universität wien

DISSERTATION / DOCTORAL THESIS

Titel der Dissertation /Title of the Doctoral Thesis

„Mono-, di- and polynucleating thiosemicarbazones, amidrazones and aminoguanisones, as well as their metal complexes as potential anticancer drugs“

verfasst von / submitted by

Kateryna Ohui

angestrebter akademischer Grad / in partial fulfilment of the requirements for the degree of

Doktorin der Naturwissenschaften (Dr. rer. Nat.)

Wien, 2019 / Vienna 2019

Studienkennzahl lt. Studienblatt / degree programme code as it appears on the student record sheet:	A 796 605 419
Dissertationsgebiet lt. Studienblatt / field of study as it appears on the student record sheet:	Chemie
Betreut von / Supervisor:	ao. Univ.-Prof. Dr. Vladimir Arion

Zusammenfassung

Diese Doktorarbeit handelt von der Synthese von Thiosemicarbazonen, Amidrazonen und Aminoguanizonen, welche ein-, zwei- und mehrkernige Metallkomplexe bilden. Diese neuen Moleküle zeigen sowohl antikrebs als auch bacterizide und antivirale Aktivität und wirken als duale Pharmazeutika. Sechs neue, wasserlösliche Morpholin-(iso)thiosemicarbazon Hybride und ihre Kupfer(II) Komplexe wurden synthetisiert. Diese Verbindungen zeigen bemerkenswerte Aktivität in cisplatinsensitiven und cisplatinresistenten Eierstockkrebszellen. Studien mit R2 RNR zeigten, dass die Kupfer(II) Komplexe mit den neuen Liganden das tyrosil Radical in Maus R2 RNR moderat inhibieren. Zusätzlich wurde gezeigt, dass Komplexierung der neuen Liganden zu einer Steigerung der bakteriziden Aktivität gegen *S. aureus* führt.

Amidrazone besitzen ein breites Spektrum an biologischen Aktivitäten und sind gute Metall-Chelatoren. In der vorgestellten Arbeit wurden neue redoxaktive einkernige Cu(II), heterozweikernige Cu(II)-Ru(II) und Cu(II)-Os(II) Komplexe mit $[CuCl_2]^-$ als Gegenion syntetisiert. Im Falle des Kupfer(II)amidrazon Komplexes war die Aldimin-Bindung stark polarisiert, was zu einer Substitution von H durch eine MeO Gruppe führte. Alle drei Komplexe zeigten moderate Aktivität in Eierstockkrebszellen und Gehirnkrebszellen im mikromolaren Konzentrationsbereich. Spin-Fallen Experimente in zellfreien Medien zeigten, dass die Verbindungen dazu in der Lage sind ROS zu generieren, was eine Erklärung für ihre antiproliferative Aktivität sein könnte.

Triapin (3-Aminopyridin-2-carboxaldehydthiosemicarbazon, 3-AP) ist eines der potentesten Antikrebswirkstoffe und ein Inhibitor von R2 RNR. Der Wirkstoff wurde bereits in über 30 klinischen Phase I und II Studien getestet. Zwei neue Derivate mit S-methyl und Pyridin Subsituenten und ihre Kupfer(II) und Eisen(III) Komplexe wurden syntetisiert und in Eierstockkrebszellen und nichtkarzinogenen embryonischen Nierenzellen getestet. Die Komplexe zeigten ein signifikante Cytotoxizität im Vergleich mit den Proliganden, bedauerlicherweise zeigten sie aber keine Selektivität für Krebszellen.

Zusätzlich wurden Versuche unternommen mehrkernige Thiosemicarbazonkomplexe zu erhalten, was zur Synthese eines neuen morpholinsubstituierten *tris*-Thiosemicarbazon und dessen *tris*-Kupfer(II)komplex führte. Diese Verbindungsklasse wird weiterhin untersucht.

Abstract

This PhD thesis is focused on the synthesis of novel mono-, di- and polynucleating thiosemicarbazones, amidrazones and/or aminoguanizones as well as their metal complexes, which could possess anticancer activity and additionally antibacterial/antiviral activity and act dual pharmaceutical agents. Six novel water-soluble morpholine-(iso)thiosemicarbazone hybrids with their copper(II) complexes were synthesized. Compounds displayed remarkable activity against cisplatin-sensitive and cisplatin-resistant ovarian carcinoma cells. Studies with R2 RNR showed that copper(II) complexes with new hybrid ligands moderately inhibit the tyrosil radical in mouse R2 RNR. Additionally it was discovered that complex formation with new hybrid ligands results in enhancement of antibacterial activity against *S. aureus*.

Amidrazones possess a broad spectrum of biological activity and are good metal chelators. In the presented work new redox-active mono- Cu(II) and heterodinuclear Cu(II)-Ru(II) and Cu(II)-Os(II) complexes with $[CuCl_2]^-$ as counteranion were synthesized. In case of copper(II)-amidrazone complex aldimine bond was highly polarized which resulted in substitution of H by MeO group. All three complexes have demonstrated moderate activity against ovarian carcinoma and cervical carcinoma cells in micromolar concentration range. Spin trapping experiment in cell-free media and confocal microscopic imaging in ovarian carcinoma cells showed that compounds are able to generate ROS, which could explain their antiproliferative activity.

Triapine (3-aminopyridine-2-carboxaldehyde thiosemicarbazone , 3-AP) is one of the most potent antitumor drug and inhibitor of R2 RNR. The drug has already entered more than 30 phase I and II clinical trials. Two new derivatives with S-methyl and pyridine substituents and their Cu(II) and Fe(III) complexes were synthesized and tested against ovarian cancer cells and non-cancerous embryonic kidney cells. Complexes showed significant cytotoxicity in comparison to proligands but unfortunately were not selective to cancer cells.

Additionally, attempts to obtain polynucleating thiosemicarbazone-derivatives were undertaken and resulted in synthesis of novel *tris*-thiosemicarbazone with morpholine moiety and its tricopper(II) complex. The investigation of this class of compounds is going on.

Table of Contents

1. General Information

1.1. Cancer

Cancer was and remains one of the biggest problems throughout the history of humanity. Cancer is a group of diseases which are characterized with specific damages in the structure of DNA leading to enhancement of the functions of genes which control cellular processes such as growth, spread and survival.[1] Normally healthy cells grow, divide and die if they got damaged, old or are not needed anymore, when in cancer cells this process does not proceed in a proper way anymore, they grow, divide but do not die. As division process is unstoppable these cells often form solid bodies called tumors. At the same time some types of cancer, e. g. leukemia do not form tumors at all.

1.2. History and Statistics

First known mentions about cancer have appeared in ancient Egypt, when descriptions of the disease were found in Edwin Smith Papyrus. During the centuries scientists accumulated knowledge and built theories, which has brought society to a much better and detailed understanding of the problem. The first sound breakthrough in this field took place in 16-17th centuries, when doctors got an opportunity to dissect bodies. Later, in 18th century certain observations were made, which brought first ideas about the reasons of cancer.[2] Globally today cancer is responsible for each 6th death all over the world which makes it the second leading reason of death worldwide. 90% of these deaths are caused by metastatic cancer.[3] Only in Austria in 2015 more than 10000 men and 9000 women died because of cancer.[4] According to a World Health Organization (WHO) statistics[5], the most common types of cancer in 2015 were:

- lung cancer (1.69 million deaths);
- liver cancer (788000 deaths);
- colorectal cancer (774000 deaths);
- stomach cancer (754000 deaths);
- breast cancer (571000 deaths).

About near 70% of cancer deaths occur in low- and middle-income countries. The number of people that live with cancer is expected to grow twice from 2000 to 2050.[6] In average 11

million cases of cancer occur annually worldwide, 6 million of them in the low- and middle-income countries.[7] It depends on abundance of infectious diseases and low vaccine coverage but also from food and water quality, generally low living standards etc. At the same time tobacco, sedentary style of life and overeating are major causes of cancer in high-income countries. Usually malignant diseases, like haematological malignancies are more common in men,[8] what can be explained with hormonal or behaviour differences. [9] Even in childhood, when these differences are not present, males have generally higher susceptibility to cancer diseases than females.[10]

Scientists distinguish large number of cancer risk factors, [11-16] such as:

- diet (excess caloric intake, low intake of fruits and vegetables);
- physical inactivity (overweight, sedentary lifestyle);
- addictions and culturally determined habits (smocking, use of alcohol);
- environmental risks (radiation, ultraviolet);
- cancer causing viruses (hepatitis B or C, Epstein-Bar, human papilloma, human immunodeficiency);
- socio-economic conditions (higher cancer incidence in low and middle-income countries in comparison with developed countries);
- genetic reasons (for some types of lung, breast cancer etc.).

1.3. Carcinogens

Substances or agents that tend to produce cancer are called carcinogens. They can be divided in genotoxic and non-genotoxic. Genotoxic carcinogens are DNA-reactive forming DNA adducts, which are essential for neoplastic transformations. Non-genotoxic or epigenetic carcinogens do not build DNA adducts but they produce effects in tissue that either are indirectly responsible for neoplastic transformations or enhance the development of tumor. [17-19]

The International Agency for Research on Cancer (IARC) which is the part of WHO divides all the known carcinogens in 4 groups:

Group 1 *carcinogenic to humans* (benzene, ethylene oxide, 4-aminobiphenyl, formaldehyde): substances or agents appear in this group when there is sufficient evidence of their carinogenity.

Group 2:

Group 2A *probably carcinogenic to humans* (acrylamide, cisplatin, diethyl sulfate, 2-nitrotoluene): agent possesses limited evidence of carcinogenicity in humans but sufficient evidence of carcinogenicity in animals.

Group 2B *possibly carcinogenic to humans* (benzophenone, nitromethane, 1,2-dichloromethane, styrene): there is limited evidence of carcinogenicity in humans and less than sufficient evidence of carcinogenicity in experimental animals.

It should be noted that terms *likely carcinogenic* and *possibly carcinogenic* are simply used to describe carcinogenicity in humans. *Likely carcinogenic* signifies higher level of it as *possibly carcinogenic*.

Group 3 is *not classifiable as to its carcinogenicity to humans* (caffeine, acrylic acid, aniline, morpholine): the evidence of carcinogenicity is inadequate in humans and inadequate or limited in animals. Agent may also be placed in this group when there is enough evidence in experimental animals, but it is proven that such mechanism of carcinogenicity does not operate in humans.

Group 4 *probably not carcinogenic to humans*: there is evidence suggesting lack of carcinogenicity in humans and experimental animals. [20]

1.4. Carcinogenesis

Decades ago Otto Warburg noticed that one of the main reasons of cancer is irreversible injuring of respiration and as a result increase of fermentation.[21] Fermentation is the metabolic process of energy release from sugar or another organic molecule, which does not need oxygen and can be measured by the amount of the formed lactic acid in the absence of oxygen.[22] This pathway is much less effective but surprisingly cancer cells use it for ATP (adenosine triphosphate) production instead of oxidative phosphorylation even in the abundance of oxygen. This was called Warburg effect.[23] Much has been changed from that moment and nowadays it is completely clear that cancer is a genetic problem. Briefly when DNA becomes damaged equilibrium between genes that control cell grows, division and apoptosis and genes that supress these effects disappears.[1,24] Therefore there is a quite large number of cancers which can be inherited. Such observations were already made over a hundred years ago, when broad pedigrees of some families have been analyzed and higher cancer incidence in some of them was noticed.[25] Nevertheless

carcinogenesis is a quite complex process which requires alterations in a large number of biological processes, which have to occur before malignance will form. In 2000 Hanahan and Weinberg described six hallmarks of cancer:[26]

(i) Alterations of the growth signals or self-sufficiency: malignant cells are able to generate a large number of their own growth signals and therefore to acquire reduced dependence from microenvironment.

(ii) Insensitivity to antigrowth signals: cancer cells have to ignore antiproliferative mechanisms to develop.

(iii) Avoidance of apoptosis: inactivation of the apoptotic pathways what makes tumors to prosper.

(iv) Limitless replicative potential: inactivation of pRb and p53 tumor suppressor proteins allows cancer cells to evade senescence (biological aging).

(v) Ability of malignant cells to form own blood vessel system through the angiogenic switch activation.

(vi) Metastasis and invasion into the healthy tissues: tumors spread cells, able to move out and may found new colonies.

Summarizing all mentioned above it becomes obvious that carcinogenesis is a complex process, in which many conditions should be fulfilled. Pathways through which cells can become malignant also differ markedly. The risk of cancer can be divided in three categories: low, moderate and high. Disease can be inherited or caused by external factors, such as influence of carcinogens, changings in lifestyle, chronic sicknesses and so on.

1.5. Anticancer Therapies

Nowadays, a variety of different anticancer therapies exists. The main are:

Surgery: This was already known much earlier than 20th century, however, already then in was noticed that nearly always disease comes back after excision. Nowadays it is mostly used in combination with other therapies.[27-30]

Hormone therapy: The most wide use this therapy has against breast and prostate cancer since it was found that removal of ovaries (in women) or testicles (in men) produces regression in cancer, thus these cancers are hormone-dependent.[31-32] Starting from this point a large number of drugs which alter hormone production has been discovered (Tamoxifen,[33] Aromatase inhibitors,[34] Degarelix[35] etc). Usually hormones are successfully

used as adjuvant therapy.[27] However there is a number of tumors that are resistant to hormonal therapy.[36]

Radiation: This procedure has traditionally been used for treatment of solid tumors. Conventional radiotherapy is inefficient to large malignancies but at the same time it shows quite good results in comparatively small ones[37] and, therefore, radiation is often used for treatment of metastases[38-40] or in combination with other therapies.[30, 41 -42]

Immunotherapy: The treatment is based on the synthesis of special biological agents which imitate or provoke the natural response of the body to uncontrollable cell growth. These agents are represented by monoclonal antibodies (Rituximab, Trastuzumab),[43] tumor reactive T-cells,[44-45] cytokines and others. Immunotherapy is also often used together with other therapies.[41-42, 46]

Targeted therapy: It is a therapy which has a certain target, like molecule or process, which is essential for the proliferation and survival of cancer cells (targeting mutant kinases, microenvironment, cancer stem cells and so on).[47]

Chemotherapy: This is a subject of my main interest and this will be discussed later in more detail.

All of the therapies described above possess their advantages and benefits and are more or less efficient in the field of their use. Nevertheless, mortality from cancer remains high and there is large number of limitations for each of the therapy used, such as high general toxicity, low selectivity, resistance against chosen treatment and so on. All these motivate researchers to discover more efficient and promising agents for chemotherapy.

2. Chemotherapy

Era of chemotherapy has begun after the Second World War when compound called aminopterin was used to treat children with acute leukemia.[48] The first known treatment of metastatic cancer was performed with methotrexate in patients with metastatic choriocarcinoma.[49] All of chemotherapeutics have their own targets depending on their mode of action. There is a variety of agents which can act as inhibitors of tyrosine kinases,[50] ribonucleotide reductase,[51] topoisomerase,[52] heat-shock protein inhibitors[53] and others. Generally, as described by Lind in 2007th in *Medicine*, chemotherapeutics can be divided on the following groups according to their type or mode of action:[54]

- ***Alkylating agents:*** drugs that damage the DNA of the cell and this latter cannot reproduce itself. In turn they can be divided in:
  - *Nitrogen mustards* (mechlorethamine, melphalan, chloroambucil);
  - *Oxazaphosphorines* (cyclophosphamide, ifosfamide);
  - *Alkyl alkane sulfonates* (busulfan);
  - *Nitrosoureas* (carmustine, lomustine, streptozotocin);
  - *Tetrazines* (dacarbazine, temozolobine);
  - *Aziridines* (thiotepa, mitomycin C);
  - *Non-classical alkyl agents* (procarbatine, hexamethylmelamine).
- ***Platinum compounds:*** anticancer drugs, containing platinum (cisplatin, carboplatin, oxaliplatin and others).
- ***Antimetabolites:*** compounds that structurally are similar to natural purines and pyrimidines:
  - *Antifolates* (methotrexate, pemetrexed);
  - *Antipyrimidines* (5-fluorouracil, gemcitabine, fludarabine);
  - *Antipurines* (6-mercaptopurine, 6-thioguanine).
- ***Topoisomerase inhibitors:*** drugs that inhibit type I or II topoisomerase, protein that control the structure of DNA (topotecan, irinotecan, epipodophyllotoxins, thiosemicarbazones).
- ***Tubulin-binding drugs:*** inhibitors of tubulin, the basic part of microtubules, which play an important role in cell functioning (vindesine, paclitaxel, taxotere etc.).
- ***Tyrosine kinase inhibitors:*** drugs (imatinib, erlotinib, lapatinib), which inhibit the enzymes, responsible for activation of the variety of proteins.

Chemotherapeutics can be combined with each other, to get synergism, or with other therapies (more often with surgery and radiotherapy) for better results in treatment. Nevertheless, research is still going on and includes many different aspects from appropriate drug design to understanding of the mode of action of each drug for the future improvement of the therapies.

2.1. Metals in Chemotherapy

In 1960th the first inorganic anticancer cisplatin was introduced in clinical practice. Its anticancer activity was discovered by the group of Rosenberg. They have accidently discovered that cisplatin is able to inhibit cell division of *Escherichia coli* and four years later reported about significant antiproliferative activity of cisplatin against sarcoma and leukemia.[55,56] From that moment metal-based anticancer compounds started to be actively investigated and era of metals in chemotherapy has begun. The mode of action of cisplatin is believed to be due to the spontaneous aquation reactions which induce the replacement of chlorido ligands with water molecules.[57] This new complex binds to DNA, forming adducts which in turn damage specific recognition proteins and bring the cell to apoptosis or take part in a process of DNA repair resulting in cell survival.[58] Unfortunately the formation of highly reacting monoaquated form of cisplatin is limited due to different intracellular reactions. Furthermore, cisplatin exhibits a number of serious side effects such as ototoxicity, nephrotoxicity, neurotoxicity, nausea, vomiting etc.[59, 60] This situation has forced scientists to search for new derivatives of platinum-containing drugs and in the followed years a number of new compounds was synthesized. The most famous of them are carboplatin, which was approved for medical use already in 1986 and nowadays its trade name is Paraplatin, oxaliplatin, approved in 1996 and marketed under the name Eloxatin, nedaplatin approved for use in 1995 in Japan, heptaplatin and others (Chart 1).[61-63] Furthermore a number of platinum based drugs have entered phase I or II clinical trials.[64-66]

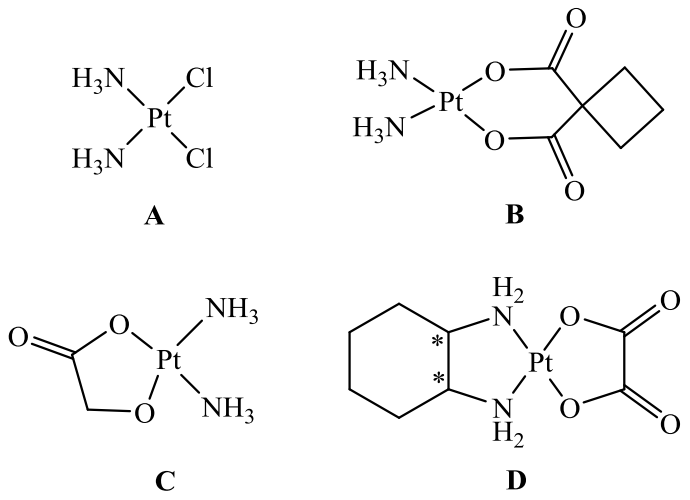

Chart 1. Platinum containing drugs approved for use: cisplatin (**A**), carboplatin (**B**), nedaplatin (**C**) and oxaliplatin (**D**).

Complexes of other metals are also widely investigated and developed as anticancer drugs. For example, compounds of gold(I) and gold(III) were discovered as effective cytotoxic agents, even though complexes of Au(III) have been underestimated for a long time due to their poor stability, higher lability in comparison to cisplatin and high toxicity *in vivo*.[67] Nevertheless, the interest in this type of complexes has been revived and still remains high. A number of gold-containing compounds which show marked antiproliferative activity, such as Au(I) phosphine and diphosphine complexes[61,68] or organogold(III) DAMP compounds, where DAMP is 2-[(dimethylamino)methyl]phenyl were investigated by Buckley *et al*.[69,70] Some of Au(I) and Au(III) complexes are toxic against specific cells, which possess resistance to cisplatin. Thus, gold compounds may have different mode of cytotoxic action from that of platinum drug.[67,71,72]

Another class of metal-containing anticancer drugs is represented by metallocenes. First metallocene with cancerostatic activity was dichlorobis(η^5-cyclopentadienyl)titanium(IV) or titanocene dichloride (Chart 2).

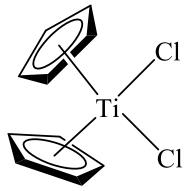

Chart 2. Line drawing of titanocene dichloride.

In 1979 Hartmut Köpf and Petra Köpf-Maier reported that this complex showed promising anticancer activity in mice.[73] Even though titanocene dichloride did not reach phase II clinical trials[74] derivatives of titanocene as well as heteronuclear bimetallic complexes with titanocene moiety are still under active investigation.[72,75-77] In addition, antitumor activity was recognized for a variety of other metallocenes containing tin, iron, vanadium, molybdenum, etc.[61,76,78]

Main group metals also play a significant role in anticancer therapy. This class is represented by complexes of rhodium, which are active against such tumor cells as Sarcoma 180 and P388 leukemia,[79] some organocobalt compounds active against L1210 leukemia and Guerin carcinoma due to its ability to generate reactive radicals,[80] arsenic trioxide, appeared to be active against acute promyelocytic leukemia,[81,82] organotin complexes,[83] gallium compounds,[84] a large variety of copper complexes.[85] Moreover, a large number of metal-based compounds are also used as radiosentisizers in radiotherapy.[61]

2.1.1. Copper in Anticancer Therapy

Copper is essential to nearly all living organisms and takes part in such important biological processes as respiration, peptide hormone production, pigmentation, oxidative stress production, normal cell growth and others.[85,86] This metal is redox active and able to cycle between two oxidation states copper(I) and copper(II) at physiologically accessible potential what makes it interesting in anticancer therapy as redox active complexes are able to generate reactive oxygen species (ROS) in cancer cells. [87] Moreover copper plays a crucial role in angiogenesis, a process of formation of the new blood and lymphatic vessels from already existing ones. Angiogenesis is important point in cancer treatment as each tumor forms its own vascular system. In addition, spread of metastases also occurs through vascular network.[88] Therefore copper chelating agents are widely used in some types of cancer.[89] One of the first works about copper complexes as anticancer agents was reported already in 1960s, when copper(II) chelate of 3-ethoxy-2-oxobutyraldehyde bis(thiosemicarbazone) was found to be active against Walker 256 carcinosarcoma in rats.[90] Later investigations demonstrated that copper complexes of thiosemicarbazones often possess higher cytotoxic activity than proligands. [91-93]

Another potent class is complexes with *N*-aromatic and π-acceptor ligands.[85] The first representative of this was copper(I) bis-phenanthroline complex. In 1979 Sigman *et al* showed that this compound was able to cleave DNA.[94] Later Zhou *et al* reported that the

same complex possess antiproliferative activity against liver carcinoma Bel-7402 cell line.[95] Unfortunately, this agent did not reach clinical use because of the number of restrictions, such as small association constant of the second phenanthroline in the complex and low selectivity to cancer cells.[96] Therefore, a large number of other derivatives of copper(I) bis-phenanthroline complex with improved properties was synthesized.[97-99]

Another class of anticancer compounds is represented by copper(II) complexes with imidazoles and their congeners.[85] Various complexes with benzimidazole derivatives showed moderate anticancer activity against different cell lines.[100] Copper(II) complex with 4-amino-1,4-dihydro-3-(2-pyridyl)-5-thioxo-1,2,4-triazole (Chart 3) exhibited marked activity comparable to that of cisplatin in HT1080 human fibroblastoma cells.[101]

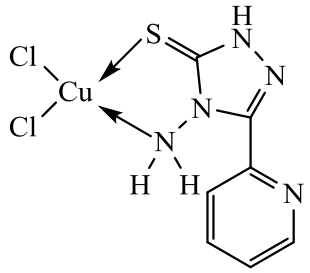

Chart 3. Line drawing of dichloride-4-amino-1,4-dihydro-3-(2-pyridyl)-5-thioxo-1,2,4-triazole copper(II).

Moreover, HT1080 fibroblastoma and HeLa cell lines appeared to be sensitive to this compound.[102] Investigations of the mechanism of action of the complex showed that despite the fact that its cytotoxic effects on HT1080 are comparable with cisplatin, programmed cell death unlike cisplatin occurs via a non-apoptotic way.[103]

A number of reports on copper complexes with Schiff-base ligands also have been published.[85] For example, in 2006 it was reported that complexes of quinoline-2-carboxaldehyde with copper are active against prostate cancer cell lines PC-3 and LNCaP.[104] Potent representatives are copper(II) complexes with isatin-Schiff bases obtained from isatin and 1,3-diaminopropane or isatin and 2-(2-aminoethyl)pyridine which induced apoptosis in neuroblastoma SH-SY5Y via the mitochondrial pathway.[105]

2.1.2. Ruthenium in Anticancer Therapy

Ruthenium is neither essential nor endogenic for the human body but in spite of this fact it has earned a large attention of the researchers as complexes with this metal displayed

potent antitumor and antimetastatic activities and some of them have already entered clinical trials. Ruthenium possesses a wide range of oxidation states, from –2 in $[Ru(CO)_4]^{2-}$ to +8 in RuO_4.[106] In biologically active compounds it is mostly present in oxidation states +2 and +3, which are both accessible under the physiological conditions.[107] It is believed that ruthenium(II) is more reactive at the tumor site than ruthenium(III). Thus, when Ru(III) reaches the tumor tissue with the lower oxygen content and pH in comparison with healthy ones, it undergoes the reduction to the more active Ru(II).[106] Second mechanism which could underlay the antiproliferative activity of ruthenium-containing drugs is the ability of ruthenium to bind with transferrin and mimicking in this respect iron.[106,107]

First mention about ruthenium as antimetastatic agent was made in 1980 by the group of Clarke, which demonstrated that *cis*-$[RuCl_2(NH_3)_4]$ and *fac*-$[RuCl_3(NH_3)_3]$ possess an excellent antiproliferative activity against P388 mouse leukemia. However, their too low aqueous solubility precluded their clinical use.[108] In 1989 Keppler *et al* have synthesized two compounds $ImH(RuIm_2Cl_4)$ (KP418) and $IndH(RuInd_2Cl_4)$ (KP1019, Chart 4), where Im = imidazole and Ind = indazole which were active against Walker 256 carcinosarcoma, Stockholm Ascitic tumor, B16 melanoma, sarcoma 180 and especially active against colorectal cancer.[109] KP1019 has already entered phase I clinical trials and showed promising results in patients with different types of cancer.[110,111]

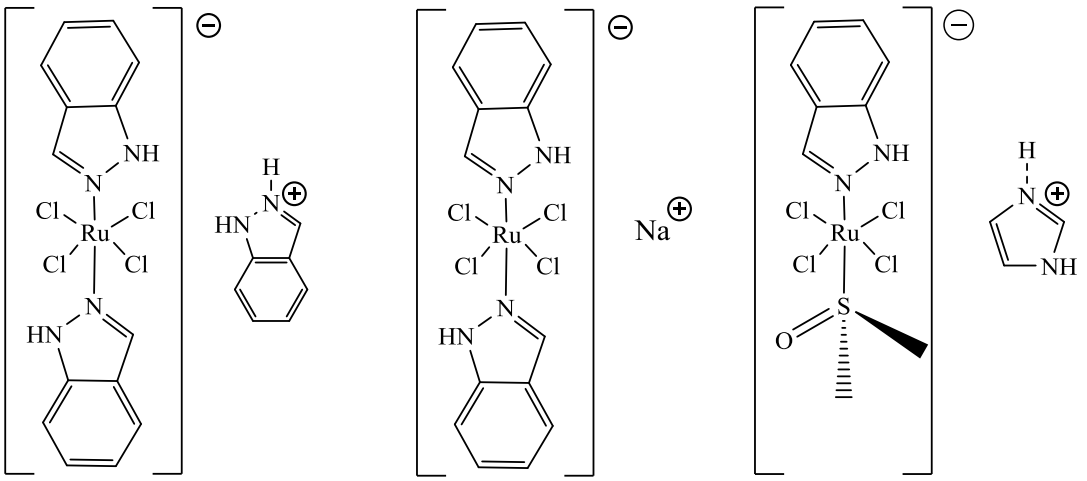

Chart 4. Ruthenium-containing drugs, which have entered clinical trials.

Sodium *trans*-[tetrachloridobis(1*H*-indazole ruthenate(III)] (NKP-1339, Chart 4) also exhibits antiproliferative activity with low general toxicity, but has higher water-solubility

what allows clinical application in higher doses.[112] The compound entered phase I clinical trials.[113]

First antimetastatic complex of ruthenium(III) which entered clinical trials was *trans*-imidazole(dimethylsulfoxide)tetrachloridoruthenate(III) ImH[*trans*-$RuCl_4$(DMSO)Im] (NAMI-A, Chart 4). Interestingly, this drug acts against metastases and does not affect the primary tumor.[114] This is likely due to the combination of anti-invasive and anti-angiogenic properties of the drug candidate. [115]

A promising class of ruthenium containing anti-cancer compounds is represented by organoruthenium(II) compounds. This field was pioneered by Sadler and Dyson. [116,117] In 2001 Morris *et al* reported that compounds with the general formula [(η^6-*p*-cymene)Ru(en)(X)]$^+$ where en = ethylenediamine and X = Cl or I and [(η^6-$C_6H_5C_6H_5$)RuCl(YZ)]$^+$ where Y, Z = ethylenediamine or *N*-ethylethylenediamine inhibit the growth of A2780 human ovarian cancer cells. Moreover, their antiproliferative effects were similar to those of carboplatin, a drug marketed under the name Paraplatin.[116] It is believed that a primary target for Ru(II)-arene complexes is DNA.[118]. Another family of related compounds with anticancer activity is shown in Chart 5.

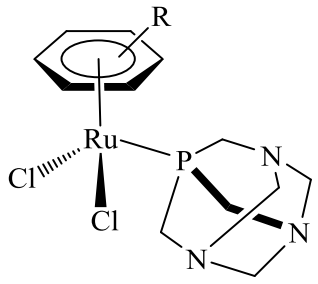

Chart 5. General formula of RAPTA compounds.

RAPTA complexes consist of ruthenium(II) coordinated with η^6-arene and 1,3,5-triaza-7-phosphatricyclo[3.3.1.1]decane (pta).[107] The most promising representatives of this group are RAPTA-C, [$RuCl_2$(η^6-cymene)(pta)], and RAPTA-T – [$RuCl_2$(η^6-toluene)](pta)]. Both of them, like NAMI-A, are only weakly cytotoxic, showing great ability to supress the growth of metastases.[119] Nowadays, RAPTA-T due to its antimetastatic action and low general toxicity is a potent candidate to enter clinical trials.[115]

In the recent years the interest of the researchers to osmium, the closest congener of ruthenium, increased as well. Compounds of ruthenium and osmium, in particularly Ru(II)-arene and Os(II)-arene, often show similar chemical behaviour as well as favorable

pharmacological properties, such as aqueous solubility, stability in plasma, bioavailability and so on.[107,120]

As mononuclear complexes of Ru(II)-arene and Os(II)-arene showed marked antiproliferative activity they are often used in combination with other metal centres in order to improve the biological properties of the final compound. Heteronuclear complexes of Ru(II)-arene with Au(I), Sn(II), Pt(IV) were reported in the literature. These complexes demonstrate marked cytotoxicity and improved selectivity to cancer cells.[121] Dinuclear ruthenium-copper complexes are still not enough developed. In 2017 Lopes *et al* reported on dinuclear Cu(I)-Ru(II) complex with 1,2-bis(diphenylphosphino)ethane (dppe) and 2,3-bis(2-pyridil)pyrazine (dpp) (Chart 6A).

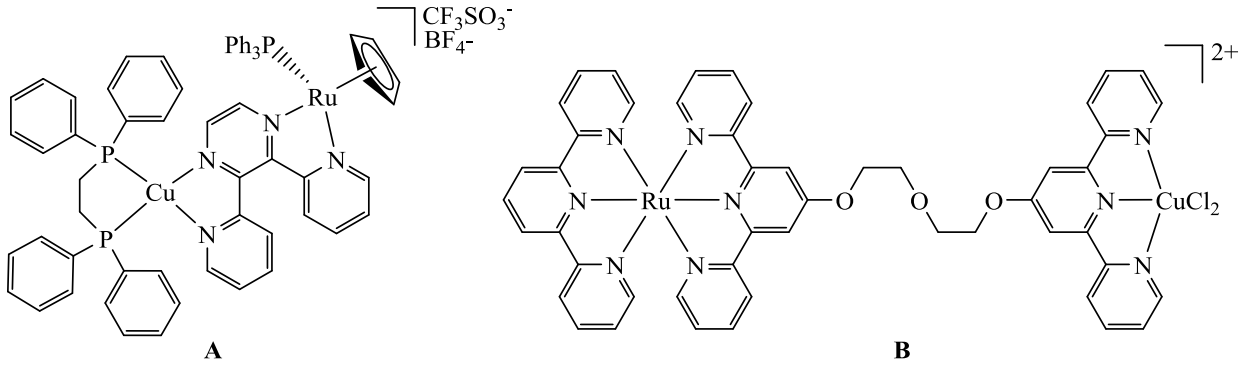

Chart 6. Heteronuclear copper-ruthenium complexes with biological activity.

The compound showed activity against human ovarian cisplatin sensitive A2780 and breast MCF7 cancer cell lines in micromolar range. However, the activity of the dinuclear complex was not significantly different from the activity of its mononuclear building blocks.[122] Nevertheless, in 2010 Reedijk *et al* reported on heteronuclear copper-ruthenium complex (Chart 6B), which was able to cleave DNA.[123] This type of compounds is still not investigated enough and continues to attract the interest of the modern researchers.

It should be noted that the activity of metal-based drugs depends not only on the metal itself but also on the ligand environment. Careful and appropriate choice of the ligands allows for modification of coordination geometry, redox properties, affects cytotoxicity and structure-activity relationships.[107]

2.2. Thiosemicarbazones (TSCs) as anicancer agents

Thiosemicarbazones have the same structure as semicarbazones where the oxygen atom is substituted by sulfur (Chart 7) and can be synthesized by the condensation reaction of appropriate aldehyde or ketone with thiosemicarbazides.

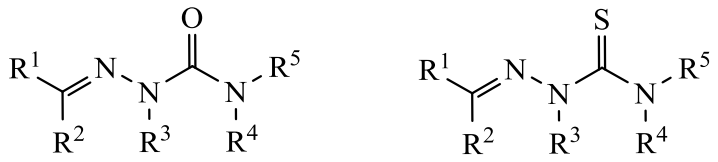

A **B**

Chart 7. General formulas of semicarbazone (**A**) and thiosemicarbazone (**B**).

They are potent inhibitors of ribonucleotide reductase,[51] topoisomerase I and II,[124,125] some of their complexes are able to generate reactive oxygen species.[126] Moreover, TSCs possess a broad spectrum of biological activity such like antiviral, antibacterial and antifungal activity[91,127,128] which makes them an interesting class of compounds for investigation.

The interest to biological properties of TSCs appeared after the works of Domagk where he showed that TSCs of cyclic aldehydes or ketones possess strong inhibiting properties against tuberculosis. Moreover, in one of his work Domagk payed attention on the fact that replacement of O-atom of semicarbazone on S-atom in thiosemicarbazone had a dramatic effect on the biological activity, as semicarbazones have showed extremely weak potency.[129] In 1956 Brockman *et al* discovered antiproliferative activity of pyridine-2-carboxaldehyde (or 2-formylpyridine) TSC against different lines of leukemia in mice. The activity found was not significant, but remarkable. Furthermore, in this work Brockman showed that isomers of 2-formylpyridine TSC have no activity against leukemia at all what brought to the idea of strong relationship between the structure of TSC and its antiproliferative activity.[130] In 1965 French and Blanz studied carcinostatic activity of α-(*N*)-heterocyclic carboxyldehyde TSCs starting with isoquinoline-1-carboxaldehyde TSC (IQ-1). The compound showed activity against two types of leukemias (L-1210 and ML-1210), adenocarcinoma 755, Ehrlich ascites carcinoma and Lewis lung carcinoma.[131] One year later they reported on anticancer activity of 3-hydroxypyridine-2-carboxaldehyde TSC (3-HP) against lymphoma L5178Y, Lewis lung carcinoma, Ehrlich ascites carcinoma,

leukemia L1210 and adenocarcinoma 755.[132] In the same year French and Blanz summarized their observations by analyzing the data of antiproliferative activity of 41 different TSC derivatives and 2 heterocyclic ketones and postulated that only those TSCs show activity whose formyl groups are attached in α-position with respect to the ring heteroatoms. This leads to a lower π-electron density on α-carbon and higher density on the ring nitrogen, forming conjugated N–N–S ligand system. They have demonstrated that no molecule, where such ligand system was absent, showed cytotoxic activity. Furthermore, some of the TSCs of this type are strong chelators for divalent transition metals, as it was already mentioned previously.[133]

2.2.1. 5-Hydroxy-2-formylpyridine Thiosemicarbazone (5-HP)

First clinically evaluated TSC was 5-hydroxy-2-formylpyridine thiosemicarbazone (Chart 8).[134]

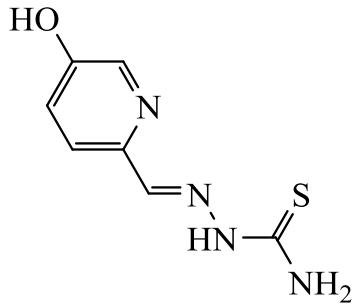

Chart 8. Line drawing of 5-hydroxy-2-formylpyridine thiosemicarbazone.

French and Blanz studied the activity of the compound against different cell lines and compared it with that of 3-HP and IQ-1, investigated before.[131,132] The behaviour of 5-HP was found to be similar but compound appeared to be less toxic as its hematologic effects were found to be reversible when treatment is stopped.[135] Of note is that 5-HP formes a water-soluble sodium salt and this facilitates its parenteral administration.[134] Sartorelli *et al* in 1971 showed that mode of action of 5-HP lies in inhibition of DNA biosynthesis.[136] In the same year they demonstrated that site of action of α-(*N*)-heterocyclic TSCs is ribonucleotide reductase.[137] The important role was given to the ability of TSCs to chelate iron(II) since it was suggested that corresponding proligands bind with the iron charged enzyme inhibiting its activity.[138]

Ribonucleotide reductase (RNR) is an enzyme which catalyzes the formation of deoxyribonucleotides from ribonucleotides. It is essential for cell proliferation as it provides precursors for DNA synthesis and repair.[139] Depending on its metal cofactors RNRs can be divided in three classes. Class I RNR contains diiron-oxygen cluster, class II has vitamin B12 as cofactor and class III contains iron-sulfur cluster coupled to *S*-adenosylmethionine.[140] Human enzyme belongs to the class I RNRs and consists of the two subunits R1 and R2.[141] The R1 subunit binds substrates and allosteric effectors and R2 subunit which is smaller than R1 contains diiron centre that takes part in tyrosyl radical stabilization, important for enzymatic activity.[142] RNR plays an important role in anticancer therapy since a strong dependence was found between its activity and progression of cancer.[143] A large number of chemotherapeutics are used to sequester the iron from diiron centre of the enzyme and/or to quench the tyrosyl radical leading to a loss of catalytic activity. One of the first agents of this class was hydroxycarbamide or hydroxyurea. Even though, it is still in the clinical use, hydroxyurea shows poor effectiveness as anticancer drug due to its low affinity to RNR and relatively fast inactivation after administration.[144] Moreover, it shows a number of side-effects like suppression of the bone marrow, genotoxicity, neutropenia, thrombocytopenia and others.[145]

At the same time, there are some TSCs which are 1000-fold more potent inhibitors of RNR than hydroxyurea.[92]

5-HP was chosen as a candidate for clinical trials since at that time it was the most potent drug against rodent transplanted tumors, could be dissolved in water in form of its sodium salt and had a good therapeutic index comparing with other representatives of this class of chemotherapeutics. Unfortunately 5-HP failed in clinical trials because of the numerous side-effects, such as high general toxicity resulted in a low therapeutic index, rapid inactivation by glucuronidation, severe hematological and gastro-intestinal side-effects.[134]

2.2.2. 3-Aminopyridine-2-carboxaldehyde Thiosemicarbazone (3-AP)

Of special attention is 3-aminopyridine-2-carboxaldehyde thiosemicarbazone, marketed under the name Triapine (Chart 9, 3-AP), which is one of the most potent antitumor drugs and inhibitors of ribonucleotide reductase nowaday. [92,144]

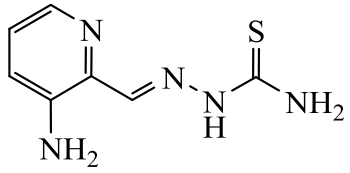

Chart 9. Line drawing of Triapine.

In 1992 Sartorelli *et al* have synthesized 12 derivatives of TSCs and demonstrated that the most effective ones in prolonging the life span of the mice bearing L1210 leukemia were 3-aminopyridine-2-carboxaldehyde (3-AP) and its 4-methyl derivative (3-AMP). Although 3-AMP showed lower toxicity, 3-AP possessed much better antitumor activity at lower dosages. Already at doses 10 mg/kg 2 times daily it produced 40% 60-day long-term survivals.[146] From this moment 3-AP gained particular attention of scientists and was actively investigated. 3-AP is a potent antiproliferative agent which showed activity against hydroxyurea-resistant cells, like leukemia L1210, murine M109 lung carcinoma, human A2780 ovarian carcinoma xenografts in mice and subline of the human KB nasopharyngeal carcinoma, which showed 15-fold resistance to hydroxyurea. Moreover, it was shown that recovery of DNA synthesis occurred in normal tissues noticeably faster than in malignant cells, which appeared to be an important point for the further clinical evaluation of the drug.[144]

Until now 3-AP has entered more than 30 phase I and II clinical trials.[147-149] It was also applied in combination with other drugs and is able to enhance the activity of cisplatin,[150] cisplatin and paclitaxel,[151] gemcitabine,[152] irinotecan,[153] doxorubicin,[154] etc. It should be noted that 3-AP showed good and promising results in leukemias, but it has failed against a number of solid tumors showing completely no responses in patients or too small to reach minimal efficiency criteria.[155-157] Nevertheless, it still can be used against solid tumors in combination with radiotherapy,[158,159] as it was shown that Triapine can be an efficient radiosensitizer.[160]

As already mentioned before, 3-AP is a strong inhibitor of ribonucleotide reductase. It is believed that loss of the activity of the enzyme occurs via destruction of tyrosyl radical, which is iron dependent. Triapine is a strong chelator for both iron(II) and iron(III) ions.[161] Moreover, 3-AP-Fe(II) complex is much more potent inhibitor of R2 RNR in comparison with 3-AP-Fe(III) or proligand. Shao *et al* reported that 3-AP-Fe(II) produces reactive oxygen species (ROS) reacting with dioxygen.[162]

Reactive oxygen species (ROS) are highly reactive chemical species which contain oxygen. Examples are singlet oxygen, superoxide, peroxide, hydroxyl radical and others.[163] In biological systems they fulfil a variety of functions, some of which are necessary, while other are harmful.[164] Specific attention in anticancer research ROS gained when it was found out that a large number of cancer cells possess an increased level of these species, which was called oxidative stress.[165] Moreover, it has been shown that redox stress correlates with the tumor aggressiveness but at the same time, if concentration of ROS reaches the level which is incompatible with the malignant cells survival, it brings to their death. From the other side normal cells are expected to survive because they do not possess any oxidative stress.[164,166] This can be used to selectively increase the efficiency in fight against cancer.

Three mechanisms of RNR inhibition by Triapine were proposed: (i) iron(III) is chelated directly from the enzyme diferric centre, (ii) drug takes iron from the intracellular iron pool and (iii) complex of Fe(III) with 3-AP is reduced to Fe(II)-3-AP that reacts then with dioxygen to produce ROS, what in turn results in the inhibition of RNR.[167]

As a number of TSCs are potent inhibitors of topoisomerase IIα,[125] inhibitory effects of Triapine towards this enzyme were also tested. Nevertheless, the drug has not showed any activity, indicating that cytotoxicity of 3-AP has another reason.[168]

Even though Triapine has entered more than 30 phase I or II clinical trials, it possesses a number of adverse effects such as methemoglobinemia, hypoxia, neutropenia and others.[157,169] Therefore, researchers continue to search for the drugs with better properties, synthesizing and investigating derivatives of 3-AP. Thus, Kowol *et al* have demonstrated that dimethylation of the terminal nitrogen increases the cytotoxicity.[170] Some of N-methylated derivatives demonstrated a significant increase in toxicity. For example, 3-aminopyridine-2-carboxaldehyde-N^4-dimethylthiosemicarbazone (Chart 10A) has shown more than 2-fold increase of cytotoxicity in ovarian carcinoma cell lines with IC_{50} 0.30 ± 0.03 μM, while 3-AP has IC_{50} 0.7 ± 0.3 μM against this cell line. In addition, it showed activity against cell lines, which are Triapine resistant, colon adenocarcinoma and lung fibroblast cell line.

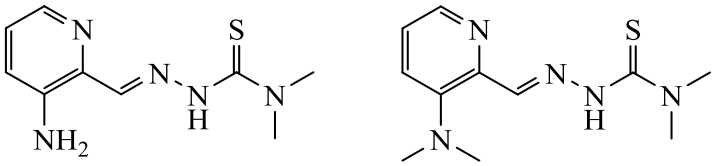

A **B**

Chart 10. Line drawings of 3-aminopyridine-2-carboxaldehyde-N^4-dimethylthiosemicarbazone (**A**) and 3-(dimethylaminopyridine)-2-carbaldehyde N,N-dimethylthiosemicarbazone (**B**).

Note that dimethylation of both, terminal nitrogen and amino group at the pyridine ring in case of 3-(dimethylaminopyridine)-2-carbaldehyde N,N-dimethylthiosemicarbazone (Chart 10B), resulted in a large increase of cytotoxicity in comparison with 3-AP with IC_{50} in low nanomolar range (0.0070 ± 0.0003 μM against ovarian carcinoma cell line).[171]
Recently, Polanski *et al* synthesized 12 novel derivatives of Triapine and demonstrated that insertion of piperazinyl fragment into the structure improves anticancer activity. Moreover, the best activity was observed for two compounds, which contained fluorine atoms within the fragment, stimulating the design of new more potent and selective anticancer agents.[172]

2.2.3. Other Thiosemicarbazones as Potent Anticancer Agents

As it can be seen from all, mentioned preciously, extensive structure-activity relationship studies are an important tool in the design of new drugs. Richardson *et al* discovered a series of novel di-2-pyridilketone thiosemicarbazones (DpT), which have shown antitumor and antimetastatic activity *in vivo* and *in vitro*.[173-175] One of the most potent and best characterized member of the first generation of DpT analogues is di-2-pyridylketone 4,4-dimethyl-3-thiosemicarbazone (Chart 11, Dp44mT).

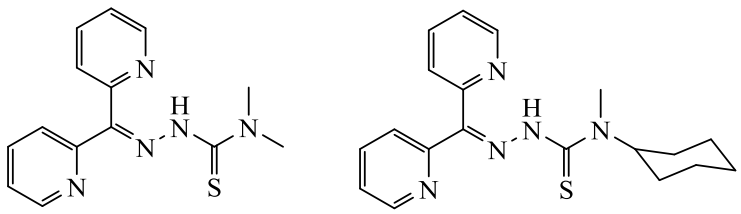

Dp44mT **DpC**

Chart 11. Line drawing of di-2-pyridylketone 4,4-dimethyl-3-thiosemicarbazone (Dp44mT) and di-2-pyridylketone 4-cyclohexyl-4-methyl-3-thiosemicarbazone (DpC).

This compound accumulates in lysosomes and takes part in ROS production what results in lysosomal membrane permeabilization and cell death.[176] It should be also noted that Dp44mT showed significantly greater antiproliferative effects in comparison with Triapine.[174] Quite recently, it was demonstrated that Dp44mT in combination therapy with doxorubicin allows to overcome drug resistance via lysosomal permeabilization.[177]

Another potent compound from the second generation of DpTs is di-2-pyridylketone 4-cyclohexyl-4-methyl-3-thiosemicarbazone (Chart 11, DpC). This compound appeared to be even more potent than Dp44mT and has shown a number of advantages, i. e., greater antitumor activity *in vivo*, possibility to administrate it orally, unlike Dp44mT, which is toxic by oral administration,[175] significantly greater plasma half-life in rats,[178] lack of some side-effects which appeared by administration of Dp44mT and others.[175,179] DpC has just entered phase I clinical trials for treating advanced tumors.[180]

As design of the new potent anticancer drugs with high activity and low toxicity is a multiparameter task computer modelling *in silico* has gained a significant importance. Different platforms use various pharmacological principles, statistical modelling. Thereby COTI-2 ((*E*)-*N*´-(6,7-dihydroquinolin-8(5*H*)-ylidene)-4-(pyridine-2-yl)piperazine-1-carbothiohydrazide, Chart 12) has been designed and synthesized recently by Koropatnick *et al.*[181]

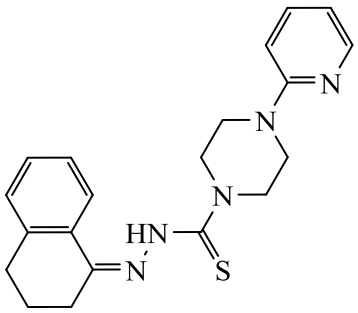

Chart 12. Line drawing of ((*E*)-*N*´-(6,7-dihydroquinolin-8(5*H*)-ylidene)-4-(pyridine-2-yl)piperazine-1-carbothiohydrazide (COTI-2).

The activity of COTI-2 against multiple human cancer cell-lines with different genetical background was tested. The compound inhibits the proliferation rate of all cell lines tested over 72 h. Moreover, COTI-2 appeared to be more effective in inhibition of the cell growth than marketed cetuximab and erlotinib.[181] COTI-2 has entered phase I clinical trials in 2016.[182] Quite recently, it has been shown that COTI-2 synergizes with other anticancer

drugs, cisplatin and paclitaxel, enhancing their activity and even does not induce resistance in cancer cells what is one of the main problems.[183]

All mentioned previously clearly shows that TSCs still remain one of the most potent and promising class of anticancer agents. They still are the subject of significant interest of the researchers. However, their use is limited by high toxicity and as a result low therapeutic index.[149,155,184] Another issue to be addressed is the low solubility of the most of TSCs. Scientists payed attention to this point already during the investigation of 5-HP, which had to be used in form of its sodium salt as it was water-soluble and allowed intravenous administration.[134] One possible way to improve the solubility is the attachment of different hydrophilic moieties, i. e., morpholine or proline to the hydrophobic scaffold of the molecule, which also allows to modulate the toxicity of the compounds. Such experiments have been successfully done by a number of research groups. [91,93,185] Furthermore, incorporation of biologically active scaffolds, such as morpholine allows to extend the biological potential of the final molecule. We reported quite recently on 6 new morpholine hybrids and their metal complexes which possess both anticancer and antibacterial properties. Compounds showed activity against two cell lines, human ovarian carcinoma A2780 and its cisplatin resistant form, as well as against *S. aureus* and *P. aeruginosa*. Should be noted that significant antibacterial activity was observed for copper(II) complexes of the hybrids, moreover, compounds were more active against Gram-positive bacteria (*S. aureus*) than Gram-negative (*P. aeruginosa*).[91]
The solubility of TSCs can also be modified in complex formation with transition metals. This issue deserves a separate chapter since there is a large variety of metal complexes with completely different from that of TSCs cytotoxic activity and mode of action, what also play an important role in anticancer therapy.

2.2.4. Metal Complexes of Thiosemicarbazones as Anticancer Agents

TSCs are strong metal chelators in both neutral and anionic forms especially for the first row transition metals such as copper(II), zinc(II) and iron(III). For coordination they usually use S and N atoms from the backbone and coordinate in bidentate fashion.[186] Coordination capacity can be increased if aldehydes or ketones used for TSCs preparation contain additional donor atoms in positions suitable for chelation. Typical tridentate

binding occurs through S, N, X atoms, where X is an atom of the additional functional group.[187] Monodentate coordination through the thione sulfur atom was reported Hg(II) and Ag(I).[188,189] It has been shown that metal complexes of TSCs are usually more cytotoxic as proligands.[87,91-93,190] For example, iron(II)-Triapine is more potent RNR inhibitor in comparison with the proligand.[162] But at the same time coordination of Fe(III) to 3-AP decreases cytoxicity up to 2-3 times.[170,191] Nevertheless, situation with other α-(*N*)-heterocyclic thiosemicarbazones is more optimistic. Coordination of copper(II) to di-2-pyridylketone 4,4-dimethyl-3-thiosemicarbazone (Dp44mT) resulted in more than 2-fold increase of cytotoxicity in SK-N-MC neuroepithelioma cells after 24 h incubation in case of [Cu(Dp44mT)(OAc)] and nearly 5-fold in case of [Cu(Dp44mT)$_2$] under the same conditions.[192] Richardson *et al* proposed the mechanism of cytotoxic action of Dp44mT, where they showed that the reason of apoptotic action of the proligand underlies in the formation of Cu-Dp44mT complex in lysosomes which further takes part in ROS production.[176] A similar was proposed for the di-2-pyridylketone 4-cyclohexyl-4-methyl-3-thiosemicarbazone (DpC).[193] Recently we reported on variety of TSCs with antineoplastic activity. For some of them coordination to copper(II) played a crucial role in their cytotoxicity. [87,91,93,190,194] For example, coordination of copper(II) to morpholine-TSC derivative resulted in nearly 5-fold increase of cytotoxicity in cervical carcinoma HeLa cell lines and more than 17-fold increase in human colon carcinoma LS174 cells.[93] Moreover, it resulted in much better aqueous solubility of TSCs.[85,93] However, coordination of metals not always leads to an increase of cytotoxicity. In particular, cordination of nickel(II) and palladium(II) to L-proline and homoproline-4-*N*-pyrrolidine-3-thiosemicarbazone hybrids have led to nearly 10-fold loss of cytotoxicity in all cell lines tested.[190]

2.3 Amidrazones as Anticancer Agents

A brief overview on amidrazones, the close congeners of thiosemicarbazones and their antiproliferative properties, is given herein. Amidrazones are compounds with general formula R–C(=NR^1)–NH–NHR^2 and can exist in two tautomeric forms, hydrazide imides and amide hydrazones (Chart 13).

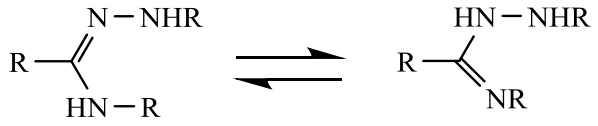

Chart 13. Tautomeric forms of amidrazones.

These molecules also possess a broad spectrum of biological activity. In literature there are reports on amidrazones as antimicrobial, antibacterial,[195-198] anticonvulsant,[199] and anticancer agents.[200-204] Like thiosemicarbazones amidrazones are good metal chelators, various complexes with copper(II), palladium(II), platinum(II) and platinum(IV) as well as with other metals have been reported.[205-209] Unlike thiosemicarbazones the number of reports about metal complexes of amidrazones is comparatively small, and studies in this direction just started to develop. Nevertheless, it was demonstrated that copper(II) complex with carboxamidrazone possesses antiproliferative activity against human breast cancer cell line MCF-7 in low micromolar range. In addition, complex appeared to be electrochemically active and potentially able to generate ROS in cancer cells.[210] Recently, it was demonstrated that incorporation of biologically active moieties like coumarine or piperazine in amidrazone backbone results in new antiproliferative agents.[203,204] Therefore coupling to another biologically active moiety like morpholine may increase cytotoxicity of the final compound. Quite recently it was shown that incorporation of morpholine unit into the thiosemicarbazone structure not only increased solubility of the compounds but also improved their anticancer activity.[91] Thus, amidrazones represent an interesting but undeveloped class of potential antitumor agents.

2.4 Dendrimers in anticancer therapy

Dendrimers are branched molecules with many arms originating from the central core. Interest in this type of molecules as possible biologically active agents appeared only in the last decades after the growth of the number of water soluble and biocompatible dendrimers.[211] The first synthesized dendrimers were polyamidoamines (PAMAMs). The core of these molecules is ammonia or ethylenediamine species.[212] Nowadays they are commercially available and PAMAM dendrimer scaffolds are mostly used for biological applications. The number of functional groups, molecular formula and molecular weight of dendrimers is a function of generation.[213] For example, in PAMAMs number of surface reactive sites is doubled with each generation, the mass of the molecule increases then

more than twice.[212, 214] In medicine dendrimers can be used, for example, as drug delivery agents, in photodynamic therapy, imaging, neutron capture therapy, etc.[215]

In anticancer therapy dendrimers are in the focus of the great interest mainly as drug delivery agents. Generally there are two main approaches for drug delivery: noncovalent encapsulation of drugs and covalent dendrimer-drug conjugates.[211] For the first time mechanism of the noncovalent incapsulation has been proposed in 1982 by Maciejewski.[216] This approach works as the "host-guest" principle. "Guest" molecules are captured within the internal cavities of "host" dendrimers. Cavity of the dendrimer, which is able to encapsulate guest molecules is called dendritic box. [217] Jansen *et al* have shown that size of approximately 5 nm is needed to physically lock guest molecules.[218] Molecules are able to diffuse in or out of the dendrimer host,[217] but it is difficult to control this process and sometimes harsh conditions are required. This makes the usage of such molecules for drug delivery more problematic. In other cases the release of the drug can occur quite rapidly, which is also often an undesired effect.[211]

The second approach implies the creation of covalent dendrimer-drug conjugates. As dendritic molecules possess multivalency, drug molecules can be attached to their periphery. Moreover, drug loading can be controlled by changing the generation number of the dendrimer.[211] This method possesses a number of advantages, in particular, increased water solubility, passive tumor targeting due to EPR-effect, prolonged plasma half-life and enhanced bioavailability.[212,219]

Enhanced permeability and retention (EPR) effect – an effect by which molecules of certain size tend to accumulate in tumor tissue more than they do in normal one. This becomes possible due to a number of pathological properties of the tumor such as extensive angiogenesis, lack of the muscle smooth layer and poor lymphatic drainage.[220,221] Thus, molecules of appropriate size can accumulate in the malignant tissue resulting in 5-10-fold higher concentration of drug in tumor tissue then in blood plasma.[219]

Therefore, dendrimers build an interesting and potent class of compounds for chemotherapy. At present compound called XYOTAX (paclitaxel, a marketed anticancer drug, conjugated to polyglutamic acid) has already entered phase III clinical trials in combination with carboplatin for the treatment of non-small cell lung cancer.[219] Attempts to synthesize dendrimers of different generations with variety of potent anticancer agents like thiosemicarbazones or ruthenium have also been reported. Govender *et al* prepared

multinuclear ruthenium-arene complexes coordinated to dendritic scaffolds. The compounds demonstrated moderate activity against A2780 human ovarian cancer cell line, but were more cytotoxic in comparison with analogous mononuclear ruthenium complexes what could be associated with better accumulation of the drug in tumor cells.[222]

Efforts to conjugate thiosemicarbazones with dendritic moiety were made by Smith *et al*. They reported on ferrocenylthiosemicarbazones with antimalarial activity.[223] In addition, palladium(II) and platinum(II) complexes of multimeric salicylaldimine TSCs which showed activity in micromolar range against oesophageal cancer WHCO1 cell line were also synthesized.[224]

Nevertheless, data on dendrimers conjugated with TSCs in this field still stays undeveloped. Moreover, drug conjugates with dendrimers still possess a number of disadvantages, such as low aqueous solubility, high general toxicity, short half-life in blood. Thus, there are still a number of problems which have to be solved.

References:

(1) Harrington, K. J. Biology of cancer. *Medicine* **2011**, *39(12)*, 689–692.

(2) The history of cancer. *Amer. Cancer Soc.* **2009**.

(3) Sporn, M. B. The war on cancer. *Lancet* **1996**, *347*, 1377–1381.

(4) From Statistik Austria, http://www.statistik.at/web_de/statistiken/menschen_und_gesellschaft/gesundheit/krebserkrankungen/krebs_im_ueberblick/index.html

(5) From the WHO, http://www.who.int/news-room/fact-sheets/detail/cancer

(6) Simmonds, M. A. Cancer Statistics, 2003: Further Decrease in Mortality Rate, Increase in Persons Living with Cancer. *C A Cancer J. Clin.* **2003**, *53*, 4.

(7) IOM, Cancer Control Opportunities in Low and Middle-Income Countries, **2007**.

(8) Molife, R.; Lorigan, P.; Macneil, S. Gender and survival in malignant tumours. *Cancer. Treat. Rev.* **2001**, *27*, 201–209.

(9) Tevfik Dorak, M.; Karpuzoglu, E. Gender differences in cancer susceptibility: an inadequately addressed issue. *Front. Gen.* **2012**, *3*, 1–11.

(10) Devarahally, S. R.; Severson, R. K.; Chuba, P.; Thomas, R.; Bhambhani, K.; Hamre, M. R. Second malignant neoplasms after primary central nervous system malignancies of childhood and adolescence. *Pediatr. Hematol. Oncol.* **2003**, *20*, 617–625.

(11) Sudhakar, A. History of Cancer, Ancient and Modern Treatment Methods. *J. Cancer Sci. Ther.* **2009**, *1*, 1–4.

(12) Anand, P.; Kunnumakara, A. B.; Sundaram, C.; Harikumar, K. B.; Tharakan, S. T.; Lai, O. S.; Sung, B.; Aggarwal, B. B. Cancer is a Preventable Disease that Requires Major Lifestyle Changes. *Pharm. Res.* **2008**, *25*, 2097–2116.

(13) Danaei, G.; Hoorn, S. V.; Lopez, A. D.; Murray, C. J. L.; Ezzati, M.; Comparative Risk Assessment collaborating group (Cancers). Causes of Cancer in the world: comparative risk assessment of nine behavioural and environmental risk factors. *Lancet* **2005**, *366*, 1784–1793.

(14) Magrath, I. Cancer in low and middle income countries. *Health G20*, 58-68.

(15) Tomatis, L. Environmental Cancer Risk Factors: A review. *Acta Oncol.* **1988**, *27*, 465–472.

(16) Henderson, B. E.; Bogdanoff, E.; Gerkins, V. R.; SooHoo, J.; Arthur, M. Evaluation of Cancer Risk Factors in a Retirement Community. *Cancer Res.* **1974**, *34*, 1045–1048.

(17) Lee, W. J.; Kim, S. C.; Lee, S. J.; Lee, J.; Park, J. H.; Yu, K.-S.; Lim, J.; Kwon, S. W. Investigating the Different Mechanisms of Genotoxic and Non-Genotoxic Carcinogens by a Gene Set Analysis. *PLoS ONE* **2014**, *9*, e86700.

(18) Williams, G. M. Mechanisms of chemical carcinogenesis and application to human cancer risk assessment. *Toxicology* **2001**, *166*, 3–10.

(19) Ellinger-Ziegelbauer, H.; Stuart, B.; Wahle, B.; Bomann, W.; Ahr, H. J. Comparison of the expression profiles induced by genotoxic and nongenotoxic carcinogens in rat liver. *Mutation Res.* **2005**, *575*, 61–84.

(20) IARC Monographs on the Evaluation of Carcinogenic Risks to Humans. Preamble. *World Health Organization* **2006**.

(21) Warburg, O. On the Origin of Cancer Cells. *Science* **1956**, *123*, 309–314.

(22) Tortora, G. J.; Funke, B. R.; Case, S. L. Microbiology: An Introduction (10 ed.). **2010**, San Francisco, CA 94111, USA: Pearson Cummings. p. 135.

(23) Vander Heiden, M. G.; Cantley, L. C.; Thompson, C. B. Understanding the Warburg Effect: The Metabolic Requirements of Cell Proliferation. *Science* **2009**, *324*, 1029–1033.

(24) Evans, D. G. Genetic predisposition to cancer. *Medicine* **2012**, *40*, 29–33.

(25) Hodson, S. V.; Foulkes, W. D., eds. Inherited susceptibility to cancer. *Cambridge: Cambridge University Press*, **1998**.

(26) Hanahan, D.; Weinberg, R. A. The Hallmarks of Cancer. *Cell* **2000**, *100*, 57–70.

(27) Perlia, C. P.; Taylor, S. G. Hormonal Treatment of Breast Cancer. *Med. Clin. North America* **1963**, *47*, 159–167.

(28) Shvero, J.; Hadar, T.; Yaniv, E.; Marshak, G.; Feinmesser, R. Segal, K. Supraglottic carcinoma: a retrospective study of 114 patients. *Eur. J. Surg. Oncol.* **1997**, *23*, 289–292.

(29) Cuzick, J.; Stewart, H.; Peto, R.; Baum, M.; Fisher, B.; Host, H.; Lythgoe, J. P.; Ribeiro, G.; Scheurlen, H.; Wallgren, A. Overview of randomized trials of postoperative adjuvant radiotherapy in breast cancer. *Cancer Treat. Rep.* **1987**, *71*, 15–29.

(30) Clarke, M.; Collins, R.; Darby, S.; Davies, C.; Elphinstone, P.; Evans, V.; Godwin, J.; Gray, R.; Hicks, C.; James, S.; MacKinnon, E.; McGale, P.; McHugh, T.; Peto, R.; Taylor, C.; Wang, Y. Effects of radiotherapy and of differences in the extent of surgery for early breast cancer on local recurrence and 15-year survival: an overview of the randomised trials. *Lancet* **2005**, *366*, 2087–2106.

(31) Beatson, G. T. On the treatment of inoperable cases of carcinoma of the mamma: suggestions for a new method of treatment, with illustrative cases. *Lancet* **1896,** *2*, 104–107.

(32) Huggins, C.; Hodges, C. V. Studies on Prostatic Cancer. I. The Effect of Castration, of Estrogen and of Androgen Injection on Serum Phosphatases in Metastatic Carcinoma of the Prostate. *Cancer Res.* **1941**, *1*, 293–297.

(33) Osborne, C. K.; Boldt, D. H.; Clark, G. M.; Trent, J. M. Effects of Tamoxifen on Human Breast Cancer Cell Cycle Kinetics: Accumulation of Cells in Early G1 Phase. *Cancer Res.* **1983**, *43*, 3583–3585.

(34) Brodie, A. M. H.; Wing, L.-Y.; Goss, P.; Dowsett, M.; Coombes, R. C. Aromatase inhibitors and the treatment of breast cancer. *J Steroid Biochem.* **1986**, *24*, 91–97.

(35) Klotz, L.; Boccon-Gibod, L.; Shore, N. D.; Andreou, C.; Persson, B.-E.; Cantor, P.; Jensen, J.-K.; Olesen, T. K.; Schröder, F. H. The efficacy and safety of degarelix: a 12-month, comparative, randomized, open-label, parallel-group phase III study in patients with prostate cancer. *BJU International* **2008**, *102*, 1531–1538.

(36) Dowsett, M. Overexpression of HER-2 as a resistance mechanism to hormonal therapy for breast cancer. *Endocrine-Related Cancer* **2001**, *8*, 191–195.

(37) Saunders, W.; Castro, J. R.; Chen, G. T. Y.; Collier, J. M.; Zink, S. R.; Pitluck, S.; Phillips, T. L.; Char, D.; Gutin, P.; Gauger, G.; Tobias, C. A.; Alpen, E. L. Helium-Ion Radiation Therapy at the Lawrence Berkeley Laboratory: Recent Results of a Northern California Oncology Group Clinical Trial. *Radiation Res.* **1985**, *104*, 227–234.

(38) Hindo, W. A.; DeTrana III, F. A.; Lee, M.-S.; Hendrickson, F. R. Large dose increment irradiation in treatment of cerebral metastases. *Cancer* **1970**, *26*, 138–141.

(39) Rusthoven, K. E.; Kavanagh, B. D.; Cardenes, H.; Stieber, V. W.; Burri, S. H.; Feigenberg, S. J.; Chidel, M. A.; Pugh, T. J.; Franklin, W.; Kane, M.; Gaspar, L. E.; Schefter, T. E. Multi-Institutional Phase I/II Trial of Stereotactic Body Radiation Therapy for Liver Metastases. *J. Clin. Oncol.* **2009**, *27*, 1572–1578.

(40) Rusthoven, K. E.; Kavanagh, B. D.; Burri, S. H.; Chen, C.; Cardenes, H.; Chidel, M. A.; Pugh, T. J.; Kane, M.; Gaspar, L. E.; Schefter, T. E. Multi-Institutional Phase I/II Trial of Stereotactic Body Radiation Therapy for Lung Metastases. *J. Clin. Oncol.* **2009**, *27*, 1579–1584.

(41) Seyedin, S. N.; Schoenhals, J. E.; Lee, D. A.; Cortez, M. A.; Wang, X.; Niknam, S.; Tang, C.; Hong, D. S.; Naing, A.; Sharma, P.; Allison, J. P.; Chang, J. Y.; Gomez, D. R.; Heymach, J. V.; Komaki, R. U.; Cooper, L. J.; Welsh, J. W. Strategies for combining immunotherapy with radiation for anticancer therapy. *Immunotherapy* **2015**, *7*, 967–980.

(42) Wang, Y.; Deng, W.; Li, N.; Neri, S.; Sharma, A.; Jiang, W.; Lin, S. H. Combining Immunotherapy and Radiotherapy for Cancer Treatment: Current Challenges and Future Directions. *Front. Pharmacol.* **2018**, *9*, 1–11.

(43) Ross, J. S.; Gray, K.; Gray, G. S.; Worland, P. J.; Rolfe, M. Anticancer Antibodies. *Am. J. Clin. Pathol.* **2003**, *119*, 472–485.

(44) Xin, G.; Schauder, D. M.; Zander, R.; Cui, W. Two is better than one: advances in pathogen-boosted immunotherapy and adoptive T-cell therapy. *Immunotherapy* **2017**, *9*, 837–849.

(45) Andersen, M. H. Immune Regulation by Self-Recognition: Novel Possibilities for Anticancer Immunotherapy. *JNCI J. Natl. Cancer Inst.* **2015**, *107*, djv154.

(46) Slamon, D. J.; Leyland-Jones, B.; Shak, S.; Fuchs, H.; Paton, V.; Bajamonde, A.; Fleming, T.; Eiermann, W.; Wolter, J.; Pegram, M.; Baselga, J.; Norton, L. Use of the chemotherapy plus a monoclonal antibody against HER2 for metastatic breast cancer that overexpress HER2. *N. Engl. J. Med.* **2001**, *344*, 783–792.

(47) Sawyers, C. Targeted cancer therapy. *Nature* **2004**, *432*, 294–297.

(48) Farber, S.; Diamond, L. K.; Mercer, R. D.; Sylvester, R. F.; Wolff, J. Temporary remissions in acute leukemia in children produced by folic acid antagonist, 4-aminopteroyl-glutamic acid (aminopterin). *New Engl. J. Med.* **1948**, *238*, 787–793.

(49) Li, M. C.; Hertz, R.; Spencer, D. B. Effect of Methotrexate Therapy upon Choriocarcinoma and Chorioadenoma. *Soc. Exp. Biol. Med.* **1956**, *93*, 361–366.

(50) Yaish, P.; Gazit, A.; Gilon, C.; Levitzki, A. Blocking of EGF-dependent cell proliferation by EGF receptor kinase inhibitors. *Science* **1988**, *242*, 933–935.

(51) Tsimberidou, A.-M.; Alvarado, Y.; Giles, F. J. Evolving role of ribonucleoside reductase inhibitors in hematologic malignancies. *Exp. Rev. Anticancer Ther.* **2002**, *2*, 437–448.

(52) D´yakonov, V. A.; Dzhemileva, L. U.; Dzhemilev, U. M. Advances in the Chemistry of Natural and Semisynthetic Topoisomerase I/II Inhibitors. *Studies Natur. Prod. Chem.* **2017**, *54*, 21–86.

(53) Den, R. B.; Lu, B. Heat shock protein 90 inhibition: rationale and clinical potential. *Adv. Med. Oncol.* **2012**, *4*, 211–218.

(54) Lind, M. J. Principles of cytotoxic chemotherapy. *Medicine* **2007**, *36*, 19–23.

(55) Rosenberg, B.; van Camp, L.; Krigas, T. Inhibition of Cell Division in *Escherichia coli* by Electrolysis Products from a Platinum Electrode. *Nature* **1965,** *205,* 698.

(56) Rosenberg, B.; van Camp, L.; Trosko, J. E.; Mansour, V. H. Platinum Compounds: a New Class of Potent Antitumor Agents. *Nature* **1969,** *222,* 385–387.

(57) El Khateeb, M.; Appleton, T. G.; Gahan, L. R.; Charles, B. G.; Bernes-Price, S. J.; Bolton, A. M. Reactions of cisplatin hydrolytes with methionine, cysteine, and plasma ultrafiltrate studied by a combination of HPLC and NMR techniques. *J. Inorg. Biochem.* **1999**, *77*, 13–21.

(58) Siddik, Z. H. Cisplatin: mode of cytotoxic action and molecular basis of resistance. *Oncogene* **2003**, *22*, 7265–7279.

(59) Rybak, L. P.; Whitworth, C. A.; Mukherjea, D.; Ramkumar, V. Mechanisms of cisplatin-induced ototoxicity and prevention. *Hearing Res.* **2007**, *226*, 157–167.

(60) O'Dwyer, P. J.; Stevenson, J. P.; Johnson, S. W. Clinical Pharmacokinetics and Administration of Established Platinum Drugs. *Drugs* **2000**, *59*, 19–27.

(61) Sykes, A. G. Advances in Inorganic Chemistry: Volume 49.

(62) Ali, I.; Wani, W. A.; Saleem, K.; Haque, A. Platinum Compounds: A Hope for Future Cancer Chemotherapy. *Anti-Cancer Agents in Med. Chem.* **2013**, *13*, 296–306.

(63) Armand, J. P.; Bolgie, V.; Raymond, E.; Fizazi, K.; Faivre, S.; Ducreux, M. Oxaliplatin in colorectal cancer: an overview. *Semin. Oncol*. **2000**, *27*, 96–104.

(64) Gietema, J. A.; Veldhuis, G. J.; Guchelaar, H. J.; Willemse, P. H. B.; Uges, D. R. A.; Cats, A.; Boonstra, H.; van der Graaf, W. T. A.; Sleijfer, D. T.; Devries, E. G. E.; Mulder, N. H. Phase II and pharmacokinetic study of lobaplatin in patients with relapsed ovarian cancer. *Br. J. Cancer* **1995**, *71*, 1302–1307.

(65) Choy, H.; Park, C.; Yao, M. Current Status and Future Prospects for Satraplatin, an Oral Platinum Analogue. *Clin. Cancer Res.* **2008**, *14*, 1633–1638.

(66) Wheate, N. J.; Walker, S.; Craig, G. E.; Oun, R. The status of platinum anticancer drugs in the clinic and in clinical trials. *Dalton Trans.* **2010**, *39*, 8113–8127.

(67) Casini, A.; Hartinger, C.; Gabbiani, C.; Mini, E.; Dyson, P. J.; Keppler, B. K.; Messori, L. Gold(III) compounds as anticancer agents: Relevance of gold–protein interactions for their mechanism of action. *J. Inorg. Biochem.* **2008**, *102*, 564–575.

(68) Berners-Price, S. J.; Bowen, R. J.; Galettis, P.; Healy, P. C.; McKeage, M. J. Structural and solution chemistry of gold(I) and silver(I) complexes of bidentate pyridyl phosphines: selective antitumour agents. *Coord. Chem. Rev.* **1999**, *185–186*, 823–836.

(69) Buckley, R. G.; Elsome, A. M.; Fricker, S. P.; Henderson, G. R.; Theobald, B. R. C.; Parish, R. V.; Howe, B. P.; Kelland, L. R. Antitumor Properties of Some 2-[(Dimethylamino)methyl]phenylgold(III) Complexes. *J. Med. Chem.* **1996**, *39*, 5208–5214.

(70) Parish, R. V.; Howe, B. P.; Wright, J. P.; Mack, J.; Pritchard, R. G.; Buckley, R. G.; Elsome, A. M.; Fricker, S. P. Chemical and Biological Studies of Dichloro(2-((dimethylamino)methyl)phenyl)gold(III). *Inorg. Chem.* **1996**, *35*, 1659–1666.

(71) Nobili, S.; Mini, E.; Landini, I.; Gabbiani, C.; Casini, A.; Messori, L. Gold Compounds as AnticancerAgents: Chemistry, Cellular Pharmacology, and Preclinical Studies. *Med. Res. Rev.* **2010**, *30*, 550–580.

(72) Wenzel, M.; Bertrand, B.; Eymin, M.-J.; Comte, V.; Harvey, J. A.; Richard, P.; Groessl, M.; Zava, O.; Amrouche, H.; Harvey, P. D.; Le Gendre, P.; Picquet, M.; Casini, A. Multinuclear Cytotoxic Metallodrugs: Physicochemical Characterization and Biological Properties of Novel Heteronuclear Gold–Titanium Complexes. *Inorg. Chem.* **2011**, *50*, 9472–9480.

(73) Köpf, H.; Köpf-Maier, P. Titanocene Dichloride – The First Metallocene with Cancerostatic Activity. *Angew. Chem.* **1979**, *91*, 509–512.

(74) Lümmen, G.; Sperling, H.; Luboldt, H.; Otto, T.; Rübben, H. Phase II trial of titanocene dichloride in advanced renal-cell carcinoma. *Cancer Chemother. Pharmacol.* **1998**, *42*, 415–417.

(75) Strohfeldt, K.; Tacke, M. Bioorganometallic fulvene-derived titanocene anti-cancer drugs. *Chem. Soc. Rev.* **2008**, *37*, 1174–1187.

(76) Harding, M. M.; Moksdi, G. Antitumour Metallocenes: Structure-Activity Studies and Interactions with Biomolecules. *Curr. Med. Chem.* **2000**, *7*, 1289–1303.

(77) González-Pantoja, J. F.; Stern, M.; Jarzecki, A. A.; Royo, E.; Robles-Escajeda, E.; Varela-Ramírez, A.; Aguilera, R. G.; Contel, M. Titanocene–Phosphine Derivatives as Precursors to Cytotoxic Heterometallic TiAu2 and TiM (M = Pd, Pt) Compounds. Studies of Their Interactions with DNA. *Inorg. Chem.* **2011**, *50*, 11099–11110.

(78) Yang, P.; Guo, M. Interactions of organometallic anticancer agents with nucleotides and DNA. *Coord. Chem. Rev.* **1999**, *185–186*, 189–211.

(79) Kadish, K. M.; Das, K.; Howard, R.; Dennis, A.; Bear, J. L. Redox Reactions and Antitumor Activity of Tetra-μ-Carboxylatdirhodium(II). *Bioelectrochem. Bioenergetics* **1978**, *5*, 741–753.

(80) Vol´pin, M.; Levitin, I.; Osinsky, S. New Course in the Search for Antitumor Agents: The Use of pH-Dependent Sources of Reactive Radicals. *Angew. Chem. Ind. Ed. Engl.* **1996**, *35*, 2395–2396.

(81) Chen, G.-Q.; Shi, X.-G.; Tang, W.; Xiong, S.-M.; Zhu, J.; Cai, X.; Han, Z.-G.; Ni, J.-H.; Shi, G.-Y.; Jia, P.-M.; Liu, M.-M.; He, K.-L.; Niu, C.; Ma, J.; Zhang, P.; Zhang, T.-G.; Paul, P.; Naoe, T.; Kitamura, K.; Miller, W.; Waxman, S.; Wang, Z.-Y. de The, H.; Chen, S.-J. Chen, Z. Use of Arsenic Trioxide (As2O3) in the Treatment of Acute Promyelocytic Leukemia (APL): I. As2O3 Exerts Dose-Dependent Dual Effects on APL Cells. *Blood* **1997**, *89*, 3345–3353.

(82) Shen, Z.-X.; Chen, G.-Q.; Ni, J.-H.; Li, X.-S.; Xiong, S.-M.; Qiu, Q.-Y.; Zhu, J.; Tang, W.; Sun, G.-L.; Yang, K.-Q.; Chen, Y.; Zhou, L.; Fang, Z.-W.; Wang, Y.-T.; Ma, J.; Zhang, P.; Zhang, T. D.; Chen, S.-J.; Chen, Z.; Wang, Z.-Y. Use of Arsenic Trioxide (As2O3) in the Treatment of Acute Promyelocytic Leukemia (APL): II. Clinical Efficacy and Pharmacokinetics in Relapsed Patients. *Blood* **1997**, *89*, 3354–3360.

(83) Gielen, M.; Bouhdid, A.; Kayser, F.; Biesemans, M.; de Vos, D.; Mahieu, B.; Willem, R. Di(n-butyl)tin Bis(dihydroxybenzoate)s: Synthesis, Spectroscopic Characterization and *in vitro* Antiturnour Activity. *Appl. Organomet. Chem.* **1995**, *9*, 251–257.

(84) Collery, P.; Domingo, J. L.; Keppler, B. K. Preclinical toxicology and tissue gallium distribution of a novel antitumour gallium compound: Tris (8-quinolinolato) gallium (III). *Anticancer Res.* **1996**, *16*, 687–692.

(85) Tisato, F.; Marzano, C.; Porchia, M.; Pellei, M.; Santini, C. Copper in Diseases and Treatments, and Copper-Based Anticancer Strategies. *Med. Res. Rev.* **2010**, *30*, 708–749.

(86) Puig, S.; Thiele, D. J. Molecular mechanisms of copper uptake and distribution. *Curr. Opin. Chem. Biol.* **2002**, *6*, 171–180.

(87) Sîrbu, A.; Palamarciuc, O.; Babak, M. V.; Lim, J. M.; Ohui, K.; Enyedy, É. A.; Shova, S.; Darvasiová, D.; Rapta, P.; Ang, W. H.; Arion, V. B. Copper(II) thiosemicarbazone complexes induce marked ROS accumulation and promote nrf2-mediated antioxidant response in highly resistant breast cancer cells. *Dalton Trans.* **2017**, *46*, 3833–3847.

(88) Nishida, N.; Yano, H.; Nishida, T.; Kamura, T.; Kojiro, M. Angiogenesis in Cancer. *Vasc. Health Risk Manag.* **2006**, *2*, 213–219.

(89) Yoshii, J.; Yoshiji, H.; Kurinama, S.; Ikenaka, Y.; Noguchi, R.; Okuda, H.; Tsujinoue, H.; Nakatani, T.; Kishida, H.; Nakae, D.; Gomez, D. E.; De Lorenzo, M. S.; Tejera, A. M.; Fukui, H. The copper-chelating agent, trientine, suppresses tumor development and angiogenesis in the murine hepatocellular carcinoma cells. *Int. J. Cancer* **2001**, *94*, 768–773.

(90) Crim, J. A.; Petering, H. G. The Antitumor Activity of Cu(II)KTS, the Copper(II) Chelate of 3-Ethoxy-2-oxobutyraldehyde Bis(thiosemicarbazone). *Cancer Res.* **1967**, *27*, 1278–1285.

(91) Ohui, K.; Afanasenko, E.; Bacher, F.; Lin Xue Ting, R.; Zafar, A.; Blanco-Cabra, N.; Torrents, E.; Dömötör, O.; May, N. V.; Darvasiova, D.; Enyedy, É. A.; Popović-Bijelić, A.; Reynisson, J.; Rapta, P.; Babak, M. V.; Pastorin, G.; Arion, V. B. New Water-Soluble Copper(II) Complexes with Morpholine-Thiosemicarbazone Hybrids: Insights into the Anticancer and Antibacterial Mode of Action. *J. Med. Chem.* **2019**, *62*, 512–530.

(92) Finch, R. A.; Liu, M.-C.; Cory, A. H.; Cory, J. G.; Sartorelli, A. C. Triapine (3-aminopyridine-2-carboxaldehyde thiosemicarbazone; 3-AP): an inhibitor of ribonucleotide reductase with antineoplastic activity. *Advan. Enzyme Regul.* **1999**, *39*, 3–12.

(93) Bacher, F.; Dömötör, O.; Chugunova, A.; Nagy, N. V.; Filipović, L.; Radulović, S.; Enyedy, É. A.; Arion, V. B. Strong effect of copper(II) coordination on antiproliferative activity of thiosemicarbazone–piperazine and thiosemicarbazone–morpholine hybrids. *Dalton Trans.* **2015**, *44*, 9071–9090.

(94) Sigman, D. S.; Graham, D. R.; D'Aurora, V.; Stern, A. M. Oxygen-dependent Cleavage of DNA by the 1,10-Phenanthroline · Cuprous Complex. *J. Biol. Chem.* **1979**, *24*, 12269–12272.

(95) Zhou, H.; Zheng, C.; Zou, G.; Tao, D.; Gong, J. G1-phase specific apoptosis in liver carcinoma cell line induced by copper-1,10-phenanthroline. *Int. J. Biochem. Cell Biol.* **2002**, *34*, 678–684.

(96) Veal, J. M.; Rill, R. L. Noncovalent DNA binding of bis(1,10-phenanthroline)copper(I) and related compounds. *Biochemistry* **1991**, *30*, 1132–1140.

(97) Pitie, M.; Donnadieu, B.; Meunier, B. Preparation of the new bis(phenanthroline) ligand "Clip-Phen" and valuation of the nuclease activity of the corresponding copper complex. *Inorg. Chem.* **1998**, *37*, 3486–3489.

(98) Pitie, M.; Boldron, C.; Gornitzka, H.; Hemmert, C.; Donnadieu, B.; Meunier, B. DNA cleavage by copper complexes of 2- and 3-Clip-Phen derivatives. *Eur. J. Inorg. Chem.* **2003**, 528–540.

(99) Deegan, C.; McCann, M.; Devereux, M.; Coyle, B.; Egan, D. A. In vitro cancer chemotherapeutic activity of 1,10-phenanthroline (phen), [Ag2(phen)3(mal)] 2H2O, [Cu(phen)2(mal)] 2H2O and [Mn(phen)2(mal)] 2H2O (malH2 = malonic acid) using human cancer cells. *Cancer Lett.* **2007**, *247*, 224–233.

(100) Saczewski, F.; Dziemidowicz-Borys, E.; Bednarski, P. J.; Gruenert, R.; Gdaniec, M.; Tabin, P. Synthesis, crystal structure and biological activities of copper(II) complexes with chelating bidentate 2-substituted benzimidazole ligands. *J. Inorg. Biochem.* **2006**, *100*, 1389–1398.

(101) Dallavalle, F.; Gaccioli, F.; Franchi-Gazzola, R.; Lanfranchi, M.; Marchio, L.; Pellinghelli, M A.; Tegoni, M. Synthesis, molecular structure, solution equilibrium, and antiproliferative activity of thioxotriazoline and thioxotriazole complexes of copper(II) and palladium(II). *J. Inorg. Biochem.* **2002**, *92*, 95–104.

(102) Tardito, S.; Bussolati, O.; Maffini, M.; Tegoni, M.; Giannetto, M.; Dall'Asta, V.; Franchi-Gazzola, R.; Lanfranchi, M.; Pellinghelli, M. A.; Mucchino, C.; Mori, G.; Marchio, L. Thio-amido coordination in a thioxo-1,2,4-triazole copper(II) complex enhances non-apoptotic programmed cell death associated with copper accumulation and oxidative stress in human cancer cells. *J. Med. Chem.* **2007**, *50*, 1916–1924.

(103) Tardito, S.; Bussolati, O.; Gaccioli, F.; Gatti, R.; Guizzardi, S.; Uggeri, J.; Marchio, L.; Lanfranchi, M.; Franchi-Gazzola, R. Non-apoptotic programmed cell death induced by a copper(II) complex in human fibrosarcoma cells. *Histochem. Cell Biol.* **2006**, *126*, 473–482.

(104) Adsule, S.; Barve, V.; Chen, D.; Ahmed, F.; Dou, Q. P.; Padhye, S.; Sarkar, F. H. Novel Schiff base copper complexes of quinoline-2 carboxaldehyde as proteasome inhibitors in human prostate cancer cells. *J. Med. Chem.* **2006**, *49*, 7242–7246.

(105) Filomeni, G.; Cerchiaro, G.; Da Costa Ferreira, A. M.; De Martino, A.; Pedersen, J. Z.; Rotilio, G.; Ciriolo, M. R. Pro-apoptotic activity of novel isatin-Schiff base copper(II) complexes depends on oxidative stress induction and organelle-selective damage. *J. Biol. Chem.* **2007**, *282*, 12010–12021.

(106) Kostova, I. Ruthenium Complexes as Anticancer Agents. *Curr. Med. Chem.* **2006**, *13*, 1085–1107.

(107) de Oliveira Silva, D. Perspectives for Novel Mixed Diruthenium-Organic Drugs as Metallopharmaceuticals in Cancer Therapy. *Anti-Cancer Agents Med. Chem.* **2010**, *10*, 312–323.

(108) Clarke, M. J. Oncological implication of the chemistry of ruthenium. *Met. Ions Biol. Syst.* **1980**, *11*, 231–283.

(109) Keppler, B. K.; Henn, M.; Juhl, U. M.; Berger, M. R.; Niebl, R.; Wagner, F. E. New Ruthenium Complexes for the Treatment of Cancer. *Clin. Biochem. Med.* **1989**, *10*, 41–69.

(110) Hartinger, C. G.; Jakupec, M. A.; Zorbas-Seifried, S.; Groessl, M.; Egger, A.; Berger, W.; Zorbas, H.; Dyson, P. J.; Keppler, B. K. KP1019, A New Redox-Active Anticancer Agent – Preclinical Development and Results of a Clinical Phase I Study in Tumor Patients. *Chem. Biodiversity* **2008**, *5*, 2140–2155.

(111) Lentz, F.; Drescher, A.; Lindauer, A.; Henke, M.; Hilger, R. A.; Hartinger, C. G.; Scheulen, M. E.; Dittrich, C.; Keppler, B. K.; Jaehde, U. Pharmacokinetics of a novel anticancer ruthenium complex (KP1019, FFC14A) in a phase I dose-escalation study. *Anti-Cancer Drugs* **2009**, *20*, 97–103.

(112) Trondl, R.; Heffeter, P.; Kowol, C. R.; Jakupec, M. A.; Berger, W.; Keppler, B. K. NKP-1339, the first ruthenium-based anticancer drug on the edge to clinical application. *Chem. Sci.* **2014**, *5*, 2925–2932.

(113) https://clinicaltrials.gov/ct2/show/NCT01415297?term=NKP-1339&rank=1

(114) Sava, G.; Capozzi, I.; Clerici, K.; Gagliardi, G.; Alessio, E.; Mestroni, G. Pharmacological control of lung metastases of solid tumours by a novel ruthenium complex. *Clin. Exp. Metastasis* **1998**, *16*, 371–379.

(115) Dyson, P. J.; Sava, G. Metal-based antitumour drugs in the post genomic era. *Dalton Trans.* **2006**, *16*, 1929–1933.

(116) Morris, R. E.; Aird, R. E.; del Socorro Murdoch, P.; Chen, H.; Cummings, J.; Hughes, N. D.; Parsons, S.; Parkin, A.; Boyd, G.; Jodrell, D. I.; Sadler, P. J. Inhibition of Cancer Cell Growth by Ruthenium(II) Arene Complexes. *J. Med. Chem.* **2001,** *44*, 3616–3621.

(117) Dyson, P. J. Systematic Design of a Targeted Organometallic Antitumour Drug in Pre-clinical Development. *Chimia* **2007**, *61*, 698–703.

(118) Zhang, C. X.; Lippard, S. J. New metal complexes as potential therapeutics. *Curr. Opin. Chem. Biol.* **2003**, *7*, 481–489.

(119) Bergamo, A.; Gaiddon, C.; Schellens, J. H. M.; Beijnen, J. H.; Sava, G. Approaching tumour therapy beyond platinum drugs Status of the art and perspectives of ruthenium drug candidates. *J. Inorg. Biochem.* **2012**, *106*, 90–99.

(120) Hanif, M.; Henke, H.; Meier, S. M.; Martic, S.; Labib, M.; Kandioller, W.; Jakupec, M. A.; Arion, V. B.; Kraatz, H.-B.; Keppler, B. K.; Hartinger, C. G. Is the Reactivity of M(II)-Arene Complexes of 3-Hydroxy-2(1H)-pyridones to Biomolecules the Anticancer Activity Determining Parameter? *Inorg. Chem.* **2010**, *49*, 7953–7963.

(121) Babak, M. V.; Ang, W. H. Multinuclear organometallic ruthenium arene complexes for cancer therapy. *MILS*, **2018**, *18*, 171–198.

(122) Lopes, J.; Alves, D.; Morais, T. S.; Costa, P. J.; Piedade, M. F. M.; Marques, F.; Villa de Brito, M. J.; Garcia, M. H. New copper(I) and heteronuclear copper(I)–ruthenium(II) complexes: Synthesis, structural characterization and cytotoxicity. *J. Inorg. Biochem.* **2017**, *169*, 68–78.

(123) van der Steen, S.; de Hoog, P.; van der Schilden, K.; Gamez, P.; Pitié, M.; Kiss, R.; Reedijk, J. Novel heteronuclear ruthenium–copper coordination compounds as efficient DNA-cleaving agents. *Chem. Commun.* **2010**, *46*, 3568–3570.

(124) Tan, K. W.; Seng, H. L.; Lim, F. S.; Cheah, S.-C.; Ng, C. H.; Koo, K. S.; Mustafa, M. R.; Ng, S. W.; Maah, M. J. Towards a selective cytotoxic agent for prostate cancer: Interaction of zinc complexes of polyhydroxybenzaldehyde thiosemicarbazones with topoisomerase I. *Polyhedron* **2012**, *38*, 275–284.

(125) de Oliveira, J. F.; Lima, T. S.; Vendramini-Costa, D. B.; Batista de Lacerda Pedrosa, S. C.; Lafayette, E. A.; Ferreira da Silva, R. M.; Vitalino de Almeida, S. M.; Olímpio de Moura, R.; Tasca Gois Ruiz, A. L.; de Carvalho, J. E.; do Carmo Alves de Lima, M. Thiosemicarbazones and 4-thiazolidinones indole-based derivatives: Synthesis, evaluation of antiproliferative activity, cell death mechanisms and topoisomerase inhibition assay. *Eur. J. Med. Chem.* **2017**, *136*, 305–314.

(126) Kowol, C. R.; Heffeter, P.; Miklos, W.; Gille, L.; Trondl, R.; Cappellacci, L.; Berger, W.; Keppler, B. K. Mechanisms underlying reductant-induced reactive oxygen species formation by anticancer copper(II) compounds. *J. Inorg. Biol. Chem.* **2012**, *17*, 409–423.

(127) Shipman Jr., C.; Smith, S. H.; Drach, J. C.; Klayman, D. L. Antiviral Activity of 2-Acetylpyridine Thiosemicarbazones Against Herpes Simplex Virus. *Antimicrobial Agents and Chemotherapy* **1981**, *19*, 682–685.

(128) Pervez, H.; Iqbal, M. S.; Tahir, M. Y.; Nasim, F.; Choudhary, M. I.; Khan, K. M. *In vitro* cytotoxic, antibacterial, antifungal and urease inhibitory activities of some N4-substituted isatin-3-thiosemicarbazones. *J. Enzym. Inhib. Med. Chem.* **2008**, *23*, 848–854.

(129) Domagk, G.; Behnisch, R.; Mietzsch, F.; Schmidt, H. Über eine neue, gegen Tuberkelbacillin *in vitro* wirksame Verbindungsklasse. *Naturwissenschaften* **1946**, *33*, 315.

(130) Brockman, R. W.; Thompson, J. R.; Bell, M. J.; Skipper, H. E. Observations on the Antileukemic Activity of Pyridine-2-carboxaldehyde Thiosemicarbazone and Thiocarbohydrazone. *Cancer Res.* **1956**, *16*, 167–170.

(131) French, F. A.; Blanz, E. J. The Carcinostatic Activity of α-(*N*) Heterocyclic Carboxaldehyde Thiosemicarbazones. I. Isoquinoline-1-carboxaldehyde Thiosemicarbazone. *Cancer Res.* **1965**, *25*, 1454–1458.

(132) French, F. A.; Blanz, E. J. The Carcinostatic Activity of α-(*N*)-Heterocyclic Carboxaldehyde Thiosemicarbazones. II. 3-Hydroxypyridine-2-carboxaldehyde Thiosemicarbazone. *Cancer Res.* **1966**, *26*, 1638–1640.

(133) French, F. A.; Blanz, E. J. The Carcinostatic Activity of Thiosemicarbazones of Formyl Heteroaromatic Compounds. III. Primary Correlation. *J. Med. Chem.* **1966**, *9*, 585–589.

(134) DeConti, R. C.; Toftness, B. R.; Agrawal, K. C.; Tomchick, R.; Mead, J. A. R.; Berlino, J. R.; Sartorelli, A. C.; Creasey, W. A. Clinical and Pharmacological Studies with 5-Hydroxy-2-formylpyridine Thiosemicarbazone. *Cancer Res.* **1972**, *32*, 1455–1462.

(135) Blanz, E. J.; French, F. A. The Carcinostatic Activity of 5-Hydroxy-2-formylpyridine Thiosemicarbazone. *Cancer Res.* **1968**, *28*, 2419–2422.

(136) Booth, B. A.; Moore, E. C.; Sartorelli, A. C. Metabolic Effects of Some Tumor-inhibitory Pyridine Carboxaldehyde Thiosemicarbazones. *Cancer Res.* **1971**, *31*, 228–234.

(137) Moore, E. C.; Booth, B. A.; Sartorelli, A. C. Inhibition of Deoxyribonucleotide Synthesis by Pyridine Carboxaldehyde Thiosemicarbazones. *Cancer Res.* **1971**, *31*, 235–238.

(138) Sartorelli, A. C.; Agrawal, K. C.; Moore, E. C. Mechanism of Inhibition of Ribonucleoside Diphosphate Reductase by α-(*N*)-Heterocyclic Aldehyde Thiosemicarbazones. *Biochem. Pharmacol.* **1971**, *20*, 3119–3123.

(139) Elledge, S. J.; Zhou, Z.; Allen, J. B. Ribonucleotide reductase: regulation, regulation, regulation. *Trends Biochem. Sci.* **1992**, *17*, 119–123.

(140) Kolberg, M.; Strand, K. R.; Graff, P.; Andersson, K. K. Structure, function, and mechanism of ribonucleotide reductases. *Biochim. Biophys. Acta* **2004**, *1699*, 1–34.

(141) Uhlin, U.; Eklund, K. Structure of ribonucleotide reductase protein R1. *Nature* **1994**, *370*, 533–539.

(142) Larsson, Å.; Sjöberg, B.-M. Identification of the stable free radical tyrosine residue in ribonucleotide reductase. *EMBO* **1986**, *5*, 2037–2040.

(143) Elford, H. L.; Freese, M.; Passamani, E.; Morris, H, P. Ribonucleotide reductase and cell proliferation. 1. Variations of ribonucleotide reductase activity with tumor growth in a series of rat hepatomas. *J. Biol. Chem.* **1970**, *245*, 5228–5233.

(144) Finch, R. A.; Liu, M.-C.; Grill, S. P.; Rose, W. C.; Loomis, R.; Vasquez, K. M.; Cheng, Y.-C.; Sartorelli, A. C. Triapine (3-Aminopyridine-2-carboxaldehyde-thiosemicarbazone): A Potent Inhibitor of Ribonucleotide Reductase Activity with Broad Spectrum Antitumor Activity. *Biochem. Pharmacol.* **2000**, *59*, 983–991.

(145) Liebelt, E. L.; Balk, S. J.; Faber, W.; Fisher, J. W.; Hughes, C. L.; Lanzkron, S. M.; Lewis, K. M.; Marchetti, F.; Mehendale, H. M.; Rogers, J. M.; Shad, A. T.; Skalko, R. J.; Stanek, E. J. NTP-CERHR Expert Panel Report on the Reproductive and Developmental Toxicity of Hydroxyurea. *Birth Defects Res. Part B* **2007**, *80*, 259–366.

(146) Liu, M-.C.; Lin, T.-S.; Sartorelli, A. C. Synthesis and Antitumor Activity of Amino Derivatives of Pyridine-2- carboxaldehyde Thiosemicarbazone. *J. Med. Chem.* **1992**, *35*, 3672–3677.

(147) Murren, J.; Modiano, M.; Clairmont, C.; Lambert, P.; Savaraj, N.; Doyle, T.; Sznol, M. Phase I and Pharmacokinetic Study of Triapine, a Potent Ribonucleotide Reductase Inhibitor, Administered Daily for Five Days in Patients with Advanced Solid Tumors. *Clin. Cancer Res.* **2003**, *9*, 4092–4100.

(148) Zeidner, J. F.; Karp, J. E.; Blackford, A. L.; Smith, B. D.; Gojo, I.; Gore, S. D.; Levis, M. J.; Carraway, H. E.; Greer, J. M.; Ivy, S. P.; Pratz, K. W.; McDevitt, M. A. A phase II trial of sequential ribonucleotide reductase inhibition in aggressive myeloproliferative neoplasms. *Haematologica* **2014**, *99*, 672–678.

(149) Nutting, C. M.; van Herpen, C. M. L.; Miah, A. B.; Bhide, S. A.; Machiels, J.-P.; Buter, J.; Kelly, C.; de Raucourt, D.; Harrington, K. J. Phase II study of 3-AP Triapine in patients with recurrent or metastatic head and neck squamous cell carcinoma. *Annals of Oncol.* **2009**, *20*, 1275–1279.

(150) Kunos, C. A.; Chu, E.; Beumer, J. H.; Sznol, M.;·Ivy, S. P. Phase I trial of daily triapine in combination with cisplatin chemotherapy for advanced‑stage malignancies. *Cancer Chemother. Pharmacol.* **2017**, *79*, 201–207.

(151) Kunos, C. A.; Chu, E.; Makower, D.; Kaubisch, A.; Sznol, M.; Ivy, S. P. Phase I Trial of Triapine– Cisplatin–Paclitaxel Chemotherapy for advanced Stage or Metastatic Solid Tumor Cancers. *Front. Oncol.* **2017**, *7*, 1–8.

(152) Mortazavi, A.; Ling, Y.; Martin, L. K.; Wei, L.; Phelps, M. A.; Liu, Z.; Harper, E. J.; Ivy, S. P.; Wu, X.; Zhou, B.-S.; Liu, X.; Deam, D.; Monk, J. P.; Hicks, W. J.; Yen, Y.; Otterson, G. A.; Grever, M. R.; Bekaii-Saab, T. A phase I study of prolonged infusion of triapine in combination with fixed dose rate gemcitabine in patients with advanced solid tumors. *Invest. New Drugs* **2013**, *31*, 685–695.

(153) Choi, B. S.; Alberti, D. B.; Schelman, W. R.; Kolesar, J. M.; Thomas, J. P.; Marnocha, R.; Eickhoff, J. C.; Ivy, S. P.; Wilding, G.; Holen, K. D. The maximum tolerated dose and biologic effects of 3-aminopyridine-2-carboxaldehyde thiosemicarbazone (3-AP) in combination with irinotecan for patients with refractory solid tumors. *Cancer Chemother. Pharmacol.* **2010**, *66*, 973–980.

(154) Schelman, W. R.; Morgan-Meadows, S.; Marnocha, R.; Lee, F.; Eickhoff, J.; Huang, W.; Pomplun, M.; Jiang, Z.; Albert, D.; Kolesar, J. M.; Ivy, P.; Wilding, G.; Traynor, A. A phase I study of Triapine in combination with doxorubicin in patients with advanced solid tumors. *Cancer Chemother. Pharmacol.* **2009** *63*, 1147–1156.

(155) Knox, J. J.; Hotte, S. J.; Kollmannsberger, C.; Winquist, E.; Fisher, B.; Eisenhauer, E. A. Phase II study of Triapine® in patients with metastatic renal cell carcinoma: a trial of the National Cancer Institute of Canada Clinical Trials Group (NCIC IND.161). *Invest. New Drugs* **2007**, *25*, 471–477.

(156) Attia, S.; Kolesar, J.; Mahoney, M. R.; Pitot, H. C.; Laheru, D.; Heun, J.; Huang, W.; Eickhoff, J.; Erlichman, C.; Holen, K. D. A phase 2 consortium (P2C) trial of 3-aminopyridine-2-carboxaldehyde thiosemicarbazone (3-AP) for advanced adenocarcinoma of the pancreas. *Invest. New Drugs* **2008**, *26*, 369–379.

(157) Chao, J.; Synold, T. W.; Morgan Jr., R. J.; Kunos, C.; Longmate, J.; Lenz, H. J.; Lim, D.; Shibata, S.; Chung, V.; Stoller, R. J.; Belani, C. P.; Gandara, D. R.; McNamara, M.; Gitlitz, B. J.; Lau, D. H.; Ramalingam, S. S.; Davies, A.; Espinoza-Delgado, I.; Newman, E. M.; Yen, Y. A phase I and pharmacokinetic study of oral 3-aminopyridine-2-carboxaldehyde thiosemicarbazone (3-AP, NSC #663249) in the treatment of advanced-

stage solid cancers: a California Cancer Consortium Study. *Cancer Chemother. Pharmacol.* **2012**, *69*, 835–843.

(158) Kunos, C. A.; Waggoner, S.; von Gruenigen, V.; Eldermire, E.; Pink, J.; Dowlati, A.; Kinsella, T. J. Phase I Trial of Pelvic Radiation, Weekly Cisplatin, and 3-Aminopyridine-2-Carboxaldehyde Thiosemicarbazone (3-AP, NSC #663249) for Locally Advanced Cervical Cancer. *Clin. Cancer Res.* **2010**, *16*, 1298–1306.

(159) Kunos, C. A.; Ivy, S. P. Triapine Radiochemotherapy in Advanced Stage Cervical Cancer. *Frontiers Oncol.* **2018**, *8*, 1–7.

(160) Barker, C. A.; Burgan, W. E.; Carter, D. J.; Cerna, D.; Gius, D.; Hollingshead, M. G.; Camphausen, K.; Tofilon, P. J. *In vitro* and *In vivo* Radiosensitization Induced by the Ribonucleotide Reductase Inhibitor Triapine (3-Aminopyridine-2-Carboxaldehyde-Thiosemicarbazone). *Clin. Cancer Res.* **2006**, *12*, 2912–2918.

(161) Enyedy, É. A.; Nagy, N. V.; Zsigó, É.; Kowol, C. R.; Arion, V. B.; Keppler, B. K.; Kiss, T. Comparative Solution Equilibrium Study of the Interactions of Copper(II), Iron(II) and Zinc(II) with Triapine (3-Aminopyridine-2-carbaldehyde Thiosemicarbazone) and Related Ligands. *Eur. J. Inorg. Chem.* **2010**, 1717–1728.

(162) Shao, J.; Zhou, B.; Di Bilio, A. J.; Zhu, L.; Wang, T.; Qi, C.; Shih, J.; Yen, Y. A. Ferrous-triapine complex mediates formation of reactive oxygen species that inactivate human ribonucleotide reductase. *Mol. Cancer Ther.* **2006**, *5*, 586–592.

(163) Hayyan, M.; Hashim, M. A.; AlNashef, I. M. Superoxide Ion: Generation and Chemical Implications. *Chem. Rev.* **2016**, *116*, 3029–3085.

(164) Trachootham, D.; Alexandre, J.; Huang, P. Targeting cancer cells by ROS-mediated mechanisms: a radical therapeutic approach? *Nature Rev.* **2009**, *8*, 579–591.

(165) Szatrowski, T. P.; Nathan, C. F. Production of large amounts of hydrogen peroxide by human tumor cells. *Cancer Res.* **1991**, *51*, 794–798.

(166) Fruehauf, J. P.; Meyskens Jr., F. L. Reactive oxygen species: a breath of life or death? *Clin. Cancer Res.* **2007**, *13*, 789–794.

(167) Aye, Y.; Long, M. J. C.; Stubbe, J. Mechanistic Studies of Semicarbazone Triapine Targeting Human Ribonucleotide Reductase *in Vitro* and in Mammalian Cells. *J. Biol. Chem.* **2012**, *287*, 35768–35778.

(168) Yalowich, J. C.; Wu, X.; Zhang, R.; Kanagasabai, R.; Hornbaker, M.; Hasinoff, B. B. The anticancer thiosemicarbazones Dp44mT and triapine lack inhibitory effects as

catalytic inhibitors or poisons of DNA topoisomerase IIα. *Biochem. Pharmacol.* **2012**, *84*, 52–58.

(169) Wadler, S.; Makower, D.; Clairmont, C.; Lambert, P.; Fehn, K.; Sznol, M. Phase I and pharmacokinetic study of the ribonucleotide reductase inhibitor, 3-aminopyridine-2-carboxaldehyde thiosemicarbazone, administered by 96-hour intravenous continuous infusion. *J. Clin. Oncol.* **2004**, *22*, 1553–1563.

(170) Kowol, C. R.; Trondl, R.; Heffeter, P.; Arion, V. B.; Jakupec, M. A.; Roller, A.; Galanski, M.; Berger, W.; Keppler, B. K. Impact of Metal Coordination on Cytotoxicity of 3-Aminopyridine-2-carboxaldehyde Thiosemicarbazone (Triapine) and Novel Insights into Terminal Dimethylation. *J. Med. Chem.* **2009**, *52*, 5032–5043.

(171) Kowol, C. R.; Miklos, W.; Pfaff, S.; Hager, S.; Kallus, S.; Pelivan, K.; Kubanik, M.; Enyedy, É. A.; Berger, W.; Heffeter, P.; Keppler, B. K. Impact of Stepwise NH2-Methylation of Triapine on the Physicochemical Properties, Anticancer Activity, and Resistance Circumvention. *J. Med. Chem.* **2016**, *59*, 6739–6752.

(172) Rejmund, M.; Mrozek-Wilczkiewicz, A.; Malarz, K.; Pyrkosz-Bulska, M.; Gajcy, K.; Sajewicz, M.; Musiol, R.; Polanski, J. Piperazinyl fragment improves anticancer activity of Triapine. *PLoS ONE* **2018**, *13*, e0188767.

(173) Richardson, D. R.; Sharpe, P. C.; Lovejoy, D. B.; Senaratne, D.; Kalinowski, D. S.; Islam, M.; Bernhardt, P. V. Dipyridyl thiosemicarbazone chelators with potent and selective antitumor activity form iron complexes with redox activity. *J. Med. Chem.* **2006**, *49*, 6510−6521.

(174) Whitnall, M.; Howard, J.; Ponka, P.; Richardson, D. R. A class of iron chelators with a wide spectrum of potent antitumor activity that overcomes resistance to chemotherapeutics. *Proc. Natl. Acad. Sci. U. S. A.* **2006**, *103*, 14901−14906.

(175) Lovejoy, D. B.; Sharp, D. M.; Seebacher, N.; Obeidy, P.; Prichard, T.; Stefani, C.; Basha, M. T.; Sharpe, P. C.; Jansson, P. J.; Kalinowski, D. S.; Bernhardt, P. V.; Richardson, D. R. Novel second generation di-2-pyridylketone thiosemicarbazones show synergism with standard chemotherapeutics and demonstrate potent activity against lung cancer xenografts after oral and intravenous administration *in vivo*. *J. Med. Chem*. **2012**, *55*, 7230−7244.

(176) Lovejoy, D. B.; Jansson, P. J.; Brunk, U. T.; Wong, J.; Ponka, P.; Richardson, D. R. Antitumor activity of metal-chelating compound Dp44mT is mediated by formation of a

redox-active copper complex that accumulates in lysosomes. *Cancer Res*. **2011**, *71*, 5871−5880.

(177) Seebacher, N. A.; Richardson, D. R.; Jansson, P. J. A mechanism for overcoming P-glycoprotein-mediated drug resistance: novel combination therapy that releases stored doxorubicin from lysosomes via lysosomal permeabilization using Dp44mT or DpC. *Cell Death and Disease* **2016**, *7*, 1–13.

(178) Sestak, V.; Stariat, J.; Cermanova, J.; Potuckova, E.; Chladek, J.; Roh, J.; Bures, J.; Jansova, H.; Prusa, P.; Sterba, M.; Micuda, S.; Simunek, T.; Kalinowski, D. S.; Richardson, D. R.; Kovarikova, P. Novel and potent anti-tumor and anti-metastatic di-2-pyridylketone thiosemicarbazones demonstrate marked differences in pharmacology between the first and second generation lead agents. *Oncotarget* **2015**, *6*, 42411−42428.

(179) Stacy, A. E.; Palanimuthu, D.; Bernhardt, P. V.; Kalinowski, D. S.; Jansson, P. J.; Richardson, D. R. Zinc(II)−Thiosemicarbazone Complexes Are Localized to the Lysosomal Compartment Where They Transmetallate with Copper Ions to Induce Cytotoxicity. *J. Med. Chem.* **2016**, *59*, 4965–4984.

(180) Guo, Z.-L.; Richardson, D. R.; Kalinowski, D. S.; Kovacevic, Z.; Tan-Un, K. C.; Chan, G. C.-F. The novel thiosemicarbazone, di-2-pyridylketone 4-cyclohexyl-4-methyl-3-thiosemicarbazone (DpC), inhibits neuroblastoma growth in vitro and in vivo via multiple mechanisms. *J. Hematol. Oncol.* **2016**, *9*, 1–16.

(181) Salim, K. Y.; Maleki Vareki, S.; Danter, W. R.; San-Marina, S.; Koropatnick, J. COTI-2, a novel small molecule that is active against multiple human cancer cell lines *in vitro* and *in vivo*. *Oncotarget* **2016**, *7*, 41363–41379.

(182) https://clinicaltrials.gov/ct2/show/NCT02433626

(183) Maleki Vareki, S.; Salim, K. Y.; Danter, W. R.; Koropatnick, J. Novel anti-cancer drug COTI-2 synergizes with therapeutic agents and does not induce resistance or exhibit cross-resistance in human cancer cell lines. *PLoS ONE* **2018**, *13*, e0191766.

(184) Traynor, A. M.; Lee, J.-W.; Bayer, G. K.; Tate, J. M.; Thomas, S. P.; Mazurczak, M.; Graham, D. L.; Kolesar, J. M.; Schiller, J. H. A phase II trial of Triapine (NSC# 663249) and Gemcitabine as second line treatment of advanced non-small cell lung cancer: Eastern Cooperative Oncology Group study 1503. *Invest. New Drugs* **2009**, *28*, 91−97.

(185) Bacher, F.; Enyedy, É. A.; Nagy, N. V.; Rockenbauer, A.; Bognár, G. M.; Trondl, R.; Novak, M. S.; Klapproth, E.; Kiss, T.; Arion, V. B. Copper(II) Complexes with Highly

Water-Soluble L- and D‑Proline−Thiosemicarbazone Conjugates as Potential Inhibitors of Topoisomerase II*α*. *Inorg. Chem.* **2013**, *52*, 8895–8908.

(186) West, D. X.; Liberta, A. E. Thiosemicarbazone complexes of copper(II): structural and biological studies. *Coord. Chem. Rev.* **1993**, *123*, 49–71.

(187) Casas, J. S.; García-Tasende, M. S.; Sordo, J. Main group metal complexes of semicarbazones and thiosemicarbazones. A structural review. *Coord. Chem. Rev.* **2000**, *209*, 197–261.

(188) Bermejo, E.; Castiñeiras, A.; García-Santosa, I.; West, D. X. Variability in the Coordination Modes of 2-Pyridineformamide Thiosemicarbazone (HAm4DH) in some Zinc(II), Cadmium(II), and Mercury(II) Complexes. *Z. Anorg. Allg. Chem.* **2005**, *631*, 2011–2019.

(189) Lobana, T. S.; Khanna, S.; Sharma, R.; Hundal, G.; Sultana, R.; Chaudhary, M.; Butcher, R. J.; Castineiras, A. Versatility of Thiosemicarbazones in the Construction of Monomers, Dimers and Hydrogen-Bonded Networks of Silver(I) Complexes. *Cryst. Growth Design* **2008**, *8*, 1203–1212.

(190) Dobrova, A.; Platzer, S.; Bacher, F.; Milunovic, M. N. M.; Dobrov, A.; Spengler, G.; Enyedy, É. A.; Novitchi, G.; Arion, V. B. Structure–antiproliferative activity studies on L-proline- and homoproline-4-*N*-pyrrolidine-3-thiosemicarbazone hybrids and their nickel(II), palladium(II) and copper(II) complexes. *Dalton Trans.* **2016**, *45*, 13427–13439.

(191) Chaston, T. B.; Lovejoy, D. B.; Watts, R. N.; Richardson, D. R. Examination of the Antiproliferative Activity of Iron Chelators: Multiple Cellular Targets and the Different Mechanism of Action of Triapine Compared with Desferrioxamine and the Potent Pyridoxal Isonicotinoyl Hydrazone Analogue 311. *Clin. Cancer Res.* **2003**, *9*, 402–414.

(192) Jansson, P. J.; Sharpe, P. C.; Bernhardt, P. V.; Richardson, D. R. Novel Thiosemicarbazones of the ApT and DpT Series and Their Copper Complexes: Identification of Pronounced Redox Activity and Characterization of Their Antitumor Activity. *J. Med. Chem.* **2010**, *53*, 5759–5769.

(193) Park, K. C.; Fouani, L.; Jansson, P. J.; Wooi, D.; Sahni, S.; Lane, D. J. R.; Palanimuthu, D.; Lok, H. C.; Kovačević, Z.; Huang, M. L. H.; Kalinowski, D. S.; Richardson, D. R. Copper and conquer: copper complexes of di-2-pyridylketone thiosemicarbazones as novel anti-cancer therapeutics. *Metallomics* **2016**, *8*, 874–886.

(194) Milunovic, M. N. M.; Enyedy, É. A.; Nagy, N. V.; Kiss, T.; Trondl, R.; Jakupec, M. A.; Keppler, B. K.; Krachler, R.; Novitchi, G.; Arion, V. B. L- and D‑Proline

Thiosemicarbazone Conjugates: Coordination Behavior in Solution and the Effect of Copper(II) Coordination on Their Antiproliferative Activity. *Inorg. Chem.* **2012**, *51*, 9309–9321.

(195) Senina, A. S.; Evdokimov, A. A.; Moskvin, A. V.; Fedorova, E. V. Synthesis, Characterization and Antimicrobial Activity of Amidrazone Derivatives. *J. Adv. Chem. Sci.* **2016**, *2*, 183–187.

(196) Ziegler-Borowska, M.; Ucherek, M.; Kutkowska, J.; Mazur, L.; Modzelewska-Banachiewicz, B.; Kędziera, D.; Kaczmarek-Kędziera, A. Reaction of N3-phenylbenzamidrazone with cis-1,2-cyclohexanedicarboxylic anhydride. *Tetrahedron Lett.* **2010**, *51*, 2951–2955.

(197) Modzelewska-Banachiewicz, B.; Matysiak, J.; Niewiadomy, A. Synthesis and mycological activity of the compounds obtained in the reaction of *N*3-substituted amidrazones with sulphinyl-bis-2,4-dihydroxybenzenethioyl. *Eur. J. Med. Chem.* **2001**, *36*, 75–80.

(198) Modzelewska-Banachiewicz, B.; Ucherek, M.; Zimecki, M.; Kutkowska, J.; Kaminska, T.; a Morak-Młodawska, B.; Paprocka, R.; Szulc, M.; Lewandowski, G.; Marciniak, J.; Bobkiewicz-Kozlowska, T. Reactions of N3-Substituted Amidrazones with cis-1,2-Cyclohexanedicarboxylic Anhydride and Biological Activities of the Products. *Arch. Pharm. Chem. Life Sci.* **2012**, *345*, 486–494.

(199) Modzelewska-Banachiewicz, B.; Banachiewicz, J.; Chodkowska, A.; Jagiełło-Wójtowicz, E.; Mazur, L. Synthesis and biological activity of new derivatives of 3-(3,4-diaryl-1,2,4-triazole-5-yl)propenoic acid. *Eur. J. Med. Chem.* **2004**, *39*, 873–877.

(200) Habashneh, A. Y.; El-Abadelah, M. M.; Zihlif, M. A.; Imraish, A.; Taha, M. O. Synthesis and antitumor activities of some new N1-(flavon-6-yl)amidrazone derivatives. *Archiv der Pharmazie* **2014**, *347*, 415–422.

(201) Sweidan, K.; Zalloum, H.; Sabbah, D. A.; Idris, G.; Abudosh, K.; Mubarak, M. S. Synthesis, characterization, and anticancer evaluation of some new *N*1-(anthraquinon-2-yl) amidrazone derivatives. *Canad. J. Chem.* **2018**, *96*, 1123–1128.

(202) Abu-Aisheh, M. N.; Mustafa, M. S.; El-Abadelah, M. M.; Naffa, R. G.; Ismail, S. I.; Zihlif, M. A.; Taha, M. O.; Mubarak, M. S. Synthesis and biological activity assays of some new *N*1-(flavon-7-yl)amidrazone derivatives and related congeners. *Eur. J. Med. Chem.* **2012**, *54*, 65–74.

(203) Mustafa, M. S.; El-Abadelah, M. M.; Zihlif, M. A.; Naffa, R. G.; Mubarak, M. S. Synthesis, and Antitumor Activity of Some *N1*-(Coumarin-7-yl) Amidrazones and Related Congeners. *Molecules* **2011**, *16*, 4305–4317.

(204) Abdel-Jalil, R. J.; El Momani, E. Q.; Hamad, M.; Voelter, W.; Mubarak, M. S.; Smith, B. H.; Peters, D. G. Synthesis, antitumor activity, and electrochemical behaviour of some piperazinyl amidrazones. *Monatsh. Chem.* **2010**, *141*, 251–258.

(205) Mazur, L.; Modzelewska-Banachiewicz, B.; Paprocka, R.; Zimecki, M.; Wawrzyniak, U. E.; Kutkowska, J.; Ziółkowska, G. Synthesis, crystal structure and biological activities of a novel amidrazone derivative and its copper(II) complex — A potential antitumor drug. *J. Inorg. Biochem.* **2012**, *114*, 55–64.

(206) Gokhale, N. H.; Padhye, S. S.; Padhye, S. B.; Anson, C. E.; Powell, A. K. Copper complexes of carboxamidrazone derivatives as anticancer agents. 3. Synthesis, characterization and crystal structure of [Cu(appc)Cl2], (appc=N1-(2-acetylpyridine)pyridine-2-carboxamidrazone). *Inorg. Chim. Acta* **2001**, *319*, 90–94.

(207) Ponticelli, G.; Miteva, M.; Synthesis, characterization, structure and cytotoxic activity of gold(III) complexes with amidrazone derivates. *Trans. Met. Chem.* **2006**, *31*, 703–707.

(208) Cocco, M. T.; Onnis, V.; Ponticelli, G.; Spanu, A. Palladium(II) and platinum(II), (IV) complexes of acetamidrazones. *Polyhedron* **1998**, *17*, 2065–2072.

(209) Cocco, M. T.; Onnis, V.; Ponticelli, G.; Meier, B.; Rehder, D.; Garribba, E.; Micera, G. Synthesis, characterisation and insulin-mimetic activity of oxovanadium(IV) complexes with amidrazone derivatives. *J. Inorg. Biochem.* **2007**, *101*, 19–29.

(210) Gokhale, N.; Padhye, S.; Rathbone, D.; Billington, D.; Lowe, P.; Schwalbe, C.; Newton, C. The crystal structure of first copper(II) complex of a pyridine-2-carboxamidrazone – a potential antitumor agent. *Inorg. Chem. Commun.* **2001**, *4*, 26–29.

(211) Gillies, E. R.; Fréchet, J. M. J. Dendrimers and dendritic polymers in drug delivery. *Drug Discovery Today* **2005**, *10*, 35–43.

(212) Szymański, P.; Markowicz, M.; Mikiciuk-Olasik, E. Nanotechnology in pharmaceutical and biomedical applications. Dendrimers. *Nano* **2011**, *6*, 509–539.

(213) Esfand, R.; Tomalia, D. A. Poly(amidoamine) (PAMAM) dendrimers: from biomimicry to drug delivery and biomedical applications. *Drug Discovery Today* **2001**, *6*, 427–436.

(214) Klajnert, B.; Bryszewska, M. Dendrimers: properties and applications. *Acta Biochim. Polon.* **2001**, *48*, 199–208.

(215) Abbasi, E.; Fekri Aval, S.; Akbarzadeh, A.; Milani, M.; Tayefi Nasrabadi, H.; Joo, S. W.; Hanifehpour, Y.; Nejati-Koshki, K.; Pashaei-Asl, R. Dendrimers: synthesis, applications, and properties. *Nanoscale Res. Lett.* **2014**, *9*, 1–10.

(216) Maciejewski, M. Concepts of Trapping Topologically by Shell Molecules. *J. Macromol. Sci.-Chem.* **1982**, *17*, 689–703.

(217) Jansen, J. F. G. A.; Meijer, E. W. The Dendritic Box: Shape-Selective Liberation of Encapsulated Guests. *J. Am. Chem. Soc.* **1995**, *117*, 4417–4418.

(218) Jansen, J. F. G. A.; de Brabander-van den Berg, E. M. M.; Meijer, E. W. Encapsulation of Guest Molecules into a Dendritic Box. *Science* **1994**, *266*, 1226–1229.

(219) Pasut, G.; Veronese, F. M. Polymer–drug conjugation, recent achievements and general strategies. *Prog. Prolym. Sci.* **2007**, *32*, 933–961.

(220) Nehoff, H.; Parayath, N. N.; Domanovitch, L.; Taurin, S.; Greish, K. Nanomedicine for drug targeting: strategies beyond the enhanced permeability and retention effect. *Int. J. Nanomed.* **2014**, *9*, 2539–2555.

(221) Kobayashi, H.; Watanabe, R.; Choyke, P. L. Improving Conventional Enhanced Permeability and Retention (EPR) Effects; What Is the Appropriate Target? *Theranostics* **2014**, *4*, 81–89.

(222) Govender, P.; Antonels, N. C.; Mattsson, J.; Renfrew, A. K.; Dyson, P. J.; Moss, J. R.; Therrien, B.; Smith, G. S. Anticancer activity of multinuclear arene ruthenium complexes coordinated to dendritic polypyridyl scaffolds. *J. Organomet. Chem.* **2009**, *694*, 3470–3476.

(223) Khanye, S. D.; Gut, J.; Rosenthal, P. J.; Chibale, K.; Smith, G. S. Ferrocenylthiosemicarbazones conjugated to a poly(propyleneimine) dendrimer scaffold: Synthesis and *in vitro* antimalarial activity. *J. Organomet. Chem.* **2011**, *696*, 3296–3300.

(224) Stringer, T.; Hendricks, D. T.; Guzgay, H.; Smith, G. S. Synthesis and characterization of multimeric salicylaldimine thiosemicarbazones and their Pd(II) and Pt(II) complexes. *Polyhedron* **2012**, *31*, 486–493.

Contribution of Kateryna Ohui to the following publications:

New Water-Soluble Copper(II) Complexes with Morpholine-Thiosemicarbazone Hybrids: Insights into the Anticancer and Antibacterial Mode of Action. *J. Med. Chem.* **2019**, *62*, 512–530:

Synthesis of starting materials, thiosemicarbazone proligands and their copper(II) complexes together with Eleonora Afanasenko (master student). Measurement and interpretation of 1D and 2D NMR spectra, ESI-MS, UV-vis and IR spectra, growth of single crystals of proligands and copper(II) complexes, descriprion of X-ray crystallography results, solution chemistry and complex-formation studies in solution under supervision of Prof. Éva Anna Enyedy, writing the manuscript.

Redox-active organoruthenium(II)- and organoosmium(II)-copper(II) complexes, with an amidrazone-morpholine hybrid and $[Cu^{I}Cl_2]^-$ as counteranion, and their antiproliferative activity. *Organometallics* 10.1021/acs.organomet.9b00229:

Synthesis of 6-(morpholinomethyl)pyridine-2-carboxaldehyde, 2-pyridinamidrazone and their Schiff-base product as proligand, $[Ru(p\text{-cymene})Cl_2]_2$, mononuclear and tetranuclear copper(II) complexes, heterodinuclear Cu(II)-Ru(II) and Cu(II)-Os(II) complexes. Measurement and interpretation of 1D and 2D NMR spectra, ESI-MS (measurement, interpreteation and simulation for heterodinuclear complexes), UV-vis and IR spectra, growth of single crystals of copper(II) tetranuclear complex, Cu(II)-Ru(II) and Cu(II)-Os(II) complexes, descriprion of X-ray crystallography results, writing the manuscript.

New Triapine Derivatives and their Metal Complexes as Anticancer Agents. Manuscript will be submitted in the nearest future:

Synthesis of thiosemicarbazone and amidrazone proligands and their metal complexes, 2-pyridinamidrazone, purification of one of the complexes by preparative HPLC. Measurement and interpretation of 1D and 2D NMR spectra, ESI-MS, UV-vis and IR spectra, growth of single crystals for X-ray diffraction of one of the proligands and copper(II) complexes, writing the manuscript.

New Water-Soluble Copper(II) Complexes with Morpholine-Thiosemicarbazone Hybrids: Insights into the Anticancer and Antibacterial Mode of Action

J. Med. Chem. **2019**, *62*, 512−530

Kateryna Ohui,[a, ≠] Eleonora Afanasenko,[a, ≠] Felix Bacher,[a] Rachel Lim Xue Ting,[b] Ayesha Zafar,[c] Núria Blanco-Cabra,[d] Eduard Torrents,[d] Orsolya Dömötör,[e] Nóra V. May,[f] Denisa Darvasiova,[g] Éva A. Enyedy,[e] Ana Popović-Bijelić,[h] Jóhannes Reynisson,[c] Peter Rapta,[g] Maria V. Babak,*[,i,j] Giorgia Pastorin,[b] Vladimir B. Arion*[,a]

[a]*University of Vienna, Institute of Inorganic Chemistry, Währinger Strasse 42, A-1090 Vienna, Austria,* [b]*Department of Pharmacy, National University of Singapore, Singapore, 3 Science Drive 2, 117543 Singapore*

[c]*School of Chemical Sciences, University of Auckland, Auckland, New Zealand*

[d]*Bacterial Infections: Antimicrobial Therapies, Institute for Bioengineering of Catalonia (IBEC), The Barcelona Institute of Science and Technology, Barcelona, Spain*

[e]*Department of Inorganic and Analytical Chemistry, University of Szeged, Dóm tér 7. H-6720 Szeged, Hungary*

[f]*Research Centre of Natural Sciences, Hungarian Academy of Sciences, Magyar tudósok körútja 2. H-1117, Budapest, Hungary*

[g]*Institute of Physical Chemistry and Chemical Physics, Slovak Technical University of Technology, Radlinského 9, 81237 Bratislava, Slovak Republic*

[h]*Faculty of Physical Chemistry, University of Belgrade, 11158 Belgrade, Serbia*

[i]*Department of Chemistry, National University of Singapore,3 Science Drive 2, 117543 Singapore*

[j]*Drug Development Unit, National University of Singapore,28 Medical Drive, 117546 Singapore*

[≠] these co-authors contributed equally

Keywords: Thiosemicarbazones, Cu(II)-TSC, solution equilibrium, stability constants, spectroelectrochemistry, molecular modelling, antitumor activity, antibacterial activity, mechanism of action, cellular accumulation, ribonucleotide reductase inhibition, ER stress, apoptosis, cell cycle

Abstract

Six morpholine-(iso)thiosemicarbazone hybrids **HL^{1}**–**HL^{6}** and their Cu(II) complexes with good-to-moderate solubility and stability in water were synthesized and characterized. Cu(II) complexes **[Cu(L$^{1–6}$)Cl]** (**1**–**6**) formed weak dimeric associates in the solid state, which did not remain intact in solution as evidenced by ESI-MS. The lead proligands and Cu(II) complexes displayed higher antiproliferative activity in cancer cells than Triapine. In addition, complexes **2**–**5** were found to specifically inhibit the growth of Gram-positive bacteria *S. aureus* with MIC_{50} values at 2 to 5 μg/mL. Insights into the processes controlling intracellular accumulation and mechanism of action were investigated for **2** and **5**, including the role of ribonucleotide reductase (RNR) inhibition, endoplasmic reticulum (ER) stress induction and regulation of other cancer signaling pathways. Their ability to moderately inhibit R2 RNR protein in the presence of DTT is likely related to Fe chelating properties of the proligands liberated upon reduction.

Introduction

Progress in modern anticancer therapy has led to significant improvements in survival rates of cancer patients. However, even though more patients achieve remission nowadays, their life-span often remains short.[1] One of the major causes of cancer death is the malignant process itself, which is associated with extensive formation of metastases, but it is not commonly mentioned that a significant number of immunocompromised cancer patients die due to infections, such as pneumonia and peritonitis.[2] Despite that cancer patients are very prone to develop infections during chemotherapy, their preventive antibiotic treatment is hampered by additional adverse effects.[3] However, recent clinical evidence demonstrated that benefits of antibiotic prophylaxis of cancer patients outweighed its risks.[4] The simultaneous suppression of pathogenic microorganisms during anticancer chemotherapy could not only interrupt or abolish tumor growth but eventually protect

cancer patients from infection. Hence, the development of novel drugs which exhibit dual anticancer and antibacterial properties in comparable concentration range would affect the malignant process and simultaneously decrease the risk of patients' death due to infection, febrile neutropenia and bacteraemia.

Both cancer and bacterial cells share similar properties, such as high rate of proliferation, rapid adjustment and quick spreading within the host and aggressive disease progression.[5] In order to sustain such rapid proliferation, cancer and bacterial cells have to support DNA replication and production of RNA by increasing *de novo* nucleotide synthesis. Ribonucleotide reductase (RNR) is the key enzyme that catalyzes the reduction of ribonucleotides to their corresponding deoxyribonucleotides, thereby initiating DNA synthesis or repair, making it an important biomolecular target for drugs with anticancer and antibacterial properties.[6,7] RNR consists of a large subunit (NrdA or R1), which contains the allosteric site that regulates and catalyzes substrate reduction, and a small subunit (NrdB or R2) with the diferric-tyrosyl radical cofactor, essential for the catalytic activity of the RNR enzyme. Small molecules, that can sequester Fe(III) from the dinuclear metal center and/or scavenge the tyrosyl radical, inhibit R2 activity, thereby preventing *de novo* DNA synthesis in cancer cells and bacteria.

α-*N*-heterocyclic thiosemicarbazones (TSCs) are excellent transition metal chelators and have a broad range of activities, including anticancer and antibacterial properties, which are believed to be at least partially due to their RNR inhibition.[8] To date, several TSC compounds, namely 3-amino-2-pyridinecarboxaldehyde thiosemicarbazone (Triapine),[9-11] di-2-pyridylketone 4-cyclohexyl-4-methyl-3-thiosemicarbazone (DpC)[12,13] and (*E*)-*N*´-(6,7-dihydroquinolin-8(5*H*)-ylidene)-4-(pyridine-2-yl)piperazine-1-carbothiohydrazide (COTI-2)[14] are undergoing phase I and II clinical trials against various types of cancer. The main caveat in the use of TSCs is their high toxicity which is reflected in a number of side-effects in clinical trials involving Triapine.[9-11] Many studies have shown that Cu(II)-TSC complexes often display better selectivity than their TSC proligands, which can be attributed to the induction of different intracellular signaling pathways.[15]

Despite advances in the design and synthesis of new TSCs and Cu(II)-TSC complexes over the years, these compounds are facing the problem of low aqueous solubility, thereby hampering their further development. Therefore, the synthesis of water-soluble and

cytotoxic TSCs and Cu(II)-TSC complexes requires a thoughtful selection of the functional groups that can be attached at the TSC backbone without reducing their biological activity.[16-20] With the aim to reach the optimal combination of aqueous solubility and high cytotoxicity, we designed new (iso)thiosemicarbazone-morpholine hybrids and their Cu(II) complexes. Notably, morpholine moiety was chosen since it confers excellent water solubility, which typically translates into an improved pharmacological effect. Additionally, morpholine derivatives possess a broad spectrum of biological activities, including anticancer and antibacterial therapeutic potential.[21] For example, commercial anticancer drugs Aprepitant and Gefinitib, as well as antibacterial drugs Finafloxacin and Levofloxacin include a morpholine fragment in their structures.

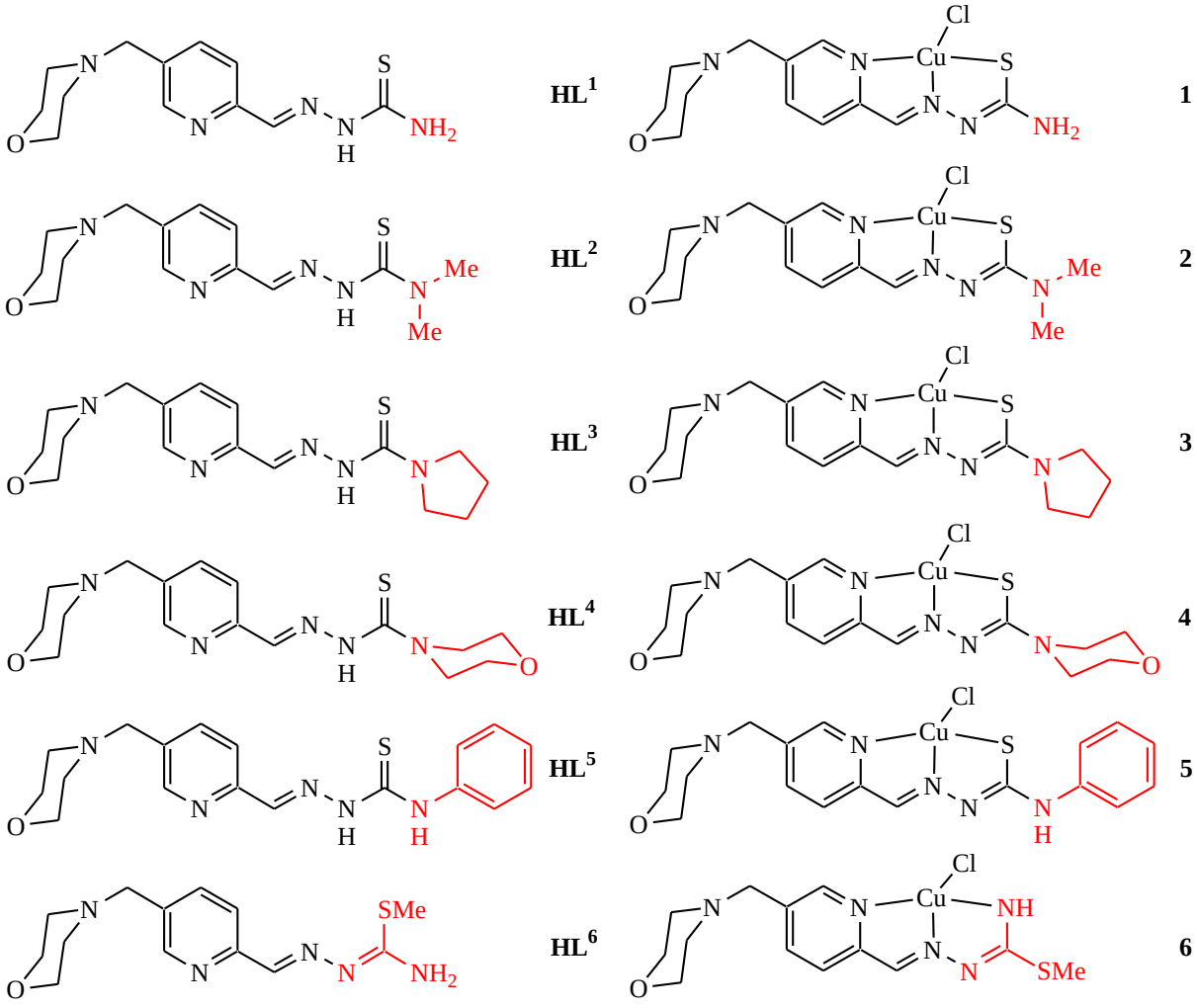

Chart 1. Line drawings of proligands **HL$^{1–6}$** and Cu(II) complexes **[Cu(L$^{1–6}$)Cl]** (**1**–**6**) reported in this work. All proligands and Cu(II) complexes, but **HL^{3}** and **2**, were investigated by single crystal X-ray crystallography.

Herein we report on the synthesis of water-soluble proligands **HL$^{1–6}$** and Cu(II) complexes **1**–**6** (Chart 1), which were characterized by analytical and various spectroscopic techniques. X-ray diffraction structures of **HL^{1}**, **HL^{2}**, **HL^{3}–HL^{6}** and **1**, **3**–**6** were established and solution equilibria studies for **HL^{1}** and Cu(II) complex formation with **HL^{1}** by pH-potentiometry, UV–vis, EPR and ^{1}H NMR spectroscopy, as well as electrochemistry were performed. Antiproliferative activity against human ovarian cancer A2780 and cisplatin resistant A2780cis cell lines, non-cancerous HEK293 cell line, as well as antibacterial activity against Gram-positive (*S. aureus*) compared to Gram-negative bacteria (*P. aeruginosa*) were investigated and structure-activity relationships discussed. The processes controlling cellular accumulation of **2** were investigated. Preliminary insights into the mode of action of **2** and **5**, including mouse R2 RNR inhibitory potential, studied by molecular modeling and tyrosyl radical quenching monitored by EPR spectroscopy, as well as by Western Blotting and flow cytometry are also presented.

Results

Synthesis and characterization of (iso)thiosemicarbazone-morpholine hybrids and their Cu(II) complexes. The 5-methylmorpholine-pyridine-2-carboxaldehyde **H** was prepared in seven steps as shown in Scheme 1 and the detailed synthesis is described in the Supporting Information. First pyridine-2,5-dicarboxylic acid **A** was converted into diester **B** that was further reduced to the diol **C**. The latter was selectively oxidized with SeO_2 to the aldehyde **D**. After protection of the aldehyde group the alcohol **E** was converted into the chloride **F** that was further reacted with morpholine to give species **G**. Finally, the hydrolysis of the methyl ester function in acidic conditions afforded the required aldehyde **H** for condensation reactions with thiosemicarbazide, 4*N*-dimethyl-3-thiosemicarbazide, 4*N*-pyrrolydinyl-3-thiosemicarbazide, 4*N*-morpholinyl-3-thiosemicarbazide, 4*N*-phenyl-3-thiosemicarbazide and *S*-methylisothiosemicarbazide hydroiodide to give the hybrids **HL$^{1–6}$** (Scheme 1), respectively. One- and two-dimensional NMR spectra were in agreement with the proposed structures for **HL$^{1–6}$**, enabling the assignment of all ^{1}H and ^{13}C resonances. The ESI mass spectra recorded in a positive ion mode showed strong peaks corresponding to $[M+H]^+$ and $[M+Na]^+$ ions, respectively. The proligands **HL$^{1–6}$** were reacted with Cu(II) chloride dihydrate and triethylamine in 1:1:1 mole ratio in methanol to give **[Cu(L$^{1–6}$)Cl]** (**1**–**6**) in 35–91% yields. Positive ion ESI mass spectra showed strong peaks attributed to $[Cu(L^{1–6})]^+$ ions. The structures of **1**, **3**–**6** were also established by single crystal X-ray diffraction (*vide infra*).

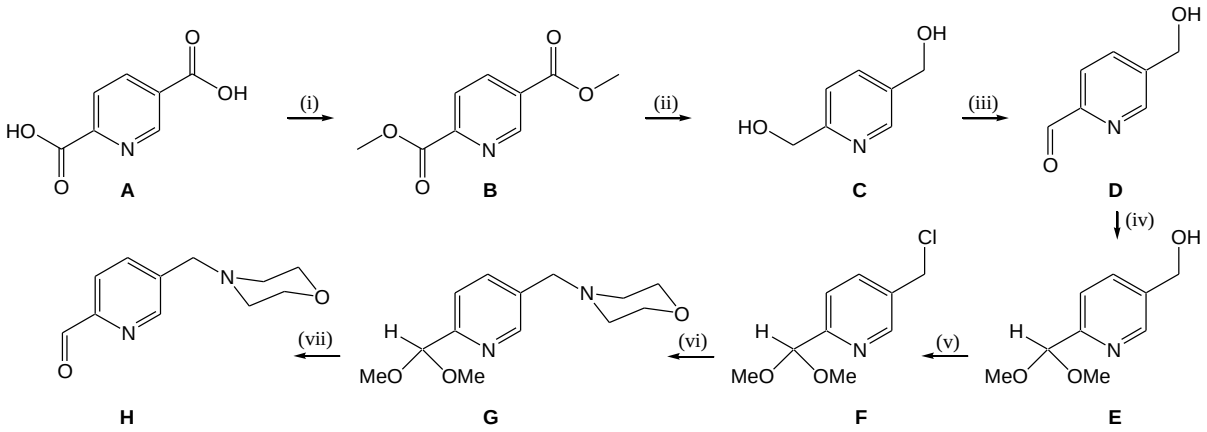

Scheme 1. Synthesis of 5-methylmorpholine-pyridine-2-carboxaldehyde. Reagents and conditions: (i) thionyl chloride, methanol, 0 °C → room temperature, 12 h;[22] (ii) sodium borohydride, ethanol, acetone, potassium carbonate, chloroform, 0 °C, 1 h → reflux, overnight;[23] (iii) selenium dioxide, dioxane, water, 100 °C, 3 h;[24] (iv) trimethyl orthoformate, methanesulfonic acid, methanol, reflux, 48 h; (v) thionyl chloride, dichloromethane, –80 °C → room temperature, overnight; (vi) moprholine, triethylamine, THF/CH_2Cl_2 1:1, 50 °C, overnight, purification by column chromatography; (vii) HCl, water, 60 °C, overnight.

X-ray Crystallography. The results of X-ray diffraction studies of **HL^1**, **HL^2** and **$HL^{4–6}$** are shown in Figure S1, while those of **[Cu(L^1)Cl]** (**1**), **[Cu(L^3)Cl]** (**3**), **[Cu(L^4)Cl]** (**4**), **[Cu(L^5)Cl]** (**5**) and **[Cu(L^1)Cl(H_2O)]** (**1´**), **[Cu(L^6)Cl]** (**6**) in Figures 1 and 2, respectively. Selected bond distances and bond angles are quoted in Tables S1 and S2. The proligands adopted different isomeric configurations in the solid state depending on substituents at the terminal nitrogen atom of the thiosemicarbazide moiety. Complexes **1**, **3**, **4** and **5** form dimeric associates as shown in Figure 1 (co-crystallized solvent was omitted for clarity). Each Cu(II) ion has a distorted square-planar coordination geometry. Intermolecular contacts supporting the dimeric associates in the crystals are of different nature in **1** and **3**–**5**, respectively. The presence of long intermolecular contacts Cu···Cl or Cu···Cl and Cu···S (see legend to Figure 1) provides evidence of weak association of complexes in dimers, which most probably dissociate in solution with formation of monomeric species. There was no evidence from ESI mass spectra on the presence of dimeric species in solution.

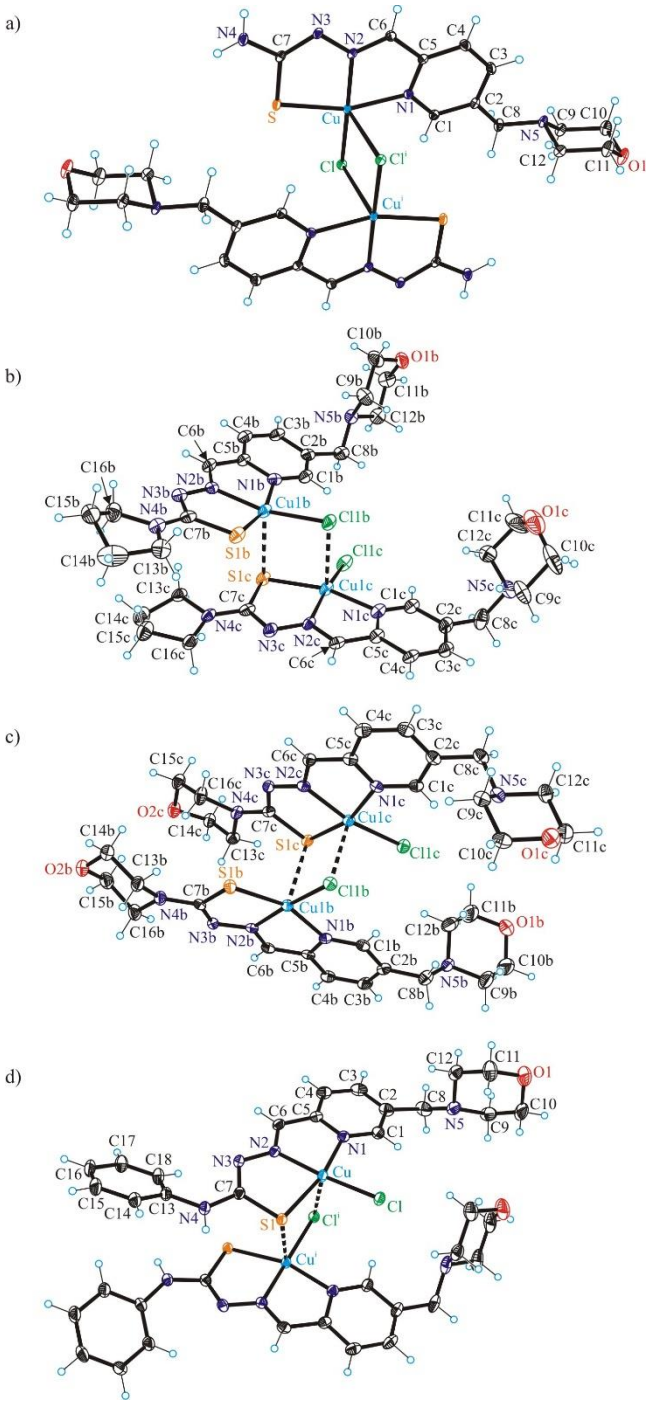

Figure 1. ORTEP views of weak dimeric associates of (a) [Cu(L^1)Cl] (**1**), (b), [Cu(L^3)Cl] (**3**), (c) [Cu(L^4)Cl]$_2$ (**4**) and (d) [Cu(L^5)Cl] (**5**).

Moreover, **HL^1** reacts with $CuCl_2$ in aqueous solution with formation of five-coordinate complex **[Cu(L^1)Cl(H_2O)]** (**1´**·2H_2O) (Figure 2b). The monomeric square-planar complex **[Cu(L^6)Cl]** forms an infinite chain via weak coordination of the morpholine oxygen atom of one complex to the Cu(II) atom of the next molecule as shown in Figure S2. The intermolecular Cu···O contact is of 2.603(3) Å.

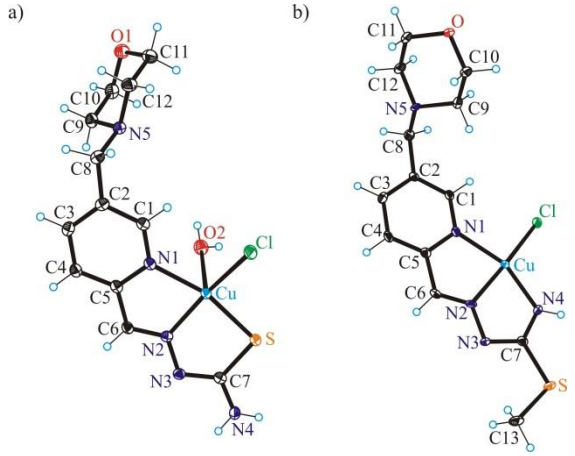

Figure 2. ORTEP views of (a) [Cu(L^1)Cl(H_2O)] (**1´**) and (b) [Cu(L^6)Cl] (**6**).

Solution Chemistry. In order to establish the presence of isomers of the proligands in aqueous solution and proton dissociation processes, in which these can be involved solution equilibrium studies have been performed. Likewise, the solution speciation of the copper(II) complexes, as well as their stability have been investigated to elucidate the species, which is the most stable and abundant at physiological pH. The proligand **HL^1** (Chart 1) was chosen for the detailed solution equilibrium studies since it has the simplest structure and the best aqueous solubility among the proligands prepared. The presence of different isomers in solution was excluded by measurements of ^{1}H NMR spectra in 10% D_2O/90% H_2O (Figure S3), which showed only one set of signals for the proligand in accordance to its low (C_1) molecular symmetry. The proligand most probably adopts the *E* configuration found in the solid state (Figure S1). The same configuration was reported previously for the reference compound 2-formylpyridine thiosemicarbazone in polar solvents.[25] Proton dissociation processes were monitored in aqueous solution by pH-potentiometric and ^{1}H NMR titrations and three pK_a values were determined by both methods (Table S3). According to the obtained pK_a values **HL^1** is mainly neutral (97% HL, 3% H_2L^+) at physiological pH (Figure S4). Inspection of ^{1}H NMR spectra revealed stepwise deprotonation of three functional groups in the following order: $N_{pyridinium}H^+ \rightarrow N_{morpholinium}H^+ \rightarrow N_{hydrazine}H$ (Figure S3).

The solution speciation of the Cu(II) complexes with **HL^1** was characterized by the combined use of pH-potentiometry, UV−vis spectrophotometry (via charge transfer (CT) and d-d bands) and EPR spectroscopy. The spectral changes (Table S4, Figures 3a and S5) in the UV and visible regions measured at 1:1 metal-to-ligand ratio show the high-extent formation of a Cu(II) complex already at strongly acidic pH values (e.g. pH 1) and its

stepwise deprotonation by increasing the pH. At pH 7.4 the dominant species is $[CuL]^+$ (Figure 3b).

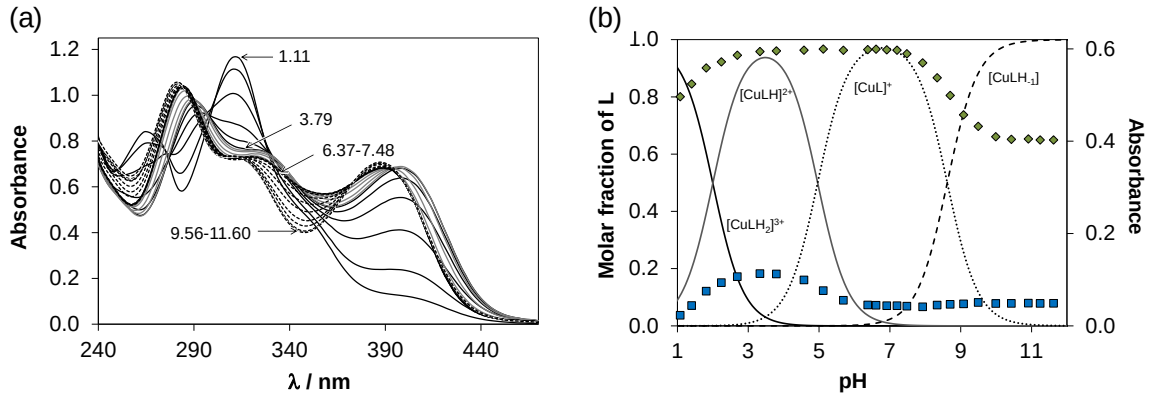

Figure 3. UV–vis spectra recorded for the Cu(II)–**HL**^{1} (1:1) system at various pH values (a), and concentration distribution curves and measured absorbance values at 346 nm (♦) and 440 nm (■) for the same system (b). {$c_{Cu(II)} = c_{lig}$ = 121 μM; T = 298 K; I = 0.10 M (KCl); l = 0.5 cm}.

Due to the high stability of the Cu(II) complexes formed, the cumulative constant (logβ) for the $[CuL]^+$ species (Table S4) was determined via EDTA displacement studies (Figure S6). Then the pK_a and the logβ values for the other type of complexes ($[CuLH_2]^{3+}$, $[CuLH]^{2+}$, $[CuLH_{-1}]$) were computed using each method and data were in a fairly good agreement (Table S4). It is worth noting that formation of a bis-ligand complex $[CuL_2]$ at ligand excess was also confirmed by the UV−vis CT and EPR titrations. The d-d bands (Figure S5) recorded from pH 3.4 to 7.5 at 1:1 metal-to-ligand ratio revealed that the proton dissociation process of $[CuLH]^{2+} \rightarrow [CuL]^+$ is accompanied by rather weak spectral changes as most probably the non-coordinating morpholinium NH^+ is deprotonating. In order to further characterize the coordination modes of the various complexes in solution EPR parameters (Table S5) obtained by the deconvolution of the recorded spectra (Figure S7) were analyzed. The isotropic g and A values of $[CuLH]^{2+}$ and $[CuL]^+$ are quite similar indicating the like coordination mode.

Comparison of the EPR parameters of the Cu(II) complexes of **HL**^{1} with those of 2-formylpyridine thiosemicarbazone[25] and Triapine[26] permitted to conclude that in the $[CuLH]^{2+}$ and $[CuL]^+$ complexes a typical coordination mode via the $N_{pyridyl}$,N,S^- binding site is realized in accordance with the X-ray diffraction data. $[CuLH_2]^{3+}$ contains the diprotonated ligand in which the protons are attributed to the non-coordinating N^2H and morpholinium NH^+ moieties, while $[CuLH_{-1}]$ is most probably a mixed hydroxido complex [CuL(OH)] formed by the deprotonation of water molecule coordinated in the fourth

equatorial position. At ligand excess besides the bis-ligand complex a minor dinuclear species $[Cu_2L_3H]^{2+}$ was detected resulting in the weak exchange coupling between neighboring Cu(II) centers smearing out the expected hyperfine structure.

Cu(II)-TSC complexes undergo quasi-reversible one-electron reduction at biologically accessible potentials. In order to assess the redox properties of **1**–**6**, detailed electrochemical and spectroscopic studies in various solvents were performed using cyclic voltammetry as well as EPR–spectroelectrochemistry. Additionally, the UV–vis spectra of **1**–**5** were measured (Figure S8). Electrochemical and spectroscopic data are summarized in Table S6. Almost reversible one-electron cathodic reduction was observed for **1**–**5** in DMSO with half-wave redox potentials from –0.77 V to –0.81 V vs Fc^+/Fc (for comparison from –0.13 V to –0.17 V vs NHE) (Table S6 and Figure S9). In general, the values of redox potentials of **1**–**6** for the first reduction step decreased in the following rank order ($E_{1/2}$(**5**) > $E_{1/2}$(**2**) = $E_{1/2}$(**3**) = $E_{1/2}$(**4**) > $E_{1/2}$(**1**) > $E_{1/2}$(**6**)). The second reduction step occurred at –1.8 V vs Fc^+/Fc (–1.16 V vs NHE) and was less reversible indicating a ligand based reduction. This was confirmed by the CVs of the corresponding proligands which exhibited the first reduction step at around –1.9 V vs Fc^+/Fc (not shown). In aqueous solutions the reduction potentials shifted to the less negative values and reduction was less reversible as shown for **2** in Figure S10. Complex **6** exhibited different redox behavior with the lowest electrochemical reversibility and the most negative reduction potential of –0.86 V vs Fc^+/Fc (–0.26 V vs NHE) (Figure S9c). Unlike the cathodic reduction, the anodic oxidation of **1**–**6** was irreversible with potential values in the region from 0.4 to 0.8 V vs Fc^+/Fc (0.68 V to 1.44 V vs NHE). Similar response was observed for the corresponding proligand $\mathbf{HL^2}$ (Figure S11), indicating ligand based oxidation in **2**.

The biologically accessible reduction of Cu(II)-TSC complexes is Cu-centered. To investigate whether the biologically accessible reduction is metal-centered, the reversible one-electron reduction of **5** was further studied by *in situ* UV–vis-spectroelectrochemistry (Figure 4a). Upon cathodic reduction at the first reduction peak two isosbestic points at 389 and 325 nm were detected. The spectral changes of the S→Cu(II) charge transfer bands (~425 nm) clearly confirmed the reduction of Cu(II) to Cu(I). Additionally, upon voltammetric reverse scan, reoxidation and a nearly full recovery of the initial optical bands were observed, attesting the chemical reversibility of the cathodic reduction even at low scan rates (Figure 4). To confirm the involvement of Cu(II) in the reduction processes,

in situ EPR electrochemistry of **1–6** in nBu$_4$NPF$_6$/DMSO and water was performed, since metal-based reduction would result in the formation of EPR-silent Cu(I) species (Figure 4b). As can be seen for electrochemical reduction of **2** in nBu$_4$NPF$_6$/DMSO in the region of the first one–electron reduction step (see inset in Figure 4b), a significant decrease of EPR signal was observed in accord with the formation of diamagnetic Cu(I) d^{10} complex. For aqueous solutions the reversibility was significantly reduced, implying a more complex mechanism involving the release of the proligand. However, by decreasing the scan rate and going to the more positive potentials upon reverse scan, a partial recovery of the initial optical bands was also observed in aqueous solutions as shown for **2** in Figure S12. Thus, electrochemical data indicated a likely reduction of Cu(II)-TSC complexes to Cu(I) species with the subsequent release of the proligands.

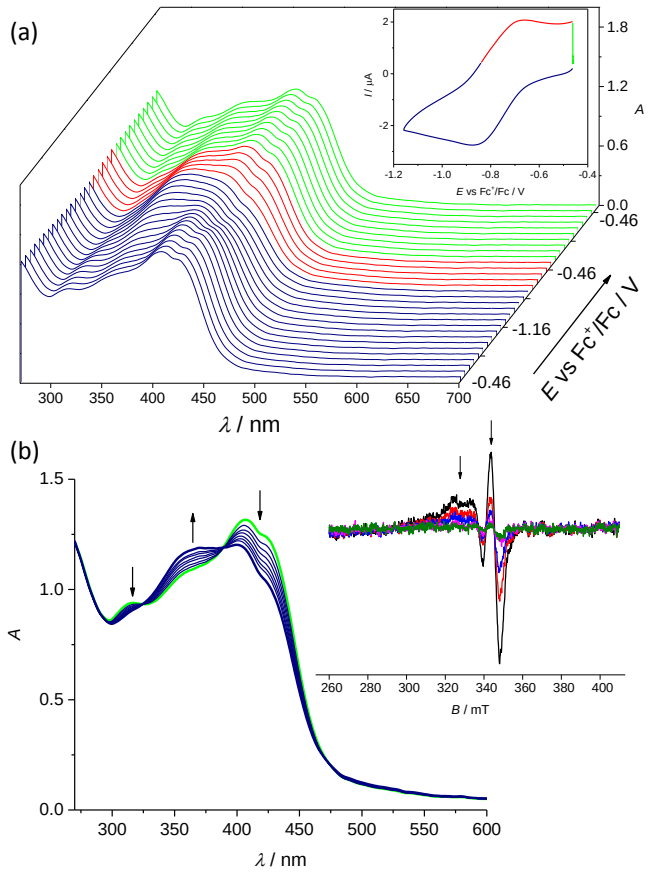

Figure 4. Spectroelectrochemistry of **2** in nBu$_4$NPF$_6$/DMSO in the region of the first cathodic peak. (a) Potential dependence of UV–vis spectra with respective cyclic voltammogram (Pt-microstructured honeycomb working electrode, scan rate v = 5 mV s^{-1}); (b) evolution of UV–vis spectra in 2D projection in forward scan (Inset: EPR spectra measured at the first reduction peak using Pt mesh working electrode).

Lead TSCs and their Cu(II) complexes exhibited marked antiproliferative activity in a nanomolar concentration range. The *in vitro* anticancer activity of **1**–**6** and their respective TSCs was determined in ovarian carcinoma cells (A2780 and A2780cisR) and non-cancerous human embryonic kidney cells (HEK293) by the colorimetric MTT assay with an exposure time of 72 h. The IC_{50} values for $\mathbf{HL^1}$–$\mathbf{HL^6}$ and **1**–**6** in comparison with Triapine, $CuCl_2$, Cu-Triapine and cisplatin are listed in Tables 1 and 2, respectively, and concentration-effect curves are depicted in Figure S13.

Table 1. Cytotoxicity of proligands $\mathbf{HL^{1–6}}$ and their *n*-octanol/water distribution coefficients ($logD_{7.4}$)

Compound	IC_{50} [μM][a]					$logD_{7.4}$[d]
	A2780	**A2780cis**	**RF**[b]	**HEK293**	**SF**[c]	
$\mathbf{HL^1}$	7.6 ± 1.9	13 ± 1	1.7	9.1 ± 1.7	1.2	+0.46 ± 0.01
$\mathbf{HL^2}$	0.010 ± 0.001	0.035 ± 0.006	3.5	0.030 ± 0.005	3.0	+0.51 ± 0.02
$\mathbf{HL^3}$	0.008 ± 0.002	0.028 ± 0.006	3.5	0.022 ± 0.005	2.8	+1.0 ± 0.1
$\mathbf{HL^4}$	0.07 ± 0.01	0.76 ± 0.06	10.9	0.35 ± 0.05	5.0	+0.37 ± 0.04
$\mathbf{HL^5}$	0.31 ± 0.08	1.1 ± 0.2	3.5	0.67 ± 0.06	2.2	≥2
$\mathbf{HL^6}$	157 ± 21	426 ± 44	2.7	89 ± 2	0.6	+0.84 ± 0.01
Triapine	0.67 ± 0.22	1.1 ± 0.1	4.6	0.39 ± 0.05	0.6	n.d.[e]

[a] 50% inhibitory concentrations (IC_{50}) in human ovarian carcinoma cell lines A2780 and A2780cisR and human embryonic kidney cell line HEK293, determined by means of the MTT assay after 72 h exposure. Values are means ± standard deviations obtained from at least three independent experiments, [b]Resistance Factor (RF) is determined as $IC_{50\ (A2780cisR)}/IC_{50\ (A2780)}$, [c] Selectivity Factor (SF) is determined as $IC_{50\ (HEK293)}/IC_{50\ (A2780)}$, [d] Distribution coefficients between *n*-octanol and buffered aqueous solution determined at physiological pH by UV–vis spectroscopy. Values are means ± standard deviations obtained from at least three independent experiments, [e] n.d. – not determined.

With the exception of $\mathbf{HL^1}$ and $\mathbf{HL^6}$, the proligands demonstrated marked antiproliferative activity in a submicromolar to nanomolar concentration range in both A2780 and A2780cisR cells. The efficacy of compounds $\mathbf{HL^2}$, $\mathbf{HL^3}$ and $\mathbf{HL^5}$ in cisplatin-resistant A2780cisR cells decreased by factor 3.5 in comparison to that in sensitive A2780 cells, whereas a 4.6- and 11-fold drop of activity was observed for Triapine and $\mathbf{HL^4}$, respectively. The activity of proligands $\mathbf{HL^{1–6}}$ and Triapine increased in the following rank order $\mathbf{HL^6 < HL^1 <}$ **Triapine** $\mathbf{< HL^5 < HL^4 << HL^2 \approx HL^3}$ (Table 1).

Table 2. Cytotoxicity of Cu(II)-TSC complexes **1**–**6**, $CuCl_2$ and cisplatin and their *n*-octanol/water distribution coefficients ($logD_{7.4}$)

Compound	IC_{50} [μM][a]					Cellular accumulation,[d] nmol Cu/ mg protein	$logD_{7.4}$[e]
	A2780	**A2780cis**	**HEK293**	**RF**[b]	**SF**[c]	**A2780**	
1	2.2 ± 0.1	13 ± 4	16 ± 2	5.9	7.3	0.63 ± 0.09	–0.81 ± 0.04
2	0.012 ± 0.002	0.030 ± 0.003	0.032 ± 0.008	2.5	2.7	3.9 ± 0.6	+0.30 ± 0.01
3	0.26 ± 0.02	0.60 ± 0.05	0.78 ± 0.20	2.3	3.0	2.2 ± 0.6	+0.86 ± 0.02
4	0.08 ± 0.01	0.26 ± 0.04	0.24 ± 0.02	3.3	3.0	3.2 ± 0.7	+0.12 ± 0.01
5	0.009 ± 0.002	0.017 ± 0.002	0.020 ± 0.003	1.9	2.2	4.1 ± 0.9	+1.49 ± 0.06
6	43 ± 3	62 ± 6	72 ± 0	1.4	1.7	0.47 ± 0.08	–0.23 ± 0.01
$CuCl_2$	83 ± 12	82 ± 3	187 ± 37	1.0	2.3	0.17 ± 0.05[f]	n.d.[g]
Cu-Triapine[h]	1.3 ± 0.1	29 ± 0.3	n.d.	22.3	-	n.d.	n.d.
Cisplatin	0.44 ± 0.13	4.6 ± 0.3	n.d.	10.5	-	-	–2.30 ± 0.79[i]

[a] 50% inhibitory concentrations (IC_{50}) in human ovarian carcinoma cell lines A2780 and A2780cisR and human embryonic kidney cell line HEK293, determined by means of the MTT assay after exposure for 72 h. Values are means ± standard deviations obtained from at least three independent experiments, [b]Resistance Factor (RF) is determined as $IC_{50\ (A2780cisR)}/IC_{50\ (A2780),}$ [c] Selectivity Factor (SF) is determined as $IC_{50\ (HEK293)}/IC_{50\ (A2780),}$ [d] Cellular accumulation in A2780 cells, determined by ICP-MS after 24 h exposure at concentration of 1 μM. Values are means ± standard deviations obtained from at least three independent experiments, [e] Distribution coefficients between *n*-octanol and buffered aqueous solution determined at physiological pH by UV–vis spectroscopy. Values are means ± standard deviations obtained from at least three independent experiments, [f] Cellular accumulation of $CuCl_2$ was detected at concentration of 2.5 μM, [g] n.d. – not determined, [h] the IC_{50} values (exposure for 72 h) were taken from the ref. 27,[i] Log $P_{o/w}$ value was taken from the ref. 28.

As can be seen in Table 2, with the exception of **3**, all Cu(II)-TSC complexes were equally or more cytotoxic than the respective proligands. The activity of complexes **1–6** increased in the following order **6 < 1 < 3** < **4** << **2** < **5**, similar to the trend in electrochemical redox potentials for Cu-based reduction step (Table S6). In order to compare the cytotoxicity of **1**–**6** with that of $[Cu(H_2O)_6]^{2+}$, A2780 cells were treated with aqueous solution of $CuCl_2$. In agreement with the literature,[29] $CuCl_2$ revealed antiproliferative activity in the high micromolar range, in contrast to high activity of **1**–**6**, which should be regarded as individual entities with their own biological, pharmacokinetic and metabolic profiles. Complexes **1**–**6** were up to ~50 times more cytotoxic than cisplatin in A2780 cells and up to ~270 times more cytotoxic in A2780cisR cells. Additionally, the differences in cytotoxicity of **1**–**6** in A2780 and A2780cisR cells were significantly lower than for

HL^{1}–**HL^{6}** and cisplatin, indicating high potential of Cu(II) complexes for the treatment of cisplatin-resistant tumors. The most active TSC proligands and their respective Cu(II) complexes were more selective towards A2780 cells over HEK293 cells; however, they did not show any selectivity towards A2780cisR cells over HEK293 cells. On the contrary, Triapine was significantly more cytotoxic towards non-cancerous HEK cells than A2780 or A2780cis cells.

Antiproliferative activity of Cu(II)-TSC complexes correlates with their cellular accumulation and lipophilicity. The ability of anticancer drugs to penetrate biological membranes, tissues and barriers underlies their biological, pharmacokinetic and metabolic properties. These properties can be predicted by calculating physicochemical characteristics of drug candidates using molecular descriptors.[30] In order to estimate if the proligands **HL^{1}**–**HL^{6}** and corresponding Cu(II) complexes demonstrate drug-like properties, they were evaluated with main stream molecular descriptors, such as molecular weight (MW), number of hydrogen bond donors and acceptors (HBD/HBA), *n*-octanol-water partition coefficient (log P), polar surface area (PSA) and rotatable bonds (RB). The results are shown in Table S7 in the Supporting Information. Based on the calculated physicochemical parameters, we determined if novel compounds belonged to the *drug-like* chemical space, which is commonly defined by the well-known Lipinski rule, or to the known drug space (KDS), which includes all small compounds in medical use.[31] As can be seen from Table S7, all compounds fell within the boundaries of *drug-like* chemical space with the exception of **HL^{4}** which demonstrated higher HBA value, referring to KDS space. Based on these results, novel compounds are expected to be sufficiently cell permeable. Following the calculations, we determined the lipophilicity of all compounds experimentally ($logD_{7.4}$, Tables 2 and 3). It is known that cancer cells accumulate hydrophilic compounds to a smaller extent relative to hydrophobic compounds, thereby affecting their activity. Hence, the differences in the lipophilicity of compounds might be related to the observed trends in cytotoxicity of **1**–**6**. In general, with the exception of morpholine derivative **HL^{4}**, proligands which were obtained by systematic substitution at the terminal thioamide nitrogen, demonstrated higher lipophilicity when compared to that of **HL^{1}**. As expected, proligands were more lipophilic than the corresponding Cu(II) species, which are positively charged at physiological pH (Figure 3b). Among Cu(II)-TSC complexes, only the least cytotoxic complexes **1** and **6**, as well as cisplatin, demonstrated negative $logD_{7.4}$ values, indicating their higher hydrophilicity. The lipophilicity of **2**–**5**

increased in the following order **4** < **2** < **3** < **5**, and correlated well with their cytotoxicity in cancer cells, with the exception of **3**. Subsequently, we determined the total cellular accumulation of Cu in A2780 cells by ICP-MS upon 24 h exposure to **1**–**6** in comparison with $CuCl_2$ (Table 4). The IC_{50} values from MTT assays with 72 h drug exposure varied from nanomolar to high micromolar concentrations; therefore, in the cellular accumulation experiment cells were treated with 1 μM of compounds of interest for 24 h to minimize cell detachment. The cellular accumulation of all Cu(II)-TSC complexes was significantly higher than for $CuCl_2$, indicating the role of lipophilic TSC ligands in the delivery of the complexes into the cells. The accumulation increased in the order **6** < **1** < **3** < **4** < **2** < **5**.

Cellular accumulation and efflux of Cu(II)-TSC complexes are energy- and/or temperature-dependent processes. Dependence of cytotoxicity on lipophilicity of **1**–**6** indicates that their cellular accumulation at least partially occurs via passive diffusion. In order to gain additional insights into the mechanisms controlling the accumulation of Cu(II)-TSC complexes, we investigated the effects of temperature and various inhibitors on total cellular accumulation of **2** with the results shown in Figure 5. A2780 cells were treated with **2** at 3 μM for 30, 60 and 120 min at 37 and 4 °C and intracellular Cu content was measured by ICP-MS. Prolonged incubation at low temperatures may result in the changes in membrane fluidity, decreasing membrane permeability and restricting drug uptake;[32] therefore, the shorter time point of 10 min was also included. The cellular accumulation of **2** dramatically decreased at low temperature even after 10 min treatment, indicating the involvement of active carrier-mediated transport or facilitated diffusion. Likewise, the decrease of cellular accumulation at low temperatures has been reported for both Cu(II)-TSC complexes and metal-free TSCs.[33,34] To further clarify whether the uptake of **2** requires energy, the cellular ATP production was blocked by incubating cells in a saline solution (HBSS), resulting in total starvation and rapid reduction of intracellular ATP content, and/or by addition of oligomycin, leading to the inhibition of oxidative phosphorylation.

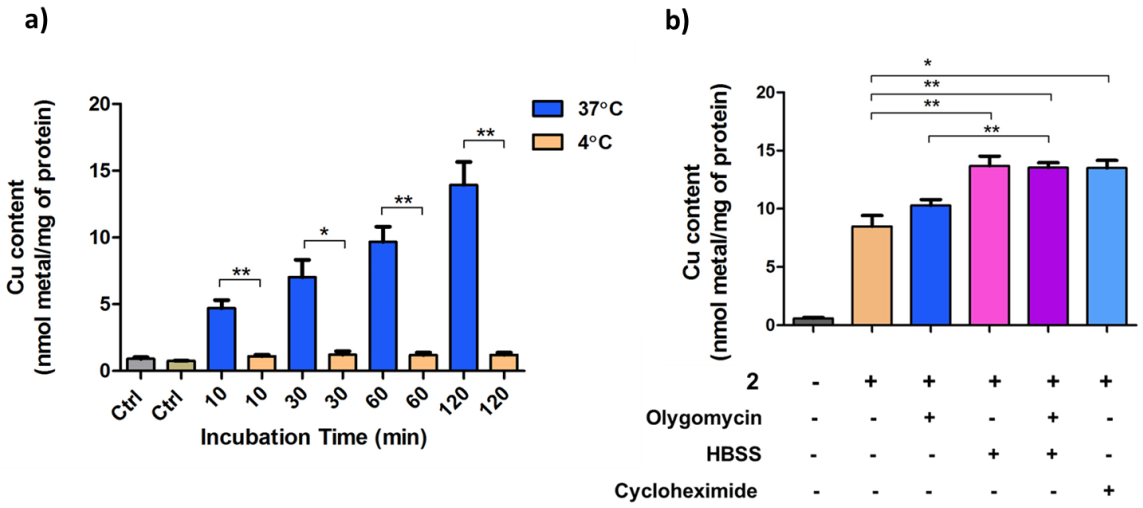

Figure 5. Effects of temperature and inhibitors on the accumulation of **2** in A2780 cells. Intracellular content was determined by ICP-MS: a) A2780 cells were treated with **2** (3 μM) at 37 or 4 °C for the indicated time periods. b) A2780 cells were pre-treated with oligomycin (5 μM), and/or pre-incubated in HBSS for 1 h, or pre-treated with cycloheximide (100 μM) for 4 h and subsequently co-treated with **2** (3 μM) for 1 h. The presence of inhibitors did not show any effects on the intracellular Cu level of untreated A2780 cells (data not shown). Statistical analysis was performed by two-tailed T-test using GraphPad Prism software (GraphPad Software Inc., CA) with $p < 0.05$ considered as significant (* $p < 0.05$, ** $p < 0.01$).

When A2780 cells were pre-treated with 5 μM of oligomycin for 1 or 4 h and subsequently co-treated with 3 μM of **2**, the intracellular Cu levels were not affected, even though the mitochondrial respiration of the cancer cells was successfully inhibited (data not shown). However, when A2780 cells were starved in HBSS for 1 h and subsequently treated with 3 μM of **2** for 1 h, an increase in intracellular Cu content was observed. Co-treatment of **2** with 5 μM of oligomycin in HBSS did not result in a further increase of intracellular Cu levels. The increase of Cu content in HBSS-starved cells might stem from the inhibition of energy-dependent efflux processes. In order to assess the role of proteins in both cellular accumulation and efflux of **2**, A2780 cells were pre-treated with cycloheximide, which is a known inhibitor of protein synthesis. Significant increase of intracellular Cu content was observed, similar to HBSS starvation, providing further evidence for the involvement of protein-dependent efflux processes. Similar effects have been reported for related Cu(II)-TSC complexes.[33] Accumulated data provide evidence that cellular accumulation of **2** occurs via carrier-facilitated diffusion, which might co-exist with passive permeation through the lipid bilayer.[35] The efflux processes, however, are actively mediated by proteins and upon inhibition of protein synthesis or energy production a strong increase of intracellular Cu concentration was observed.

Cu(II)-TSC complexes demonstrated high antibacterial activity against *S. aureus* in a comparable concentration range to ciprofloxacin. The antibacterial activity of **HL^{1}**–**HL^{6}** and **1**–**6** on planktonic cells of *P. aeruginosa* and *S. aureus* was investigated by determination of MIC_{50} and MIC_{100} values (Table 3). Overall, compounds showed a higher antimicrobial activity against Gram-positive (*S. aureus*) compared to Gram-negative bacteria (*P. aeruginosa*). The highest activity against *S. aureus* was observed for **2**–**5**, which specifically inhibited its growth with MIC_{50} values ranging between 2 and 5 μg/mL and completely abolished its growth at 10 μg/mL (MIC_{100}). This activity is comparable but slightly lower that the antibacterial activity of a well-known benchmarked antibiotics ciprofloxacin (CPX). On the contrary, *P. aeruginosa* exhibited high resistance to most of the compounds tested with the exception of **HL^{2}** and **2** with MIC_{50} values at 70 and 50 μg/mL, respectively.

Table 3. Antibacterial activity of **HL$^{1–6}$** and **1**–**6**[a]

	***S. aureus* (μg/mL)**		***P. aeruginosa* (μg/mL)**	
	MIC_{50}	**MIC_{100}**	**MIC_{50}**	**MIC_{100}**
HL^{1}	100	>400	NA	NA
HL^{2}	10	400	50	100
HL^{3}	10	300	100	NA
HL^{4}	100	>400	NA	NA
HL^{5}	10	300	NA	NA
HL^{6}	NA	NA	NA	NA
1	100	>500	NA	NA
2	2	10	70	200
3	3	10	100	400
4	5	10	100	400
5	3	10	200	450
6	NA	NA	200	NA
Ciprofloxacin	0.5	1	0.5	2

[a]See experimental section for details. NA denotes no antibacterial activity detected (>500 μg/mL).

Compounds **HL^{6}** and **6** based on S-methylisothiosemicarbazide were completely devoid of antibacterial activity and no inhibition of bacterial growth was observed at the whole concentration range tested. Interestingly, metal-free thiosemicarbazones **HL^{1}**–**HL^{5}** displayed relatively low antibacterial activity (MIC_{100} > 300 μg/mL), which was significantly enhanced upon coordination to Cu(II). Subsequently, the mode of action of

the most active compounds **2**–**5** was evaluated in *S. aureus* and *P. aeruginosa* using the Live/Dead viability assay. As shown in Figure 6, compounds **2**–**5** greatly reduced cell replication, reflected by the lower number of cells compared to the untreated sample and high percentage of PI-stained cells, indicating compromised cell membrane allowing the penetration of propidium iodide and a bacteriostatic action of these compounds.

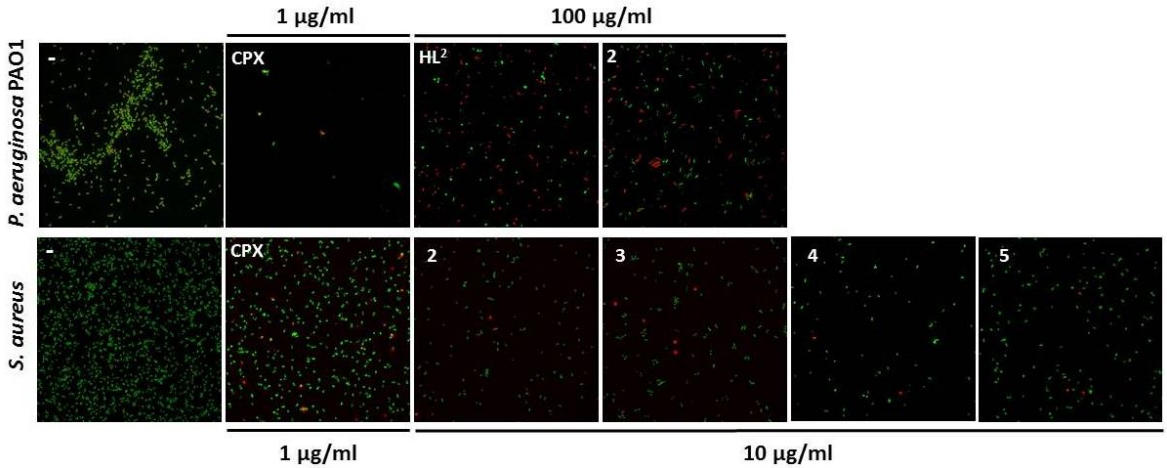

Figure 6. Live/dead bacterial cells are shown by staining with green fluorescence indicating live cells and red fluorescence indicating dead cells.

TSCs and their Cu(II) complexes are located in a close proximity to the active site of mouse R2 RNR protein. Next, the RNR inhibitory potential of the TSC proligands **HL^1**–**HL^6** and their corresponding Cu(II) complexes **1**–**6** was investigated. The proligands **HL^1**–**HL^6** and Cu(II) complexes **1**–**6** were docked into the crystal structure of mouse R2 RNR subunit (PDBid:1W68)[36] using GOLD software.[37] To predict the binding of **1**–**6**, the GoldScore function was used and its parameters were modified to include Cu since they are not in GOLD's database.[38] The scoring functions are presented in Table S8. Overall, similar docking results were observed for all proligands and their Cu(II) complexes**,** suggesting a plausible binding to the mouse R2 protein. The compounds were deeply embedded into the pocket of the R2 subunit, close to the diferric center (Fe_2O), and the enzymatically essential tyrosyl residue (Tyr177). The docked configuration of **5** in comparison with Triapine into the binding site is shown in Figure 7. An overlap with Triapine was predicted, resulting in a partial reproduction of a hydrogen-bonding pattern (Figure S14, Table S8).

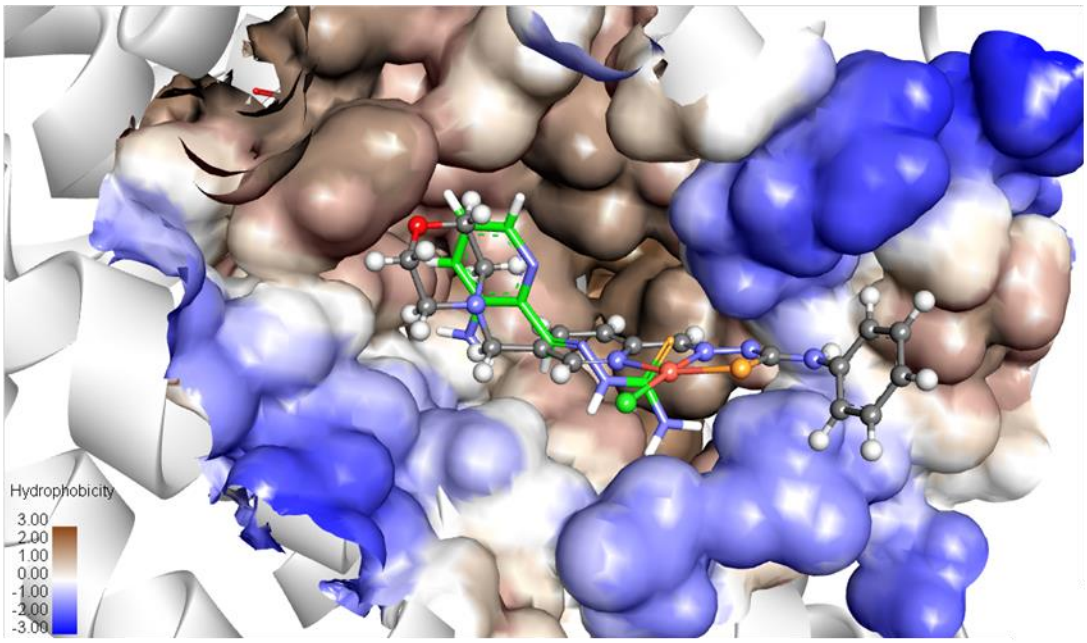

Figure 7. The overlay of docked configurations of Cu(II) complex **5** (grey) and Triapine (green) in the binding site of the mouse R2 RNR protein (PDB ID: 1W68). The surface is rendered. Blue and brown depict hydrophilic and hydrophobic areas, respectively.

Lead TSCs and their Cu(II) complexes cause moderate inhibition of a mouse R2 RNR protein in a reducing environment as a result of iron chelation. The effects of the most cytotoxic complexes **2** and **5**, and the corresponding proligands $\mathbf{HL^2}$ and $\mathbf{HL^5}$, on the mouse R2 tyrosyl radical were investigated by EPR spectroscopy at 30 K. The proligands and their Cu(II) complexes were incubated with the mouse R2 RNR protein at 1:1 protein-to-compound mole ratio at 298 K in the presence or absence of the reducing agent dithiothreitol (DTT), and the time-dependent reduction of the tyrosyl radical was monitored.[39] Tyrosyl radical reduction by the investigated compounds was observed only in the presence of DTT. Upon incubation with $\mathbf{HL^2}$, $\mathbf{HL^5}$ and **2**, **5**, 50% of tyrosyl radical was reduced within 90 s, after which no further reduction was observed (Figure S15). Since the diferric center of the mouse R2 protein is expected to be reduced upon addition of DTT,[40,41] the ability of proligands $\mathbf{HL^2}$ and $\mathbf{HL^5}$ to form stable Fe(II) complexes was investigated by monitoring these reactions by UV–vis measurements in buffered aqueous solutions at pH 7.4. $\mathbf{HL^2}$ and $\mathbf{HL^5}$ (λ_{max} = 312 and 320 nm, respectively) readily reacted with $FeSO_4 \cdot 7H_2O$ affording Fe(II) bis-ligand complexes (λ_{max} = 373, 610 nm and λ_{max} = 385, 645 nm, respectively) at both 1:1 and 1:2 Fe-to-ligand mole ratios. Additionally, the formation of Fe(III) complexes with the subsequent reduction by DTT was investigated (Figure S15). $\mathbf{HL^2}$ and $\mathbf{HL^5}$ reacted with $FeCl_3 \cdot 6H_2O$ (at 1:1 or 1:2 Fe-to-ligand mole

ratios) to give $[Fe^{III}(L^2)_2]^+$ and $[Fe^{III}(L^5)_2]^+$ complexes (λ_{max} = 378 nm, 612 nm and λ_{max} = 386 nm, 635 nm, respectively). The formation of $[Fe^{III}(L^5)_2]^+$ species was confirmed by ESI-MS (Figure S16). The absorption spectra of reduced forms were almost identical to those of Fe(II) bis-ligand species, and to the previously reported spectra of other Fe^{II}-TSC complexes.[42]

HL^2 and 2 induced unfolded protein response (UPR), antioxidant defense and cell cycle perturbations. In order to get further insight into the mechanism of action of **2**, Western Blotting of ER stress-related protein markers, namely IRE1α, CHOP, BiP/GRP78 and p-ERK, was performed (Figure 8). When A2780 cells were treated with increasing concentrations of **2** for 24 h, the dose-dependent upregulation of IRE1α and CHOP proteins, decrease of ER stress chaperone BiP/GRP78, as well as phosphorylation of ERK were observed as a response to ER stress. To assess the effects of **2** on the cell cycle, we examined the expression of cyclin D1 and cyclin B1 which serve as cell cycle regulatory switches in actively proliferating cells and are required for cell cycle progression in G_1 and G_2 phases, respectively. Complex **2** displayed significant inhibition of cyclin D1 expression, indicating cell cycle arrest at G_1/S phase, whereas no changes in cyclin B1 expression were detected. Subsequently, we compared the effects of **2** and the respective proligand **HL^2** on the expression of p-ERK1/2 and the marker of antioxidant defence NRF2. Both **HL^2** and **2** demonstrated phosphorylation of ERK1/2; however, the effects on NRF2 were markedly different. Whereas no increase of NRF2 expression was observed, when cells were treated with **HL^2**, complex **2** induced increased expression of NRF2 even at low concentration, indicating activated antioxidant defense, possibly as a result of ROS insult caused by Cu(II) reduction.

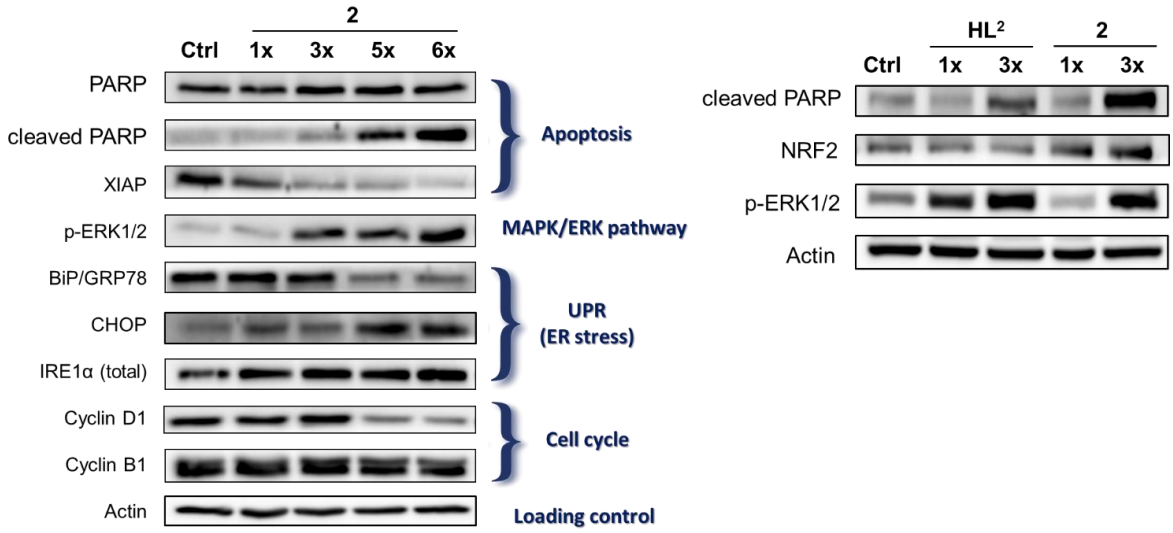

Figure 8. Western Blot analysis of various proteins. A2780 cells were treated with increasing concentrations of proligand **HL**^{2} and complex **2** (corresponding to IC_{50} value from MTT experiment with exposure time of 72 h) for 24 h. Total lysates were isolated and examined by Western Blot. Actin was used as a loading control.

HL^2 **and 2 induced dose-dependent apoptosis accompanied by PARP cleavage and XIAP inhibition.** To elucidate if observed cytotoxicity of new compounds described in this study was a result of apoptosis induction, we conducted Annexin V/PI apoptosis assay. In brief, fluorochrome-labeled Annexin V reagent is used for detection of membrane phosphatidylserine (PS), which translocates to the cellular surface from the inner side of plasma membrane in the event of early apoptosis. Simultaneously, propidium iodide (PI) is used for detection of later stages of apoptosis or necrosis, which are characterized by loss of membrane integrity and accumulation of PI inside the cells. A2780 cells were treated with $2IC_{50}$ and $6IC_{50}$ concentrations of **HL**^{2} and **2** (IC_{50} values were obtained from MTT experiment in A2780 cells with the exposure time of 72 h). Results are illustrated in Figure 9. Upon incubation of A2780 cells with increasing concentrations of **HL**^{2} and **2**, the dose-dependent increase of apoptotic cells was observed.

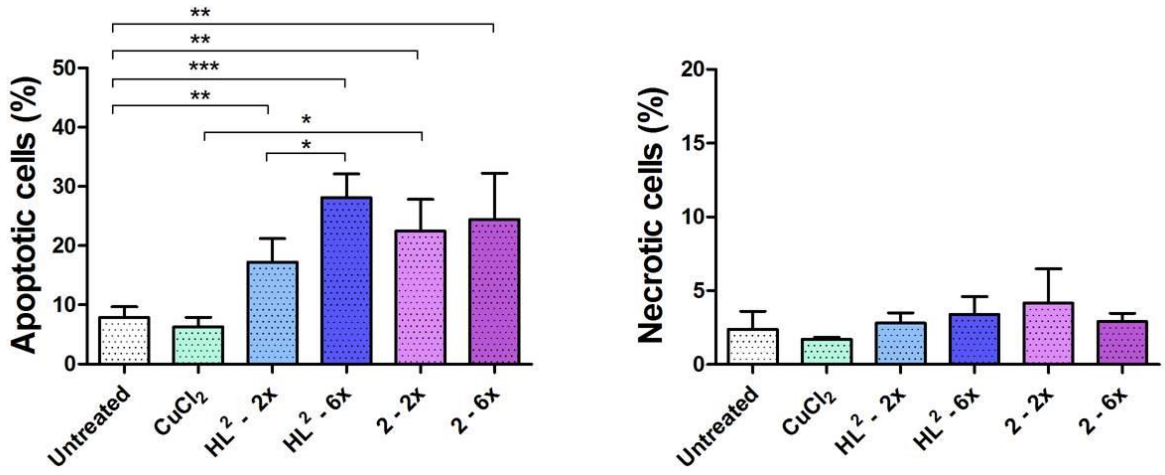

Figure 9. Bar graphs showing the percentage of cell death due to apoptosis (left) and necrosis (right) in A2780 cells treated with increasing concentrations of **HL²**, **2** ($2IC_{50}$ and $6IC_{50}$) and $CuCl_2$ and detected by Annexin V/PI apoptosis assay. Statistical analysis was performed by two-tailed T-test using GraphPad Prism software (GraphPad Software Inc., CA) with $p < 0.05$ considered as significant (* $p < 0.05$, ** $p < 0.01$).

At low concentrations both the proligand and Cu(II) complex induced a 2- to 3-fold increase of apoptotic cells in comparison with untreated cells (7.8 ± 1.8 %, 17.2 ± 3.9 % and 22.5 ± 5.3 % for untreated cells, **HL²** ($2IC_{50}$) and **2** ($2IC_{50}$), respectively). At high concentrations a further increase of apoptotic cells was observed (28.1 ± 4.0% and 24.4 ± 7.8.% for **HL²** ($6IC_{50}$) and **2** ($6IC_{50}$)). No significant differences between the apoptosis-inducing properties of the proligand **HL²** and **2** were noticed. When $CuCl_2$ was incubated with the cells at the concentration, corresponding to Cu content in **2** at $2IC_{50}$, no induction of apoptosis was detected, which can be explained by poor cellular accumulation of $CuCl_2$. The proportion of necrotic cells was negligible and no significant deviation from untreated cells was detected; therefore, the induction of necrosis by **HL²** and **2** was ruled out. Subsequently, the effects of **HL²** and **2** on apoptotic signaling in cells were investigated by Western Blotting. A2780 cells were treated with increasing concentrations of the drug for 24 h, and the cleavage of poly (ADP-ribose) polymerase-1 (PARP) was investigated (Figure 8). Cleavage of poly (ADP-ribose) polymerase-1 (PARP) through suicidal proteases such as caspases has been widely accepted as an indicator of apoptosis.[43] As can be seen in Figure 8, both **HL²** and **2** revealed a dose-dependent PARP cleavage, indicating apoptosis induction in agreement with the results of Annexin V/PI assay. Additionally, expression of X-linked inhibitor of apoptosis (XIAP) was markedly reduced in a dose-dependent manner upon treatment with increasing concentrations of **2**.

Discussion

The diverse biological and chemical properties of Triapine and other TSCs, as well as their transition metal complexes, have been extensively studied for decades. [41,44-51] Their antiproliferative and antibacterial activity varies greatly, from low nanomolar to high micromolar range, depending on the substituents at the TSC backbone.[16,20,52] Even though clinical trials demonstrated some benefits of patient treatment with Triapine, its low aqueous solubility and high toxicity prevent it from further clinical progress. In a continuous effort to improve the bioavailability and therapeutic profile of TSCs and Cu(II)-TSC complexes, novel thiosemicarbazone hybrids with bioactive L-proline, homoproline, piperazine or iminodiacetate moieties, using the molecular hybridization approach, have been designed and synthesized.[16-20] However, the improvement of the aqueous solubility was often accompanied by a significant decrease in cytotoxicity. In this study, the attachment of N-substituted morpholine moiety at the TSC backbone resulted in a simultaneous improvement of aqueous solubility and cytotoxicity (up to ~50 times in comparison with Triapine). To ensure the selectivity of novel TSCs towards cancer cells over healthy cells, their cytotoxicity against A2780 cancer cells and noncancerous HEK293 cells was compared. It was shown that new compounds were 2–5 fold more toxic towards cancer cells than healthy cells (Tables 1 and 2), whereas Triapine was more toxic towards noncancerous cells, which is in agreement with its known high toxicity. The coordination of TSCs to Cu(II) resulted in Cu(II)-TSC complexes with similar or improved antiproliferative activity. In general, when TSCs are coordinated to Cu(II), an increase in cytotoxicity is observed;[17,18,53] however, Cu(II)-Triapine complex was shown to be significantly less cytotoxic than Triapine itself.[27] The activity of the Cu(II) complexes **1–6** was in a good correlation with their lipophilicity, cellular accumulation, as well as their electrochemical redox potentials (Tables S6 and 2). Interestingly, metal-free TSCs exhibited only low antibacterial properties against *S. aureus*, whereas Cu(II)-TSC complexes revealed significant antibacterial activity similar to that of the commonly used antibiotic ciprofloxacin (Table 4). These results indicate that coordination of TSCs to Cu(II) improved their therapeutic potential. It should be noted that the replacement of N,N,S- with N,N,N-chelating moiety in **6** resulted in a drop of cytotoxicity and antibacterial activity, which is in agreement with the previously reported data.[20]

The antiproliferative activity of Triapine and other TSC proligands is often related to their Fe-chelating properties.[54] To sustain their high proliferation rate, cancer cells rely on

increased uptake of Fe from Fe-transporting proteins; therefore, Fe chelation is a valuable therapeutic strategy for cancer treatment. Based on UV–vis and ESI-MS experiments, it was demonstrated that irrespective of metal-to-ligand ratio, proligands **HL^2** and **HL^5** readily reacted with Fe(III) to form $[Fe^{III}(L^2)_2]^+$ and $[Fe^{III}(L^5)_2]^+$ species, which could be reduced to Fe(II) bis-ligand complexes by the reducing agent DTT. These results indicate that morpholine-TSC hybrids, investigated in this study, may act as Fe chelators. Additionally, spectroelectrochemical experiments revealed that under reducing conditions, the Cu(II)-TSC complexes could undergo reversible reduction to Cu(I) species, with simultaneous release of proligands, suggesting that these complexes may act as Fe chelators, also in cancer cells. In addition, the presence of the Cu(II) ion in the cells may lead to the production of ROS *in vivo*, due to Cu(II)/Cu(I) redox cycling.[55]

It is well known that one of the mechanisms contributing to the cytotoxic effects of Fe chelators is inhibition of the RNR enzyme, which is highly expressed in cancer cells, and essential for their DNA synthesis. The mechanism of RNR inhibition by Triapine has been extensively studied by several research groups.[41-56] It has been proposed that Triapine interferes with the assembly of the differic-tyrosyl radical cofactor in R2, necessary for the catalytic activity of RNR.[46,56] Moreover, it has been shown that the presence of Fe is required for effective R2 inhibition,[44,45] and that it is actually the Fe(II)-Triapine species that is responsible for the R2-specific RNR inhibitory effect of Triapine.[41,46,47,51,58] The Fe(II)-Triapine complex may be formed by chelation of Fe from the differic cofactor in R2 *in vitro*,[44,41] and/or from intracellular iron pools *in vivo*.[46,56] The potent inhibition of human,[47] and mouse[41] R2 RNR *in vitro* by catalytic amounts of Fe(II)-Triapine has been proposed to involve ROS. Namely, ROS had been spin-trapped, and detected by EPR spectroscopy, in the aerobic reaction between human R2 RNR and Fe(II)-Triapine, which had implicated that O_2 is important in tyrosyl radical destruction, and that ROS may ultimately be responsible for the pharmacologic effects of Triapine *in vivo*.[47] In another study of time-dependent tyrosyl radical reduction in mouse R2 by Triapine, and its Zn, Ga, Cu, and Fe complexes, the requirement of O_2 in R2 inhibition was also suggested.[41] This was based on the observation that substoichiometric amounts of Fe(III)-Triapine relative to R2 (protein-to-complex mole ratio, 5:1) reduced only 20% tyrosyl radical in anaerobic conditions, compared to 100% in aerobic conditions. However, more recently, in a different experimental setup, namely in the presence of a 10-fold excess of Fe(II)-Triapine over R2 protein, the role of ROS (and O_2) in human R2 inhibition was excluded.[51] This

study showed that the principle mechanism of human R2 RNR inhibition by Triapine, based on kinetic measurements of tyrosyl radical, and ^{55}Fe loss, is direct radical quenching, in an iron-loaded protein. Furthermore, it implied that Fe(II)-Triapine can rapidly reduce the tyrosyl radical, while leaving the protein in the met-state.

In order to investigate if R2 RNR could be the potential biomolecular target for the novel morpholine-TSC hybrids, and their Cu(II) complexes, molecular docking studies, and R2 RNR tyrosyl radical reduction kinetic experiments, were performed. It has been suggested that the efficiency of R2 inhibition is likely to depend on the access of the inhibitors to the differic center of R2;[41,47] therefore, we estimated the likelihood of the binding of TSC proligands **HL^1**–**HL^6** and their corresponding Cu(II) complexes **1**–**6** to the surface of the R2 protein. It was demonstrated that new TSCs, and their Cu(II) complexes were deeply embedded into the pocket of the R2 protein and exhibited hydrogen bonding patterns similar to Triapine (Figure 7). Based on the results of the molecular docking studies suggesting plausible binding to the mouse R2 protein, the time-dependent tyrosyl radical reduction in the mouse R2 protein upon incubation with the most cytotoxic complexes, **2** and **5**, and the corresponding proligands **HL^2** and **HL^5**, at a 1:1 protein-to-compound ratio, was measured by EPR spectroscopy. Only in the presence of DTT (which can reduce Fe(III) to Fe(II) in the R2 differic cofactor),[40] **HL^2** and **HL^5** caused 50% tyrosyl radical reduction (Figure S15a). These results show that R2 inactivation by **HL^2** and **HL^5** is not as efficient as with Triapine, which causes 100% tyrosyl radical loss in mouse R2 after 5 min (in the same experimental conditions).[41] The most plausible explanation for this observation is that different mechanisms are likely to be involved in R2 inhibition by **HL^2**, **HL^5** and Triapine. The R2 inhibitory activity of the corresponding Cu(II) complexes **2** and **5** was found to be similar to that of the proligands (Figure S15a). This is likely due to the fact that in the presence of DTT, the reduction of Cu(II) to Cu(I) leads to the release of the proligands, which is in agreement with the results of spectroelectrochemical experiments (*vide supra*). Since the UV–vis, and ESI-MS experiments showed that **HL^2** and **HL^5** act as tridentate ligands, and form stable Fe(II)L_2 complexes (Figure S15), it is possible to propose that the mechanism of R2 inhibition by the TSC proligands involves Fe chelation from the differic cofactor. Based on the extent of tyrosyl radical reduction, it is tempting to speculate that the subsequently formed Fe(II) complexes are not potent inhibitors like the Fe(II)-Triapine complex. However, as this was not the aim of this paper, it is reasonable to refrain from any conclusions prior to the detailed mechanistic studies of mouse, human,

and p53 R2 RNR inhibition by the morpholine-TSC hybrids. Moreover, a separate study should be dedicated only to the comparison of the inhibitory potentials of selected TSCs, and their Fe(II) complexes, in order to comprehensively understand the structure-activity relationship, which in turn may explain the mechanism of R2 RNR inhibition. Finally, even though R2 inhibition can be partially attributed to the marked anticancer activity of **2** and **5,** other biomolecular targets are likely to be involved (Figure 10).

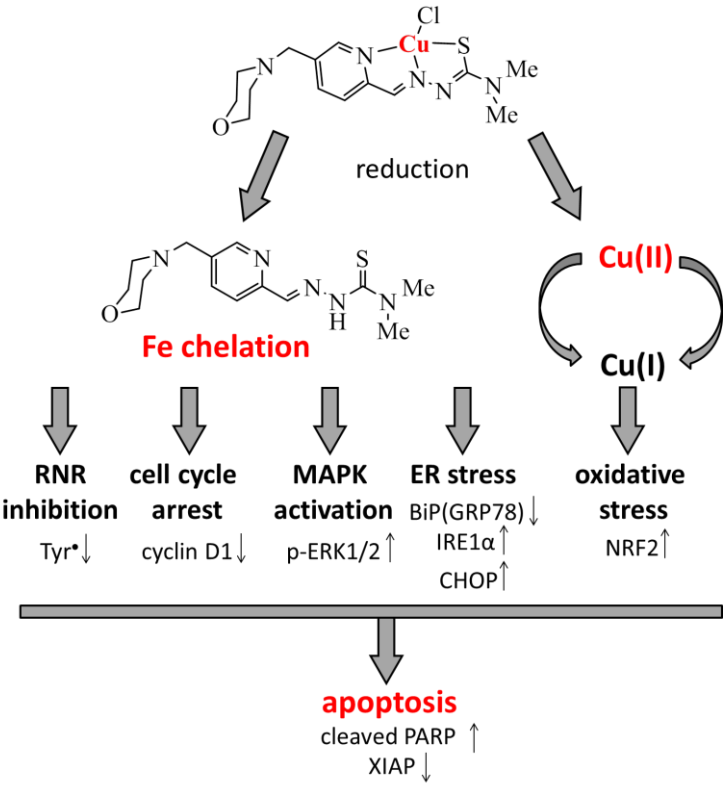

Figure 10. Proposed molecular mechanism of complex **2.**

Fe homeostasis is an intrinsically complex process; hence, Fe sequestration results in the alteration of various biomolecular pathways. Besides RNR, Fe depletion affects multiple molecular targets including those regulating the cell cycle.[57] It has been reported that the expression of cyclin D1, which ensures the progression through the G_1/S phase, was strongly dependent on the cellular Fe status.[58] It is believed that in Fe-depleted conditions, down-regulation of cyclin D1 prevents cells from entering the S phase, where Fe is needed for the activity of the RNR enzyme and DNA synthesis.[59] Fe chelation by TSCs often results in the down-regulation of cyclin D1 and subsequent cell cycle arrest at the G_1/S phase.[60,61] As expected, complex **2** was shown to induce strong dose-dependent down-regulation of cyclin D1, whereas the protein expression of cyclin B1, which is responsible for G_2/M progression, remained unchanged. In order to further investigate the potential

biomolecular targets of Fe-chelating compounds of interest, we studied the phosphorylation of ERK protein, which belongs to the MAPK family. The MAP kinases occupy the central position in cell growth and apoptosis and each MAP kinase member plays a different role in cellular responses.[62] It was reported that some Fe chelators induced cancer cell death associated with the activation of p38 MAPK and ERK.[63] Moreover, the MAPK-mediated cell death was characterized by the decreased expression of cyclin D1.[64] Complex **2**, as well as the corresponding proligand **HL^2** caused dose-dependent phosphorylation ERK in line with its activation, suggesting that MAPK pathway might be a potential mediator of the cell death, induced by this complex.

Recently, it was discovered that chelation and depletion of intracellular Fe leads to the activation of certain ER stress-response proteins.[65,66] Previously, several TSCs and their Cu(II) complexes were reported to induce ER stress, characterized by UPR activation,[67,68] ER expansion and release of intracellular calcium.[69] Since under reducing conditions, the novel TSCs and their Cu(II) complexes demonstrated formation of Fe(II)-TSC complexes, it may be suggested that they could possibly induce sequestration of cellular Fe resulting in the ER stress. It occurs due to the accumulation of misfolded and/or unfolded proteins in ER, resulting in the disruption of cellular homeostasis. In order to overcome stress, cells activate a rescue program known as UPR, which operates via several signaling pathways, namely ATF6, PERK and IRE1α. However, in case of severe ER stress, the pro-survival program is switched off and pro-apoptotic signaling takes place, characterized by the enhanced expression of CHOP protein. Complex **2** was shown to induce dose-dependent increase in the expression of IRE1α and CHOP proteins, indicating the induction of UPR signaling as a result of ER stress. Cell treatment with **2** resulted in a concentration-dependent decrease of BiP/GRP78 protein marker. The ER chaperon BiP/GRP78 plays a central role in the survival machinery and its overexpression is associated with tumor progression and metastases.[70] The inhibition of BiP/GRP78 indicates severe ER stress, resulting in the suppression of pro-survival chaperones. The antibacterial properties of novel Cu(II)-TSC complexes can be also related to ER stress induction, since it was recently demonstrated *in vitro* and *in vivo* experiments that chemical modulation of ER stress might result in the overload of its machinery that can be effective in elimination of bacterial infection.[71] Additionally, it was reported that efficient killing of methicillin-resistant *S. aureus* was dependent on the induction of IRE1α UPR pathway and required sustained generation of ROS.[72] Based on the observations that **2**, but not proligand **HL^2**

induced antioxidant defence in cancer cells characterized by NRF2 induction, it may be speculated that the ability of **2**, but not proligand **HL^2**, to induce oxidative and ER stress, may be related to the beneficial antibacterial activity of Cu(II)-TSC complexes over metal-free TSCs. However, it is not clear yet why new complexes **1**–**6** did not inhibit the growth of *P. aeruginosa* and their mechanism of action should be investigated in more detail.

In order to cope with the severe perturbations imposed by drug treatment, cancer cells develop adaptive responses to provide them with survival advantage. However, novel TSCs and their Cu(II) complexes significantly disturbed cellular life-death balance towards cell death resulting in the induction of apoptosis. Both proligand **HL^2**, and complex **2** were demonstrated to induce apoptosis characterized by PARP cleavage, decreased expression of XIAP and increased PS translocation. It should be noted that XIAP is a determining factor of cisplatin chemoresistance in ovarian cancer cells as it effectively suppresses apoptosis via caspase-3 and caspase-7 inhibition.[73] Therefore, the ability of **2** to decrease XIAP expression is highly important and to the best of our knowledge has not been previously reported for TSCs and metal thiosemicarbazonates, with the exception of Triapine.[74] Some TSCs and their respective Cu(II) complexes have been reported to simultaneously induce various types of cell death including apoptosis,[75,76] autophagy[76,77] and methuosis, which is a very special form of non-apoptotic cell death involving massive cytoplasmic vacuolization.[78] Therefore, induction of other forms of cell death by new TSCs and their Cu(II) complexes presented in this study cannot be excluded. The results show that the attachment of the morpholine moiety at the TSC backbone and the subsequent coordination to Cu(II), resulted in new drug candidates, likely with better therapeutic profile than Triapine and a promising potential for further clinical development.

Conclusions

One of the reasons hindering the clinical development of Cu(II) thiosemicarbazone complexes is their low aqueous solubility. The decoration of the TSC backbone with functional groups that increase the aqueous solubility and bioavailability often results in a significant decrease of the compound activity. In this work, attachment of a morpholine moiety to 2-formylpyridine (iso)thiosemicarbazone in position 5 of 2-formylpyridine moiety yielded new water-soluble TSC-morpholine hybrids and their Cu(II) complexes, which demonstrated high antiproliferative activity against cisplatin-sensitive and cisplatin-

resistant ovarian carcinoma cells, in a nanomolar to submicromolar concentration range. Sufficient aqueous solubility of the new compounds enabled the study of their solution behavior and electrochemical properties under conditions similar to the intracellular environment. Solution speciation studies of **1** revealed that the dissociation of the complex does not occur at the physiological pH, even at micromolar concentrations, indicating its high stability in aqueous media. However, under reducing conditions associated with the cancer cell environment, the reversible reduction of Cu(II) with subsequent release of the proligand within the biologically accessible electrochemical window is plausible. Since the R2 RNR protein is believed to be one of the biomolecular targets of TSCs, and the fact that the proligands form 2:1 complexes with Fe(II), the chelation of Fe(II) from R2 was expected. The Cu(II)-TSCs and their corresponding proligands showed only moderate Tyrosyl radical reduction in mouse R2. Therefore, the marked anticancer activity of the compounds investigated in this work was not solely related to their RNR inhibitory potential, but also to the induction of apoptosis as a result of ER stress, MAPK activation and cell cycle perturbations. Studies of the mechanisms controlling cellular accumulation of the lead drug **2** have shown that it accumulates in cancer cells as a result of passive and/or facilitated diffusion. Finally, it was discovered that coordination of TSC ligands to Cu(II) resulted in a significant enhancement of their antibacterial properties against *S. aureus*. The combination of excellent antiproliferative and antibacterial activity, as well as water-solubility, is a sound basis for further development of this class of Cu(II) thiosemicarbazonates as dual pharmaceutical agents.

Experimental

1. Chemicals. 2,5-Pyridinecarboxylic acid was purchased from Alfa Aesar. Ethylenediaminetetraacetic acid (EDTA), KOH and 4-(2-hydroxyethyl)-1-piperazineethanesulfonic acid (HEPES) were purchased from Sigma-Aldrich in puriss quality. KCl, $CuCl_2$, hydrochloric acid and *n*-octanol are products of Molar Chemicals. $CuCl_2$ stock solution was prepared from anhydrous $CuCl_2$ and water and its exact concentration was determined by complexometry through the EDTA complex. All solvents were of analytical grade and used without further purification. Milli-Q water was used for sample preparation. The synthesis of the 5-methylmorpholine-pyridine-2-carboxaldehyde **H** (Scheme 1) is described in detail in Supporting Information. Chemical grade cisplatin (1 mg/mL) was purchased from Hospira Pty Ltd (Melbourne, Australia). IGEPAL CA-630, DL-dithiothreitol (DTT), tetramethylethylenediamine (TEMED), sodium deoxycholate,

non-fat dried milk bovine, TWEEN® 20, ponceau S, propidium iodide (PI) were purchased from Sigma-Aldrich (St Louis, MO, USA). Thiazolyl Blue tetrazolium bromide (MTT) was purchased from Alfa Aesar. Tris was purchased from Vivantis Technologies. Glycine, Hyclone™ Trypsin Protease 2.5% (10×) solution, RPMI 1640, DMEM medium, Fetal bovine serum (FBS), Bovine Serum Albumin (BSA), Hank's Balanced Salt Solution (HBSS) and Pierce™ Protease and Phosphatase Inhibitor Mini Tablets were purchased from Thermo Fisher Scientific. Hyclone™ Dulbecco's Phosphate-Buffered Saline (10×), were purchased from GE Healthcare Life Sciences. Biorad protein assay dye reagent concentrate, 30% Acrylamide/Bis solution, 5× Laemmli Sample Buffer, Nitrocellulose Membrane (0.2 μm) were purchased from Bio-rad Laboratories. Luminata™ Classico and Crescendo Western HRP substrate were purchased from Merck Millipore Corporation. Milli-Q-grade purified water was obtained from a Milli-Q UV purification system (Sartorius Stedim Biotech S.A., Aubagne Cedex, France). All antibodies were obtained from Cell Signaling Technologies (Beverly, MA, USA). Nitric acid (65% to 71%, *Trace*SELECT Ultra) for ICP-MS analysis and $n\text{Bu}_4\text{NPF}_6$ for cyclic voltammetry experiments were obtained from Fluka (Sigma Aldrich) and used without further purification. Cu and In standards for ICP-MS measurements were obtained from CPI international (Amsterdam, The Netherlands). Cycloheximide, oligomycin, annexin V-FITC apoptosis detection reagent (500X) were purchased from Abcam (Cambridge, UK).

2. Synthesis of proligands.

The yields, m.p. and analytical data for **HL^1**–**HL^6** and **1**–**6** are presented in Tables S9 and S10. The experimental CHNS contents were within ±0.4 with those calculated, providing evidence for ≥95% purity.

5-(morpholinomethyl)pyridine-2-carboxaldehyde thiosemicarbazone (HL^1). 5-morpholinomethyl-pyridine-2-carboxaldehyde (0.29 g, 1.41 mmol), thiosemicarbazide (0.13 g, 1.41 mmol) and EtOH (5 mL) were mixed in a 25 mL Shlenk tube. The reaction mixture was stirred at 78 °C overnight. The next day the reaction mixture was cooled to room temperature and stored at 4 °C for 4 h. The white crystalline precipitate was filtered off, washed with cold EtOH and dried in vacuo. Yield: 0.34 g. ^{1}H NMR 500 MHz (DMSO-d_6, *δ*, ppm): ^{1}H NMR (500 MHz, DMSO) δ 11.62 (s, 1H, NH^{16}), 8.48 (d, *J* = 1.3 Hz, 1H, H^6), 8.34 (s, 1H, NH^{19}), 8.24 (d, *J* = 8.1 Hz, 1H, H^3), 8.15 (s, 1H, NH^{19}), 8.09 (s, 1H, H^{14}), 7.74 (dd, *J* = 8.2, 1.7 Hz, 1H, H^4), 3.59 – 3.54 (m, 4H, H^{10}, H^{12}), 3.51 (s, 2H, H^7), 2.36 (s,

4H, H^9, H^{13}). ^{13}C NMR (126 MHz, DMSO) δ 178.74 (C_q, C^{17}), 152.73 (C_q, C^2), 150.12 (CH, C^6), 142.85 (CH, C^{14}), 137.51 (CH, C^4), 134.23 (C_q, C^5), 120.23 (CH, C^3), 66.57 ($2CH_2$, C^{10}, C^{12}), 59.74 (CH_2, C^7), 53.49 ($2CH_2$, C^9, C^{13}). IR (ATR, selected bands, $\tilde{\upsilon}_{max}$): 1612, 1527, 1468, 1400, 1339, 1274, 1102, 1004, 938, 859, 626 cm^{-1}.

5-(morpholinomethyl)pyridine-2-carboxaldehyde 4,4-dimethyl-3-thiosemicarbazone (HL^2). 5-(morpholinomethyl)pyridine-2-carboxaldehyde (0.29 g, 1.41 mmol) and 4,4-dimethyl-3-thiosemicarbazide (0.17 g, 1.41 mmol) were dissolved in EtOH (5 mL) and stirred in a Shlenk tube at 78 °C for 2 h until the solution became clear. The reaction mixture was left to stand at 4 °C for 6 h. The yellow crystalline precipitate was filtered off, washed with cold EtOH and dried in vacuo. Yield: 0.25 g. ^1H NMR (500 MHz, DMSO) δ 15.08 (s, 1H, NH^{16}), 8.71 (s, 1H, H^3), 8.49 (s, 1H, H^6), 8.23 (d, 1H, H^{14}), 7.76 (dd, *J* = 13.9, 8.1 Hz 1H, H^4), 3.59 (s, 4H, H^{10}, H^{12}), 3.52 (s, 2H, H^7), 3.38 (s, 4H, H^{20}, H^{21}), 2.37 (s, 4H, H^9, H^{13}).^{13}C NMR (126 MHz, DMSO) δ 180.02 (C_q, C^{17}), 153.06 (C_q, C^2), 150.27 (CH, C^6), 148.84 (CH, C^3), 144.29 (CH, C^{14}), 137.75 (CH, C^4), 134.06 (C_q, C^5), 66.61 ($2CH_2$, C^{10}, C^{12}), 59.77 (CH_2, C^7), 53.53 ($2CH_2$, C^9, C^{13}), 42.72 ($2CH_3$, C^{20}, C^{21}). IR (ATR, selected bands, $\tilde{\upsilon}_{max}$): 1497, 1443, 1362, 1303, 1209, 1158, 1108, 1064, 1003, 901, 862, 716, 627 cm^{-1}.

5-(morpholinomethyl)pyridine-2-carboxaldehyde *N*-pyrrolidinylthiosemicarbazone (HL^3). 5-(morpholinomethyl)pyridine-2-carboxaldehyde (0.29 g, 1.41 mmol) and *N*-pyrrolidine-3-thiosemicarbazide (0.20 g, 1.41 mmol) were dissolved in EtOH (5 mL) and stirred in a Shlenk tube at 78 °C for 2 h until the solution became clear. The mixture was left to stand at 4 °C for 12 h. The yellow crystalline precipitate was filtered off, washed with cold EtOH and dried in vacuo. Yield: 0.36 g. ^1H NMR (500 MHz, DMSO) δ 11.23 (s, 1H, NH^{16}), 8.49 (d, J = 1.4 Hz, 1H, H^3), 8.20 (s, 1H, H^6), 8.01 (dd, J = 8.0, 2.1 Hz, 4H, H^{21}, H^{22}), 7.84 (s, 1H, H^{14}), 7.77 (d, J = 1.9 Hz, 1H, H^4), 3.76 (s, 4H, H^{20}, H^{23}), 3.59 (dd, J = 8.1, 5.3 Hz, 4H, H^9, H^{13}), 3.52 (s, 2H, H^7), 2.42 – 2.32 (m, 4H, H^{10}, H^{12}). ^{13}C NMR (126 MHz, DMSO) δ 177.02 (C, C^{17}), 153.11 (C, C^2), 150.17 (CH, C^6), 149.02 (CH, C^3), 143.48 (CH, C^{14}), 139.44, ($2CH_2$, C^{21}, C^{22}), 138.08 (CH, C^{16}), 134.05 (C, C^5), 119.43 (CH, C^3), 66.62 ($2CH_2$, C^9, C^{13}), 59.91 (CH_2, C^7), 53.53 ($2CH_2$, C^{20}, C^{23}), 40.00 ($2CH_2$, C^{10}, C^{12}, overlapped with residual DMSO signal). IR (ATR, selected bands, $\tilde{\upsilon}_{max}$): 1585, 1529, 1419, 1347, 1287, 1108, 1001, 855, 796, 741 cm^{-1}.

5-(morpholinomethyl)pyridine-2-carboxaldehyde *N*-morpholinylthiosemicarbazone (HL^4). 5-(morpholinomethyl)pyridine-2-carboxaldehyde (0.29 g, 1.41 mmol) and *N*-morpholinyl-3-thiosemicarbazide (0.23 g, 1.41 mmol) were dissolved in EtOH (5 mL) and

stirred in a Shlenk tube at 78 °C for 2.5 h until the solution became clear. Light-yellow crystals formed within 3 weeks at 4 °C after concentration of the reaction mixture. These were filtered off, washed with cold EtOH and dried in vacuo. Yield: 0.12 g. ^{1}H NMR (500 MHz, DMSO) δ 11.43 (s, 1H, NH^{16}), 8.50 (d, J = 1.3 Hz, 1H, H^{6}), 8.18 (s, 1H, H^{14}), 7.83 (d, J = 8.1 Hz, 1H, H^{4}), 7.78 (dd, J = 8.2, 1.9 Hz, 1H, H^{3}), 3.98 – 3.91 (m, 4H, H^{20}, H^{24}), 3.72 – 3.66 (m, 4H, H^{21}, H^{23}), 3.60 – 3.55 (m, 4H, H^{9}, H^{13}), 3.52 (s, 2H, H^{7}), 2.36 (br. s, 4H, H^{10}, H^{12}). ^{13}C NMR (126 MHz, DMSO) δ 181.27 (C_q, C^{17}), 152.75 (C_q, C^{4}), 150.33 (CH, C^{6}), 144.44 (CH, C^{14}), 137.83 (CH, C^{3}), 134.27 (CH, C^{2}), 119.60 (C_q, C^{4}), 66.60 ($2CH_2$, C^{21}, C^{23}), 66.48 (CH_2, C^{7}), 59.73 ($2CH_2$, C^{9}, C^{13}).

5-(morpholinomethyl)pyridine-2-carboxaldehyde 4-phenylthiosemicarbazone (**HL^{5}**). 5-(morpholinomethyl)pyridine-2-carboxaldehyde (0.29 g, 1.41 mmol) and 4-phenyl-3-thiosemicarbazide (0.24 g, 1.41 mmol) were dissolved in EtOH (5 mL) and stirred in a Shlenk tube at 78 °C for 3 h until the solution became clear. Then the reaction mixture was allowed to stand at 4 °C for 12 h. The yellow crystalline precipitate was filtered off, washed with cold EtOH and dried in vacuo. Yield: 0.32 g. ^{1}H NMR (500 MHz, DMSO) δ 12.02 (s, 1H, NH^{16}), 10.24 (s, 1H, NH^{18}), 8.52 (s, 1H, H^{6}), 8.41 (d, *J* = 8.1 Hz, 1H, H^{3}), 8.21 (s, 1H, H^{14}), 7.78 (d, *J* = 10.1 Hz, 1H, H^{4}), 7.56 (d, *J* = 8.6 Hz, 2H, H^{21}, H^{25}), 7.40 (t, *J* = 7.9 Hz, 2H, H^{22}, H^{24}), 7.24 (t, *J* = 7.4 Hz, 1H, H^{23}), 3.59 (s, 4H, H^{10}, H^{12}), 3.54 (s, 2H, H^{7}), 2.38 (s, 4H, H^{9}, H^{13}).^{13}C NMR (126 MHz, DMSO) δ 176.84 (C_q, C^{17}), 152.62 (C_q, C^{2}), 150.25 (CH, C^{6}), 143.45 (C_q, C^{14}), 139.44 (C_q, C^{20}), 137.51 (CH, C^{4}), 134.46 (C_q, C^{5}), 128.59 (2CH, C^{22}, C^{24}), 126.56 (2CH, C^{21}, C^{25}), 120.68 (CH, C^{3}), 66.62 ($2CH_2$, C^{10}, C^{12}), 53.54 ($2CH_2$, C^{9}, C^{13}), 40.00 (CH_2, C^{7}). IR (ATR, selected bands, $\tilde{\upsilon}_{max}$): 1592, 1505, 1466, 1338, 1291, 1188, 1105, 1060, 1000, 944, 909, 863, 791, 751, 689, 634 cm^{-1}.

5-(morpholinomethyl)pyridine-2-carboxaldehyde S-methylisothiosemicarbazone (**HL^{6}**). To a solution of 5-(morpholinomethyl)pyridine-2-carboxaldehyde (0.29 g, 1.41 mmol) in EtOH (6 mL) was added a solution of S-methylisothiosemicarbazide hydroiodide (0.33 g, 1.41 mmol) in water (2 mL). Then the raction mixture was heated to 60 °C and a solution of $NaHCO_3$ (0.118 g, 1.41 mmol) in water (4 mL) was added dropwise. When bubbles of CO_2 disappeared, the mixture was allowed to cool to room temperature. The solvent was removed under reduced pressure and the residue dissolved in water. The product was extracted with chloroform. After removal of the solvent the residue was dissolved in a small amount of EtOH and allowed to stand at –20 °C overnight. Light-brown crystalline product was obtained the next day. Yield: 0.14 g. ^{1}H NMR (500 MHz, DMSO) δ 8.49 (d, J = 1.4 Hz, 1H, H^{4}), 8.21 (d, J = 8.1 Hz, 1H, H^{14}), 8.17 (s, 1H, H^{6}), 7.84

(d, J = 8.1 Hz, 1H, H^3), 7.16 (s, 2H, H^{18}), 3.60-3.55 (m, 8H, H^9, H^{13}), 3.51 (s, 2H, H^7), 2.40 (br. s, 3H, H^{20}), 2.36 (d, J = 6.0 Hz, 8H, H^{10}, H^{12}). ^{13}C NMR (126 MHz, DMSO) δ 164.19 (C, C^{17}), 154.02 (C, C^5), 151.84 (CH, C^6), 150.12 (CH, C^4), 137.35 (CH, C^3), 133.89, (C, C^2), 120.68 (CH, C^{14}), 66.61 ($2CH_2$, C^9, C^{13}), 59.84 (CH_2, C^7), 53.53 ($2CH_2$, C^{10}, C^{12}), 12.52 (CH_3, C^{20}). IR (ATR, selected bands, $\tilde{\upsilon}_{max}$): 1600, 1497, 1472, 1335, 1290, 1111, 1069, 1015, 931, 870, 790, 752, 714, 626 cm^{-1}.

3. Synthesis of Cu(II) complexes.

[Cu(L^1)Cl] (1). To **HL^1** (100 mg, 0.36 mmol) in MeOH (20 mL) was added triethylamine (50 µl, 0.36 mmol) and then $CuCl_2 \cdot 2H_2O$ (60 mg, 0.36 mmol) in MeOH (5 mL) at 60 °C. The solution was stirred for 5 min and left to stand at room temperature overnight. The precipitate formed was filtered off, washed with cold EtOH and dried in air. Yield: 123 mg. IR (ATR, selected bands, $\tilde{\upsilon}_{max}$): 1631, ´1426, 1310, 1158, 1107, 1060, 907, 722, 688 cm^{-1}.

[Cu(L^2)Cl] (2). To **HL^2** (100 mg, 0.32 mmol) in MeOH (20 mL) was added triethylamine (44.5 µL, 0.32 mmol) and then $CuCl_2 \cdot 2H_2O$ (54 mg, 0.32 mmol) in MeOH (5 mL) at 60 °C. The solution was stirred for 5 min and left to stand at room temperature overnight. The precipitate formed was filtered off, washed with cold EtOH and dried in air. Yield: 104 mg. IR (ATR, selected bands, $\tilde{\upsilon}_{max}$): 1505, 1372, 1310, 1252, 1111, 1000, 913, 872, 749, 626 cm^{-1}.

[Cu(L^3)Cl] (3). To **HL^3** (100 mg, 0.3 mmol) in MeOH (20 mL) was added triethylamine (42 µl, 0.28 mmol) and then $CuCl_2 \cdot 2H_2O$ (50 mg, 0.3 mmol) in MeOH (5 mL) at 60 °C. The solution was stirred for 5 min and left to stand at room temperature overnight. The precipitate formed was filtered off, washed with cold EtOH and dried in air. Yield: 74 mg. IR (ATR, selected bands, $\tilde{\upsilon}_{max}$): 1444, 1375, 1281, 1242, 1111, 1004, 913, 885, 623 cm^{-1}.

[Cu(L^4)Cl] (4). To **HL^4** (50 mg, 0.28 mmol) in MeOH (20 mL) was added triethylamine (20 µl, 0.28 mmol) and then $CuCl_2 \cdot 2H_2O$ (25 mg, 0.28 mmol) in MeOH (5 mL) at 60 °C. The solution was stirred for 5 min and left to stand at room temperature overnight. The precipitate formed was filtered off, washed with cold EtOH and dried in air. Yield: 22 mg. IR (ATR, selected bands, $\tilde{\upsilon}_{max}$): 1465, 1429, 1381, 1313, 1265, 1229, 1109, 1028, 932, 888, 860 cm^{-1}.

[Cu(L^5)Cl] (5). To **HL^5** (100 mg, 0.28 mmol) in MeOH (20 mL) was added triethylamine (39 µl, 0.28 mmol) and then $CuCl_2 \cdot 2H_2O$ (47 mg, 0. 82 mmol) in MeOH (5 mL) on heating. The solution was stirred for 5 min and left to stand at room temperature overnight. The precipitate formed was filtered off, washed with cold EtOH and dried in air. Yield: 67

mg. IR (ATR, selected bands, $\tilde{\upsilon}_{max}$): 1600, 1550, 1493, 1417, 1182, 1111, 1000, 899, 863, 799, 752, 691 cm^{-1}.

[Cu(L^6)Cl] (6). To **HL^6** (100 mg, 0.34 mmol) in MeOH (20 mL) was added triethylamine (47 µl, 0.34 mmol). Then the reaction was heated to 40 °C and $CuCl_2 \cdot 2H_2O$ (58 mg, 0.34 mmol) in MeOH (5 mL) was added. The solution was stirred for 5 min at 50 °C and left to stand at –20 °C overnight. The precipitate formed was filtered off, washed with ethanol, ether and dried in air. Yield: 75 mg. IR (ATR, selected bands, $\tilde{\upsilon}_{max}$): 1599, 1491, 1431, 1320, 1115, 1035, 1004, 973, 911, 796, 724 cm^{-1}.

4. Solution equilibrium studies in aqueous phase

pH-potentiometric measurements. These measurements were performed as described previously.[16] The initial volume of the samples was 10.0 mL. The ligand concentration was 1 mM and metal ion-to-ligand ratios of 1:1 − 1:3 were used. The exact concentration of the ligand stock solutions together with the proton dissociation constants were determined by pH-potentiometric titrations with the use of the computer program HYPERQUAD.[79] HYPERQUAD was also utilised to establish the stoichiometry of the complexes and to calculate the stability constants ($\log\beta(M_pL_qH_r)$). $\beta(M_pL_qH_r)$ is defined for the general equilibrium $pM + qL + rH \rightleftharpoons M_pL_qH_r$ as $\beta(M_pL_qH_r) = [M_pL_qH_r]/[M]^p[L]^q[H]^r$, where M denotes the metal ion and L the completely deprotonated ligand. The uncertainties (standard deviations, SD) of the equilibrium constants are shown in parentheses for the species determined in the present work.

5. Instrumentation. ICP-OES determination of Cu content was performed in Chemical, Molecular and Analysis Centre, National University of Singapore with Optima ICP-OES (Perkin Elmer, Watham, MA, USA). The absorbance of thiazolyl blue tetrazolium bromide (MTT) was measured by synergy H1 hybrid multimode microplate reader (Bio-Tek, Winoosky, VT, USA). Cu and Re contents in cells were determined by Agilent 7700 Series ICP-MS (Agilent Technologies, Santa Clara, CA, USA). Flow cytometry was performed on BD LSRFortessa Cell Analyzer (BD Biosciences, Franklin Lakes, NJ, USA). Western blot images were generated from G:Box (Syngene, Cambride, UK). The UV–vis spectrophotometric measurements were performed on a Hewlett Packard 8452A diode array spectrophotometer and a Thermo Scientific Evolution 220 spectrophotometer. CW-EPR spectra were recorded with a BRUKER EleXsys E500 spectrometer. *In situ* ultraviolet-visible-near-infrared (UV–vis–NIR) spectroelectrochemical measurements were performed on a spectrometer (Avantes, Model AvaSpec-2048x14-USB2.

6. UV–vis spectrophotometric, ^{1}H NMR, EPR and lipophilicity measurements. UV–vis spectra were recorded in the ranges 200–800 nm and 450–1050 nm, respectively. The path length was 0.5, 1 or 2 cm. Stability constants of the complexes and the molar absorbance spectra of the individual species were calculated with the computer program PSEQUAD.[80] The spectrophotometric titrations were performed on samples containing the proligand with or without Cu(II) ions and the concentration of the proligand was 120 μM to 1.4 mM. The metal-to-proligand ratios were 1:1 and 1:2 in the pH range from 1.0 to 11.5 at 25.0 ± 0.1 °C at an ionic strength of 0.10 M (KCl). pH values in the range 1.0–2.0, were calculated from the strong acid and strong base content. The conditional stability constant of [CuL] at pH 6.0 (50 mM MES) for **1** was determined from competition titrations of the Cu(II) complex of EDTA with the proligand **HL^1**. Samples contained 34 μM Cu(II) ion and 34 μM **HL^1**, and the concentration of the EDTA was varied in the range of 0–83 μM. Absorbance data were recorded after 0.5 h incubation. ^{1}H NMR studies for **HL^1** were carried out on a Bruker Avance III HD Ascend 500 Plus instrument in a 10% (v/v) D_2O/H_2O mixture at ionic strength of 0.10 M (KCl). All CW-EPR spectra were recorded with a BRUKER EleXsys E500 spectrometer (microwave frequency 9.85 GHz, microwave power 10 mW, modulation amplitude 5 G, modulation frequency 100 kHz. The pH dependent series of isotropic EPR spectra were recorded in a circulating system, at room temperature. A Heidolph Pumpdrive 5101 peristaltic pump was used for circulate the solution from the titration pot through a capillary tube into a Bruker flat cell placed in the cavity of the instrument. The titrations were carried out under nitrogen atmosphere. EPR spectra were recorded at 1.00 mM Cu(II) and 0.75 mM ligand concentration, and at 1.00 mM $CuCl_2$ and 1.50 mM ligand concentration, both between pH = 1 – 11.5. The ionic strength of 0.1 M was adjusted with KCl. Before the simulation of the room temperature spectra, the measured spectra were corrected by subtracting the spectra of aqua solution measured in the same circulating system. The series of pH-dependent isotropic EPR spectra recorded in the equimolar solution were simulated by the „two-dimensional" method using the 2D_EPR program[81] and EPR parameters were computed as published previously.[16,25] Distribution coefficients ($D_{7.4}$) values of complexes **1**–**6** and **HL^1**–**HL^6** were determined by the traditional shake-flask method in *n*-octanol/buffered aqueous solution at pH 7.40 (20 mM HEPES, 0.10 M KCl) at 25.0 ± 0.2 °C as described previously.[82]

7. Crystallographic Structure Determination. X-ray diffraction quality single crystals of **HL^1**, **HL^2**, **HL^4**–**HL^6** were obtained by recrystallization in ethanol, while **1** and **3**–**6** by

slow diffusion of diethyl ether into the DMF and methanolic solution of the complexes, respectively. The measurements were performed on a Bruker X8 APEX-II CCD (**HL^1**, **HL^2**, **HL^4**, **HL^5**, **1´**, **3**–**6**), Bruker D8 Venture (**1**) or Gemini (**HL^6**) diffractometer. Single crystals were positioned at 35, 35, 35, 35 and 55 mm from the detector, and 388, 1110, 946, 1108 and 2935 frames were measured, each for 40, 3, 60, 3 and 32s over 0.5, 0.5, 0.5, 0.5 and 1.0° scan width for **HL^1**–**HL^6**, respectively. For Cu(II) complexes **1**, **1´**, **3**–**6** the single crystals were placed at 24, 35, 35, 33, 35 and 24 mm from the detector, and 8088, 2692, 794, 1212, 1261 and 567 fames were measured, each for 3, 2, 60, 60, 60 and 3s over 0.6, 0.5, 0.5, 0.5, 0.4 and 0.5° scan width, respectively. The data were processed using SAINT or CrysAlis software.[83,84] Crystal data, data collection parameters, and structure refinement details are given in Tables S11 and S12. The structures were solved by direct methods and refined by full-matrix least-squares techniques. Non-H atoms were refined with anisotropic displacement parameters. H atoms were inserted in calculated positions and refined with a riding model. The morpholine group and the N-piperidinyl unit in one of three crystalographically independent molecules in the asymmetric unit were found to be disordered over two positions with s.o.f. 0.5:0.5 and 0.6:0.4 in **3·0.25MeOH**. The morpholine moiety attached to pyridine unit in one of the three crystallographically independent molecules of **4·0.58MeOH** was found to be disordered over two positions with s.o.f. 0.7:0.3, while one molecule of methanol over two positions with s.o.f. 0.75:0.25. The positional parameters of disordered atoms were refined by using PART, DFIX and SADI tools implemented in SHELX. The following computer programs and hardware were used: structure solution, *SHELXS-2014* and refinement, *SHELXL-2014*;[85] molecular diagrams, ORTEP;[86] computer, Intel CoreDuo. CCDC 1850567–1850577.

8. Electrochemistry and spectroelectrochemistry. Cyclic voltammetric experiments were performed as described previously.[53] The cyclic voltammograms were measured in the catodic region in different solvents (DMSO, methanol, DMSO/H_2O). The analytical purity grade $LiClO_4$ (Sigma-Aldrich) and distilled and deionized water were used for preparation of 1 mM aqueous solutions of the investigated complexes **1**–**6**. EPR spectra were recorded with the EMX plus. *In situ* ultraviolet-visible-near-infrared (UV–vis–NIR) spectroelectrochemical measurements were performed on a spectrometer (Avantes, Model AvaSpec-2048x14-USB2 in the spectroelectrochemical cell kit (AKSTCKIT3) with the Pt-microstructured honeycomb working electrode, purchased from Pine Research Instrumentation. The cell was positioned in the CUV–UV Cuvette Holder (Ocean Optics) connected to the diode-array UV–vis–NIR spectrometer by optical fibers. UV–vis–NIR

spectra were processed using the AvaSoft 7.7 software package. Halogen and deuterium lamps were used as light sources (Avantes, Model AvaLight-DH-S-BAL). The *in situ* EPR spectroelectrochemical experiments were carried out under an argon atmosphere in the EPR flat cell equipped with a large platinum mesh working electrode. The freshly prepared solutions were carefully purged with argon and the electrolytic cell was polarized in the galvanostatic mode directly in the cylindrical EPR cavity TM-110 (ER 4103 TM) and the EPR spectra were measured in situ.

9. Cell lines and culture conditions. Human ovarian carcinoma cells A2780 and A2780cisR, and human embryonic kidney HEK293 were obtained from ATCC. A2780 and A2780cisR cells were cultured in RPMI 1640 medium containing 10% fetal bovine serum (FBS). HEK293 were cultured in DMEM medium containing 10% FBS. All cells were grown in tissue culture 25 cm^2 flasks (BD Biosciences, Singapore) at 37 °C in a humidified atmosphere of 95% air and 5% CO_2. All drug stock solutions were prepared in sterile water. The amount of Cu was determined by ICP-OES. All compounds were soluble in water; more specifically, the solubility of **1**, **2** and **5** was moderate and did not exceed 2 mM, whereas **3** was less soluble (0.3 mM) in water.

10. Inhibition of cell viability assay. The cytotoxicity of the compounds was determined by colorimetric microculture assay (MTT assay, MTT = 3-(4,5-dimethyl-2-thiazolyl)-2,5-diphenyl-2H-tetrazolium bromide) as described previously.[53]

11. Cellular accumulation. Cellular accumulation of **1**–**6** was determined in A2780 cells. Cells were seeded into Cellstar 6-well plates (Greiner Bio-one) at a density of 60×10^4 cells/well (2 mL per well). After the cells were allowed to resume exponential growth for 24 h, they were exposed to **1**–**6** at 1 μM for 24 h at 37 °C. The cells were washed twice with 1 mL of PBS and lysed with RIPA lysis buffer for 5–10 min at 4 °C. The cell lysates were scraped from the wells and transferred to separate 1.5 mL microtubes. The supernatant was then collected after centrifugation (13 000 rpm, 4 °C for 15 min) and total protein content of each sample was quantified via Bradford's assay. Cell lysates were transferred to 2 mL glass vials and then digested with ultrapure 65% HNO_3 at 100 °C for 24 h. The resulting solution was diluted to 1 mL (2–4% *v/v* HNO_3) with ultrapure Milli-Q water. Cu content of each sample was quantified by ICP-MS. In was used as an internal standard. Cu and In were measured at *m*/*z* 64 and *m*/*z* 115, respectively. Metal standards for calibration curve (0, 0.5, 1, 2, 5, 10, 20, 40 ppb) were freshly prepared before each measurement. All readings were made in triplicates in He mode. For temperature-dependent cellular accumulation experiments, A2780 cells were seeded into 35×10 mm

tissue culture plates at a density of 60×10^4 cells/plate. After the cells were allowed to resume exponential growth for 24 h, they were exposed to **2** at 3 μM for 10, 30, 60 and 120 min at 37 and 4 °C. The subsequent analysis was performed as described above. For energy-dependent experiments, A2780 cells were seeded into 35×10 mm tissue culture plates at a density of 1×10^6 cells/plate. After the cells were allowed to resume exponential growth for 24 h, they were pre-incubated with oligomycin (5 μM) for 1 h or 4 h or with cycloheximide (100 μM) for 4 h and further co-incubated with 3 μM of **2** at 37 °C. To induce total starvation, after the cells were allowed to resume exponential growth for 24 h, RPMI media was replaced with Hanks' Balanced Salt Solution (HBSS) and cells were pre-incubated in HBSS for 1 h and further incubated with 3 μM of **2** for 1 h at 37 °C. The subsequent analysis was performed as described above.

12. Western blot analysis. A2780 cells were seeded into Cellstar 6-well plates (Greiner Bio-One) at a density of 60×10^4 cells/well (2 mL per well). After the cells were allowed to resume exponential growth for 24 h, they were exposed to **HL^2** and **2** at different concentrations for 24 h. The experiment was performed essentially as described previously.[53] The membranes were blocked in 5% BSA (w/v) in TBST wash buffer for 1 h and subsequently incubated with the appropriate primary antibodies in 5% BSA (w/v) in TBST wash buffer (actin antibody) at 4 °C overnight. The membranes were washed with a wash buffer 3 times for 5 min. After incubation with horseradish peroxidase-conjugated secondary antibodies (room temperature, 1.5 h), the membranes were washed with a wash buffer 4 times for 5 min. Immune complexes were detected with Luminata HRP substrates and analyzed using enhanced chemiluminescence imaging. Actin was used as a loading control. The following antibodies were used: NRF2 (sc13032) from Santa Cruz Biotechnologies, ECL Antirabbit IgG (NA934 V) and ECL Antimouse IgG (NA931) from GE Healthcare Life Sciences, cleaved PARP (Asp214) (D64E10), PARP, CHOP (D46F1), BiP (C50B12), IRE1α (14C10), β-actin (13E5), phospho-p44/p42 MAPK (Erk1/2) (Thr202/Tyr204) (D13.14.4E), cyclin D1 (92G2), cyclin B1 (D5C10), XIAP antibodies from Cell Signalling Technologies. All antibodies were used at 1 : 500 dilutions except for actin (1 : 10 000), anti-mouse and anti-rabbit (1 : 5000).

13. Annexin V/PI apoptosis assay. A2780 cells were seeded into Cellstar 12-well plates (Greiner Bio-One) at a density of 20×10^4 cells/well (1 mL per well). The cells were allowed to resume exponential growth for 24 h and subsequently they were exposed to **HL^2** and **2** at different concentrations for 24 h. After the supernatant solution was collected

in 1.5 mL microtubes, the cells were washed with 100 μl of trypsin, which was combined with the supernatant. Subsequently, cells were trypsinized with 200 μl of trypsin for 5 min at 37 °C, 5% CO_2, washed with 200 μl of PBS and combined with the supernatant. The cells were centrifuged at 2.5×10^3 rpm for 5 min and the pellets were washed once with PBS and resuspended in 500 μl of Annexin V binding buffer and stained with Annexin V-FITC and PI reagents. The fluorescence was immediately analyzed by flow cytometry. The resulting dot blots were acquired from 10 000 events and quantified using Flowjo software (Flowjo LLC, Ashland, OR, USA).

14. Tyrosyl radical reduction in mouse R2 ribonucleotide reductase protein. The 9.4 GHz EPR spectra were recorded at 30 K on a Bruker EleXsys II E540 EPR spectrometer with an Oxford Instruments ESR900 helium cryostat, essentially as described previously.[51] The small mouse R2 subunit without diferric-tyrosyl cofactor was produced from *E.coli* carrying a mouse R2 cDNA plasmid. The cofactor was further regenerated, resulting in the formation of the cluster with 0.38 tyrosyl radical/Fe(III) ratio, which is in agreement with the literature.[41]

15. Molecular docking calculations. The calculations were performed as described previously.[20]. The centre of the binding pocket was defined (x = 102.276, y = 87.568, z = 80.588)[87] with 10 Å radius. The basic amino acids lysine and arginine were defined as protonated. Furthermore, aspartic and glutamic acids were assumed to be deprotonated. The GoldScore (GS),[37] ChemScore (CS),[88,89] Chem Piecewise Linear Potential (ChemPLP)[90] and Astex Statistical Potential (ASP)[90] scoring functions were implemented to validate the predicted binding modes and relative energies of the ligands using the GOLD v5.4 software suite. The parameter file for GS was augmented for Cu according to Sciortino et al.[38] The QikProp 4.6[91] and Marvin software package[92] was used to calculate the molecular descriptors of the compounds. The reliability of QikProp is established for the molecular descriptors.[93]

16. Bacterial Strains and antibacterial activity. *Wild-type Pseudomonas aeruginosa PAO1 strain CECT 4122 (ATCC 15692)* and *Staphylococcus aureus CECT 86 (ATCC 12600)* were obtained from the Spanish Type Culture Collection (CECT). All strains were routinely cultivated in TSB medium (Sharlab, Spain) at 37 ºC. Minimal inhibitory concentration (MIC) assays were determined by the microdilution method using TSB broth following the method described by the Clinical and Laboratory standards Institute.[94] In brief, compounds were diluted in a 96-well microtiter plate (tissue culture-treated polystyrene; Costar 3595, Corning Inc., Corning, NY) to a final concentration ranging

from 0.1 to 100 µg/mL. A 100-µl aliquot of the bacterial suspension (around 5×10^5 colony forming units/mL (CFU/mL)) was inoculated, incubated at 37 ºC for 8 h at 150 rpm, and absorbance at 550 nm was read every 15 min in an Infinity 200 Pro microplate reader (Tecan). The MIC_{100} was determined as the lowest concentration that completely inhibited bacterial growth, and MIC_{50} in which bacterial growth was inhibited at 50%.

17. Bacterial viability test analysis. Cultures of *S. aureus* and *P. aeruginosa* were diluted in fresh TSB medium and grown overnight to the beginning of exponential phase (A550 0.3) and different compounds were added. After 3 h of incubation at 37 ºC in shaking conditions, cells were harvested and stained using the LIVE/DEAD BactLight Bacterial Viability Kit (Thermofisher) for 30 min. Fluorescent bacteria were visualized by a Nikon inverted fluorescent microscope ELIPSE Ti-S/L100 (Nikon) coupled with a DS-Qi2 Nikon camera.

ASSOCIATED CONTENT

Supporting Information Available: Synthetic details, atom numbering scheme for NMR spectra (Scheme 1), ORTEP views of **HL^1**, **HL^2**, **HL$^{4–6}$** (Figure S1), portion of the crystal structure of **6** (Figure S2), low field region of the ^{1}H NMR spectra of **HL^1** recorded at pH 0.75–12.50 (Figure S3), concentration distribution curves of **HL^1** (Figure S4), UV–vis and EPR spectra for Cu(II) containing systems (Figures S5–S7), cyclic voltammograms and UV–vis spectra of **1**–**6** and one of the proligands (Figures S8–S11), plot with potential dependence of UV–vis spectra of **2** (Figure S12), concentration–effect curves (Figure S13), hydrogen binding of **5** to R2 protein (Figure S14), EPR spectrum of R2 RNR tyrosyl radical, complex formation reactions of Fe^{III} and Fe^{II} with **HL^2** and **HL^5** monitored by UV–vis spectroscopy (Figure S15), ESI MS spectrum of $[Fe^{III}(HL^5)]^+$ (Figure S16), selected bond distances and angles in Cu(II) complexes (Tables S1 and S2), proton dissociation constants for HL^1 (Table S3), cumulative stability and proton dissociation constants of Cu(II) complexes of HL^1 (Table S4), formation constants for Cu(II)–HL^1 complexes (Table S5), electrochemical data for **1**–**6** (Table S6), Molecular descriptors for **HL^1**–**HL^6** and **1**–**6** (Table S7), details of molecular docking calculations (Table S8), analytical data (Tables S9 and S10), details of data collection and refinement of proligands (Table S11) and Cu(II) complexes (Table S12). Molecular formula strings (CSV). This material is available free of charge via the Internet at http://pubs.acs.org.

Author Information

Corresponding Authors

* E-mail: maria.babak@nus.edu.sg (M.V.B).

* E-mail: vladimir.arion@univie.ac.at (V.B.A.).

ORCID

Vladimir B. Arion: 0000-0002-1895-6460

Maria V. Babak: 0000-0002-2009-7837

Eleonora Afanasenko: 0000-0003-0434-1753

Éva A. Enyedy: 0000-0002-8058-8128

Orsolya Dömötör: 0000-0001-8736-3215

Nóra V. May: 0000-0003-4770-4681

Jóhannes Reynisson: 0000-0003-4147-9512

Acknowledgments. Austrian Science Fund (FWF) is acknowledged for the grant no. P28223-N34. This work was supported in part by grants to ET from the Spanish Ministerio de Economia y Competitividad (MINECO / FEDER) (BIO2015-63557-R), Generalitat de Catalunya (2014 SGR01260 and CERCA programme), the Catalan and Spanish Cystic Fibrosis foundations and La Caixa Foundation. This work was also supported by the National Research, Development and Innovation Office FK 124240 project, and the J. Bolyai Research Scholarship of the Hungarian Academy of Sciences (ÉAE and NVM). PR and DD acknowledge the support of Slovak Research and Development Agency (APVV-15-0053) and Slovak Scientific Grant Agency VEGA (1/0416/17). This work was supported by the National University of Singapore (NUS), Department of Pharmacy (C148-000-003-001 (FYP)). We thank A. Roller for collection of X-ray data.

ABBREVIATIONS

TSC, thiosemicarbazone, COTI-2, (*E*)-*N´*-(6,7-dihydroquinolin-8(5*H*)-ylidene)-4-(pyridine-2-yl)piperazine-1-carbothiohydrazide, DpC, di-2-pyridylketone 4-cyclohehyl-4-methyl-3-thiosemicarbazone, ROS, reactive oxygen species, GSH, glutathione, UPR, unfolded protein response, TEMED, tetrmethylethylenediamine, PI, propidium iodide, FBS, Foetal Bovine Serum, BSA, Bovine Serum Albumine, HBSS, Hank's Balanced Salt Solution, PS, phosphatidylserine, KDS, known drug space.

Accession Codes

PDB ID of the complexes of Triapine and **5** docked in mouse R2 protein: 1w68-5-T. Authors will release the atomic coordinates upon article publication.

References:

(1) Chabner, B. A.; Roberts, T. G. Chemotherapy and the war on cancer. *Nat. Rev. Cancer* **2005**, *5*, 65–72.

(2) Inagaki, J.; Rodriguez, V.; Bodey, G. P. Proceedings: causes of death in cancer patients. *Cancer* **1974**, *33*, 568–573.

(3) Alibek, K.; Bekmurzayeva, A.; Mussabekova, A.; Sultankulov, B. Using antimicrobial adjuvant therapy in cancer treatment: a review. *Infect. Agent Cancer* **2012**, *7*: 33, 10 pp.

(4) Kardas, J.; Buraczewska, A. The use of antibiotic prophylaxis in patients with solid tumors – when and to whom? *Oncol. Clin. Pract*. **2016**, *12*, 128–135.

(5) Benharroch, D.; Osyntsov, L. Infectious diseases are analogous with cancer. Hypothesis and implications. *J. Cancer* **2012**, *3*, 117–121.

(6) Elledge, S. J.; Zhou, Z.; Allen, J. B. Ribonucleotide reductase: regulation, regulation, regulation. *Trends Biochem. Sci.* **1992**, *17*, 119–123.

(7) Torrents, E. Ribonucleotide reductases: essential enzymes for bacterial life. *Frontiers in Cellular and Infection Microbiology*, **2014**, 4, 52.

(8) Beraldo, H.; Gambino, D. The wide pharmacological versatility of semicarbazones, thiosemicarbazones and their metal complexes. *Mini-Rev. Med. Chem.* **2004**, *4*, 31–39.

(9) Knox, J. J.; Hotte, S. J.; Kollmannsberger, C.; Winquist, E.; Fisher, B.; Eisenhauer, E. A. Phase II study of Triapine in patients with metastatic renal cell carcinoma: a trial of the National Cancer Institute of Canada Clinical Trials Group (NCIC IND.161). *Invest. New Drugs* **2007**, *25*, 471–477.

(10) Nutting, C. M.; van Herpen, C. M. L.; Miah, A. B.; Bhide, S. A.; Machiels, J.-P.; Buter, J.; Kelly, C.; de Raucourt, D.; Harrington, K. J. Phase II study of 3-AP Triapine in patients with recurrent or metastatic head and neck squamous cell carcinoma. *Ann. Oncol.* **2009**, *20*, 1275–1279.

(11) Traynor, A. M.; Lee, J.-W.; Bayer, G. K.; Tate, J. M.; Thomas, S. P.; Mazurczak, M.; Graham, D. L.; Kolesar, J. M.; Schiller, J. H. A phase II trial of Triapine (NSC# 663249) and Gemcitabine as second line treatment of advanced non-small cell lung cancer: Eastern Cooperative Oncology Group study 1503. *Invest. New Drugs* **2010**, *28*, 91–97.

(12) Stacy, A. E.; Palanimuthu, D.; Bernhardt, P. V.; Kalinowski, D. S.; Jansson, P. J.; Richardson, D. R. Structure-activity relationships of di-2-pyridylketone, 2-

benzoylpyridine, and 2-acetylpyridine thiosemicarbazones for overcoming Pgp-mediated drug resistance. *J. Med. Chem.* **2016**, *59*, 8601–8620.

(13) https://clinicaltrials.gov/ct2/show/NCT02688101 (accessed Feb. 23, 2016).

(14) Salim, K. Y.; Danter, W. R.; Maleki, V. S.; Koropatnick, J. COTI-2, a novel small molecule that is active against multiple human cancer cell lines in vitro and in vivo. *Oncotarget* **2016**, *7*, 41363–41379.

(15) West, D. X.; Liberta, A. E.; Padhye, S. B.; Chikate, R. C.; Sonawane, P. B.; Kumbhar, A. S.; Yerande, R. G. Thiosemicarbazone complexes of copper(II): structural and biological studies. *Coord. Chem. Rev.* **1993**, *123*, 49–71.

(16) Bacher, F.; Dömötör, O.; Kaltenbrunner, M.; Mojovic, M.; Popovic-Bijelic, A.; Gräslund, A.; Ozarowski, A.; Filipovic, L.; Radulovic, S.; Enyedy, E. A.; Arion, V. B., Effects of terminal dimethylation and metal coordination of proline-2-formylpyridine thiosemicarbazone hybrids on lipophilicity, antiproliferative activity, and hR2 RNR inhibition. *Inorg. Chem.* **2014**, *53*, 12595–12609.

(17) Milunovic, M. N. M.; Enyedy, E. A.; Nagy, N. V.; Kiss, T.; Trondl, R.; Jakupec, M. A.; Keppler, B. K.; Krachler, R.; Novitchi, G.; Arion, V. B. L- and D-proline thiosemicarbazone conjugates: coordination behavior in solution and the effect of copper(II) coordination on their antiproliferative activity. *Inorg. Chem.* **2012**, *51*, 9309–9321.

(18) Bacher, F.; Dömötör, O.; Chugunova, A.; Nagy, N. V.; Filipovic, L.; Radulovic, S.; Enyedy, E. A.; Arion, V. B. Strong effect of copper(II) coordination on antiproliferative activity of thiosemicarbazone-piperazine and thiosemicarbazone-morpholine hybrids. *Dalton Trans.* **2015**, *44*, 9071–9090.

(19) Dobrova, A.; Platzer, S.; Bacher, F.; Milunovic, M. N. M.; Dobrov, A.; Spengler, G.; Enyedy, E. A.; Novitchi, G.; Arion, V. B. Structure-antiproliferative activity studies on L-proline- and homoproline-4*N*-pyrrolidine-3-thiosemicarbazone hybrids and their nickel(II), palladium(II) and copper(II) complexes. *Dalton Trans.* **2016**, *45*, 13427–13439.

(20) Zaltariov, M. F.; Hammerstad, M.; Arabshahi, H. J.; Jovanovic, K.; Richter, K. W.; Cazacu, M.; Shova, S.; Balan, M.; Andersen, N. H.; Radulovic, S.; Reynisson, J.; Andersson, K. K.; Arion, V. B., New iminodiacetate-thiosemicarbazone hybrids and their copper(II) complexes are potential ribonucleotide reductase R2 inhibitors with high antiproliferative activity. *Inorg. Chem.* **2017**, *56*, 3532–3549.

(21) Naim, M. J.; Alam, O.; Alam, M. J.; Alam, P.; Shrivastava, N. A review on pharmacological profile of morpholine derivatives. *Int. J. Pharmacol. Pharm. Sci.* **2016**, *3*, 40–51.

(22) Boehm, M. F.; Heyman, R. A. Compounds Having Selective Activity for Retinoid X Receptors, and Means for Modulation of Processes Mediated by Retinoid X Receptors. US7655699 B1, 2010.

(23) Warr, R. J.; Willis, A. C.; Wild, S. B. Inorganic asymmetric synthesis: asymmetric synthesis of a two-bladed propeller, octahedral metal complex. *Inorg. Chem.* **2006**, *45*, 8618–8627.

(24) Dawson, M. I.; Chan, R.; Hobbs, P. D.; Chao, W. R.; Schiff, L. J. Aromatic retinoic acid analogues. 2. Synthesis and pharmacological activity. *J. Med. Chem.* **1983**, *26*, 1282–1293.

(25) Dömötör, O.; May, N. V.; Pelivan, K.; Kiss, T.; Keppler, B. K.; Kowol, C. R.; Enyedy, É. A. A comparative study of α-*N*-pyridyl thiosemicarbazones: spectroscopic properties, solution stability and copper(II) complexation. *Inorg. Chim. Acta* **2018**, *472*, 264–275.

(26) Enyedy, E. A.; Zsigo, E.; Nagy, N. V.; Kowol, C. R.; Roller, A.; Keppler, B. K.; Kiss, T. Complex-formation ability of salicylaldehyde thiosemicarbazone towards ZnII, CuII, FeII, FeIII and GaIII ions. *Eur. J. Inorg. Chem.* **2012**, *2012*, 4036–4047.

(27) Kowol, C. R.; Heffeter, P.; Miklos, W.; Gille, L.; Trondl, R.; Cappellacci, L.; Berger, W.; Keppler, B. K. Mechanisms underlying reductant-induced reactive oxygen species formation by anticancer copper(II) compounds. *J. Biol. Inorg. Chem.* **2012**, *17*, 409–423.

(28) Goeschl, S.; Varbanov, H. P.; Theiner, S.; Jakupec, M. A.; Galanski, M.; Keppler, B. K. The role of the equatorial ligands for the redox behavior, mode of cellular accumulation and cytotoxicity of platinum(IV) prodrugs. *J. Inorg. Biochem.* **2016**, *160*, 264–274.

(29) Primik, M. F.; Mülgassner, G.; Jakupec, M. A.; Zava, O.; Dyson, P. J.; Arion, V. B.; Keppler, B. K. Highly cytotoxic copper(II) complexes with modified paullone ligands. *Inorg. Chem.* **2010**, *49*, 302–311.

(30) Waring, M. J. Lipophilicity in drug discovery. *Expert Opin. Drug Discovery* **2010**, *5*, 235–248.

(31) Zhu, F.; Logan, G.; Reynisson, J. Wine compounds as a source for HTS screening collections. A feasibility study. *Mol. Inf.* **2012,** *31*, 847–855.

(32) Los, D. A.; Murata, N. Membrane fluidity and its roles in the perception of environmental signals. *Biochim. Biophys. Acta, Biomembr.* **2004**, *1666*, 142–157.

(33) Price, K. A.; Crouch, P. J.; Volitakis, I.; Paterson, B. M.; Lim, S.; Donnelly, P. S.; White, A. R. Mechanisms controlling the cellular accumulation of copper bis(thiosemicarbazonato) complexes. *Inorg. Chem.* **2011**, *50*, 9594–9605.

(34) Merlot, A. M.; Pantarat, N.; Menezes, S. V.; Sahni, S.; Richardson, D. R.; Kalinowski, D. S. Cellular uptake of the antitumor agent Dp44mT occurs via a carrier/receptor-mediated mechanism. *Mol. Pharmacol.* **2013**, *84*, 911–924.

(35) Sugano, K.; Kansy, M.; Artursson, P.; Avdeef, A.; Bendels, S.; Di, L.; Ecker, G. F.; Faller, B.; Fischer, H.; Gerebtzoff, G.; Lennernaes, H.; Senner, F. Coexistence of passive and carrier-mediated processes in drug transport. *Nat. Rev. Drug Discovery* **2010**, *9*, 597–614.

(36) Strand, K. R.; Karlsen, S.; Kolberg, M.; Rohr, A. K.; Goerbitz, C. H.; Andersson, K. K. Crystal structural studies of changes in the native dinuclear iron center of ribonucleotide reductase protein R2 from mouse. *J. Biol. Chem.* **2004**, *279*, 46794–46801.

(37) Jones, G.; Willett, P.; Glen, R. C.; Leach, A. R.; Taylor, R. Development and validation of a genetic algorithm for flexible docking. *J. Mol. Biol.* **1997**, *267*, 727–748.

(38) Sciortino, G.; Rodriguez-Guerra Pedregal, J.; Lledos, A.; Garribba, E.; Marechal, J.-D. Prediction of the interaction of metallic moieties with proteins: an update for protein-ligand docking techniques. *J. Comput. Chem.* **2018**, *39*, 42–51.

(39) Gräslund, A.; Ehrenberg, A.; Thelander, L. Characterisation of the free radical of mammalian ribonucleotide reductase. *J. Biol. Chem*. **1982**, *257*, 5711–5715.

(40) Thelander, L.; Graslund, A. Mechanism of inhibiton of mammalian ribonucleotide reductase by the iron chelate of 1-formylisoquinonline thiosemicarbazone. *J. Biol. Chem.* **1983**, *258*, 4063–4066.

(41) Popović-Bijelić, A.; Kowol, C. R.; Lind, M. E.; Luo, J.; Himo, F.; Enyedy, E. A.; Arion, V. B.; Gräslund, A. Ribonucleotide reductase inhibition by metal complexes of Triapine (3-aminopyridine-2-carboxaldehyde thiosemicarbazone): a combined experimental and theoretical study. *J. Inorg. Biochem*. **2011**, *105*, 1422–1431.

(42) Enyedy, A. E.; Primik, M. F.; Kowol, C. R.; Arion, V. B.; Kiss, T.; Keppler, B. K. Interaction of Triapine and related thiosemicarbazones with iron(III)/(II) and gallium(III): a comparative solution equilibrium study. *Dalton Trans.* **2011**, *40*, 5895–5905.

(43) Mullen, P. PARP cleavage as a means of assessing apoptosis. *Methods Mol. Med.* **2004**, *88*, 171–181.

(44) Finch, R. A.; Liu, M. C.; Cory, A. H.; Cory, J. G.; Sartorelli, A. C. Triapine (3-aminopyridine-2-carboxaldehyde thiosemicarbazone (3-AP)). An inhibitor of ribonucleotide reductase with antineoplastic activity. *Adv. Enzyme Regul.* **1999**, *39*, 3–12.

(45) Finch, R. A.; Liu, M.; Grill, S. P.; Rose, W. C.; Loomis, R.; Vasquez, K. M.; Cheng, Y.; Sartorelli, A. C. Triapine (3-aminopyridine-2-carboxaldehyde-thiosemicarbazone). A potent inhibitor of ribonucleotide reductase activity with broad spectrum of antitumor activity. *Biochem. Pharm.* **2000**, *59*, 983–991.

(46) Yu. Y.; Wong, J.; Lovejoy, D. B.; Kalinowski, D. S.; Richardson, D. R. Chelators at the cancer coalface. Desferrioxamine to triapine and beyond. *Clin. Cancer Res.* **2006**, *12*, 6876–6883.

(47) Shao, J.; Zhou, B.; Di Bilio, A. J.; Zhu, L.; Wang, T.; Qi, C.; Shih, J.; Yen, Y. A ferrous-triapine complex mediates formation of reactive oxygen species that inactivate human ribonucleotide reductase. *Mol. Cancer Ther*. **2006**, *5*, 586–592.

(48) Kowol, C. R.; Trondl, R.; Heffeter, P.; Arion, V. B.; Jakupec, M. A.; Roller, A.; Galanski, M.; Berger, W.; Keppler, B. K. Impact of metal coordination on cytotoxicity of 3-aminopyridine-2-carboxaldehyde thiosemicarbazone (triapine) and novel insights into terminal demethylation. *J. Med. Chem.* **2009**, *52*, 5032–5043.

(49) Yu, Y.; Gutierrez, E.; Kovacevic, Z.; Saletta, F.; Obeidy, P.; Suryo Rahmanto, Y.; Richardson, D. R. Iron chelators for the treatment of cancer. *Curr. Med. Chem.* **2012**, *19*, 2869–2702.

(50) Merlot, A. M.; Kalinowski, D. S.; Richardson, D. R. Novel chelators for cancer treatment: where are we now? *Antioxid. Red. Signal* **2013**, *18*, 973–1006.

(51) Aye, Y.; Long, M. J. C.; Stubbe, J. Mechanistic studies of semicarbazide triapine targeting human ribonucleotide reductase in vitro and in mammalian cells. Tyrosyl radical quenching not involving reactive oxygen species. J. Biol. Chem. **2012**, *287*, 35768–35778.

(52) Pandeya, S. N.; Sriram, D.; Nath, G.; DeClercq, E. Synthesis, antibacterial, antifungal and anti-HIV activities of Schiff and Mannich bases derived from isatin derivatives and *N*-[4-(4′-chlorophenyl)thiazol-2-yl] thiosemicarbazide]. *Eur. J. Pharm. Sci.* **1999**, *9*, 25–31.

(53) Sirbu, A.; Palamarciuc, O.; Babak, M. V.; Lim, J. M.; Ohui, K.; Enyedy, E. A.; Shova, S.; Darvasiova, D.; Rapta, P.; Ang, W. H.; Arion, V. B. Copper(II) thiosemicarbazone

complexes induce marked ROS accumulation and promote nrf2-mediated antioxidant response in highly resistant breast cancer cells. *Dalton Trans.* **2017**, *46*, 3833–3847.

(54) Yu. Y.; Kalinowski, D. S.; Kovacevic, Z.; Siafakas, A. R.; Jansson, P. J.; Stefani, C.; Lovejoy, D. B.; Sharpe, P. C.; Bernhardt, P. V.; Richardson, D. R. Thiosemicarbazones from the old to new: iron chelators that are more than just ribonucleotide reductase inhibitors. *J. Med. Chem.* **2009**, *52*, 5271–5294.

(55) Antholine, W.; Knight, J.; Whelan, H.; Petering, D. H. Studies of the reaction of 2-formylpyridine thiosemicarbazone and its iron and copper complexes with biological systems. *Mol. Pharmacol.* **1977**, *13*, 89–98.

(56) Chaston, T.B.; Lovejoy, D.B.; Watts, R.N.; Richardson, D.R.Examination of the antiproliferative activity of iron chelators: multiple cellular targets and the different mechanism of action of triapine compared with desferrioxamine and the potent pyridoxal isonicotinoyl hydrazone analogue 311. Clin Cancer Res. **2003** 9, 402–414.

(57) Yu, Y.; Kovacevic, Z.; Richardson, D. R. Tuning cell cycle regulation with an iron key. *Cell Cycle* **2007**, *6*, 1982–1994.

(58) Nurtjahja-Tjendraputra, E.; Fu, D.; Phang, J. M.; Richardson, D.R. Iron chelation regulates cyclin D1 expression via the proteasome: a link to iron deficiency-mediated growth suppression. *Blood* **2007**, *109*, 4045–4054.

(59) Thelander, L.; Graslund, A.; Thelander, M. Continual presence of oxygen and iron required for mammalian ribonucleotide reduction: Possible regulation mechanism. *Biochem. Biophys. Res. Commun*. **1983**, *110*, 859–865.

(60) Lui, G. Y. L.; Kovacevic, Z.; Menezes, S. V.; Kalinowski, D. S.; Merlot, A. M.; Sahni, S.; Richardson, D. R. Novel thiosemicarbazones regulate the signal transducer and activator of transcription 3 (STAT3) pathway: inhibition of constitutive and interleukin 6-induced activation by iron depletion. *Mol. Pharmacol.* **2015**, *87*, 543–560.

(61) Yu, Y.; Rahmanto, Y. S.; Richardson, D. R. Bp44mT: an orally active iron chelator of the thiosemicarbazone class with potent anti-tumour efficacy. *Br. J. Pharmacol.* **2012**, *165*, 148–166.

(62) Karin, M. The regulation of AP-1 activity by mitogen-activated protein kinases. *J. Biol. Chem*. **1995**, *270*, 16483–16486.

(63) Lee, S.-K.; Jang, H.-J.; Lee, H.-J.; Lee, J.; Jeon, B.-H.; Jun, C.-D.; Lee, S.-K.; Kim, E.-C. p38 and ERK MAP kinase mediates iron chelator-induced apoptosis and –suppressed

differentiation of immortalized and malignant human oral keratinocytes. *Life Sciences* **2006**, *79*, 1419–1427.

(64) Moon, S. K.; Jung, S. Y.; Choi, Y. H.; Lee, Y.C.; Patterson, C.; Kim, C. H. PDTC, metal chelating compound, induces G1 phase cell cycle arrest in vascular smooth muscle cells through inducing p21Cip1 expression: Involvement of p38 mitogen activated protein kinase. *J. Cell Physiol*. **2004**, *198*, 310–323.

(65) Lane, D. J. R.; Mills, T. M.; Shafie, N. H.; Merlot, A. M.; Saleh Moussa, R.; Kalinowski, D. S.; Kovacevic, Z.; Richardson, D. R. Expanding horizons in iron chelation and the treatment of cancer: role of iron in the regulation of ER stress and the epithelial-mesenchymal transition. *Biochim. Biophys. Acta Rev. Cancer* **2014**, *1845*, 166–181.

(66) Lane, D. J. R.; Saletta, F.; Rahmanto, Y. S.; Kovacevic, Z.; Richardson, D. R. N-myc downstream regulated 1 (NDRG1) is regulated by eukaryotic initiation factor 3a (eIF3a) during cellular stress caused by iron depletion. *PLoS One* **2013**, *8*, e57273.

(67) Trondl, R.; Flocke, L. S.; Kowol, C. R.; Heffeter, P.; Jungwirth, U.; Mair, G. E.; Steinborn, R.; Enyedy, E. A.; Jakupec, M. A.; Berger, W.; Keppler, B. K. Triapine and a more potent dimethyl derivative induce endoplasmic reticulum stress in cancer cells. *Mol. Pharmacol.* **2014**, *85*, 451–459.

(68) Merlot, A. M.; Shafie, N. H.; Yu, Y.; Richardson, V.; Jansson, P. J.; Sahni, S.; Lane, D. J. R.; Kovacevic, Z.; Kalinowski, D. S.; Richardson, D. R. Mechanism of the induction of endoplasmic reticulum stress by the anti-cancer agent, di-2-pyridylketone 4,4-dimethyl-3-thiosemicarbazone (Dp44mT): activation of PERK/eIF2α, IRE1α, ATF6 and calmodulin kinase. *Biochem. Pharmacol.* **2016**, *109*, 27–47.

(69) Fu, Y.; Liu, Y.; Wang, J.; Li, C.; Zhou, S.; Yang, Y.; Zhou, P.; Lu, C.; Li, C., Calcium release induced by 2-pyridinecarboxaldehyde thiosemicarbazone and its copper complex contributes to tumor cell death. *Oncol. Rep.* **2017**, *37*, 1662–1670.

(70) Lee, A. S. GRP78 induction in cancer: therapeutic and prognostic implications. *Cancer Res.* **2007**, *67*, 3496–3499.

(71) Pillich, H.; Loose, M.; Zimmer, K-P.; Chakraborty, T. Diverse roles of endoplasmic reticulum stress sensors in bacterial infection. *Molecular and Cellular Pediatrics* **2016**, *3*, 1–6.

(72) Abuaita, B. M.; Burkholder, K. M.; Boles, B. R.; O'Riordan, M. X. The endoplasmic reticulum stress sensor inositol-requiring enzyme 1α augments bacterial killing through sustained oxidant production. *mBio* **2015**, *6*, e00705–e00715.

(73) Li, J.; Sasaki, H.; Sheng, Y. L.; Schneiderman, D.; Xiao, C. W.; Kotsuji, F.; Tsang, B. K. Apoptosis and chemoresistance in human ovarian cancer: is Xiap a determinant? *Biol. Signals Recept.* **2000**, *9*, 122–130.

(74) Alvero, A. B.; Chen, W.; Sartorelli, A. C.; Schwartz, P.; Rutherford, T.; Mor, G. Triapine (3-aminopyridine-2-carboxaldehyde thiosemicarbazone) induces apoptosis in ovarian cancer cells. *J. Soc. Gynecol. Invest.* **2006**, *13*, 145–152.

(75) Karlsson, H.; Fryknas, M.; Strese, S.; Gullbo, J.; Larsson, R.; Sjoblom, T.; Pandzic, T.; Nygren, P.; Westman, G.; Bremberg, U. Mechanistic characterization of a copper containing thiosemicarbazone with potent antitumor activity. *Oncotarget* **2017**, *8*, 30217–30234.

(76) Bisceglie, F.; Alinovi, R.; Pinelli, S.; Galetti, M.; Pioli, M.; Tarasconi, P.; Mutti, A.; Goldoni, M.; Pelosi, G. Autophagy and apoptosis: studies on the effects of bisthiosemicarbazone copper(II) complexes on p53 and p53-null tumour cell lines. *Metallomics* **2016**, *8*, 1255–1265.

(77) Hancock, C. N.; Stockwin, L. H.; Han, B.; Divelbiss, R. D.; Jun, J. H.; Malhotra, S. V.; Hollingshead, M. G.; Newton, D. L. A copper chelate of thiosemicarbazone NSC 689534 induces oxidative/ER stress and inhibits tumor growth in vitro and in vivo. *Free Radical Biol. Med.* **2011**, *50*, 110–121.

(78) De, B. M.; Taverna, E.; Bongarzone, I.; Maffioli, E.; Tedeschi, G.; Casalini, P.; Crisafi, F.; Kumar, V.; Polli, D.; Caccia, C. Lipid accumulation in human breast cancer cells injured by iron depletors. *J. Exp. Clin. Cancer Res.* **2018**, *37*, 75.

(79) Gans, P.; Sabatini, A.; Vacca, A. Investigation of equilibria in solution. Determination of equilibrium constants with HYPERQUAD suite of programms. *Talanta* **1996**, *43*, 1739–1753.

(80) Zékány, L.; Nagypál, I. in: Computational Methods for the Determination of Stability Constants, ed. D. L. Leggett, Plenum Press, New York, **1985**, p. 291.

(81) Rockenbauer, A.; Szabó-Plánka, T.; Árkosi, Zs.; Korecz, L. A two-dimensional (magnetic field and concentration) electron paramagnetic resonance method for analysis of multispecies complex equilibrium systems. Information content of EPR spectra. *J. Am. Chem. Soc.* **2001**, *123*, 7646–7654.

(82) Enyedy, É. A.; Hollender, D.; Kiss, T. Lipophilicity of kinetically labile metal complexes through the example of antidiabetic Zn(II) and VO(IV) compounds. *J. Pharm. Biomed. Anal.* **2011**, *54*, 1073–1081.

(83) *SAINT-Plus*, version 8.32B and APEX2; Bruker-Nonius AXS Inc.: Madison, WI, 2016.

(84) *CrysAlis RED*, Version 1.171.36.32; Oxford Diffraction Ltd, 2003.

(85) Sheldrick, G. M. A short history of SHELX. *Acta Crystallogr., Sect. A: Found. Crystallogr.* **2008**, *64*, 112–122.

(86) Burnett, M. N.; Johnson, G. K. ORTEPIII. Report ORNL-6895. OAK Ridge National Laboratory; Tennessee, **1996**.

(87) Mooij, W. T. M.; Verdonk, M. L., General and targeted statistical potentials for protein–ligand interactions. *Proteins* **2005,** *61*, 272–287.

(88) Eldridge, M. D.; Murray, C.; Auton, T. R.; Paolini, G. V.; Mee, P. M. Empirical scoring functions: I. The development of a fast empirical scoring function to estimate the binding affinity of ligands in receptor complexes. *J. Comp. Aid. Mol. Design* **1997,** *11*, 425–445.

(89) Verdonk, M. L.; Cole, J. C.; Hartshorn, M. J.; Murray, C. W.; Taylor, R. D. Improved protein-ligand docking using GOLD. *Proteins* **2003**, *52*, 609–623.

(90) Korb, O.; Stuetzle, T.; Exner, T. E. Empirical scoring functions for advanced protein-ligand docking with PLANTS. *J. Chem. Inf. Model.* **2009**, *49*, 84–96.

(91) Schrödinger *Small-Molecule Drug Discovery Suite 2015-4: QikProp*, 4.6; 2015.

(92) ChemAxon-Marvin, ChemAxon. Ltd: 15.7.13.0, 2015, http://www.chemaxon.com.

(93) Ioakimidis, L.; Thoukydidis, L.; Mirza, A.; Naeem, S.; Reynisson, J., Benchmarking the reliability of QikProp. Correlation between experimental and predicted values. *QSAR & Combinatorial Science* **2008,** *27*, 445–456.

(94) Clinical and laboratory standards institute. Methods for dilution antimicrobial susceptibility test for bacteria that grow aerobically; approved standard, CLSI document M7-A7, 7th ed. *Clinical and Laboratory Standards Institute, Wayne, PA* **2006**.

Supporting Information

for

New Water-Soluble Copper(II) Complexes with Morpholine-Thiosemicarbazone Hybrids: Insights into the Anticancer and Antibacterial Mode of Action

Kateryna Ohui,[a, ≠] Eleonora Afanasenko,[a, ≠] Felix Bacher,[a] Rachel Lim Xue Ting,[b] Ayesha Zafar,[c] Núria Blanco-Cabra,[d] Eduard Torrents,[d] Orsolya Dömötör,[e] Nóra V. May,[f] Denisa Darvasiova,[g] Éva A. Enyedy,[e] Ana Popović-Bijelić,[h] Jóhannes Reynisson,[c] Peter Rapta,[g] Maria V. Babak,*[,i,j] Giorgia Pastorin,[b] Vladimir B. Arion*[,a]

[a]*University of Vienna, Institute of Inorganic Chemistry, Währinger Strasse 42, A-1090 Vienna, Austria,* [b]*Department of Pharmacy, National University of Singapore, Singapore, 3 Science Drive 2, 117543 Singapore*

[c]*School of Chemical Sciences, University of Auckland, Auckland, New Zealand*

[d]*Bacterial Infections: Antimicrobial Therapies, Institute for Bioengineering of Catalonia (IBEC), The Barcelona Institute of Science and Technology, Barcelona, Spain*

[e]*Department of Inorganic and Analytical Chemistry, University of Szeged, Dóm tér 7. H-6720 Szeged, Hungary*

[f]*Research Centre of Natural Sciences, Hungarian Academy of Sciences, Magyar tudósok körútja 2. H-1117, Budapest, Hungary*

[g]*Institute of Physical Chemistry and Chemical Physics, Slovak Technical University of Technology, Radlinského 9, 81237 Bratislava, Slovak Republic*

[h]*Faculty of Physical Chemistry, University of Belgrade, 11158 Belgrade, Serbia*

[i]*Department of Chemistry, National University of Singapore,3 Science Drive 2, 117543 Singapore*

[j]*Drug Development Unit, National University of Singapore,28 Medical Drive, 117546 Singapore*

[≠] these co-authors contributed equally

Keywords: Thiosemicarbazones, Cu(II)-TSC, solution equilibrium, stability constants, spectroelectrochemistry, molecular modelling , antitumor activity, antibacterial activity, mechanism of action, cellular accumulation, ribonucleotide reductase inhibition, ER stress, apoptosis, cell cycle

Synthesis of proligand precursors

Scheme S1. Atom numbering used for proton and carbon resonances assignment in ^{1}H and ^{13}C NMR spectra of **HL$^{1–6}$**.

Figure S1. ORTEP view of **HL^{1}**, **HL^{2}** and **HL$^{4–6}$**

Figure S2. A fragment of an infinite chain formed in the crystal of **6**.

Figure S3. Low field region of the ^{1}H NMR spectra of **HL^{1}** recorded at pH 0.75–12.50

Figure S4. Concentration distribution curves of **HL^{1}** and pH-dependent chemical shift values (δ / ppm) for the C*H*(=N) proton measured by ^{1}H NMR spectroscopic titration.

Figure S5. UV–vis spectra recorded for the Cu(II)–**HL^{1}** (1:1) system at various pH values.

Figure S6. UV–vis spectra of the Cu(II) – **HL^{1}** – EDTA system recorded at pH 6.00 at various EDTA-to-**HL^{1}** ratios. Inset shows the measured absorbance values at 320 nm (■) and 394 nm (Δ) plotted against the EDTA-to-**HL^{1}** ratios.

Figure S7. Experimental (black) and simulated (red) solution EPR spectra recorded for Cu(II) – **HL^{1}** 1:0.75 (a) and 1:1.5 (b) systems together with the calculated component EPR spectra obtained for various complexes (c) at room temperature.

Figure S8. (a) UV–vis spectra of **1–5** in DMSO; (b) UV–vis spectrum of **2** in H_2O; (c) UV–vis spectra of **2** in DMSO (red line), MeOH (black line) and in H_2O (blue line).

Figure S9. (a) Cyclic voltammograms of **5** in *n*Bu_4NPF_6/DMSO in the region of the first cathodic peak (black line) as well as going to the second reduction step (red line). (b) Cyclic

voltammetry of Cu(II) complexes **1**–**5** in DMSO in the region of the first electron transfer in the presence of ferrocene. (c) Cyclic voltammetry of **6** (two consecutive scans) in *n*Bu_4NPF_6/DMSO.

Figure S10. (a) Cyclic voltammograms of **2** in $H_2O/LiClO_4$ at different scan rates in the region of the first cathodic peak (GC-disc working electrode). (b) Cyclic voltammetry of **2** in the region of the first electron transfer in different solvents (red line – DMSO, black line – MeOH, blue line – H_2O) in the presence of ferrocene.

Figure S11. Cyclic voltammograms of **2** in $MeOH/LiClO_4$ in the cathodic (green line) and anodic (blue line) region as well as the cyclic voltammograms of the corresponding proligand $\mathbf{HL^2}$ in the cathodic (black line) and anodic (red line) part.

Figure S12. Potential dependence of UV–vis spectra of **2** in $H_2O/LiClO_4$ measured in the region of the first cathodic peak.

Figure S13. Concentration-effect curves for $\mathbf{HL^{1–6}}$, **1**–**6** and cisplatin in A2780, A2780cis and HEK293 cells lines upon 72 h exposure.

Figure S14. The hydrogen bond interactions of Triapine (a) and **5** (b) with aminoacids inside R2 RNR binding pocket.

Figure S15. a) Time-dependent Tyrosyl radical reduction in mouse R2 RNR protein by $\mathbf{HL^2}$, $\mathbf{HL^5}$, **2**, and **5** at 1:1 protein-to-drug ratio in the presence of DTT. b) EPR spectrum of the Tyrosyl radical in mouse R2 RNR protein at 30 K. c) UV–vis spectra of $\mathbf{HL^2}$ (black line), $\mathbf{HL^2}$ + $FeCl_3{\cdot}6H_2O$ at 2:1 mole ratio (red trace), $\mathbf{HL^2}$ + $FeCl_3{\cdot}6H_2O$ + DTT at 2:1:5 mole ratio measured immediately after DTT addition (blue trace) and after 5 min (green trace), as well as UV–vis spectrum of the complex prepared by mixing $\mathbf{HL^2}$ + $FeSO_4{\cdot}7H_2O$ at 2:1 ratio (violet trace), all in buffered water solution (using pH 7 buffer capsules from Sentec) and measured aerobically (1 cm quartz UV–vis cuvette). d) UV–vis spectra of $\mathbf{HL^5}$ + $FeCl_3{\cdot}6H_2O$ at 2:1 mole ratio (red trace), $\mathbf{HL^5}$ + $FeCl_3{\cdot}6H_2O$ + DTT at 2:1:5 mole ratio measured immediately after DTT addition (green trace).

Figure S16. ESI mass spectrum of $[Fe^{III}(L^5)_2]^+$ obtained *in situ* from $FeCl_3$ and **HL^5** in 1:1 molar ratio.

Table S1. Selected bond distances (Å) and bond angles (deg) in **1**, **1´**, **5** and **6**.

Table S2. Selected bond distances (Å) and bond angles (deg) in **3** and **4**.

Table S3. Proton dissociation constants of **HL^1** determined by pH-potentiometry and EPR spectroscopy.

Table S4. Cumulative stability (logβ) and proton dissociation constants of the Cu(II) complexes of **HL^1** determined by UV–vis, pH-potentiometry and EPR spectroscopy

Table S5. Formation constants and isotropic EPR parameters of the components obtained for Cu(II) – **HL^1** complexes.

Table S6. Electrochemical and optical spectral data of **1**–**6**.

Table S7. Molecular descriptors for **HL^1**–**HL^6** and **1**–**6.**

Table S8. The results of the scoring functions for the ligands **HL$^{1–6}$** and and their Cu(II) complexes **1**–**6**.

Table S9. Yields, m.p. and analytical data for **HL^1**–**HL^6**.

Table S10. Yields and analytical data for **1**–**6**.

Table S11. Crystal data and details of data collection for **HL^1**, **HL^2**, **HL$^{4–6}$**.

Table S12. Crystal data and details of data collection for Cu(II) complexes

Synthesis of proligand precursor

Synthesis of **B** (as described in ref. 43). To a slurry of the 2,5-pyridinecarboxylic acid **A** (34 g, 0.2 mol) in 120 ml of methanol at 0 °C was added dropwise 15 ml of thionyl chloride and the resulting slurry was warmed up to room temperature, giving rise to a clear solution. The mixture then was heated at reflux for 12 h to afford yellow slurry. Filtration of the reaction mixture provided dimethyl-2,5-pyridinecarboxylate **B** in a quantitative yield as a yellow crystalline solid.

Synthesis of 2,5-Pyridinedimethanol (**C**) (as described in ref. 44). Dimethyl -2,5-pyridinecarboxylate **B** (5.03 g, 0.03 mol) was suspended in ethanol (70 ml), and the mixture was cooled to 0 °C in the ice bath. Sodium borohydride (4.53 g, 0.12 mol) was added in small portions to the mixture. After the reaction mixture was stirred for 1 h at 0 °C, the ice bath was removed; the outgoing exothermic reaction caused the solution to warm and boil under reflux. Stirring of the mixture was continued for 3 h, and then it was heated overnight under reflux. The solvent was removed by distillation, and the residue was dissolved in acetone (70 ml). Saturated aqueous potassium carbonate (70 ml) was added, and the mixture was heated at boiling temperature for 1 h. This resulted in a yellow layer separating from the reaction mixture, which was isolated and extracted continuously with chloroform (ca 14 h) to yield the product as yellow oil. Yield: 3.07 g (84%). ^{1}H NMR (D_2O, 300 MHz): δ 4.68 (s, 2H, C*H*$_2$), 4.72 (s, 2H, C*H*$_2$), 7.51 (d, 1H, $^{3}J_{HH}$ = 7.8 Hz, py*H*), 8.43 (d, 1H, $^{3}J_{HH}$ = 6.1 Hz, py*H*), 8.45 (s, 1H, py*H*-6); ^{1}H NMR (DMSO-d_6, 60 MHz): δ 4.55 and 4.59 (2s, 4H, C*H*$_2$OH), 5.23 (br s, 2H, CH_2O*H*), 7.42 (d, *J* = 8 Hz, 1H, 3´-H), 7.72 (dd, *J* = 2 and 8 Hz, 1H, 4´-H), 8.42 (d, *J* = 2 Hz, 1H, 6´-H).

Synthesis of 2-formyl-5-hydroxymethylpyridine (**D**) (as described in ref. 45). The crude diol **C** (10.5 g, 0.076 mol) was dissolved in 80 ml of dioxane and 2 ml of water, and 4.0 g (0.036 mol) of SeO_2 was added. The mixture was degassed three times under argon and then heated at 100 °C for 3 h. The cooled reaction mixture was filtered through Celite (30-ml dioxane wash). The filtrate and washings were concentrated to about a 10 ml volume and chromatographed on 150 g of silica gel (50% EtOAc/Hexane and 75% EtOAc/Hexane) to give 6.2 g (59% yield) of the aldehyde as a pale yellow solid. A portion was recrystallized from EtOAc/Hexane to give white plates: mp 75 °C; ^{1}H NMR ($CDCl_3$, 60 MHz): δ 4.23 (br s, 1H,

OH), 4.90 (s, 2H, CH_2), 7.95 and 7.97 (2s, 2H, 3´- and 4´-H), 8.77 (s, 1H, 6´-H), 10.07 (s, 1H, CHO); MS calcd for $C_7H_7NO_2$, 137.0478; found, 137.0471.

(6-(dimethoxymethyl)pyridine-3-yl)methanol (**E**). 5-(hydroxymethyl)pyridinecarboxaldehyde (1.22 g, 8.92 mmol), trimethyl orthoformate (3.83 ml, 35.0 mmol), methanesulfonic acid (140 µl, 0.21mmol) and absolute methanol (14 ml) were combined in a 50 ml Shlenk tube. The reaction mixture was stirred at 78 °C for 48 h. After cooling down the solvent was evaporated under reduced pressure. The residue was dissolved in $CHCl_3$ (50 ml) and washed with saturated aqueous K_2CO_3 and brine. The aqueous phase was extracted with $CHCl_3$ (3 x 40 ml). The combined organic layers were dried over $MgSO_4$ and the solvent was removed under reduced pressure to give a red-brown oil. Yield: 1.61 g, 98%. ^{1}H NMR (500 MHz, DMSO-d_6) δ 8.52 – 8.44 (m, 1H, C$H_{(Ar)}$), 7.77 (dd, J = 8.0, 2.2 Hz, 1H, C$H_{(Ar)}$), 7.46 (d, J = 8.0 Hz, 1H, C$H_{(Ar)}$), 5.34 (t, J = 5.5 Hz, 1H, O*H*), 5.28 (s, 1H, *H*C$(OCH_3)_2$), 4.55 (d, J = 4.8 Hz, 2H, CH_2OH), 3.30 (s, 6H, (OCH_3)$_2$).

5-(chloromethyl)-2-(dimethoxymethyl)pyridine (**F**). (6-(dimethoxymethyl)pyridine-3-yl)methanol (0.50 g, 2.73 mmol) was dissolved in dry CH_2Cl_2 (20 ml) in a 100 ml nitrogen flask and cooled to -80 °C. A solution of thionyl chloride (218 µl, 3.00 mmol) in dry CH_2Cl_2 (15 ml) was added dropwise via dropping funnel. After complete addition the reaction mixture was stirred overnight, while it was allowed to slowly reach room temperature. Next day the reaction mixture was cooled to -70 °C and trimethylamine (454 µl, 3.28 mmol) was added dropwise. The reaction mixture was allowed to reach room temperature, stirred for 1 h at room temperature and then poured into iced water (50 ml). Then saturated aqueous Na_2CO_3 (50 ml) was added and the resulting mixture was extracted with CH_2Cl_2 (3 x 50 ml). The combined organic layers were dried over $MgSO_4$ and the solvent was removed under reduced pressure to give a dark-red oil. Yield: 0.44 g, 80%. ^{1}H NMR (500 MHz, DMSO-d_6) δ 8.63 (d, J = 2.2 Hz, 1H, C$H_{(Ar)}$), 7.93 (dd, J = 8.0, 2.2 Hz, 1H, C$H_{(Ar)}$), 7.53 (d, J = 8.1 Hz, 1H C$H_{(Ar)}$), 5.31 (s, 1H, *H*C$(OCH_3)_2$), 4.85 (s, 2H, CH_2Cl), 3.31 (s, 6H, (OCH_3)$_2$).

4-((6-(dimethoxymethyl)pyridine-3-yl)methyl)morpholine (**G**). To a solution of 5-(chloromethyl)-2-(dimethoxymethyl)pyridine (0.44 g, 2.18 mmol) in 1:1 mixture of dry CH_2Cl_2 and dry THF (11 ml) were added morpholine (285 µl, 3.27 mmol) and trimethylamine (907 µl, 6.54 mmol). The reaction mixture was stirred overnight at 50 °C (50 ml Shlenk tube).

The next day the mixture was cooled to room temperature and the white precipitate of triethylammonium chloride was filtered off and washed with THF. The solvent was removed under reduced pressure and the brown, oily raw product was purified on a silica gel column, using CH_2Cl_2/MeOH 95:5 as eluent, to give the product as pale yellow oil. Yield: 0.38 g, 69%. ^{1}H NMR (500 MHz, DMSO-d_6) δ 8.47 (d, J = 1.5 Hz, 1H, C$H_{(Ar)}$), 7.77 (dd, J = 8.0, 2.1 Hz, 1H, C$H_{(Ar)}$), 7.46 (d, J = 8.0 Hz, 1H, C$H_{(Ar)}$), 5.28 (s, 1H, HC(OCH$_3$)$_2$), 3.60-3.55 (m, 4H, C$H_{2(morph)}$), 3.51 (s, 2H, CH_2), 3.30 (s, 6H, (OCH_3)$_2$), 2.40-2.32 (m, 4H, C$H_{2(morph)}$).

5-(morpholinomethyl)pyridinecarbaldehyde (**H**). 4-((6-(dimethoxymethyl)pyridine-3-yl)methyl)morpholine (0.38 g, 1.87 mmol) was mixed with water (20 ml) and 12 M HCl (0.49 ml, 5.88 mmol). The reaction mixture was stirred at 60 °C for 6 h. After reaching room temperature the reaction was mixed with saturated aqueous K_2CO_3 and extracted with CH_2Cl_2 (3 x 40 ml). The combined organic layers were dried over $MgSO_4$ and the solvent was removed under reduced pressure to give colorless oil, which crystallized after a few hours to give a beige solid. Yield: 0.29 g, 75%. ^{1}H NMR (500 MHz, DMSO-d_6) δ 9.99 (s, 1H, CHO), 8.76 (d, J = 1.5 Hz, 1H, C$H_{(Ar)}$), 7.98 (dd, J = 7.9, 1.7 Hz, 1H, C$H_{(Ar)}$), 7.93 (d, J = 7.9 Hz, 1H, C$H_{(Ar)}$), 3.63 (s, 2H, CH_2), 3.61-3.55 (m, 4H, C$H_{2(morph)}$), 2.42-2.34 (m, 4H, C$H_{2(morph)}$).

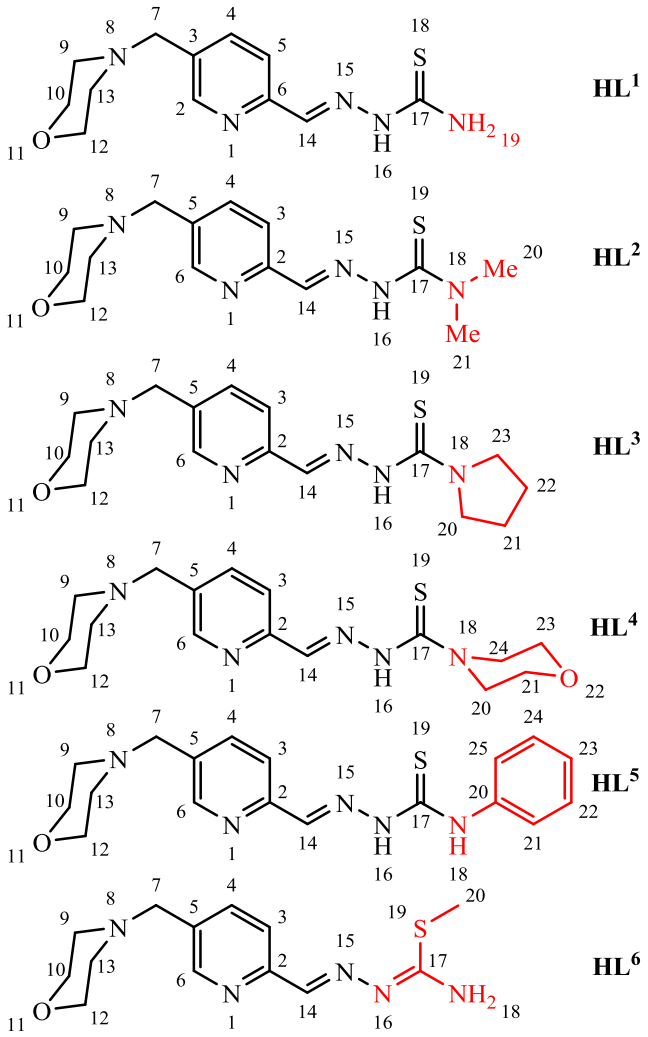

Scheme S1. Atom numbering used for proton and carbon resonances assignment in ^{1}H and ^{13}C NMR spectra of **HL^{1}**–**HL^{6}**.

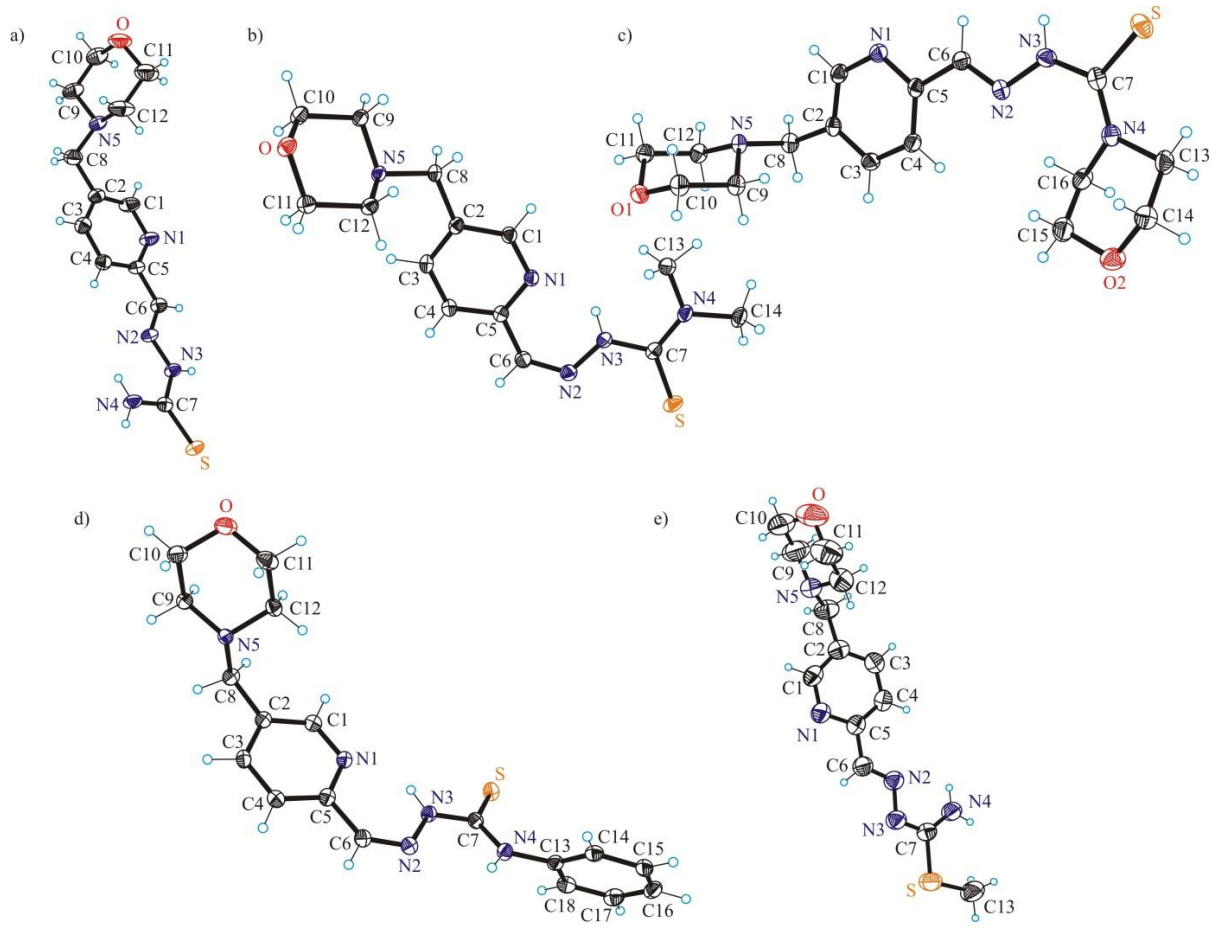

Figure S1. ORTEP views of proligands: a) **HL**[1], b) **HL**[2], c) **HL**[4], d) **HL**[5] and e) **HL**[6]. Selected bond distances (Å) and bond angles (deg) in **HL**[1]: C6–N2 1.276(4), N2–N3 1.374(3), N3–C7 1.355(4), C7–N4 1.325(4), C7–S 1.690(3), N1–C5–C6–N2 177.0(3), N2–N3–C7–N4 1.9(4); in **HL**[2]: C6–N2 1.292(2), N2–N3 1.3651(17), N3–C7 1.3746(19), C7–N4 1.343(2), C7–S 1.6783(16), N1–C5–C6–N2 –3.8(3), N2–N3–C7–N4 177.87(13); in **HL**[4]: C6–N2 1.280(2), N2–N3 1.372(2), N3–C7 1.361(2), C7–N4 1.333(3), C7–S 1.692(2), N1–C5–C6–N2 176.22(16), N2–N3–C7–N4 14.7(3); in **HL**[5]: C6–N2 1.2870(19), N2–N3 1.3612(18), N3–C7 1.3673(19), C7–N4 1.3410(19), C7–S 1.6752(16), N1–C5–C6–N2 –3.9(2), N2–N3–C7–N4 –13.29(19); in **HL**[6]: C6–N2 1.276(2), N2–N3 1.3888(17), N3–C7 1.315(2), C7–N4 1.319(2), C7–S 1.7549(14), S–C13 1.775(2), N1–C5–C6–N2 176.04(14), N2–N3–C7–N4 0.0(2).

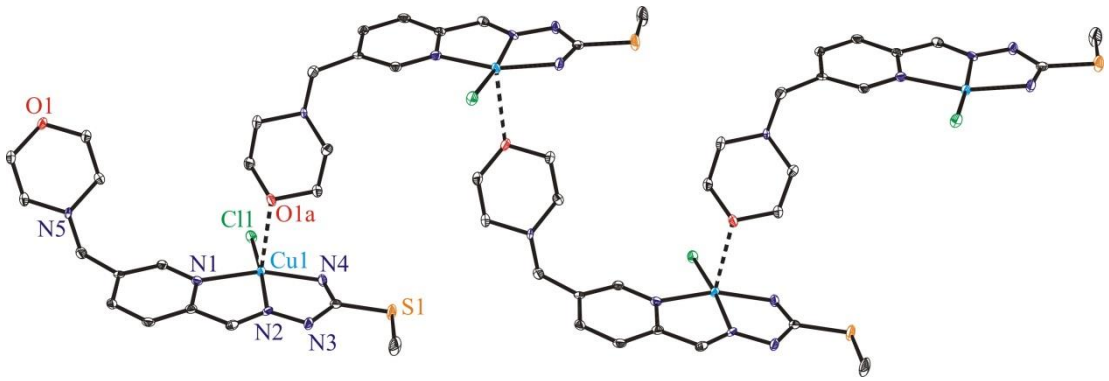

Figure S2. A fragment of an infinite chain formed in the crystal of **6**.

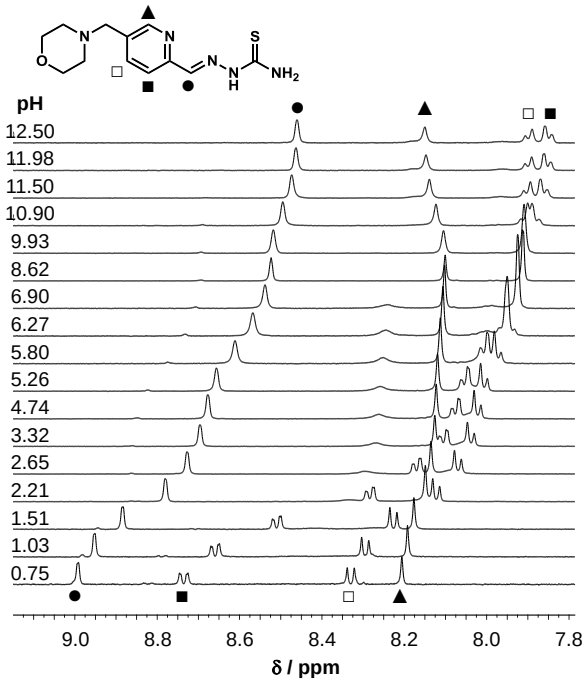

Figure S3. Low field region of the ^{1}H NMR spectra of **HL^{1}** recorded at pH 0.75–12.50 {$c_{proligand}$ = 0.84 mM; 10% D_2O/H_2O, I = 0.1 M (KCl)}. Exact pH values at pH < 2 and at pH > 11.5 were calculated based on the strong acid or strong base content of the sample.

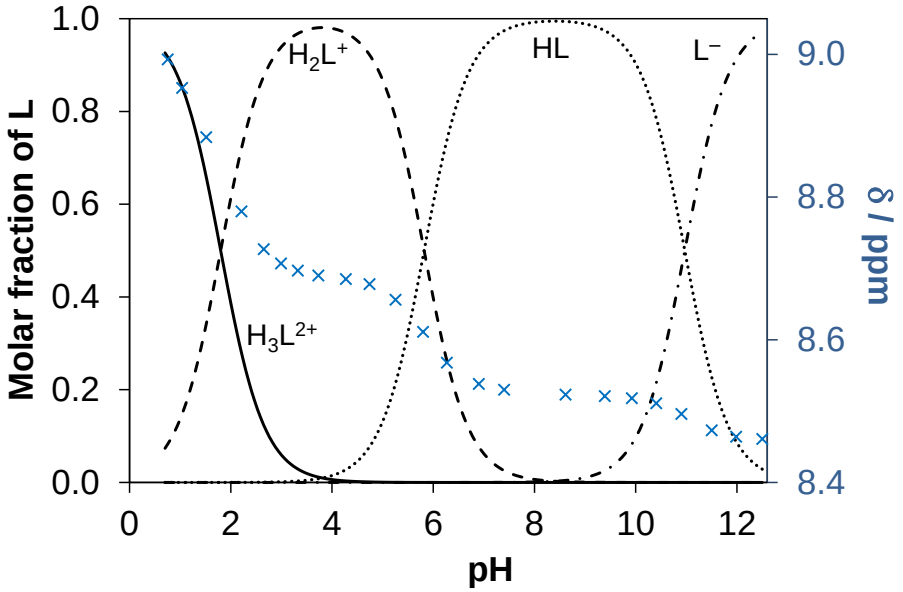

Figure S4. Concentration distribution curves of **HL**[1] and pH-dependent chemical shift values (δ / ppm) for the C*H*(=N) proton measured by ^{1}H NMR spectroscopic titration. {^{1}H NMR: $c_{proligand}$ = 0.84 mM; t = 25.0 °C; in 10 % D_2O/H_2O; I = 0.1 M (KCl)}.

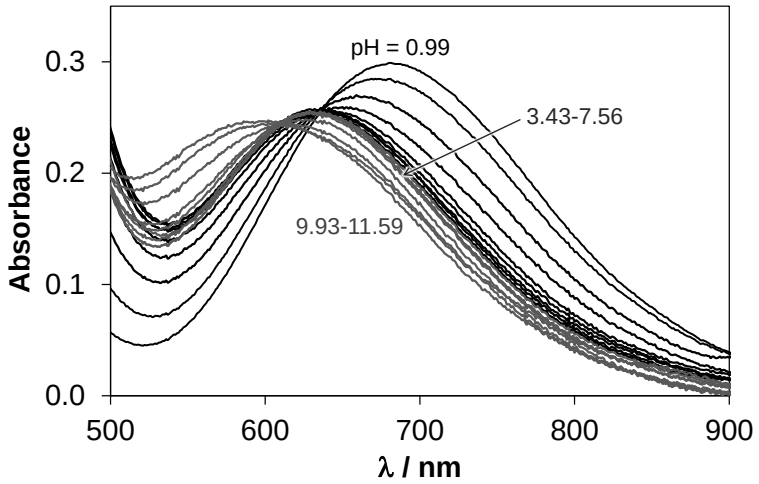

Figure S5. UV–vis spectra recorded for the Cu(II)–**HL**[1] (1:1) system at various pH values {$c_{Cu(II)}$ = c_{lig} = 745 μM; T = 25 ˚C; I = 0.10 M (KCl); *l* = 2 cm}.

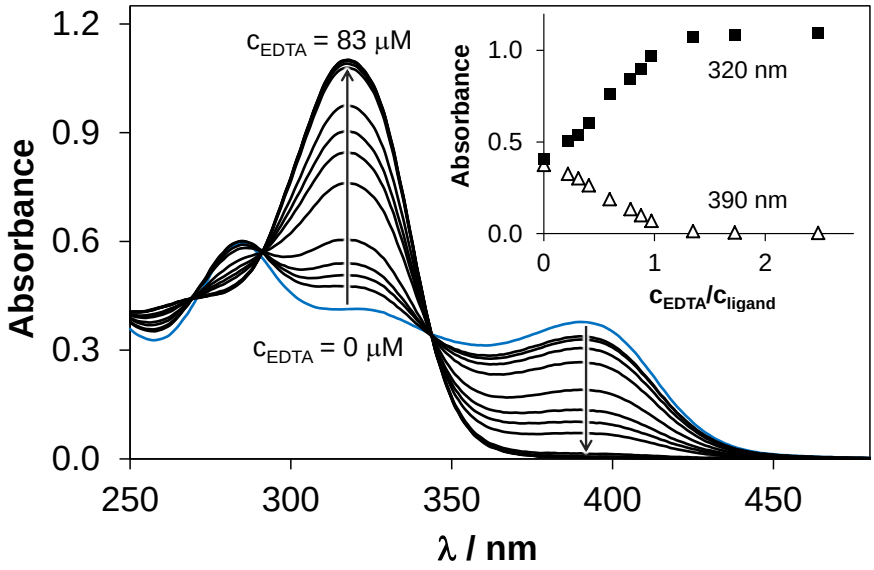

Figure S6. UV–vis spectra of the Cu(II) – **HL**^{1} – EDTA system recorded at pH 6.00 at various EDTA-to-**HL**^{1} ratios. Inset shows the measured absorbance values at 320 nm (■) and 394 nm (Δ) plotted against the EDTA-to-**HL**^{1} ratios. {$c_{Cu(II)}$ = c_{lig} = 34 μM; c_{EDTA} = 0–83 μM; pH = 6.00 (50 mM MES buffer); incubation time = 30 min; T = 25 ˚C; I = 0.10 M (KCl); l = 1 cm}.

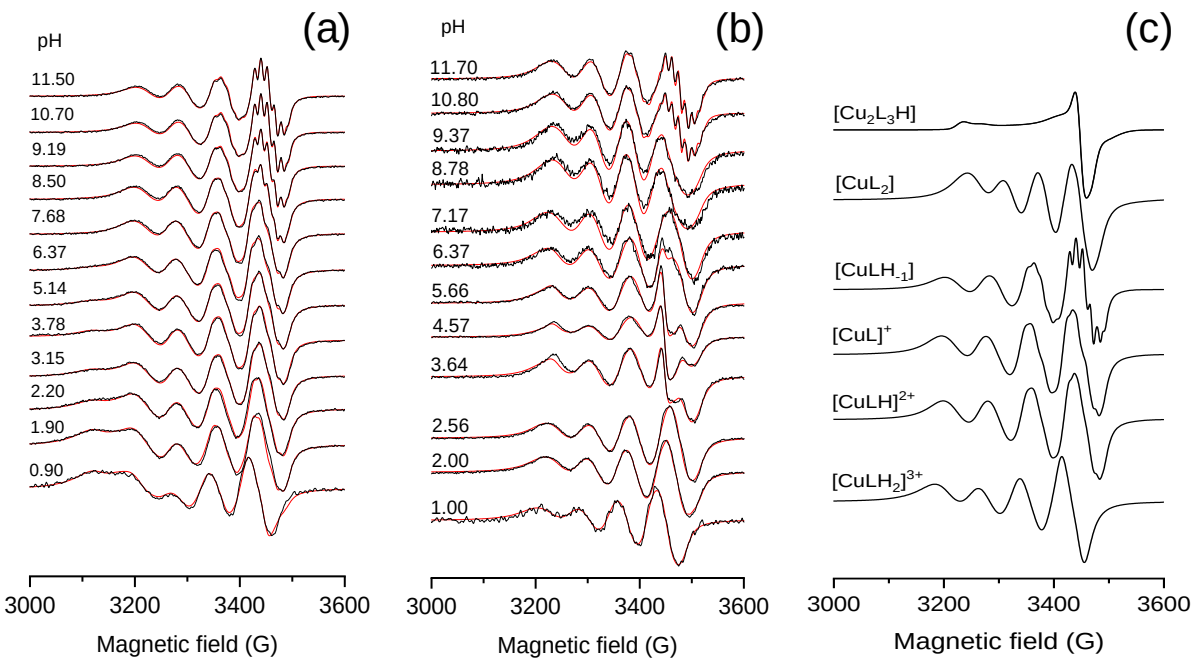

Figure S7. Experimental (black) and simulated (red) solution EPR spectra recorded for Cu(II) – **HL**[1] 1:0.75 (a) and 1:1.5 (b) systems together with the calculated component EPR spectra obtained for various complexes (c) at room temperature. Spectra were normalised to the maximum intensity {c_{Cu} = 1 mM; t = 25.0 °C; I = 0.1 M (KCl)}.

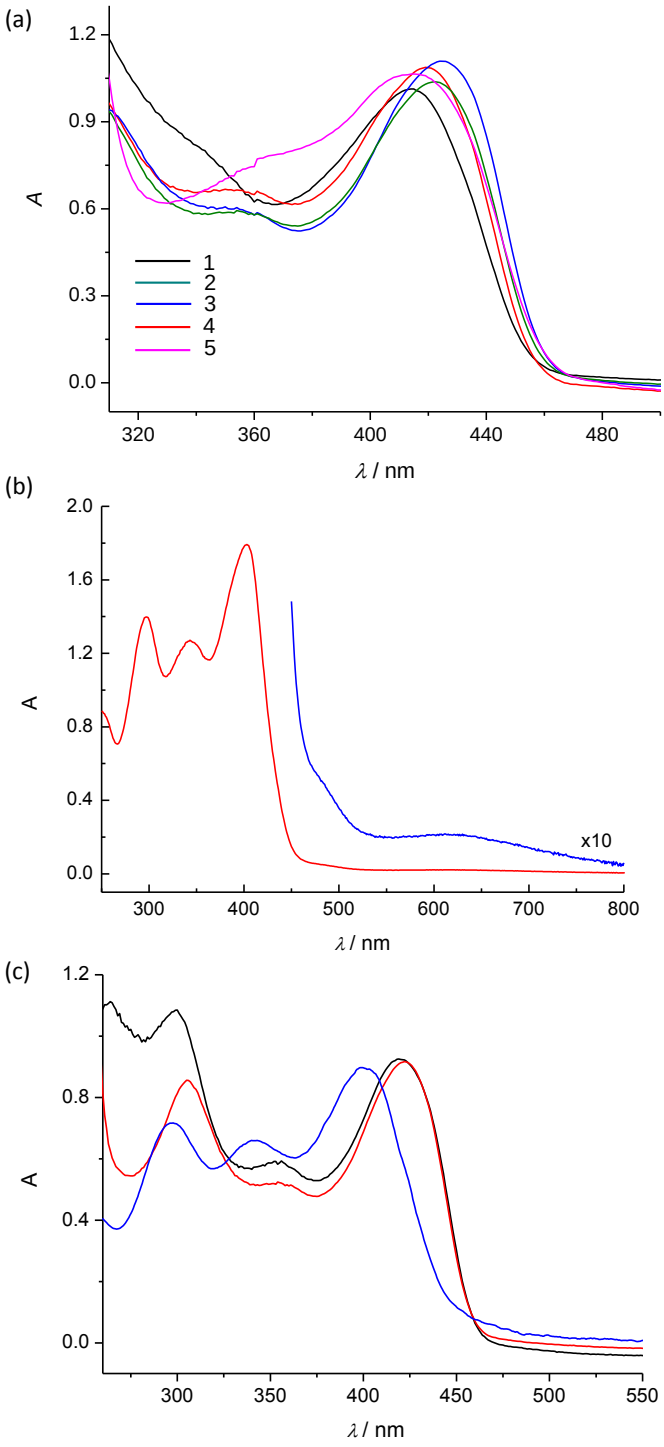

Figure S8. (a) UV–vis spectra of **1–5** in DMSO; (b) UV–vis spectrum of **2** in H_2O; (c) UV–vis spectra of **2** in DMSO (red line), MeOH (black line) and in H_2O (blue line).

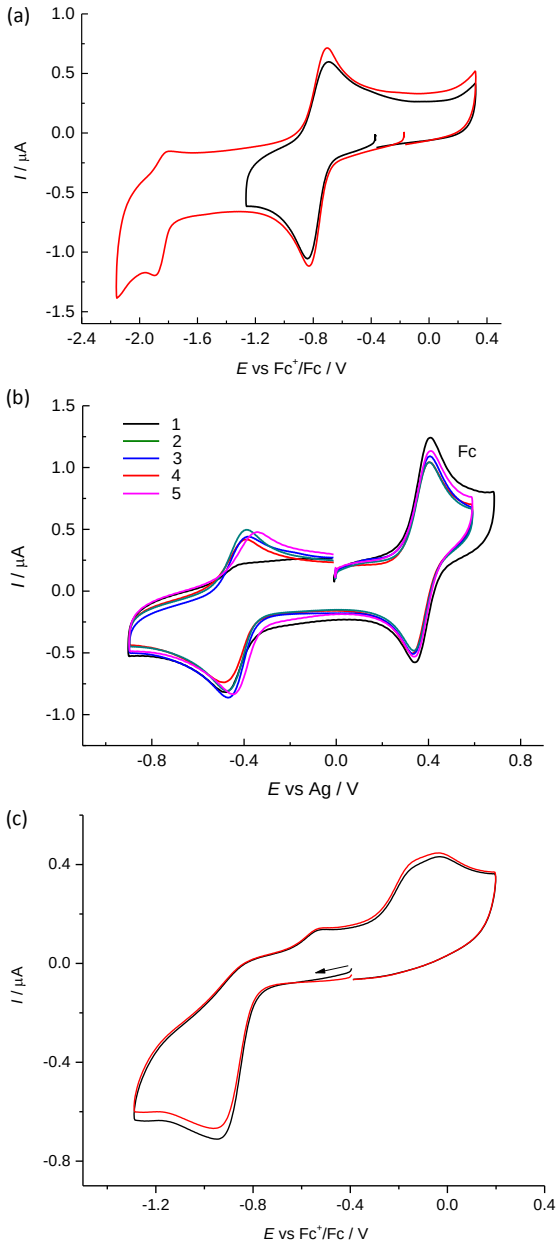

Figure S9. (a) Cyclic voltammograms of **5** in nBu$_4$NPF$_6$/DMSO in the region of the first cathodic peak (black line) as well as going to the second reduction step (red line). (b) Cyclic voltammetry of copper(II) complexes **1**–**5** in DMSO in the region of the first electron transfer

in the presence of ferrocene. (c) Cyclic voltammetry of **6** (two consecutive scans) in nBu$_4$NPF$_6$/DMSO (Pt-disc working electrode, scan rate 100 mV s^{-1}).

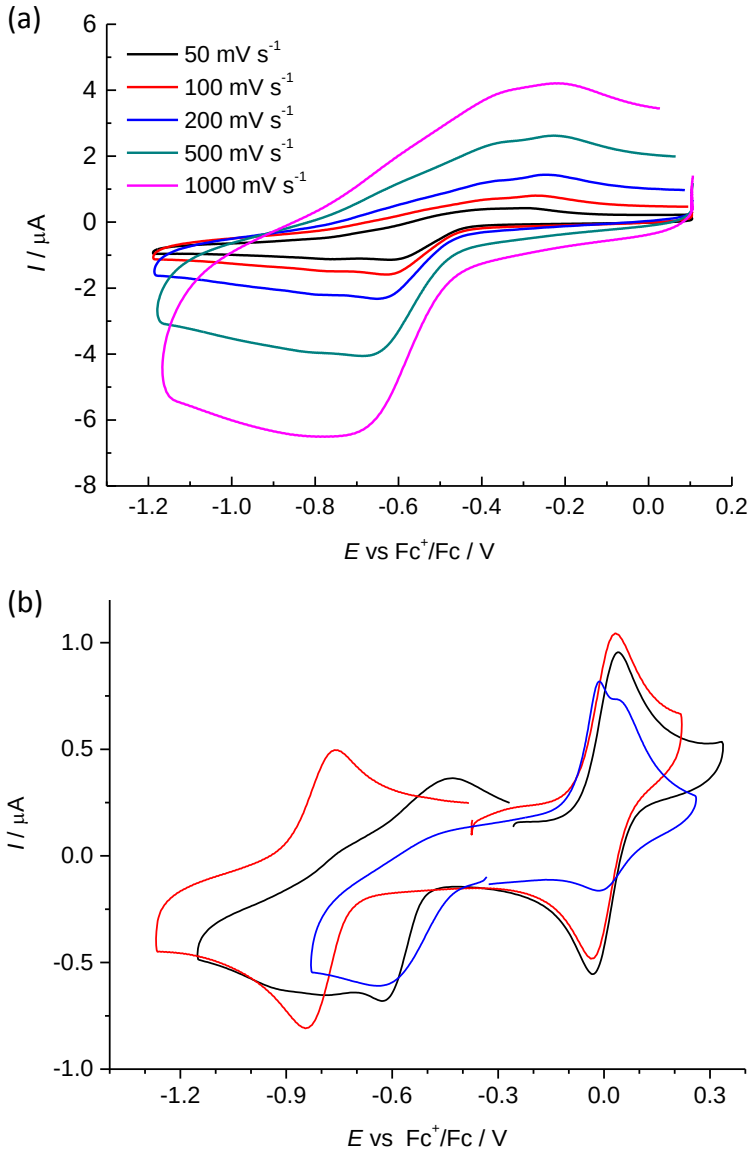

Figure S10. (a) Cyclic voltammograms of **2** in H_2O/$LiClO_4$ at different scan rates in the region of the first cathodic peak (GC-disc working electrode). (b) Cyclic voltammetry of **2** in the region of the first electron transfer in different solvents (red line – DMSO, black line – MeOH, blue line – H_2O) in the presence of ferrocene (in the case of water solution ferrocene dissolved in small amount of DMSO was added).

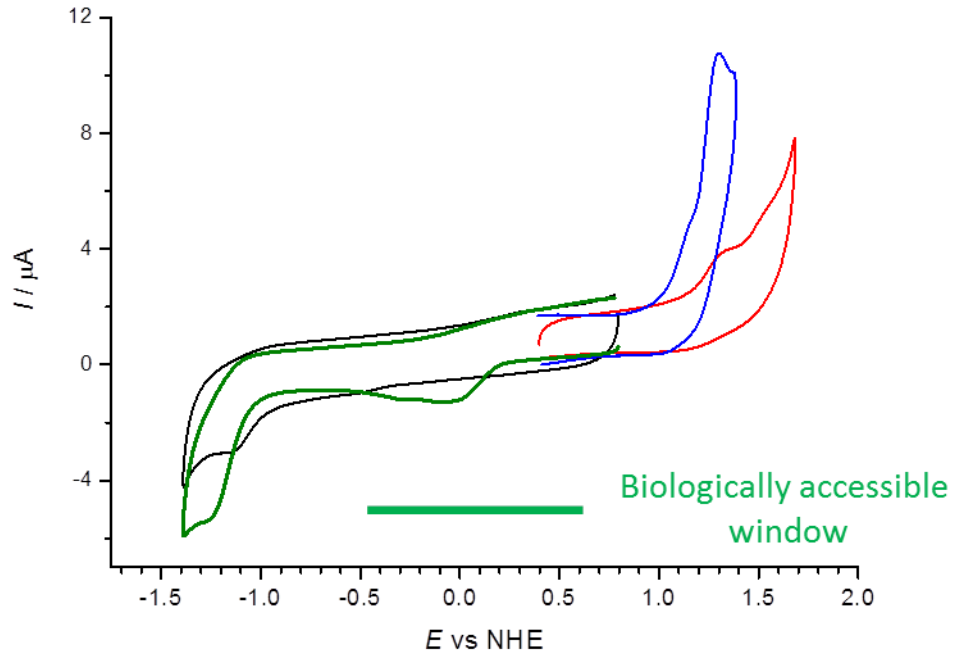

Figure S11. Cyclic voltammograms of **2** in MeOH/$LiClO_4$ in the cathodic (green line) and anodic (blue line) region as well as the cyclic voltammograms of the corresponding proligand **HL**^{2} in the cathodic (black line) and anodic (red line) part (GC-disc working electrode, scan rate 100 mV s^{-1}). The potentials were recalculated vs normal hydrogen electrode (NHE) reference using the known $E_{1/2}$ of ferricenium/ferrocene (+0.64 V) vs NHE [V. V. Pavlishchuk and A. W. Addison, *Inorg. Chim. Acta*, **2000**, *298*, 97–102].

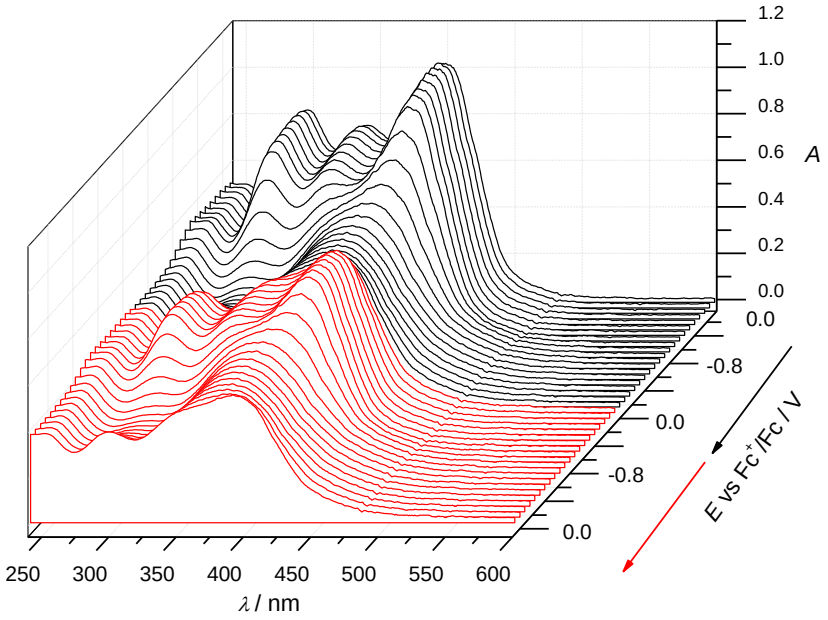

Figure S12. Potential dependence of UV–vis spectra of **2** in $H_2O/LiClO_4$ measured in the region of the first cathodic peak (two consecutive scans: black lines – the first voltammetric scan, red lines – the second voltammetric scan, Pt-microstructured honeycomb working electrode, scan rate v = 10 mV s^{-1}).

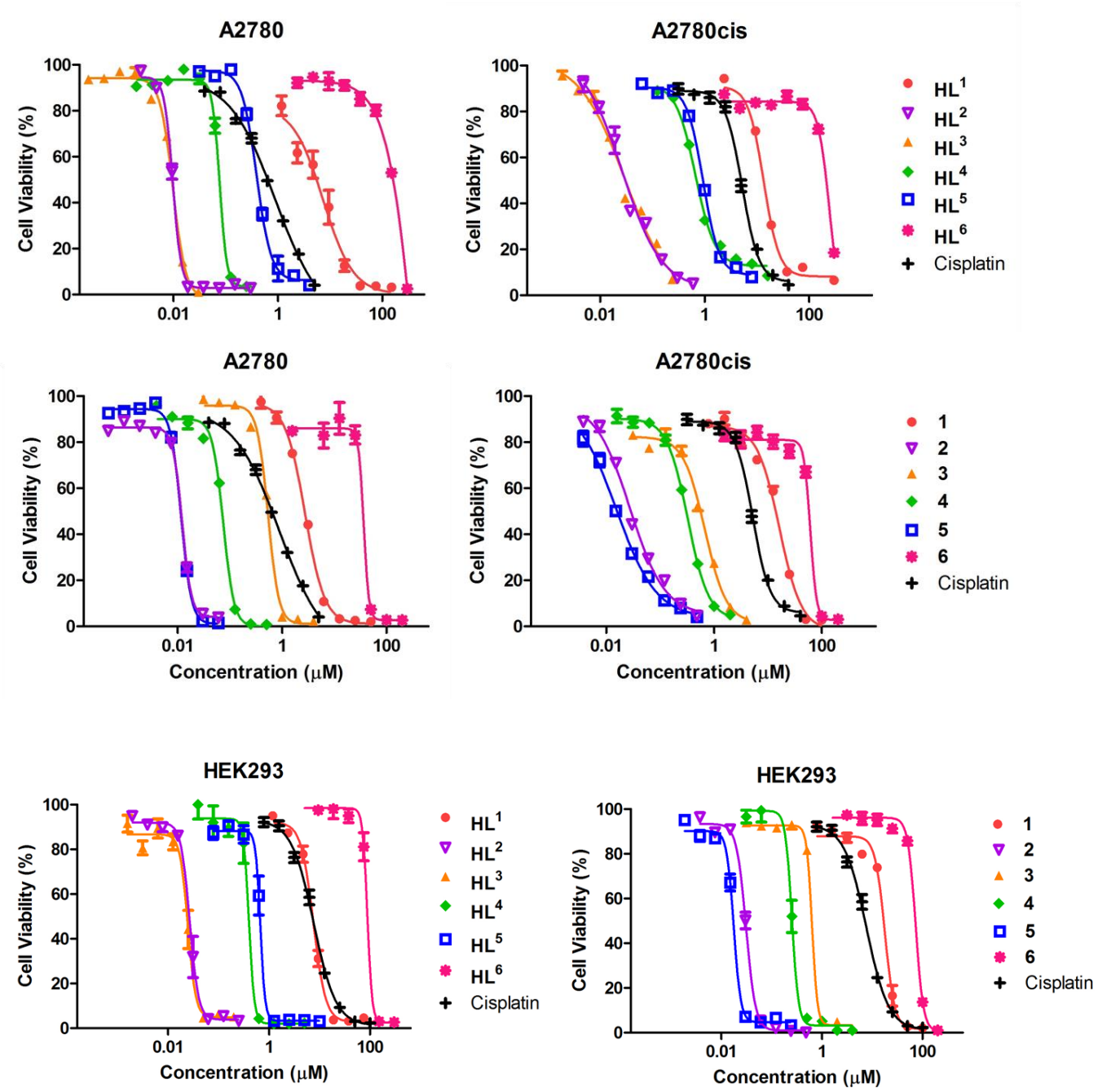

Figure S13. Concentration-effect curves for **HL**$^{1–6}$, **1**–**6** and cisplatin in A2780, A2780cis and HEK293 cells lines upon 72 h exposure.

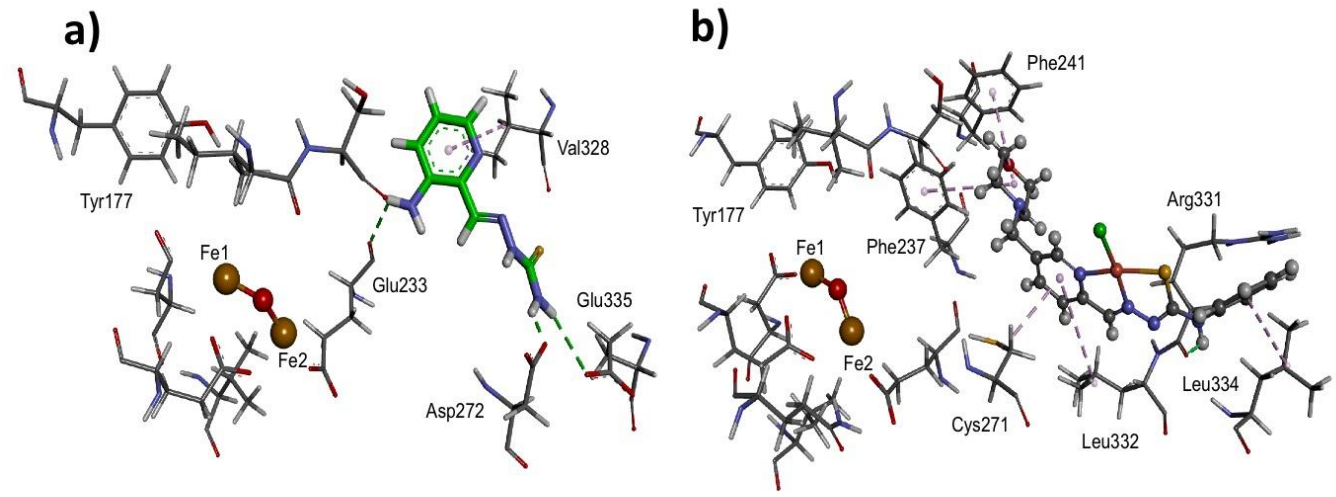

Figure S14. The hydrogen bond interactions of Triapine (a) and **5** (b) with aminoacids inside R2 RNR binding pocket. The hydrogen bond interactions are depicted as green lines. Lipophilic contacts are shown as purple dashed lines.

Complex **5** exhibited lipophilic contacts to Phe237, Phe241, Leu332, Leu334 and Cys271 amino acids residues and was involved in hydrogen-bonding interactions with Arg331. Likewise, it was reported that the pyridine ring of Triapine was located in the pocket formed by Phe237, Phe241, Ser238 and Tyr324 and hydrogen-bonding interactions with Glu233, Glu335, Asp272 and Arg331 were detected [*Journal of inorganic biochemistry* **2011,** *105* (11), 1422-1431]. It should be noted that Cys271 and Phe237 are close to Fe_2O and the enzymatically essential tyrosyl residue (Tyr177).

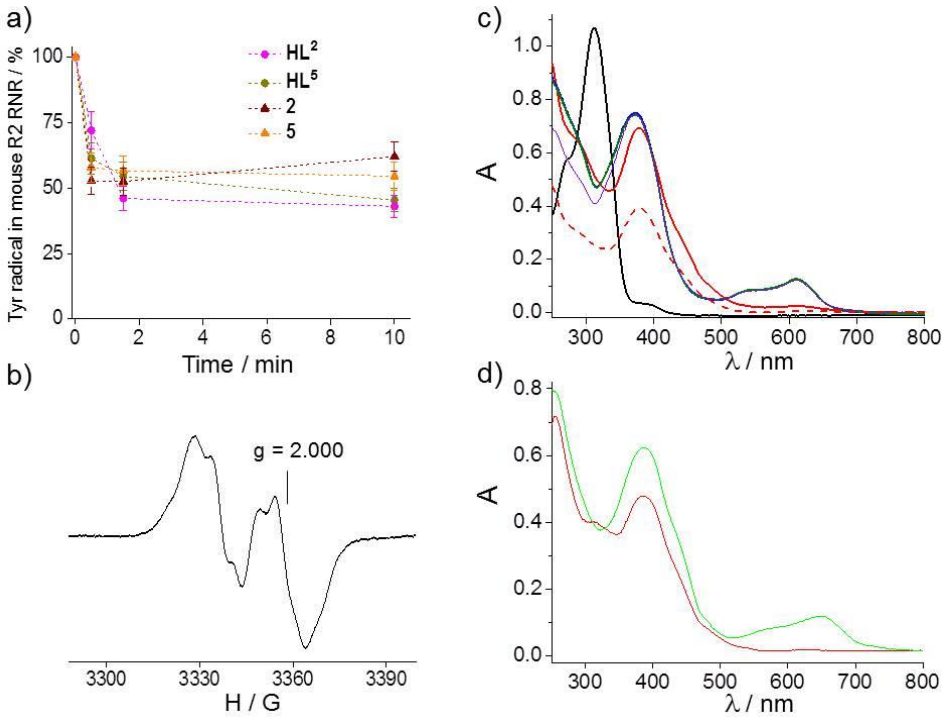

Figure S15. a) Time-dependent Tyrosyl radical reduction in mouse R2 RNR protein by **HL^2**, **HL^5**, **2**, and **5** at 1:1 protein-to-drug ratio in the presence of DTT. b) EPR spectrum of the Tyrosyl radical in mouse R2 RNR protein at 30 K. c) UV–vis spectra of **HL^2** (black line), **HL^2** + $FeCl_3 \cdot 6H_2O$ at 2:1 mole ratio (red trace), **HL^2** + $FeCl_3 \cdot 6H_2O$ + DTT at 2:1:5 mole ratio measured immediately after DTT addition (blue trace) and after 5 min (green trace), as well as UV–vis spectrum of the complex prepared by mixing **HL^2** + $FeSO_4 \cdot 7H_2O$ at 2:1 ratio (violet trace), all in buffered water solution (using pH 7 buffer capsules from Sentec) and measured aerobically (1 cm quartz UV–vis cuvette). d) UV–vis spectra of **HL^5** + $FeCl_3 \cdot 6H_2O$ at 2:1 mole ratio (red trace), **HL^5** + $FeCl_3 \cdot 6H_2O$ + DTT at 2:1:5 mole ratio measured immediately after DTT addition (green trace).

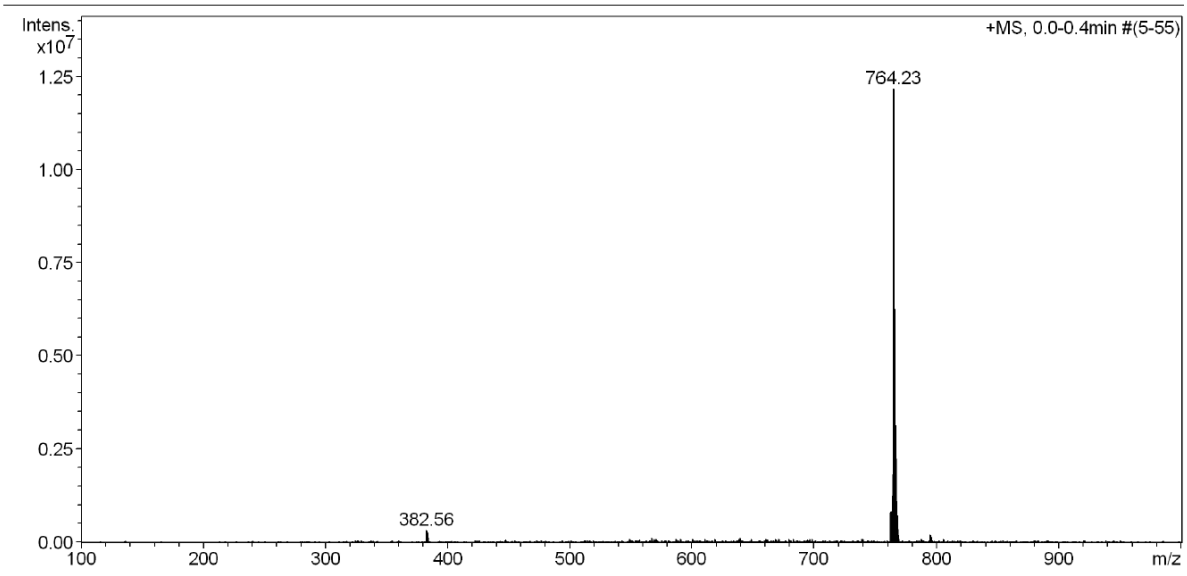

Figure S16. ESI mass spectrum of $[Fe^{III}(L^5)_2]^+$ obtained *in situ* from $FeCl_3$ and **HL^5** in 1:1 molar ratio.

Table S1. Selected bond distances (Å) and bond angles (deg) in **1**, **1´**, **5** and **6**.

Complex	**1**[a]	**1´**[b]	**5**	**6**
Cu–N1	2.0385(13)	2.0268(9)	2.0349(16)	2.050(3)
Cu–N2	1.9733(13)	1.9740(10)	1.9632(15)	1.961(3)
Cu–N4				1.942(3)
Cu–S	2.2585(4)	2.2673(3)	2.2704(5)	
Cu–Cl	2.2543(4)	2.2459(3)		2.2281(9)
Cu–O2		2.4266(10)		
Cu–Cl^{i}	2.7312(4)		3.0893(6)	
S–Cu^{i}			3.0233(6)	
N2–N3	1.3589(17)	1.3638(12)		1.362(4)
C7–S	1.7408(16)	1.7451(12)		1.757(4)
S–C13				1.805(4)
N1–Cu–N2	80.74(5)	80.58(4)		79.93(12)
N2–Cu–N4				78.58(13)
N2–Cu–S	84.10(4)	83.62(3)		
S–Cu–Cl	96.557(15)	96.609(13)		
N1–Cu–O2		80.81(3)		
N1–Cu–Cl	97.57(4)	98.09(3)		97.87(9)
N4–Cu–Cl				102.79(10)
N1–Cu–Cl^{i}	87.03(4)			
Cu–Cl–Cu^{i}	88.11(1)			
Cu–S–Cu^{i}		88.12(2)	88.12(2)	
Cu–Cl^{i}–Cu^{i}		87.31(2)	87.31(2)	

[a] symmetry code i for generation of symmetry equivalent atoms: $-x + 1, -y + 1, -z + 1$.

[b] symmetry code i for generation of symmetry equivalent atoms: $x, -y + 1.5, z - 0.5$.

Table S2. Selected bond distances (Å) and bond angles (deg) in **3** and **4**.

Complex	**3**[a]	**4**[b]
Cu1b–N1b	2.033(5)	2.026(2)
Cu1b–N2b	1.978(5)	1.976(2)
Cu1b–S1b	2.2492(18)	2.2503(8)
Cu1b–Cl1b	2.2677(15)	2.2537(8)
Cu1b–S1c	2.8010(16)	2.8860(8)
Cu1c–N1c	2.012(5)	2.044(2)
Cu1c–N2c	1.962(5)	1.978(2)
Cu1c–S1c	2.2576(16)	2.2888(8)
Cu1c–Cl1c	2.2363(17)	2.2519(8)
Cu1c–Cl1b	2.8411(6)	2.7273(8)
Cu1b–Cl1b–Cu1c	89.61(5)	90.94(3)
Cu1b–S1c–Cu1c	90.84(5)	86.31(3)

Table S3. Proton dissociation constants of **HL**[1] determined by pH-potentiometry and EPR spectroscopy.

Method	pK_1	pK_2	pK_3
pH potentiometry	≤1.8	5.77(1)	10.92(1)
^{1}H NMR spectroscopy	≤1.8	5.82(1)	10.99(1)

Table S4. Cumulative stability (logβ) and proton dissociation constants of the Cu(II) complexes of **HL^1** determined by UV–vis, pH-potentiometry and EPR spectroscopy. {T = 298 K, I = 0.10 M (KCl)}.

Method	Logβ					pK_a[b]		
	$[CuLH_2]^{3+}$	**$[CuLH]^{2+}$**	**$[CuL]^{+}$**	**$[CuLH_{-1}]$**	**$[CuL_2]$**	**$[CuLH_2]^{3+}$**	**$[CuLH]^{2+}$**	**$[CuL]^{+}$**
UV–vis via CT-bands	≤26.0	24.00(1)	19.04(2)[a]	10.42(1)	26.69(4)	≤2.0	4.96	8.63
UV–vis via d-d bands	≤26.0	23.96(1)	-	10.45(1)	-	≤2.0	4.92	8.59
pH-metry	-	24.09(3)	-	10.45(4)	26.83(7)	-	5.05	8.59
EPR	25.4(1)	24.00(1)	-	10.22(1)	-	1.4	5.04	8.82

[a] Determined via EDTA displacement study. [b] pK_a $[CuLH_2]^{3+}$ = logβ $[CuLH_2]^{3+}$ − logβ $[CuLH]^{2+}$; pK_a $[CuLH]^{2+}$ = logβ $[CuLH]^{2+}$ − logβ $[CuL]^{+}$; pK_a $[CuL]^{+}$ = logβ $[CuL]^{+}$ − logβ $[CuLH_{-1}]$.

Table S5. Formation constants and isotropic EPR parameters of the components obtained for Cu(II) – **HL^1** complexes[a]

Complex	***g***	**A_{Cu} / G**	**a_N / G**	**α / G**	**β / G**	**γ / G**
$[CuLH_2]^{3+}$	2.1065(2)	72.9(2)	13.6(2)	30.2(2)	–8.5(2)	0.2(1)
$[CuLH]^{2+}$	2.0941(2)	75.2(1)	15.4(2), 9.9(2)	19.4(2)	–7.9(1)	1.7(1)
$[CuL]^{+}$	2.0954(2)	75.0(2)	16.4(2), 9.8(2)	19.148(5)	–8.250(4)	1.98(1)
$[CuLH_{-1}]$	2.0927(1)	74.9(1)	14.0(1), 11.4(1)	17.272(4)	–9.160(4)	1.797(4)
$[CuL_2]$	2.1001(3)	59.4(3)	16(1), 11(2)	21.0	–6.9	1.5
$[Cu_2L_3H]^{2+}$	2.042, 2.156					

[a] Uncertainties (SD) of the last digits are shown in parentheses.

Table S6. Electrochemical and optical spectral data of **1**–**6**. Half-wave redox potentials for the first reduction step ($E_{1/2}^{Red1}$) are in V vs Fc^+/Fc and vs NHE (*in brackets*) respectively.

Complex	$E_{1/2}^{Red1}$ (DMSO)	$E_{1/2}^{Red1}$ (MeOH)	$E_{1/2}^{Red1}$ (H_2O)*	λ_{max} (DMSO)	λ_{max} (H_2O)*
1	–0.81 (*–0.17*)	–0.57 (*+0.07*)	-	414 nm	-
2	–0.80 (*–0.16*)	–0.54 (*+0.10*)	–0.52 (*+0.12*)	423 nm	403 nm
3	–0.80 (*–0.16*)	–0.49 (*+0.15*)	-	425 nm	-
4	–0.80 (*–0.16*)	–0.49 (*+0.15*)	-	419 nm	-
5	–0.77 (*–0.13*)	–0.48 (*+0.16*)	-	415 nm	-
6	–0.86 (*–0.26*)	-	-	-	-

*Electrochemical and optical spectra of complex **2** were additionally measured in aqueous solution, wherein the decrease of the reduction potential and λ_{max} was observed.

Table S7. Molecular descriptors for **HL^1**–**HL^6** and **1**–**6** and the maximum values for each descriptor defining drug-like and known drug space.

Compound	Molecular Weight (g mol^{-1})	Lipophilicity (Log*P*)	Hydrogen Bond Donors	Hydrogen Bond Acceptors	Polar Surface Area ($Å^2$)	Rotatable Bonds
HL^1	279.4	0.5	3	8.7	80.3	5
HL^2	307.4	1.6	1	8.7	53.3	5
HL^3	333.5	2.1	1	8.7	54.0	5
HL^4	349.5	1.4	1	10.4	62.4	5
HL^5	355.5	2.5	2	8.7	63.5	6
HL^6	293.4	1.3	2	7.7	79.9	6
1	377.4	1.0	2	5	89.4	2
2	405.5	2.1	0	5	66.6	2
3	431.5	2.4	0	5	66.6	2
4	447.5	1.7	0	6	75.8	2
5	453.5	3.0	1	5	75.4	3
6	391.4	1.3	1	5	75.4	3
Triapine	195.2	0.5	5	3	89.3	2
Drug-like space	500	5	5	10	140	10
Known Drug Space	800	6.5	7	15	180	17

Table S8. The results of the scoring functions for the ligand and their copper (II) complexes.

Compound	GS	ChemPLP	CS	ASP	H-Bonding(HB)/ Lipophilic Contact(LC)
HL^1	47.2	47.9	22.3	31.4	Arg331(HB), Tyr324(HB), Phe237(LC), Phe241(LC), Leu332(LC), Cys271(LC)
HL^2	45.3	55.7	23.2	22.6	Arg331(HB), Phe237(LC), Phe241(LC), Leu332(LC), Cys271(LC)
HL^3	48.1	61.6	26.2	25.7	Arg331(HB), Tyr324(HB), Phe237(LC), Leu332(LC), Cys271(LC)
HL^4	49.5	60.5	24.6	24.1	Tyr324(HB), Phe237(LC), Phe241(LC), Cys271(LC)
HL^5	60.5	60.1	28.3	30.4	Tyr324(HB), Arg331(HB), Phe237(LC), Leu332(LC), Cys271(LC)
HL^6	50.1	53.8	21.9	26.7	Phe237(LC), Phe241(LC), Leu332(LC), Cys271(LC), Val328(LC)
1	47.6				Arg331(HB), Phe237(LC), Phe241(LC), Cys271(LC)
2	49.7				Cys271(LC), Val328(LC), Phe237(LC),Phe241(LC), Leu332(LC)
3	54.6				Phe237(LC), Phe241(LC), Leu332(LC), Cys271(LC), Val328(LC)
4	50.3				Phe237(LC), Phe241(LC), Leu332(LC), Cys271(LC), Val328(LC)
5	56.4				Arg331(HB), Phe237(LC), Phe241(LC), Leu332(LC), Leu334(LC), Cys271(LC)
6	48.4				Cys271(LC), Val328(LC), Phe237(LC), Phe241(LC), Leu332(LC), Arg331(LC)

Table S9. Yields, m.p. and analytical data for **HL[1]**–**HL[6]**.

		HL[1]	**HL[2]**	**HL[3]**	**HL[4]**	**HL[5]**	**HL[6]**
Yield (%)		89	58	76	24.5	64	34
Brutto formula		$C_{12}H_{17}N_5OS$	$C_{14}H_{21}N_5OS$	$C_{16}H_{23}N_5OS$	$C_{16}H_{22}N_5O_2S$	$C_{18}H_{21}N_5OS$	$C_{13}H_{19}N_5OS$
***M*r**		279.36	307.42	333.45	348.44	355.46	293.39
mp (°C)		228.5	157	168.5	151.1	159.9	142.6
C (%)	**calcd**	51.59	4.70	57.63	55.15	60.82	53.22
	found	51.50	54.76	57.67	55.12	60.86	53.27
H (%)	**calcd**	6.13	6.89	6.95	6.37	5.95	6.53
	found	6.02	6.91	6.93	6.75	5.95	6.51
N (%)	**calcd**	25.07	22.78	21.00	20.10	19.70	23.87
	found	24.79	22.38	20.76	20.02	19.65	23.50
S (%)	**calcd**	11.48	10.43	9.62	9.20	9.02	10.93
	found	11.25	10.44	9.63	9.07	8.97	10.73
O (%)	**calcd**		5.20	4.80		4.50	
	found		5.22	4.69		4.57	
ESI-MS (methanol)	**[M + Na]$^+$**	302	330	356	372	378	316
	[M + H]$^+$	280	308	334	350	356	294
X-ray structure		Yes	yes	no	yes	yes	yes

Table S10. Yields and analytical data fo1 **1**–**6**.

		1	**2**	**3**	**4**	**5**	**6**
Yield (%)		91.0	80.6	57.4	34.9	52.6	51.7
Brutto formula		$C_{12}H_{16}ClCuN_5OS$ ·0.4DMF	$C_{14}H_{20}ClCuN_5OS$	$C_{16}H_{22}ClCuN_5OS$ ·0.4CH_3OH	$C_{16}H_{22}ClCuN_5O_2S$ ·0.5CH_3OH· 0.3H_2O	$C_{18}H_{20}ClCuN_5OS$	$C_{13}H_{18}ClCuN_5OS$ ·0.25H_2O
***M*r**		406.6	405.41	444.26	465.27	471.45	395.88
C (%)	**calcd**	38.99	41.58	44.34	42.26	45.86	39.44
	found	38.90	41.59	44.30	41.86	45.85	39.17
H (%)	**calcd**	4.66	4.99	5.35	5.29	4.70	4.71
	found	4.81	4.94	5.09	4.90	4.50	4.56
N (%)	**calcd**	18.59	17.33	15.76	14.94	14.85	17.69
	found	18.20	16.92	15.74	14.83	14.80	17.18
S(%)	**calcd**	7.89	7.91	7.22	6.84	6.80	8.10
	found	7.63	7.92	7.24	6.92	6.84	7.86
ESI-MS (methanol)	**[M - Cl]$^+$**	341	369	395	412	417	354
	[2M - Cl]$^+$	719	775	827	591	871	
X-ray structure		yes	no	yes	yes	yes	yes

Table S11. Crystal data and details of data collection for **HL[1]**, **HL[2]**, **HL[4–6]**.

Compound	**HL[1]**	**HL[2]**	**HL[4]**	**HL[5]**	**HL[6]**
empirical	$C_{12}H_{17}N_5OS$	$C_{14}H_{21}N_5OS$	$C_{16}H_{23}N_5O_2S$	$C_{18}H_{21}N_5OS$	$C_{13}H_{19}N_5OS$
Fw	279.37	307.42	349.45	355.46	293.39
Space group	$P2_1/c$	$P2_1/c$	$P2_1/c$	$P2_1/n$	$P2_1/c$
α, Å	11.544(3)	6.1236(4)	13.3622(18)	7.1287(2)	22.7776(4)
b, Å	13.204(3)	7.9500(6)	5.8899(6)	15.0536(6)	6.8585(1)
c, Å	10.086(3)	30.956(2)	21.414(3)	16.4704(6)	9.8800(2)
β, °	112.081(7)	92.419(4)	97.465(1)	97.810(2)	104.877(2)
V [Å^3]	1424.6(6)	1505.68(19)	1684.6(4)	1751.09(11)	1524.92(5)
Z	4	4	4	4	4
λ [Å]	0.71073	0.71073	0.71073	0.71073	1.54178
ρ_{calcd}, g cm^{-3}	1.303	1.356	1.378	1.348	1.278
Cryst size, mm^3	0.20 × 0.18 ×	0.27 × 0.26 ×	0.15 × 0.03 ×	0.20 × 0.06 ×	0.37 × 0.25 ×
T [K]	130(2)	100(2)	100(2)	100(2)	293(2)
μ, mm^{-1}	0.228	0.222	0.212	0.202	1.920
R_1[a]	0.0578	0.0443	0.0535	0.0454	0.0478
wR_2[b]	0.1609	0.1187	0.1221	0.1330	0.1434
GOF[c]	1.025	1.038	1.012	1.033	1.048

[a] $R_1 = \Sigma||F_o| - |F_c||/\Sigma|F_o|$. [b] $wR_2 = \{\Sigma[w(F_o^2 - F_c^2)^2]/\Sigma[w(F_o^2)^2]\}^{1/2}$. [c] GOF = $\{\Sigma[w(F_o^2 - F_c^2)^2]/(n - p)\}^{1/2}$, where n is the number of reflections and p is the total number of parameters refined.

Table S12. Crystal data and details of data collection for Cu(II) complexes

Compound	**1´ [Cu(L^1)Cl(H$_2$**	**1 [Cu(L^1)Cl]·**	**3 [Cu(L^3)Cl]·0.**	**4 [Cu(L^4)Cl]·0.**	**5 [Cu(L^5)Cl]·**	**6 [Cu(L^6)Cl]**
empirical	$C_{12}H_{22}ClCuN_5O_4$	$C_{15}H_{23}ClCuN$	$C_{16.25}H_{22.33}ClCu$	$C_{16.58}H_{24.33}ClCu$	$C_{19}H_{24}ClCuN$	$C_{13}H_{18}ClCu$
Fw	431.40	450.44	439.44	466.13	485.48	391.38
space group	*P*-1	$P2_1/c$	$P2_1/n$	$P2_1/n$	$P2_1/c$	$C2/c$
α, Å	9.2626(8)	9.3959(3)	24.702(4)	22.2413(7)	16.5043(12)	15.7566(11)
b, Å	9.5087(8)	19.8889(6)	9.1959(4)	8.3324(2)	17.7857(12)	14.2967(9)
c, Å	11.0617(9)	10.9744(3)	25.064(5)	31.9121(9)	7.1311(6)	14.2703(10)
α, °	89.565(2)					
β, °	76.519(2)	108.3661(7)	100.971(6)	90.565(1)	96.241(3)	92.971(3)
γ, °	67.742(2)					
V [Å^3]	873.29(13)	1946.37(10)	5589.5(2)	5913.8(3)	2080.9(3)	3210.3(4)
Z (Z´)	2	4	4 (12)	4 (12)	4	8
λ [Å]	0.71073	1.54178	0.71073	0.71073	0.71073	0.71073
ρ_{calcd}, g cm^{-3}	1.641	1.537	1.567	1.571	1.550	1.620
cryst size,	0.30 × 0.22 ×	0.22 × 0.14 ×	0.20 × 0.17 ×	0.15 × 0.08 ×	0.20 × 0.06 ×	0.20 × 0.10
T [K]	100(2)	100(2)	100(2)	100(2)	100(2)	100(2)
μ, mm^{-1}	1.550	4.046	1.445	1.375	1.305	1.665
R_1[a]	0.0215	0.0256	0.0572	0.0357	0.0368	0.0424
wR_2[b]	0.0577	0.0706	0.1693	0.0861	0.0913	0.1128
GOF[c]	1.061	1.061	1.062	1.037	1.022	1.053

[a] $R_1 = \Sigma||F_o| - |F_c||/\Sigma|F_o|$. [b] $wR_2 = \{\Sigma[w(F_o^2 - F_c^2)^2]/\Sigma[w(F_o^2)^2]\}^{1/2}$. [c] GOF = $\{\Sigma[w(F_o^2 - F_c^2)^2]/(n - p)\}^{1/2}$, where n is the number of reflections and p is the total number of parameters refined.

Redox-active organoruthenium(II)- and organoosmium(II)-copper(II) complexes, with an amidrazone-morpholine hybrid and $[Cu^{I}Cl_2]^-$ as counteranion, and their antiproliferative activity

Organometallics 10.1021/acs.organomet.9b00229

Kateryna Ohui,[a,] Maria V. Babak,[b,c] Denisa Darvasiova,[d] Alexander Roller,[a] Daniel Vegh,[e] Peter Rapta,[d] Grace Rui Shi Guan,[f] Yi Hsuan Ou,[f] Giorgia Pastorin,[f] Vladimir B. Arion*,[a]

[a]*University of Vienna, Institute of Inorganic Chemistry, Währinger Strasse 42, A-1090 Vienna, Austria*

[b]*Department of Chemistry, National University of Singapore,3 Science Drive 2, 117543 Singapore*

[c]*Drug Development Unit, National University of Singapore,28 Medical Drive, 117546 Singapore*

[d]*Institute of Physical Chemistry and Chemical Physics, Slovak Technical University of Technology, Radlinského 9, 81237 Bratislava, Slovak Republic*

[e]*Institute of Organic Chemistry, Catalysis and Petrochemistry, Department of Organic Chemistry, Slovak Technical University of Technology, Radlinského 9, 81237 Bratislava, Slovak Republic*

[f]*Department of Pharmacy, National University of Singapore, Singapore*

Abstract. A novel proligand HL^H has been prepared from 2-pyridinamidrazone and 6-(morpholinomethyl)pyridine-2-carboxaldehyde. Subsequently starting from HL^H and $CuCl_2·2H_2O$ in the presence of triethylamine a series of homo- and heterometallic complexes with $[Cu^{I}Cl_2]^-$ as counteranion, namely mononuclear complex $[Cu^{II}Cl(HL^{OMe})][Cu^{I}Cl_2]$ (**1**), dinuclear Ru(II)-Cu(II) complex $[Cu^{II}Ru^{II}(\eta^6\text{-}p\text{-cymene})Cl_2(L^H)][Cu^{I}Cl_2]·1.5H_2O$ (**2**·1.5H_2O), Os(II)-Cu(II) complex $[Cu^{II}Os^{II}(\eta^6\text{-}p\text{-cymene})Cl_2(L^H)][Cu^{I}Cl_2]·H_2O$ (**3**·H_2O) and tetranuclear complex $[Cu^{II}_4(L^1)_2(L^2)_2Cl_2]Cl_2·5MeOH$ (**4**·5MeOH), where HL^{OMe}, L^1 and L^2 are Schiff base ligands derived from HL^H, were synthesized. The structures of metal complexes were established by X-ray diffraction. Complexes **1**–**3** demonstrated quasireversible one-electron reduction of Cu(II) in complex cations and one-electron oxidation of $[Cu^{I}Cl_2]^-$ counterion, confirmed by UV–vis and EPR spectroelectrochemical measurements. They exhibited moderate antiproliferative activity against ovarian carcinoma and cervical adenocarcinoma cell lines in a micromolar concentration range, which was superior to the

activity of HL^H, $CuCl_2$ and $[Cu^ICl_2]^-$. The observed anticancer effects might be related to the ability of novel complexes to generate ROS, which was established by spin trapping experiments in cell-free media, as well as by confocal microscopic imaging in ovarian carcinoma cells.

Keywords: heterometallic complexes, amidrazones, organometallics, ruthenium(II)-copper(II), osmium(II)-copper(II), spectroelectrochemistry, antiproliferative activity, ROS

Introduction

The clinical success of anticancer drug cisplatin fuelled rapid development of various transition metal complexes with therapeutic properties. As an alternative to highly toxic platinum drugs, ruthenium anticancer complexes have been reported and subsequently introduced into clinical trials.[1] Organometallic M(Arene) pharmacophores with M = Ru, Os have also been widely investigated due to the accessible synthetic pathways, easy structural fine-tuning and low toxicity.[2] One valuable strategy to further enhance the therapeutic potential of M(Arene) complexes is to design multinuclear and heteronuclear scaffolds.[3] An emerging approach involves the combination of M(Arene) moieties with other metal fragments, thereby taking advantage of beneficial therapeutic properties of both entities. Synchronous delivery of different metal components to the intended site of action is expected to result in better pharmacological properties, since all therapeutic entities would act on the biological targets simultaneously. Additionally, high toxicity or low solubility of mononuclear metal complexes can be significantly improved upon coordination to low toxic or water-soluble metal entities. Mononuclear Ru(Arene) and Os(Arene) complexes demonstrated marked anticancer properties and their use *in vivo* was in general characterized by low toxicity and good aqueous solubility.[4-8] Therefore, these organometallic species are widely exploited as building blocks for higher-order multinuclear M(Arene) anticancer complexes. Conjugation of Ru(Arene) fragments with Pt(II), Pt(IV), Au(I), Sn(II) and other metal-based building blocks resulted in an improved selectivity to cancer cells over healthy cells and excellent cytotoxicity.[3]

Surprisingly, the biological properties of heterometallic Ru/Cu complexes are barely investigated. Copper(II) complexes are well known for their marked anticancer properties,[9] linked to the ability of a Cu atom to cycle between Cu(II) and Cu(I) oxidation states,[10] leading to the production of reactive oxygen species (ROS), which are deadly for cancer

cells.[11,12] It was reported that the attachment of $CpRu^+$ to a Cu(I)-dppe (1,2-bis(diphenylphosphino)ethane) yielded the heterodinuclear Ru(II)-Cu(I) complex **A** with cytotoxicity in a low micromolar range (Chart 1).[13] However, no differences between antiproliferative activity and ROS-inducing properties of a heteronuclear complex and its corresponding mononuclear counterparts have been observed. To our knowledge, the only other example of biologically active Ru/Cu complexes was reported by Reedijk *et al.*, where DNA-intercalating ruthenium(II)-terpyridine moiety was designed to direct ROS-inducing copper(II) unit into DNA followed by its oxidative damage.[14] Complex **B** and its trinuclear and tetranuclear analogues indeed demonstrated DNA cleavage. However, their anticancer activity has not been studied. The biological activity of heteronuclear Os/Cu complexes has never been reported.

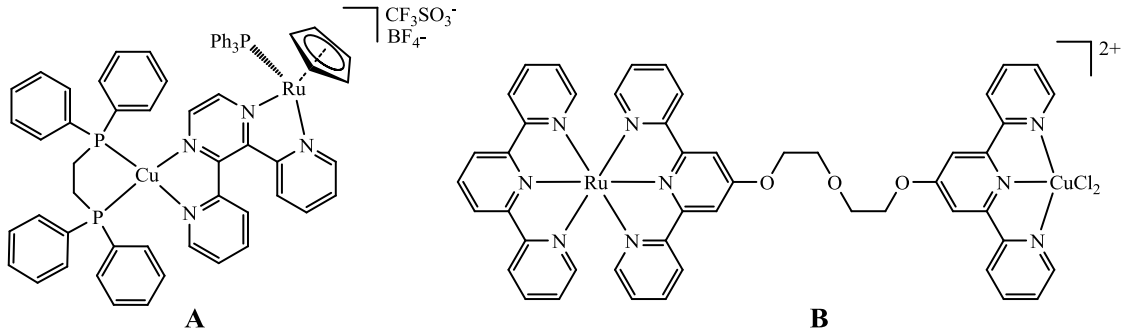

Chart 1. Examples of previously reported Ru/Cu heteronuclear complexes.

In this work we have prepared heterodinuclear Cu(II)-Ru(II) and Cu(II)-Os(II) complexes linked by a morpholine-substituted amidrazone proligand. The amidrazone backbone was chosen due to its coordination capacity, as well as a broad spectrum of biological activities, including antimicrobial,[15] antimycobacterial,[16] antiviral,[17] antibacterial,[18] anticonvulsant,[19] and anticancer properties.[20-22] However, there is only a limited number of literature reports on the metal complexes of amidrazones.[23-27] It was shown that coordination of amidrazones to copper(II) yielded complexes with anticancer activity in a low micromolar range. Moreover, these copper(II)-amidrazone complexes were reported to be electrochemically active and were expected to induce ROS in cancer cells.[27]

The incorporation of a morpholine moiety into amidrazone scaffold not only provides an additional coordination site, but is also expected to increase the aqueous solubility and bioactivity of resulting metal complexes. In general, addition of morpholine moiety to the chemical structures yields drugs with better pharmacological profiles, such as widely used

anticancer drugs Aprepitant and Gefitinib (Chart 2).[28,29] Previously, we demonstrated that incorporation of a morpholine structural moiety into thiosemicarbazone backbones led to a marked improvement of their cytotoxicity and aqueous solubility.[30] Similarly, conjugation of N1-(flavon-6-yl)amidrazone with morpholine (Chart 2, amidrazone-morpholine hybrid) resulted in higher antiproliferative activity in comparison with other structurally similar amidrazones.[20]

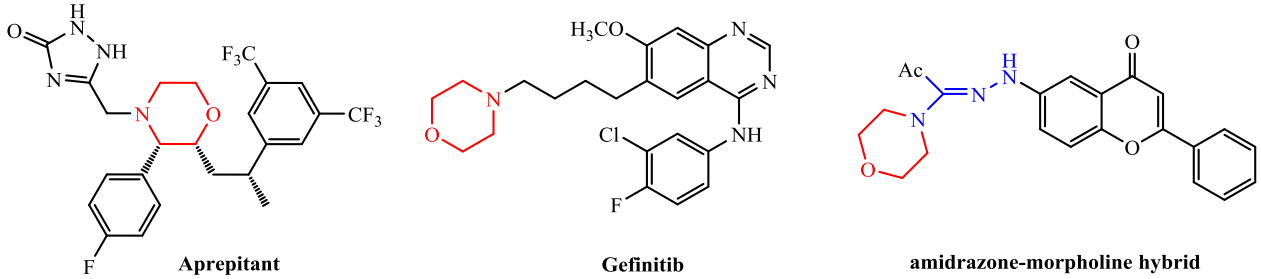

Chart 2. Marketed anticancer drugs with morpholine moiety and previously published amidrazone-morpholine hybrid with high anticancer activity (the amidrazone backbone is highlighted in blue).

Herein we report on the synthesis of the novel amidrazone proligand HL^{H} prepared from 2-pyridinamidrazone and 6-(morpholinomethyl)pyridine-2-carboxaldehyde, as well as three metal complexes, namely the homonuclear Cu(II) complex $[Cu^{II}(HL^{OMe})Cl][Cu^{I}Cl_2]\cdot 0.2H_2O$ (**1**$\cdot 0.2H_2O$) and heterodinuclear Cu(II)-Ru(II) $[Cu^{II}(L^{H})Ru^{II}(\eta^6\text{-}p\text{-cymene})Cl_2][Cu^{I}Cl_2]\cdot 1.5H_2O$ (**2**$\cdot 1.5H_2O$) and Cu(II)-Os(II) $[Cu^{II}(L^{H})Os^{II}(\eta^6\text{-}p\text{-cymene})Cl_2][Cu^{I}Cl_2]\cdot H_2O$ (**3**$\cdot H_2O$) complexes, shown in Chart 3. Full analytical, standard spectroscopic and X-ray diffraction characterization of **1**–**3**, as well as their spectroelectrochemistry and antiproliferative activity in three cancerous and one non-cancerous cell lines along with the ability to generate ROS are also presented and discussed.

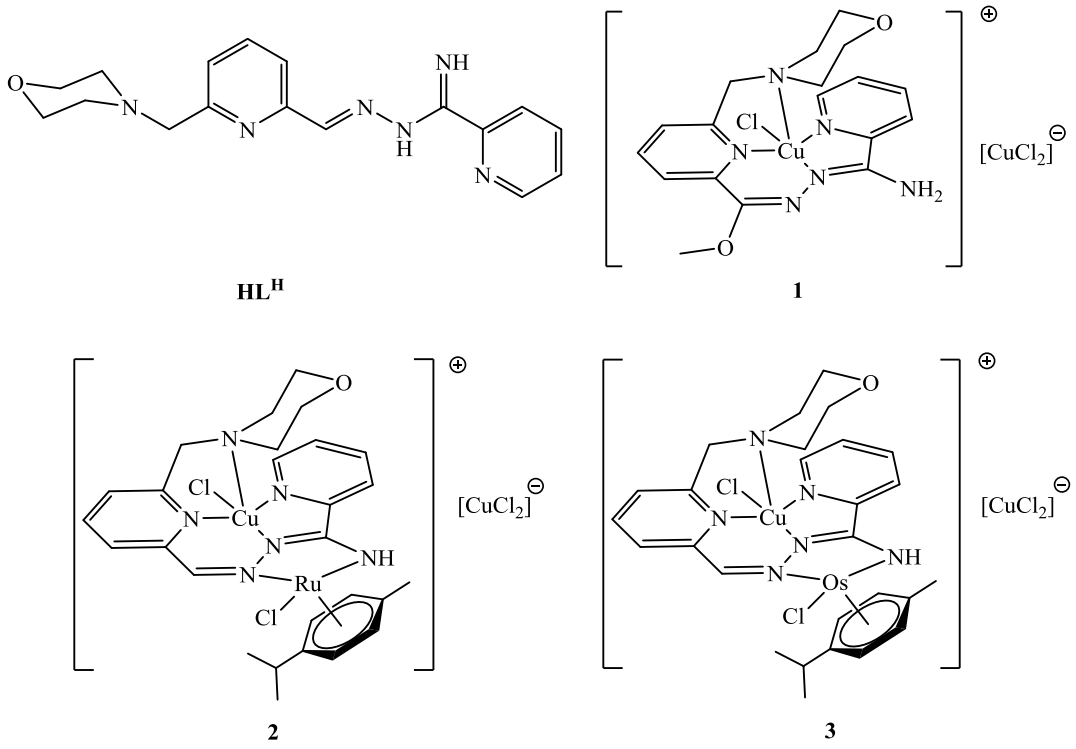

Chart 3. Line drawings of proligand **HL^{H}** and complexes **1**–**3** reported in this work. The structures of all complexes were established by single crystal X-ray crystallography.

Results and Discussion

Synthesis and characterization of the HL^{H}, Cu(II) complex 1 and heterodinuclear complexes 2 and 3. The proligand HL^{H} was obtained by the reaction of the 6-(morpholinomethyl)pyridine-2-carboxaldehyde with 2-pyridinamidrazone in 1:1 mol ratio in ethanol in 92% yield. The ESI mass spectrum recorded in positive ion mode showed a peak with *m*/*z* 325.0 attributed to $[M+H]^+$. The ^{1}H NMR spectrum was in agreement with the suggested structure for the HL^{H}. The reaction of the latter with $CuCl_2{\cdot}2H_2O$ in the presence of triethylamine in methanol in 1:2:1 mol ratio afforded a solid that was removed by filtration. The filtrate was concentrated and allowed to stand at –20 °C overnight producing bright-green crystals. Slow diffusion of diethyl ether into the solution of the crude product redissolved in methanol afforded the complex $[Cu^{II}Cl(HL^{OMe})][Cu^{I}Cl_2]{\cdot}0.2H_2O$ (**1**$\cdot 0.2H_2O$) in 17% yield. The positive ESI mass spectrum showed a peak with *m*/*z* 452.0, which could be assigned to $[Cu^{II}Cl(HL^{OMe})]^+$, while the negative ion mass spectrum confirmed the formation of $[Cu^{I}Cl_2]^-$ by the presence of a strong peak at *m*/*z* 134.7. The insertion of methoxy group into the aldimine C–H bond was further confirmed by X-ray diffraction (*vide infra*). Substitution of aldimine hydrogen atom by an alkoxy group was reported for some Schiff bases when reacted with copper(II)

salts in alcohols.[31,32] Two different mechanisms for the transformation observed were proposed.[33] One which appears to be plausible for our case as well, is the addition of ROH to the polarized aldimine group followed by oxidation to the final product (see Scheme S1 in Supporting Information). A part of the initially formed complex with HL^H, presumably $[Cu^{II}Cl(HL^H)]^+$, acts as an oxidant. This is evidenced by the presence of $[Cu^ICl_2]^-$ as counteranion in **1** and the low yield of the product. There is no other source for generation of $[Cu^ICl_2]^-$, taking into account that copper(II) salt was allowed to react with HL^H in 1:1 mol ratio. Addition of 0.5 mol equiv of $[Ru(\eta^6\text{-}p\text{-cymene})Cl_2]_2$ to the 1:1:1 mixture of HL^H, $CuCl_2{\cdot}2H_2O$ and triethylamine in ethanol and reflux of the dark-red solution produced a dark-red crystalline product, which after re-crystallization in ethanol afforded X-ray diffraction quality crystals of $[Cu^{II}Ru^{II}(\eta^6\text{-}p\text{-cymene})Cl_2(L^H)][Cu^ICl_2]{\cdot}1.5H_2O$ (**2**$\cdot 1.5H_2O$) in 23% yield. The osmium(II) sibling species **3**$\cdot H_2O$ was prepared similarly in 25% yield. Characteristic signatures for both **2** and **3** were the presence of strong peaks with *m*/*z* 694.10 and 782.09 in positive ion ESI mass spectra attributed to $[Cu^{II}Ru^{II}(\eta^6\text{-}p\text{-cymene})Cl_2(L^H)]^+$ and $[Cu^{II}Os^{II}(\eta^6\text{-}p\text{-cymene})Cl_2(L^H)]^+$, respectively (Figures S1 and S2 in Supporting Information, and a peak at *m*/*z* 134.7 in negative ion mass spectrum assigned to $[Cu^ICl_2]^-$. The reaction of HL^H with $CuCl_2{\cdot}2H_2O$ in the presence of triethylamine in 1:1:1 mol ratio in methanol afforded a solid that was isolated by filtration and dissolved in methanol. Slow diffusion of diethyl ether into the methanolic solution afforded brown crystals of **4** which were investigated by X-ray diffraction (*vide infra*).

X-ray crystallography. The results of X-ray diffraction studies of **1–3** are shown in Figures 1 and 2, while that of tetranuclear copper(II) complex **4** in Figure S3 in Supporting Information. Complexes **2** and **3** are chiral, but crystallize as enantiomeric mixtures in the monoclinic centrosymmetric space group *C*2/*c*. The Cu(II) ion in **1** adopts a slightly distorted square-pyramidal coordination geometry (τ parameter 0.16)[34] with the new ligand formed via insertion of methoxy group into the aldimine C–H bond as shown in Scheme S1 in Supporting Information. The ligand HL^{OMe} acts as a monoanion and occupies the basal plane and the chloride as co-ligand the apical position.

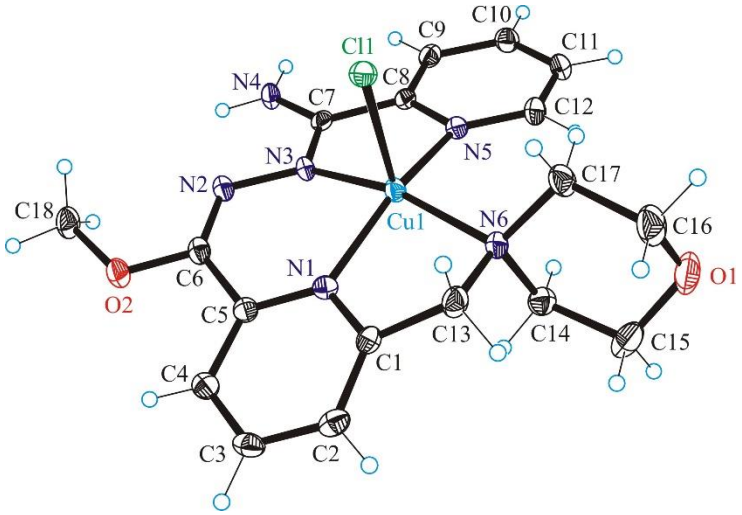

Figure 1. ORTEP plot of $[Cu^{II}(HL^{OMe})Cl][Cu^{I}Cl_2]$ (**1**). Selected bond distances (Å), bond angles (deg) and torsion angles (deg): Cu1–N1 2.005(2), Cu1–N3 1.971(3), Cu1–N5 2.071(3), Cu1–N6 2.071(3), Cu1–Cl1 2.4701(9); N1–Cu1–N3 88.37(10), N3–Cu1–N5 80.09(10), N5–Cu1–N6 102.27(10), N1–Cu1–N6 83.99(10); N1–C1–C13–N6 –34.4(4).

The distortion of Cu(II) coordination geometry enhances upon coordination of $[Cu^{II}(L^{H})Cl]$ moiety to Ru(II)- and/or Os(II)-*p*-cymene building blocks. An intermediate coordination geometry between square-pyramidal and trigonal-bipyramidal for Cu(II) in isostructural complexes **2** and **3** has been established with τ-parameter of 0.53 and 0.52, respectively. The Ru(II) and Os(II) adopt the usual three-leg piano-stool configuration, in which the two nitrogen atoms N2 and N4 along with one chloride atom act as the legs.

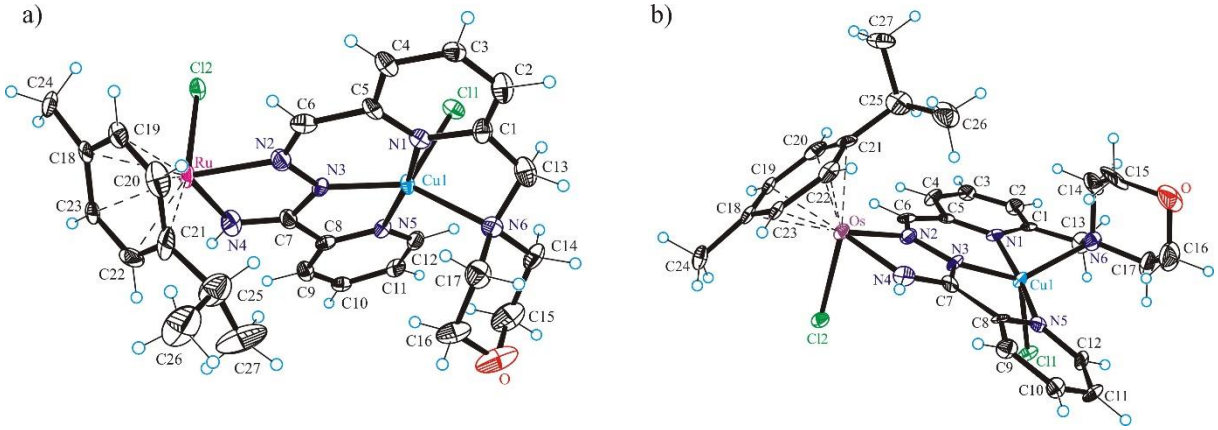

Figure 2. ORTEP plots of heterodinuclear species a) $[Cu^{II}(L^{H})Ru^{II}(\eta^6\text{-}p\text{-cymene})Cl_2]^+$ in **2** and b) $[Cu^{II}(L^{H})Os^{II}(\eta^6\text{-}p\text{-cymene})Cl_2]^+$ in **3**. Selected bond distances (Å), bond angles (deg) and torsion angles (deg) in the complex cation of **2**: Cu1–N1 1.985(7), Cu1–N3

1.938(6), Cu1–N5 2.000(6), Cu1–N6 2.172(7), Cu1–Cl1 2.388(2), Ru–N2 2.068(6), Ru–N4 2.063(8), Ru–Cl2 2.4194(19), Ru–C_{av}(*p*-cym) 2.19(3); N1–Cu1–N3 89.1(3), N3–Cu1–N5 81.5(3), N5–Cu1–N6 107.5(3), N1–Cu1–N6 78.3(3); N1–C1–C13–N6 –23.6(10). Selected bond distances (Å), bond angles (deg) and torsion angles (deg) in the complex cation of **3**: Cu1–N1 1.963(5), Cu1–N3 1.943(6), Cu1–N5 2.016(5), Cu1–N6 2.175(6), Cu1–Cl1 2.379(2), Os–N2 2.085(6), Os–N4 2.063(6), Os–Cl2 2.420(2), Os–C_{av}(*p*-cym) 2.20(4); N1–Cu1–N3 89.6(2), N3–Cu1–N5 80.9(2), N5–Cu1–N6 107.6(2), N1–Cu1–N6 78.6(2); N1–C1–C13–N6 –26.3(10).

The structure of $[Cu^{II}_4(L^1)_2(L^2)_2Cl_2]Cl_2 \cdot 5MeOH$ (**4**·5MeOH) in Figure S3 (Supporting Information) shows that two new ligands L^1 and L^2 are formed from HL^H (see Charts S1 and S2 in Supporting Information) and corroborates the high reactivity of the coordinated Schiff base. The first ligand L^1 is formed by addition of water to the Cu(II) coordinated HC=N group of HL^H and conversion to an amide presumably via oxidation, a rare type of transformation documented in the literature, i.e. for Re^{IV} and Ru^{III}.[35] Intermediates resulted from addition of H_2O and/or ROH to aldimine functions were also isolated and characterized.[36,37] The second ligand L^2 is produced via cyclization reaction by nucleophilic attack of terminal nitrogen atom at the polarized aldimine carbon. Taking into account the redox activity of Cu(II) in reported copper(II) complexes with amidrazones,[26,27] the spectroelectrochemical properties of **1–3** were investigated.

Cyclic voltammetry and spectroelectrochemistry. Cyclic voltammograms of Cu(II) complex **1** and heterodinuclear complexes **2** and **3** in DMSO/*n*-Bu_4NPF_6 by using platinum or glassy-carbon working electrodes are very similar and show one reduction peak in the cathodic part at E_{pc} = –0.73 V for **1** (Figure 3a, red trace), –0.75 V for **2** (Figure 3a, black trace) and –0.72 V for **3** (Figure S4a in Supporting Information), and one oxidation peak in the anodic part at E_{pa} = +0.04 V with a markedly shifted counterion peak at around –0.28 V (all vs Fc^+/Fc at scan rate of 100 mV s^{-1}). The proligand HL^H is not redox active in the potential window available (Figure S4b in Supporting Information). Almost the same voltammetric response was found also for methanolic solutions with E_{pc} at around –0.68 vs Fc^+/Fc at scan rate of 100 mV s^{-1} (Figure S5 in Supporting Information). Therefore the reduction event can be attributed to the Cu(II) → Cu(I) reduction in the corresponding $[Cu^{II}Ru/Os(\eta^6\text{-}p\text{-cymene})Cl_2(L^H)]^+$ cation, while the oxidation peak corresponds to the oxidation of the $[Cu^ICl_2]^-$ anion in **1**–**3**. The shape of cyclic voltammogram of *n*-

$Bu_4N[CuCl_2]$ salt in DMSO is very similar to that observed for **1**–**3** in the anodic part with a slightly shifted potential to the higher value (see blue line in Figure S4a in Supporting Information) confirming the oxidation of $[Cu^{I}Cl_2]^-$. Similar broadened cyclic voltammogram was already reported for anodic oxidation of triethylammonium dichloridocuprate(I).[38] To provide further evidence that the reduction is metal-centered, the nearly reversible one-electron reduction of **2** was studied by *in situ* UV–vis-spectroelectrochemistry. A new absorption band at 408 nm arose upon cathodic reduction of **2** in DMSO/*n*-Bu_4NPF_6 at the first electron transfer with a simultaneous decrease of the initial optical bands at 446 and 348 nm via isosbestic points at 434 and 365 nm (Figure 3b). A strong decrease of the initial EPR signal (originating from the $[Cu^{II}Ru(\eta^6\text{-}p\text{-cymene})Cl_2(L^H)]^+$ cation) was observed in the analogous spectroelectrochemical experiment directly in the EPR cavity using a large platinum working electrode and a flat spectroelectrochemical cell (see Figure S6a in Supporting Information), thus confirming the reduction of Cu(II) with formation of a diamagnetic d^{10} EPR-silent Cu(I) species. The spectral changes of the S→Cu(II) charge transfer bands (~446 nm) are also in line with the reduction of Cu(II) to Cu(I). Additionally, upon voltammetric reverse scan, reoxidation and a nearly full recovery of the initial optical bands were observed, attesting the chemical reversibility of the cathodic reduction even at low scan rates (Figure S7 in Supporting Information). As can be seen for electrochemical oxidation of **2** in DMSO/*n*-Bu_4NPF_6 in the region of the first one-electron oxidation step (Figure S6b in Supporting Information), a new EPR signal was observed which is different from the EPR signal of the $[Cu^{II}Ru(\eta^6\text{-}p\text{-cymene})Cl_2(L^H)]^+$ cation and characteristic for $[Cu^{II}(solv)_6]Cl_2$ species. So the first oxidation peak is due to the oxidation of $[Cu^{I}Cl_2]^-$ anion. A new absorption band at 302 nm arises upon anodic oxidation of **2** in DMSO/*n*-Bu_4NPF_6 at the first electron transfer with no changes of the initial optical band at 446 nm, again in agreement with the oxidation of $[Cu^{I}Cl_2]^-$ (Figure S8 in Supporting Information). Thus it can be concluded that the Ru^{II} and Os^{II} centers are not redox active in the biologically accessible redox window but slightly affect the redox potential of the Cu(II)-centered reduction in **2** and **3**.

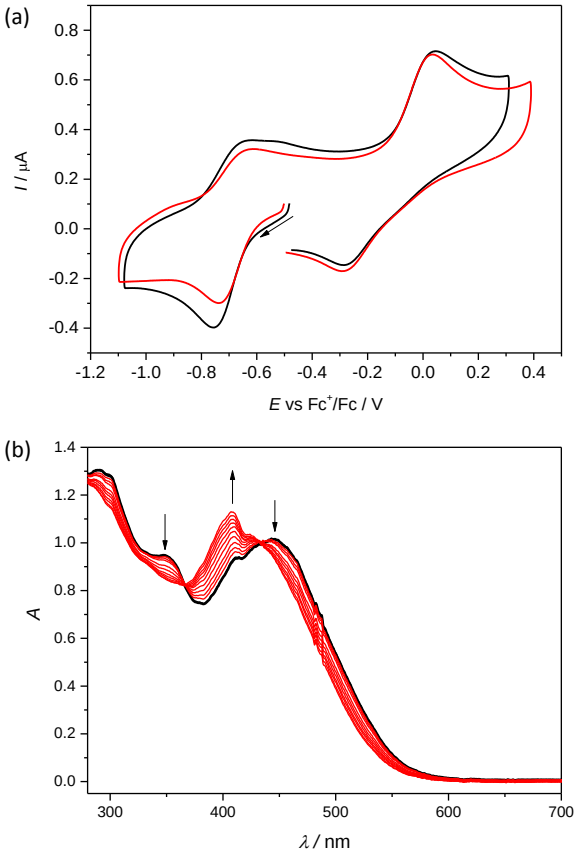

Figure 3. (a) Cyclic voltammograms of **1** (red trace) and heterodinuclear complex **2** (black trace) in DMSO/*n*-Bu_4NPF_6 at glassy-carbon working electrode at scan rate of 100 mV s^{-1}; (b) UV–vis spectra measured upon cathodic reduction of **2** at the first reduction peak by using honeycomb Pt working electrode.

Hydrolysis. The aqueous stability of **1–3** was investigated by UV–vis spectrophotometry to predict their behaviour under physiological conditions. Samples were incubated in water at 298 K and their absorption spectra were monitored over 24 h. The absorption bands of **2** and **3** decreased with time, while those for **1** remain unchanged indicating resistance to hydrolysis of the latter compound (Figure S9 in Supporting Information). The aqueous stability of **1** was confirmed by ESI mass spectra, which remain unchanged over 24 h and showed a peak with *m*/*z* 452, corresponding to $[Cu^{II}Cl(HL^{OMe})]^+$. In the presence of 24 μM NaCl the optical spectra of **2** and **3** did not change significantly, indicating that hydrolysis was effectively suppressed by the excess of Cl^- (Figure S10 in Supporting Information). In agreement with UV–vis studies, ESI mass spectra of complexes **2** and **3** in the presence of 24 μM NaCl indicated their enhanced aqueous stability.

Antiproliferative activity. The cytotoxicity of complexes **1**–**3** and proligand HL^H in comparison with cisplatin, $CuCl_2$ and *n*-$Bu_4N[Cu^ICl_2]$ was studied by MTT assays against ovarian carcinoma cell lines A2780 and A2780cisR, cervical adenocarcinoma HeLa cell line, as well as human embryonic kidney HEK293 cell line with an exposure time of 72 h. Results shown in Table 1 and Figure S11 in Supporting Information represent the mean IC_{50} values with standard deviations, and the resistance factor (RF).

Table 1. Cytotoxicity of amidrazone-morpholine hybrid HL^H, metal complexes **1–3**, $CuCl_2$, *n*-$Bu_4N[CuCl_2]$ and cisplatin.

Compound	IC_{50}[a] [μM]					
	A2780	**A2780cisR**	**RF**[b]	**HeLa**	**HEK293**	**SF**[c]
HL^H	138 ± 36	438 ± 54	3.2	>500	>100	-
1·0.2H_2O	15 ± 3	23 ± 5	1.5	51 ± 4	103 ± 30	6.9
2·1.5H_2O	22 ± 1	59 ± 6	2.7	91 ± 29	>100	>5
3·H_2O	45 ± 1	45 ± 4	1.0	32 ± 7	70 ± 15	1.5
$CuCl_2$	83 ± 12	82 ± 3	1.0	217 ± 42	187 ± 37	2.3
***n*-$Bu_4N[CuCl_2]$**	83 ± 13	156 ± 16	1.9	215 ± 16	145 ± 46	1.7
Cisplatin	0.44 ± 0.13	4.6 ± 0.3	10.5	4.4 ± 0.8	3.4 ± 1.1	7.7

[a] 50% inhibitory concentrations (IC_{50}) in human ovarian carcinoma cell lines A2780 and A2780cisR, human cervical adenocarcinoma cell line HeLa and human embryonic kidney cell line HEK293, determined by the MTT assay after exposure for 72h. Values are means ± standard error of mean (SEM) obtained from at least three different independent experiments. [b] RF is determined as $IC_{50(A2780cisR)}/IC_{50(A2780)}$. [c] SF is determined as $IC_{50(HEK293)}/IC_{50(A2780)}$.

As can be seen from Table 1, in all tested cell lines complexes **1**–**3** demonstrated antiproliferative activity in a micromolar concentration range, which is significantly lower than the activity of cisplatin. However, the differences in the activity of **1**–**3** in the cisplatin-resistant and cisplatin-sensitive cell lines reflected by their RF values were smaller than that of cisplatin, which typically demonstrates a 10–20 fold decrease of cytotoxicity in A2780cisR. The lack of cross resistance of **1**–**3** with cisplatin is expected, since these compounds operate via different mechanisms of action. Importantly, complexes **1** and **2** demonstrated high selectivity to cancer cell lines over noncancerous HEK293 cells, which might be beneficial for their further clinical development.

All metal complexes displayed greater cytotoxicity than HL^H, indicating that the binding of amidrazone-morpholine ligand to the metal is beneficial for their cytotoxicity. Similar increase of cytotoxicity was previously observed upon chelation of thiosemicarbazones to copper(II).[39,40] However, the subsequent coordination of the second metal (Ru or Os) to a copper(II)-amidrazone backbone did not lead to a further increase of activity. Of note is that **2** and **3** cannot be directly compared to **1**, since their amidrazone backbones are different. Also, it is important to point out that the activity of **1**–**3** was higher than the activity of $CuCl_2$ and $[CuCl_2]^-$, suggesting that anticancer effects of the complexes were not solely determined by the Cu(II) or counteranion, but by the combination of Cu(II) and amidrazone-morpholine ligand.

Intracellular accumulation. To determine whether the relative cytotoxicity of the copper(II)-amidrazone complexes was related to their cellular uptake, intracellular Cu(II) accumulation was determined at equimolar concentrations (100 μM) using ICP-MS (Figure 4). The intracellular Cu(II) accumulation increased in the following order **1** < **2** < **3**, indicating that coordination of Ru(II) or Os(II)-based fragments resulted in the improved uptake of these complexes into cells. However, the trend in cellular accumulation did not correlate with the trend in cytotoxicity in A2780 cell line (**1** > **2** > **3**), suggesting that the activity of the complexes is not directly related to their cellular uptake. In general, the accumulation of the complexes was very poor and did not significantly increase in comparison with $CuCl_2$, with the exception of **3** (***** $p<0.05$).

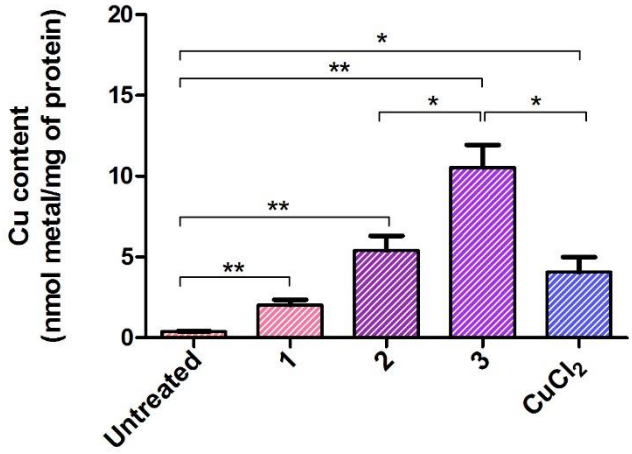

Figure 4. Intracellular Cu content determined upon 24 h exposure of A2780 cells to 100 μM of complexes **1**–**3** and $CuCl_2$ by means of ICP-MS. Statistical analysis was performed

by two-tailed T-test using GraphPad Prism software (GraphPad Software Inc., CA) with $p < 0.05$ considered as significant (* $p < 0.05$, ** $p < 0.01$).

ROS generation. To ascertain the ability of **1**–**3** and *n*-$Bu_4N[CuCl_2]$ to generate ROS in cell-free media in aerated DMSO/H_2O solutions the EPR spin trapping technique was used. The addition of 5,5-dimethyl-1-pyrroline *N*-oxide (DMPO) as a spin trap to DMSO/H_2O solutions of **1**–**3** and *n*-$Bu_4N[CuCl_2]$ saturated with pure molecular oxygen led to the appearance of EPR signals characteristic of mainly oxygen centered spin adducts[41] (Figures 5 and 6). The intensity of the corresponding EPR signal increased proportionally with the concentration of **2** (Figure 5a) providing evidence that ROS is produced in the presence of the heterometallic heterovalent complex. Note that only minor formation of these radicals was seen in the absence of **2** (see black line in Figure 5a), confirming the involvement of the latter in generation of ROS. The dominating spin adduct in DMSO/aqueous (4:1, v/v) solutions was simulated by the following spin-Hamiltonian parameters $A_N = 1.397$ mT, $A_H^{\beta} = 1.228$ mT and can be attributed to the $^{\bullet}$DMPO-OH spin-adduct in accord with literature data.[42] Experiments with increased amount of added water into the system (Figure 5b) confirmed the formation of hydroxyl radical spin-adduct. In DMSO/H_2O (2:3, v/v) mixed solvent the characteristic EPR signal of $^{\bullet}$DMPO-OH with 1:2:2:1 line intensities dominates the spectrum (see red line in Figure 5b) and can be simulated by the nearly equal values of hyperfine couplings ($A_N = 1.450$ mT, $A_H^{\beta} = 1.367$ mT).[43] The minor component ($A_N = 1.5240$ mT, $A_H^{\beta} = 2.246$ mT) corresponds to the carbon centered spin adduct $^{\bullet}$DMPO-R. No EPR signal was observed for reference sample in the absence of investigated complexes in DMSO/H_2O (2:3, v/v) system. The integral EPR intensity of DMPO spin-adducts (OH radicals dominated) of **1–3** in DMSO/H_2O/O_2/DMPO solutions, corresponding to the ROS-generating ability of complexes, decreased in the following order **1** > **2** > **3** (Figure 6b). This is in a good correlation with the cytotoxicity trend (Table 1) and might explain the reduced activity of complexes **2** and **3** despite their higher intracellular accumulation. The presence of $[CuCl_2]^-$ in **1–3** might be important for ROS generation, since *n*-$Bu_4N[CuCl_2]$ also demonstrated strong ROS induction.

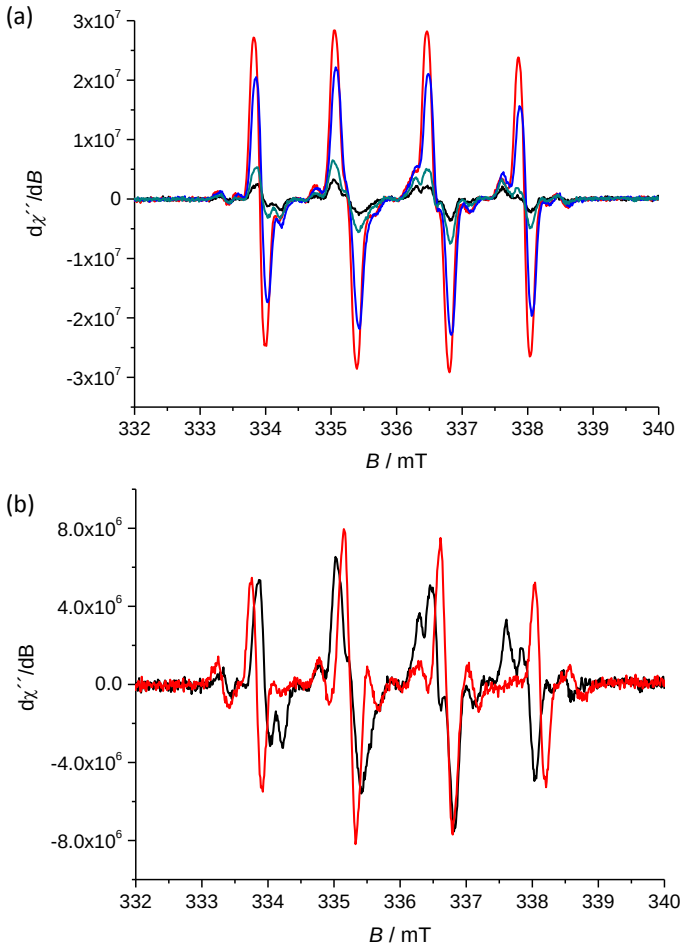

Figure 5. (a) EPR spectra of DMPO spin-adducts monitored for the DMSO/aqueous (4:1, v/v) solutions saturated with oxygen containing different concentrations of **2** and DMPO. c_0(DMPO) = 0.04 M and c_0(**2**) = 0.3 mM (red line), 0.1 mM (blue line), 0.02 mM (green line) and 0.00 mM (black line); (b) EPR spectra of DMPO spin-adducts measured in the **2**/DMSO/H_2O/O_2/DMPO solutions at 298 K with different amount of water in the system (black line: 400uL DMSO + 100 uL H_2O, red line: 200 uL DMSO + 300 uL H_2O). c_0(**2**) = 0.3 mM, c_0(DMPO) = 0.04 M.

When ROS generation experiments were performed for **1**–**3** in neat DMSO, a broadening of EPR signals was observed, as illustratively shown for **2** in Figure S12a in Supporting Information. A better resolution was obtained by bubbling Ar through the solution (Figure S12b in Supporting Information), indicating the formation of mainly oxygen-centered spin adducts. The dominating spin adduct was best simulated by the following spin-Hamiltonian parameters A_N = 1.375 mT, A_H^{β} = 1.161 mT in agreement with the formation of alkoxy-radical •DMPO-OR spin-adduct.[43] Only minor formation of these adducts was

seen in the absence of metal complexes, again providing evidence for their involvement in ROS generation.

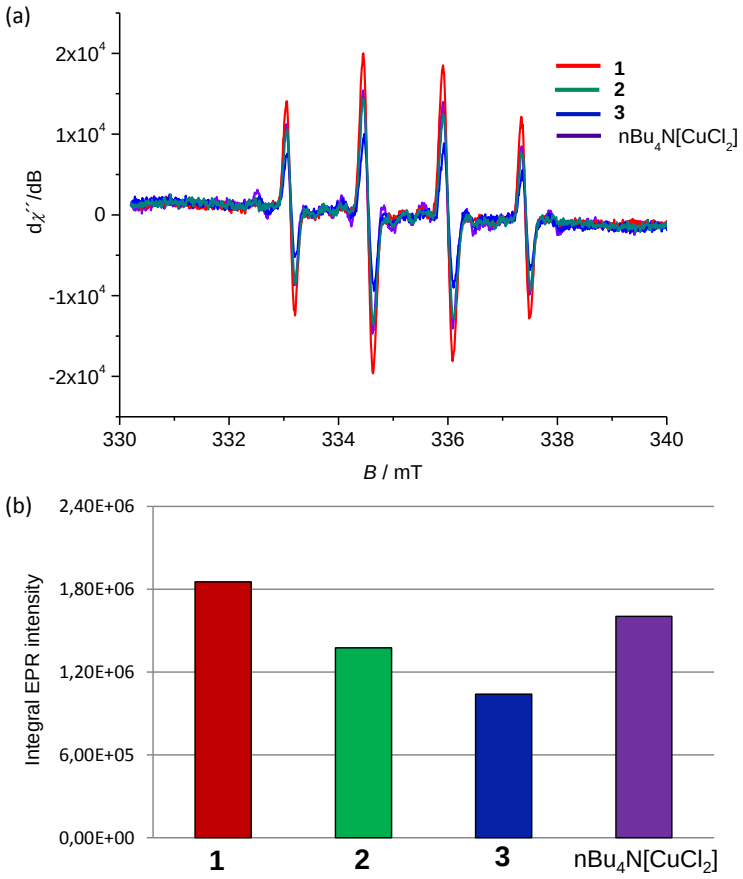

Figure 6. (a) EPR spectra of DMPO spin-adducts measured in the DMSO/H_2O/O_2/DMPO solutions at 298 K for 200 µL DMSO + 300 µL H_2O system and c_0(sample) = 60 µM, c_0(DMPO) = 0.04 M (red line – complex **1**, green line – complex **2**, blue line – complex **3**, violet line – sample *n*-$Bu_4N[CuCl_2]$) and (b) the corresponding integral EPR intensity (red column – complex **1**, green column – complex **2**, blue column – complex **3**, violet column – sample *n*-$Bu_4N[CuCl_2]$).

To support the results of EPR spin trapping experiments, we performed immunostaining of A2780 cells for the *in vitro* ROS detection. A2780 cells were treated with complex **3** (135 μM) for 24 h and subsequently co-incubated with cell permeable dye 2′,7′-dichlorodihydrofluorescein diacetate H_2DCF-DA, which is commonly used for the intracellular ROS detection, and Hoechst nuclear stain. As can be seen from Figure 7, untreated cells were characterized by basal intracellular ROS levels. However, when cells were treated with **3**, increase of ROS production was observed in agreement with the initial

hypothesis. Interestingly, drug treatment affected cellular morphology, resulting in the appearance of vacuoles, possibly of lysosomal-endosomal nature, and vacuolated cells demonstrated the highest DCFDA intensity. This might indicate that ROS induction by complex **3** might be involved in the mediation of non-apoptotic cell death accompanied by vacuolization, such as methuosis or paraptosis, but this hypothesis requires deeper investigation in the future.[44]

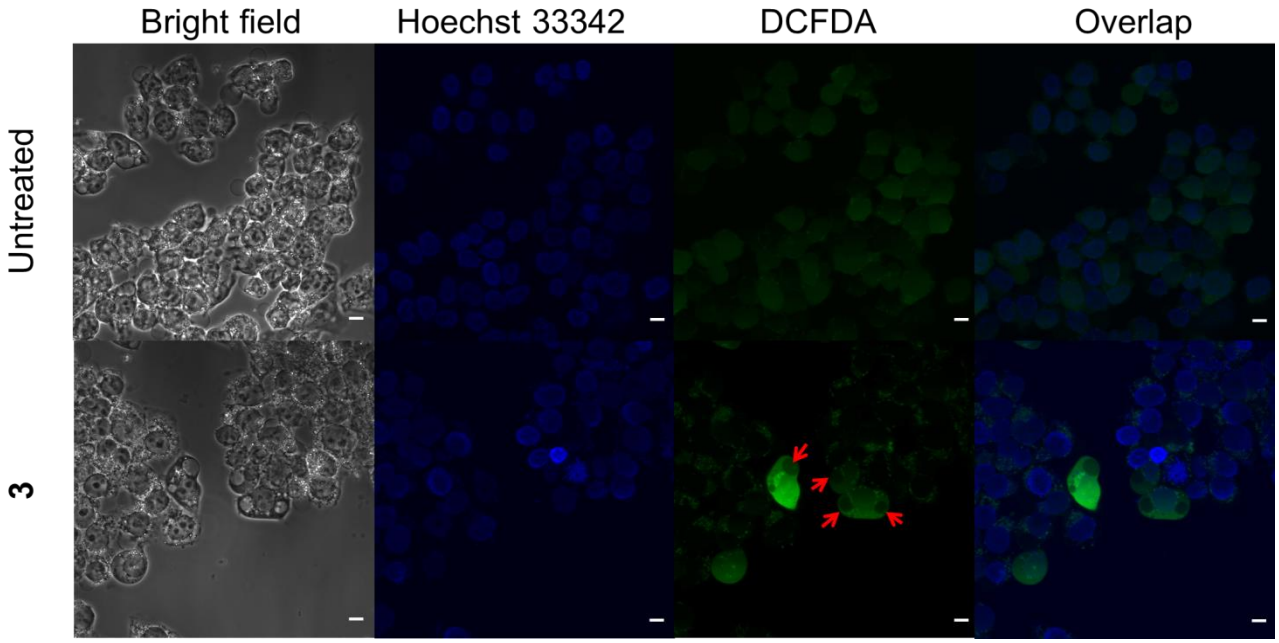

Figure 7. ROS detection by immunostaining. A2780 cells were incubated with complex **3** (100 μM) for 24 h and subsequently stained with H_2DCFDA (20 μM) for 15 min and visualized by confocal microscopy imaging. Hoechst 33342 dye was used for nuclear staining. Red arrows indicate cellular vacuoles. The scale bar represents 10 μM.

Conclusions

In this work, we prepared several novel homo- (**1**) and hetero- (**2**, **3**) metallic copper(II) complexes with amidrazone scaffold and $[CuCl_2]^-$ as a counterion. The heterometallic species, **2** and **3**, were obtained by a combination of copper(II) species, where a Cu(II) center was coordinated in a traditional manner by nitrogen donors, and a typical organoruthenium(II)/osmium(II) three leg piano stool moiety. The aldimine bond in copper(II)-amidrazone complexes was highly polarized, giving rise to novel unexpected species, mono- and tetranuclear copper(II) complexes (**1** and **4**), which were characterized by spectroscopic techniques and/or X-ray diffraction. Complexes **1**–**3** demonstrated superior anticancer activity in comparison to the amidrazone-morpholine proligand HL^H.

In addition, all complexes were selective to cancer cells over healthy cells. The anticancer activity of complexes **1**–**3** is due to the production of deadly ROS. The ability of investigated metal-based amidrazone-morpholine hybrids to generate ROS in cell-free media, as well as in cancer cells, was confirmed by spin trapping experiments by EPR spectroscopy and confocal microscopic imaging. Heterometallic complexes **2** and **3** were less active than the mononuclear complex **1**, even though their intracellular accumulation was higher, which might be explained by their less efficient ROS production. To specify the role of counterion in the biological activity of complexes **1**–**3**, we compared their anticancer properties with those of *n*-$Bu_4N[Cu^ICl_2]$. It was demonstrated that despite the ability of *n*-$Bu_4N[Cu^ICl_2]$ to induce significant ROS production, its cytotoxicity was significantly lower, suggesting that high activity of complexes **1**–**3** was a result of synergistic action of all metal-containing entities. To conclude, we proposed a viable approach for the assembly of redox-active anticancer organometallic compounds **2** and **3**. The redox potentials of copper(II) complex **1** and heterometallic complexes **2** and **3** are similar. The Cu-centered nature of redox events was further confirmed by UV–vis and EPR spectroelectrochemical measurements. Thus the redox activity of the whole, bimetallic assembly is confined to the Cu sites, not involving the Ru(II)/Os(II) centers.

Experimental section

Chemicals. All reagents used were received from commercial sources. 2-cyanopyridine, $RuCl_3 \cdot nH_2O$, $OsCl_3 \cdot nH_2O$ and $CuCl_2 \cdot 2H_2O$ were purchased from Sigma-Aldrich. The 6-(morpholinomethyl)pyridine-2-carboxaldehyde was synthesized via a multistep procedure as described elsewhere.[39] 2-pyridinamidrazone was prepared as a white solid by reaction of 2-cyanopyridine with excess hydrazine hydrate as reported previously.[45] Tetrabutylammonium dichloridocuprate(I) was synthesized as white crystals by reaction of copper(I) chloride with tetrabutylammonium hydrogen sulfate in the presence of sodium chloride in dichloromethane as described in the literature.[46] $[Ru(p\text{-cymene})Cl_2]_2$[47] and $[Os(p\text{-cymene})Cl_2]_2$[48] were prepared following literature procedures. Anhydrous dimethyl sulfoxide (SeccoSolv®, max. 0.025% H_2O) from Merck (Darmstadt, Germany), methanol (spectroscopic grade, Lachema, Brno, Czech Republic) and ferrocene (98%, Aldrich) were used as received. Tetrabutylammonium hexafluorophosphate (*n*-Bu_4NPF_6) of puriss quality (from Fluka) was dried under reduced pressure at 70 °C for 24 h before use. Distilled and deionized water was used for preparation of DMSO/water solutions. The spin trapping agent 5,5-dimethyl-1-pyrroline *N*-oxide (DMPO; Sigma-Aldrich) was distilled prior to the

application. Chemical grade cisplatin (1 mg/mL) was purchased from Hospira Pty Ltd (Melbourne, Australia). IGEPAL CA-630, DL-dithiothreitol (DTT), H_2DCF-DA were purchased from Sigma-Aldrich (St Louis, MO, USA). Thiazolyl Blue tetrazolium bromide (MTT) was purchased from Alfa Aesar. Hyclone™ Trypsin Protease 2.5% (10×) solution, RPMI 1640, DMEM medium, Fetal bovine serum (FBS) and Pierce™ Protease and Phosphatase Inhibitor Mini Tablets were purchased from Thermo Fisher Scientific. Biorad protein assay dye reagent concentrate was purchased from Bio-rad Laboratories. Milli-Q-grade purified water was obtained from a Milli-Q UV purification system (Sartorius Stedim Biotech S.A., Aubagne Cedex, France). Nitric acid (60–61%, for trace metal analysis) for ICP-MS analysis was obtained from Fluka (Sigma Aldrich) and used without further purification. Cu and In standards for ICP-MS measurements were obtained from CPI international (Amsterdam, The Netherlands).

Instrumentation. ICP-OES determination of Cu content was performed in Chemical, Molecular and Analysis Centre, National University of Singapore with Optima ICP-OES (Perkin Elmer, Watham, MA, USA). The absorbance of thiazolyl blue tetrazolium bromide (MTT) was measured by synergy H1 hybrid multimode microplate reader (Bio-Tek, Winoosky, VT, USA). Cu and Re contents in cells were determined by Agilent 7700 Series ICP-MS (Agilent Technologies, Santa Clara, CA, USA). The UV–vis spectrophotometric measurements were performed on a Hewlett Packard 8452A diode array spectrophotometer and a Thermo Scientific Evolution 220 spectrophotometer. The UV–vis spectrophotometric measurements were performed on a Hewlett Packard 8452A diode array spectrophotometer and a Thermo Scientific Evolution 220 spectrophotometer. Confocal microscope images were collected through a laser scanning confocal microscope (Fluoview FV3000, Olympus).

Synthesis of proligand and complexes

N-((6-(morpholinomethyl)pyridin-2-yl)methyleneamino)picolinamidine (HL^H). To 6-(morpholinomethyl)pyridine-2-carboxaldehyde (1.11 g, 5.39 mmol) in ethanol (50 ml) 2-pyridinamidrazone (0.734 g, 5.39 mmol) was added. The mixture was left under stirring and reflux overnight. Next day orange clear solution was allowed to cool to ambient temperature. The solvent was removed under reduced pressure to give a bright-orange oil, which was dried in vacuo. Yield: 1.61 g, 92.0%. Anal. Calcd for $C_{17}H_{20}N_6O \cdot 0.25H_2O$ (M_r

= 328.9), %: C, 62.08; H, 6.28; N, 25.55. Found, %: C, 62.07; H, 6.09; N, 25.67. ^{1}H NMR (500.10 MHz, DMSO-d_6): δ 8.68 (ddd, J = 4.8, 1.6, 0.9 Hz, 1H, H^{23}), 8.39 (s, 1H, H^{14}), 8.29-8.25 (m, 2H, H^{4}, H^{21}), 7.95 (td, J = 7.7, 1.7 Hz, 1H, H^{24}), 7.84 (t, J = 7.7 Hz, 1H, H^{3}), 7.56 (ddd, J = 7.5, 4.8, 1.2 Hz, 1H, H^{22}), 7.46 (d, J = 7.1 Hz, 1H, H^{5}), 7.36 (s, 1H, H^{18}), 7.26 (s, 1H, H^{16}), 3.63 (s, 2H, H^{7}), 3.62-3.58 (m, 4H, H^{9}, H^{13}), 2.45 (d, J = 3.8 Hz, 4H, H^{10}, H^{12}). ^{13}C NMR (125.76 MHz, DMSO-d_6): δ 158.43 (Cq, C^{6}), 157.96 (Cq, C^{17}), 154.69 (CH, C^{14}), 154.09 (Cq, C^{2}), 150.54 (Cq, C^{19}), 149.06 (CH, C^{23}), 137.56 (CH, C^{24}), 137.28 (CH, C^{3}), 126.14 (CH, C^{22}), 123.57 (CH, C^{5}), 121.94 (CH, C^{21}), 119.96 (CH, C^{4}), 66.69 (CH_2, C^{7}), 64.42 (CH_2, C^{9}, C^{13}), 53.81 (CH_2, C^{10}, C^{12}). ESI-MS (positive): *m/z* 325 ($[L + H]^+$). UV–vis (MeOH), λ_{max}, nm (ε, $M^{-1}cm^{-1}$): 337 (20280). The atom labelling scheme for ^{1}H and ^{13}C resonance assignment is given in Chart S1 in Supporting Information.

$[Cu^{II}Cl(HL^{OMe})][Cu^{I}Cl_2]\cdot 0.2H_2O$ (1·0.2H_2O)**.** To a solution of HL^{H} (0.190 g, 0.59 mmol) in methanol (5 ml) was added a solution of copper(II) chloride dihydrate (0.200 g, 1.17 mmol) in methanol (10 ml) and triethylamine (0.082 ml, 0.59 mmol). Bright-green suspension was stirred at 60 ºC for 20 min and the precipitate was filtered off. The filtrate was concentrated and allowed to stand at –20 ºC overnight to give a bright-green crystalline product. Crystals of X-ray diffraction quality were obtained by slow diffusion of diethyl ether into solution of the raw product in methanol. Yield: 0.058 g, 16.9%. Anal. Calcd for $C_{18}H_{22}N_6O_2Cu_2Cl_3\cdot 0.2H_2O$ (M_r = 591.5), %: C, 36.55; H, 3.82; N, 14.21. Found, %: C, 36.53; H, 3.87; N, 13.90. ESI-MS (positive): *m/z* 452 ($[M]^+$). UV–vis (MeOH), λ_{max}, nm (ε, $M^{-1}cm^{-1}$): 724 (144), 367 (4909), 260 (10755). IR (ATR, selected bands, $\tilde{\upsilon}_{max}$): 3357, 1633, 1584, 1555, 1429, 1307, 1269, 1108, 1011, 972, 854, 799, 698, 652 cm^{-1}.

$[Cu^{II}(L^{H})Ru^{II}(\eta^{6}$-*p*-cymene$)Cl_2][Cu^{I}Cl_2]\cdot 1.5H_2O$ (**2**·1.5H_2O). To a solution of HL^{H} (0.100 g, 0.31 mmol) in ethanol (5 ml) was added a solution of copper(II) chloride dihydrate (0.053 g, 0.31 mmol) in ethanol (5 ml) and triethylamine (0.043 ml, 0.31 mmol). Green-brown suspension was stirred under reflux for 20 min and then [Ru(η^6-p-cymene)$Cl_2]_2$ (0.095 g, 0.16 mmol) was added. Dark-red clear solution was left under stirring and reflux overnight. Next day the solvent was removed under reduced pressure to give a dark-red crystalline precipitate, which was filtered off, washed with ethanol and diethyl ether and dried in air. X-ray diffraction quality single crystals of **2** were obtained by re-crystallization of the product in ethanol. Yield: 0.06 g, 22.8%. Anal. Calcd for $C_{27}H_{33}N_6OCu_2RuCl_4\cdot 1.5H_2O$ (M_r = 854.6), %: C, 37.95; H, 4.25; N, 9.83. Found, %: C, 37.93; H, 4.13; N, 9.79. ESI-MS (positive): *m/z* calcd for $[Cu^{II}Ru^{II}(L^{H})Cl_2]^+$ 694.06; for

$[Cu^{II}Ru^{II}(L^{H})Cl]^{2+}$ 329.54. Found: *m/z* 694.10 and 329.57 ($[Cu^{II}Ru^{II}(L^{H})Cl]^{2+}$). ESI-MS (negative): *m/z* 134.74 ($[CuCl_2]^-$). UV–vis (MeOH), λ_{max}, nm (ε, $M^{-1}cm^{-1}$): 489sh, 440 (4169), 415 (4222), 343 (4529), 290sh. IR (ATR, selected bands, $\tilde{\upsilon}_{max}$): 3049, 1599, 1567, 1458, 1382, 1250, 1167, 1107, 868, 798, 654 cm^{-1}.

$[Cu^{II}(L^{H})Os^{II}(\eta^6$-*p*-cymene)$Cl_2][Cu^{I}Cl_2]\cdot H_2O$ (**3**·H_2O). To a solution of HL^H (0.10 g, 0.31 mmol) in ethanol (5 ml) was added a solution of copper(II) chloride dihydrate (0.05 g, 0.31 mmol) in ethanol (5 ml) and triethylamine (0.043 ml, 0.31 mmol). Green-brown suspension was stirred under reflux for 20 min and then $[Os(\eta^6$-*p*-cymene)$Cl_2]_2$ (0.126 g, 0.16 mmol) was added. A dark-red clear solution was left under stirring and reflux for 1.5 h, cooled down thereafter and left to stand in air at ambient temperature. Dark-red crystals of X-ray diffraction quality were obtained after 3 days. Yield: 0.037 g, 25.1%. Anal. Calcd for $C_{27}H_{33}N_6OCu_2OsCl_4\cdot H_2O$ (M_r = 934.7), %: C, 34.69; H, 3.77; N, 8.99. Found, %: C, 34.56; H, 3.25; N, 8.78. ESI-MS (positive): *m/z* calcd for $[Cu^{II}Os^{II}(L^{H})Cl_2]^+$ 782.10; for $[Cu^{II}Os^{II}(L^{H})Cl]^{2+}$ 373.57. Measured: *m/z* 782.09 and 373.53 ($[Cu^{II}Ru^{II}(L^{H})Cl]^{2+}$). ESI-MS (negative): *m/z* 134.64 ($[CuCl_2]^-$). UV–vis (MeOH), λ_{max}, nm (ε, $M^{-1}cm^{-1}$): 537sh, 458 (3734), 353 (4291), 317 (4682), 274sh. IR (ATR, selected bands, $\tilde{\upsilon}_{max}$): 3239, 1598, 1565, 1459, 1254, 1169, 1102, 1056, 1027, 863, 798, 659 cm^{-1}.

$[Cu^{II}_4(L^1)_2(L^2)_2Cl_2]Cl_2\cdot 5MeOH\cdot 5.5H_2O$ (4·5MeOH·5.5H_2O**)**. To a solution of HL^H (0.500 g, 1.54 mmol) in methanol (20 ml) was added a solution of copper(II) chloride dihydrate (0.263 g, 1.54 mmol) in methanol (10 ml) and triethylamine (0.21 ml, 1.54 mmol). Dark-green suspension was stirred at 60 ºC for 20 min. Then the mixture was cooled down, the precipitate filtered off. By diffusion of diethyl ether into a methanolic solution of the raw product brown crystals of X-ray diffraction quality were grown within three days and investigated by X-ray crystallography.

Crystallographic Structure Determination. X-ray diffraction measurements were performed on a Bruker X8 APEXII CCD (**1**), Bruker D8 Venture (**2**–**4**) diffractometers. Single crystals were positioned at 35, 24, 24 and 24 mm from the detector, and 2300, 720, 713 and 1342 frames were measured, each for 26, 60, 60 and 37 s over 0.5, 0.5, 0.4 and 0.5° scan width for **1**–**4**, respectively. The data were processed using SAINT software.[49] Crystal data, data collection parameters, and structure refinement details are given in Table 2. The structures were solved by direct methods and refined by full-matrix least-squares techniques. Non-H atoms were refined with anisotropic displacement parameters. H atoms

were inserted in calculated positions and refined with a riding model. The residual electron density in the structures **2**, **3** and **4**·5MeOH was removed by using SQUEEZE option implemented in PLATON. Solvent accessible voids of 442, 445 and 163 $Å^3$ are present in the crystal structures of **2**, **3** and **4**·5MeOH, respectively. The following computer programs and hardware were used: structure solution, *SHELXS-2014* and refinement, *SHELXL-2014*;[50] molecular diagrams, ORTEP;[51] computer, Intel CoreDuo. CCDC – 1884326 for **1**, 1884327 for **2**, 1884328 for **3**, 1884329 for **4**·5MeOH.

Electrochemistry. Cyclic voltammetry experiments with 1 mM solutions of **1**–**3** in 0.1 M *n*-Bu_4NPF_6 supporting electrolyte in DMSO or in methanol were performed under argon atmosphere using a three electrode arrangement with glassy-carbon 1 mm disc working electrode (from Ionode, Australia), platinum wire as counter electrode, and silver wire as pseudoreference electrode. Ferrocene served as the internal potential standard. A Heka PG310USB (Lambrecht, Germany) potentiostat with a PotMaster 2.73 software package served for the potential control in voltammetric studies.

Spectroelectrochemistry. *In situ* ultraviolet-visible-near-infrared (UV–vis–NIR) spectroelectrochemical measurements were performed on a spectrometer (Avantes, Model AvaSpec-2048x14-USB2) in the spectroelectrochemical cell kit (AKSTCKIT3) with the Pt-microstructured honeycomb working electrode, purchased from Pine Research Instrumentation. The cell was positioned in the CUV–UV Cuvette Holder (Ocean Optics) connected to the diode-array UV–vis–NIR spectrometer by optical fibers. UV–vis–NIR spectra were processed using the AvaSoft 7.7 software package. Halogen and deuterium lamps were used as light sources (Avantes, Model AvaLight-DH-S-BAL). The *in situ* EPR spectroelectrochemical experiments were carried out under an argon atmosphere in the EPR flat cell equipped with a large platinum mesh working electrode. The freshly prepared solutions were carefully purged with argon and the electrolytic cell was polarized in the galvanostatic mode directly in the cylindrical EPR cavity TM-110 (ER 4103 TM) and the EPR spectra were measured *in situ*. The EPR spectra were recorded at room temperature with the EMX Bruker spectrometer.

Cell lines and culture conditions. Human ovarian carcinoma cells A2780 and A2780cisR, human cervical adenocarcinoma cells HeLa and healthy embryonic kidney cells HEK293 were obtained from ATCC. A2780cisR cells were exposed to cisplatin (1 μM) every third

passage to maintain resistance. A2780 and A2780cisR cells were cultured in RPMI 1640 medium containing 10% fetal bovine serum (FBS). HeLa and HEK293 cells were cultured in DMEM medium containing 10% FBS. All cells were grown in tissue culture 25 cm^2 flasks (BD Biosciences, Singapore) at 37 °C in a humidified atmosphere of 95% air and 5% CO_2. All drug stock solutions except cisplatin were prepared in DMSO and the final concentration of DMSO in medium did not exceed 1% (v/v) at which cell viability was not inhibited. The amount of actual Cu and Ru concentration in the stock solutions was determined by ICP-OES.

Inhibition of cell viability assay. The cytotoxicity of the compounds was determined by colorimetric microculture assay (MTT assay). The cells were harvested from culture flasks by trypsinization and seeded into Cellstar 96-well microculture plates (Greiner Bio-One) at the seeding density of 6000 cells per well (100 μl per well) or 10000 cells per well for HEK293 cells. After the cells were allowed to resume exponential growth for 24 h, they were exposed to drugs at different concentrations in media for 72 h. The drugs were diluted in complete medium at the desired concentration and 100 μl of the drug solution was added to each well and serially diluted to other wells. After exposure for 72 h, drug solutions were replaced with 100 μL of MTT in media (5 mg ml^{-1}) and incubated for additional 45 min. Subsequently, the medium was aspirated and the purple formazan crystals formed in viable cells were dissolved in 100 μl of DMSO per well. Optical densities were measured at 570 nm with a microplate reader. The quantity of viable cells was expressed in terms of treated/control (T/C) values by comparison to untreated control cells, and 50% inhibitory concentrations (IC_{50}) were calculated from concentration-effect curves by interpolation. Evaluation was based on means from at least three independent experiments, each comprising six replicates per concentration level.

Intracellular accumulation. Intracellular accumulation of **1**–**3** and $CuCl_2$ was determined in A2780 cells. Cells were seeded into Cellstar 6-well plates (Greiner Bio-one) at a density of 20×10^4 cells/well (2 mL per well). After the cells were allowed to resume exponential growth for 48 h, they were exposed to **1**–**3** and $CuCl_2$ at 100 μM for 24 h at 37 °C. The cells were washed twice with 1 mL of PBS and lysed with 100 μL of RIPA lysis buffer (ultrapure water, 5M NaCl, 1M Tris-HCl pH 8.0, 2% sodium deoxycholate, 10% SDS, IGEPAL, protease and phosphatase inhibitor) for 5–10 min at 4 °C. The cell lysates were scraped from the wells and transferred to separate 1.5 mL microtubes. The supernatant was then collected after centrifugation (13 000 rpm, 4 °C for 15 min) and total protein content

of each sample was quantified via Bradford's assay. Cell lysates were transferred to 2 mL glass vials and then digested with ultrapure 60% HNO_3 (50 μL) at 110 °C for 96 h. The resulting solution was diluted to 1 mL (2–4% *v/v* HNO_3) with ultrapure Milli-Q water, sonicated for 45 min and filtered through 0.45 μm filters. Cu content of each sample was quantified by ICP-MS and expressed as per mg of protein. Re was used as an internal standard. Cu and Re were measured at *m*/*z* 64 and 186, respectively. Metal standards for calibration curve (0, 1, 2, 5, 10, 20, 40 ppb) were prepared. All readings were made in six replicates in He mode.

Cell-free ROS generation. The generation of paramagnetic intermediates was monitored by cw-EPR spectroscopy using the EMXplus spectrometer. Freshly prepared 0.4 mM solution of **2** in DMSO was mixed with DMSO or water (final amount 400 μL) and bubbled with pure oxygen for 5 min. After this step the solution of spin trapping agent 100 μL of 0.21 M DMPO in DMSO was added and immediately transferred into a flat EPR quartz cell. The EPR spectra were measured with following experimental parameters: X-band, room temperature, microwave frequency, 9.431 GHz; 100 kHz field modulation amplitude, 2 G; time constant, 10 ms; scan time, 41s (ten scans).

Fluorescence staining. A2780 cells were seeded onto 100 mm cell culture dishes at a seeding density of 2×10^5 cells per dish. After the cells were allowed to resume exponential growth for 24 h, the media was changed and the cells were exposed to 100 μM of complex **3** for 24 h at 37 °C. Subsequently, the cells were stained with Hoechst 33342 nuclear stain (0.1 μg/ml) for 10 min and then washed twice with 1x PBS and replaced with H_2DCFDA (20 μM) in colorless RPMI media (without FBS). The cells were then incubated at 37 °C for 15 min, washed twice with 1x PBS and fixed with 10% paraformaldehyde in 0.1 M phosphate buffer (pH 7.4) at room temperature for 30 min. Subsequently, the cells were washed twice with 1x PBS and analyzed by confocal microscopy using Fluoview FV3000 Olympus confocal microscope.

Table 2. Crystal Data and Details of Data Collection for **$[Cu^{II}(HL^{OMe})Cl][Cu^{I}Cl_2]$ (1)**, **$[(Cu^{II}(Ru(p\text{-cymene})Cl_2(L^{H})][Cu^{I}Cl_2]$ (2)**, **$[(Cu^{II}Os(p\text{-cymene})Cl_2(L^{H})][Cu^{I}Cl_2]$ (3)** and **$[Cu^{II}_4Cl_2(L^1)_2(L^2)_2]Cl_2\cdot 5MeOH$ (4·5MeOH)**

Compound	**1**	**2**	**3**	**4·5MeOH**
empirical	$C_{18}H_{22}Cl_3Cu_2N_6$	$C_{27}H_{33}Cl_4Cu_2N_6O$	$C_{27}H_{33}Cl_4Cu_2N_6O$	$C_{73}H_{92}Cl_4Cu_4N_{24}O_{11}$
fw	587.84	827.54	916.67	1877.66
space group	*P*-1	*C*2/*c*	*C*2/*c*	$P2_1/n$
α, Å	6.9042(14)	31.6782(17)	31.528(3)	13.9260(6)
b, Å	12.424(2)	12.8500(7)	12.846(1)	15.8732(7)
c, Å	13.264(3)	21.729(2)	21.868(2)	21.0395(9)
α, °	83.869(6)			
β, °	82.030(7)	128.987(1)	128.844(3)	92.474(2)
γ, °	77.462(6)			
V [Å^3]	1096.5(4)	6875.2(9)	6898.1(10)	4646.5(3)
Z	2	8	8	2
λ [Å]	0.71073	0.71073	0.71073	0.71073
ρ_{calcd}, g cm^{-3}	1.780	1.599	1.765	1.342
cryst size, mm^3	0.20 × 0.15 ×	0.14 × 0.04 × 0.01	0.10 × 0.02 × 0.02	0.12 × 0.12 × 0.07
T [K]	100(2)	100(2)	100(2)	100(2)
μ, mm^{-1}	2.334	2.001	5.237	1.083
R_1[a]	0.0331	0.0713	0.0442	0.0699
wR_2[b]	0.0852	0.1476	0.0990	0.2104
GOF[c]	1.028	1.094	0.953	1.083

[a] $R_1 = \Sigma||F_o| - |F_c||/\Sigma|F_o|$. [b] $wR_2 = \{\Sigma[w(F_o^2 - F_c^2)^2]/\Sigma[w(F_o^2)^2]\}^{1/2}$. [c] GOF = $\{\Sigma[w(F_o^2 - F_c^2)^2]/(n - p)\}^{1/2}$, where n is the number of reflections and p is the total number of parameters refined.

ASSOCIATED CONTENT

Supporting Information Available: Atom numbering scheme for NMR spectra (Chart S1), line drawings of the ligands in tetranuclear Cu(II) complex **4** (Chart S2), ESI mass spectra of **2** and **3** (Figure S1 and S2), X-ray diffraction structure of **4** (Figure S3), cyclic volammograms of **3**, *n*-$Bu_4N[CuCl_2]$ and HL^H (Figure S4), and **2** (Figure S5), EPR spectra for **2** and its one-electron reduced and one-electron oxidized species (Figure S6), UV-vis-NIR spectra of **2** after in situ reduction of **2** and upon back reoxidation (Figure S7), UV-vis-NIR spectra of **2** upon in situ oxidation (Figure S8), absorption spectra of 1–3 in aqueous solutions in the absence and in the presence of NaCl (Figures S9 and S10), concentration-effect curves for HL^H and **1**–**3** (Figure S11), EPR spectra of $^{\bullet}$DMPO-X spin adducts in the presence of **2** (Figure S12). This material is available free of charge via the Internet at http://pubs.acs.org.

Author Information

Corresponding Author

* E-mail: vladimir.arion@univie.ac.at (V.B.A.).

ORCID

Vladimir B. Arion: 0000-0002-1895-6460

Maria V. Babak: 0000-0002-2009-7837

Notes

The authors declare no competing financial interests.

Acknowledgments. Austrian Science Fund (FWF) is acknowledged for the grant no. P28223-N34. This work was also supported by the National University of Singapore (NUS), Department of Pharmacy (C148-000-003-001 (FYP)), by the Science and Technology Assistance Agency under the contract no. APVV-15-0053 and SK-AT-2017-

0017, and by the Slovak Grant Agency VEGA under contract no. 1/0416/17 and 1/0466/18.

References

(1) Bergamo, A.; Gaiddon, C.; Schellens, J. H. M.; Beijnen, J. H.; Sava, G. Approaching tumor therapy beyond platinum drugs. J. Inorg. Biochem. **2012**, *106*, 90–99.

(2) Thota, S.; Rodrigues, D. A.; Crans, D. C.; Barreiro, E. J. Ru(II) compounds: Next-generation anticancer metallotherapeutics? J. Med. Chem. **2018**, *61*, 5805–5821.

(3) Babak, M. V.; Ang, W. H. Multinuclear organometallic ruthenium-arene complexes for cancer therapy. In Metallo-Drugs: Development and Action of Anticancer Agents; Sigel, A., Sigel, H., Freisinger, E., Sigel, R. K. O., Eds.; De Gruyter: Berlin, Boston, **2018**, 171–198.

(4) van Rijt, S. H.; Peacock, A. F. A.; Johnstone, R. D. L.; Parsons, S.; Sadler, P. J. Organometallic osmium(II) arene anticancer complexes containing picolinate derivatives. *Inorg. Chem.* **2009**, *48*, 1753–1762.

(5) Grozav, A.; Miclaus, V.; Vostinaru, O.; Ghibu, S.; Berce, C.; Rotar, I.; Mogosan, C.; Therrien, B.; Loghin, F.; Popa, D.-S. Acute toxicity evaluation of a thiazolo arene ruthenium(II) complex in rats. *Regul. Toxicol. Pharm.* **2016**, *80*, 233–240.

(6) Aird, R. E.; Cummings, J.; Ritchie, A. A.; Muir, M.; Morris, R. E.; Chen, H.; Sadler, P. J.; Jodrell, D. I. In vitro and in vivo activity and cross resistance profiles of novel ruthenium(II) organometallic arene complexes in human ovarian cancer. *Br. J. Cancer* **2002**, *86*, 1652–1657.

(7) Murray, B. S.; Babak, M. V.; Hartinger, C. G.; Dyson, P. J. The development of RAPTA compounds for the treatment of tumors. *Coord. Chem. Rev.* **2016**, *306*, 86–114.

(8) Hanif, M.; Babak, M. V.; Hartinger, C. G. Development of anticancer agents: wizardry with osmium. *Drug Discovery Today* **2014**, *19*, 1640–1648.

(9) Denoyer, D.; Clatworthy, S. A. S.; Cater, M. A. Copper complexes in cancer therapy. In *Metallo-Drugs: Development and Action of Anticancer Agents*; Sigel, A., Sigel, H., Freisinger, E., Sigel, R. K. O., Eds.; De Gruyter: Berlin, Boston, **2018**; 469–506.

(10) Jungwirth, U.; Kowol, C. R.; Keppler, B. K.; Hartinger, C. G.; Berger, W.; Heffeter, P. Anticancer activity of metal complexes: involvement of redox processes. *Antioxidants & Redox Signaling* **2011**, *15*, 1085–1127.

(11) Schumacker, P. T. Reactive oxygen species in cancer cells: live by the sword, die by the sword. *Cancer Cell* **2006**, *10*, 175–176.
(12) Trachootham, D.; Alexandre, J.; Huang, P. Targeting cancer cells by ROS-mediated mechanisms: a radical therapeutic approach? *Nat. Rev. Drug Disc.* **2009**, *8*, 579–591.
(13) Lopes, J.; Alves, D.; Morais, T. S.; Costa, P. J.; Piedade, M. F. M.; Marques, F.; Villa de Brito, M. J.; Helena Garcia, M. New copper(I) and heteronuclear copper(I)–ruthenium(II) complexes: synthesis, structural characterization and cytotoxicity. *J. Inorg. Biochem.* **2017**, *169*, 68–78.
(14) van der Steen, S.; de Hoog, P.; van der Schilden, K.; Gamez, P.; Pitié, M.; Kiss, R.; Reedijk, J. Novel heteronuclear ruthenium–copper coordination compounds as efficient DNA-cleaving agents. *Chem. Commun.* **2010**, *46*, 3568–3570.
(15) Senina, A. S.; Evdokimov, A. A.; Moskvin, A. V.; Fedorova, E. V. Synthesis, characterization and antimicrobial activity of amidrazone derivatives. *J. Adv. Chem. Sci.* **2016**, *2*, 183–187.
(16) Modzelewska-Banachiewicz, B.; Matysiak, J.; Niewiadomy, A. Synthesis and mycological activity of the compounds obtained in the reaction of N(3)-substituted amidrazones with sulphinyl-bis-2,4-dihydroxybenzenethioyl. *Eur. J. Med. Chem.* **2001**, *36*, 75–80.
(17) Modzelewska-Banachiewicz, B.; Ucherek, M.; Zimecki, M.; Kutkowska, J.; Kaminska, T.; Morak-Młodawska, B.; Paprocka, R.; Szulc, M.; Lewandowski, G.; Marciniak, J.; Bobkiewicz-Kozlowska, T. Reactions of N^3-substituted amidrazones with *cis*-1,2-cyclohexanedicarboxylic anhydride and biological activities of the products. *Arch. Pharm.* **2012**, *345*, 486–494.
(18) Ziegler-Borowska, M.; Ucherek, M.; Kutkowska, J.; Mazur, L.; Modzelewska-Banachiewicz, B.; Kędziera, D.; Kaczmarek-Kędziera, A. Reaction of N3-phenylbenzamidrazone with cis-1,2-cyclohexanedicarboxylic anhydride. *Tetrahedron Lett.* **2010**, *51*, 2951–2955.
(19) Modzelewska-Banachiewicz, B.; Banachiewicz, J.; Chodkowska, A.; Jagiełło-Wójtowicz, E.; Mazur, L. Synthesis and biological activity of new derivatives of 3-(3,4-diaryl-1,2,4-triazole-5-yl)propenoic acid. *Eur. J. Med. Chem.* **2004**, *39*, 873–877.
(20) Habashneh, A. Y.; El-Abadelah, M. M.; Zihlif, M. A.; Imraish, A.; Taha, M. O. Synthesis and antitumor activities of some new *N*1-(flavon-6-yl)amidrazone derivatives: antitumor activities of *N*1-(flavon-6-yl)amidrazone derivatives. *Arch. Pharm.* **2014**, *347*, 415–422.

(21) Abdel-Jalil, R. J.; El Momani, E. Q.; Hamad, M.; Voelter, W.; Mubarak, M. S.; Smith, B. H.; Peters, D. G. Synthesis, antitumor activity, and electrochemical behavior of some piperazinyl amidrazones. *Monatsh. Chem.* **2010**, *141*, 251–258.
(22) Abu-Aisheh, M. N.; Mustafa, M. S.; El-Abadelah, M. M.; Naffa, R. G.; Ismail, S. I.; Zihlif, M. A.; Taha, M. O.; Mubarak, M. S. Synthesis and biological activity assays of some new N1-(flavon-7-yl)amidrazone derivatives and related congeners. *Eur. J. Med. Chem.* **2012**, *54*, 65–74.
(23) Pelova, R.; Spassowska, N.; Maneva, L.; Taxirov, S. Antibacterial and antitumor activity of platinum complexes of hydrazinopyrimidines and amidrazones. *Pharmazie* **1987**, *42*, 251–252.
(24) Ponticelli, G.; Mitewa, M. Synthesis, characterization, structure and cytotoxic activity of gold(III) complexes with amidrazone derivates. *Transition Met. Chem.* **2006**, *31*, 703–707.
(25) Mazur, L.; Modzelewska-Banachiewicz, B.; Paprocka, R.; Zimecki, M.; Wawrzyniak, U. E.; Kutkowska, J.; Ziółkowska, G. Synthesis, crystal structure and biological activities of a novel amidrazone derivative and its copper(II) complex — a potential antitumor drug. *J. Inorg. Biochem.* **2012**, *114*, 55–64.
(26) Gokhale, N. H.; Padhye, S. S.; Padhye, S. B.; Anson, C. E.; Powell, A. K. Copper complexes of carboxamidrazone derivatives as anticancer agents. 3. Synthesis, characterization and crystal structure of [Cu(Appc)Cl_2], (Appc = N1-(2-acetylpyridine)pyridine-2-carboxamidrazone). *Inorg. Chim. Acta* **2001**, *319*, 90–94.
(27) Gokhale, N.; Padhye, S.; Rathbone, D.; Billington, D.; Lowe, P.; Schwalbe, C.; Newton, C. The crystal structure of first copper(II) complex of a pyridine-2-carboxamidrazone – a potential antitumor agent. *Inorg. Chem. Commun.* **2001**, *4*, 26–29.
(28) Dando, T. M.; Perry, C. M. Aprepitant: a review of its use in the prevention of chemotherapy-induced nausea and vomiting. *Drugs* **2004**, *64*, 777–794.
(29) Mok, T. S.; Wu, Y.-L.; Thongprasert, S.; Yang, C.-H.; Chu, D.-T.; Saijo, N.; Sunpaweravong, P.; Han, B.; Margono, B.; Ichinose, Y.; Nishiwaki, Y.; Ohe, Y.; Yang, J. J.; Chewaskulyong, B.; Jiang, H.; Duffield, E. L.; Watkins, C. L.; Armour, A. A.; Fukuoka, M. Gefitinib or Carboplatin–Paclitaxel in pulmonary adenocarcinoma. *New England J. Med.* **2009**, *361*, 947–957.
(30) Ohui, K.; Afanasenko, E.; Bacher, F.; Ting, R. L. X.; Zafar, A.; Blanco-Cabra, N.; Torrents, E.; Dömötör, O.; May, N. V.; Darvasiova, D.; Enyedy, E. A.; Popović-Bijelić, A.; Reynisson, J.; Rapta, P.; Babak, M. V.; Pastorin, G.; Arion, V. B. New water-soluble

copper(II) complexes with morpholine–thiosemicarbazone hybrids: Insights into the anticancer and antibacterial mode of action. *J. Med. Chem.* **2019**, *2*, 512–530.
(31) Bera, P.; Butcher, R. J.; Saha, N. Synthesis, spectral and structural characterisation of chloro{S-benzyl-β-N-(5-methylpyrazole-3-yl)ethoxymethylenedithiocarbazato} copper(II) derived from S-benzyl-β-N-(5-methylpyrazole-3-yl)methylenedithio-carbazide. *Chem. Lett.* **1998**, *27*, 559–560.
(32) Ali, M. A.; Mirza, A. H.; Ting, W. Y.; Hamid, M. H. S. A.; Bernhardt, P. V.; Butcher, R. J. Mixed-ligand nickel(II) and copper(II) complexes of tridentate ONS and NNS ligands derived from S-alkyldithiocarbazates with the saccharinate ion as a co-ligand. *Polyhedron* **2012**, *48*, 167–173.
(33) Sangeetha, N. R.; Pal, S.; Pal, S. Copper(II)-activated transformation of azomethine to imidate: synthetic and structural studies. *Polyhedron* **2000**, *19*, 2713–2717.
(34) Addison, A. W.; Rao, T. N.; Reedijk, J.; van Rijn, J.; Verschoor, G. C. Synthesis, Structure, and spectroscopic properties of copper(II) compounds containing nitrogen–sulphur donor ligands; the crystal and molecular structure of aqua[1,7-bis(N-methylbenzimidazol-2′-yl)-2,6-dithiaheptane]copper(II) perchlorate. *J. Chem. Soc., Dalton Trans.* **1984**, 1349–1356.
(35) Menon, M.; Choudhury, S.; Pramanik, A.; Deb, A. K.; Chandra, S. K.; Bag, N.; Goswami, S.; Chakravorty, A. Oxidation of coordinated azomethine to amide. Synthetic and structural studies on a rhenium and a ruthenium system. *J. Chem. Soc., Chem. Commun.* **1994**, 57–58.
(36) Busch, D. H.; Bailar, J. C. The iron(II)-methine chromophore. *J. Am. Chem. Soc.* **1956**, *78*, 1137–1142.
(37) Harris, C. M.; McKenzie, E. D. Addition of alcohols to a Schiff base co-ordinated to copper(II). *Nature* **1962**, *196*, 670–671.
(38) Silkey, J. R.; Joke, J. T. Electrochemical studies of triethylammonium dichlorocuprate(I), a room temperature fused salt. *J. Electrochem. Soc.* **1980**, *127*, 1091–1095.
(39) Bacher, F.; Dömötör, O.; Chugunova, A.; Nagy, N. V.; Filipović, L.; Radulović, S.; Enyedy, É. A.; Arion, V. B. Strong effect of copper(II) coordination on antiproliferative activity of thiosemicarbazone–piperazine and thiosemicarbazone–morpholine hybrids. *Dalton Trans.* **2015**, *44*, 9071–9090.
(40) Sîrbu, A.; Palamarciuc, O.; Babak, M. V.; Lim, J. M.; Ohui, K.; Enyedy, E. A.; Shova, S.; Darvasiová, D.; Rapta, P.; Ang, W. H.; Arion, V.B. Copper(II) thiosemicarbazone

complexes induce marked ROS accumulation and promote nrf2-mediated antioxidant response in highly resistant breast cancer cells. *Dalton Trans.* **2017**, *46*, 3833–3847.
(41) Dvoranová, D.; Barbieriková, Z.; Brezová, V. Radical intermediates in photoinduced reactions on TiO_2 (an EPR spin trapping study). *Molecules* **2014**, *19*, 17279–17304.
(42) Zalibera, M.; Rapta, P.; Staško, A.; Brindzová, L.; Brezová, V. Thermal generation of stable spin trap adducts with super-hyperfine structure in their EPR spectra: an alternative EPR spin trapping assay for radical scavenging capacity determination in dimethylsulphoxide. *Free Rad. Res.* **2009**, *43*, 457–469.
(43) Hricovíni, M.; Mazúr, M.; Sîrbu, A.; Palamarciuc, O.; Arion, V. B.; Brezová, V. Copper(II) thiosemicarbazone complexes and their proligands upon UVA irradiation: an EPR and spectrophotometric steady-state study. *Molecules* **2018**, *23*, 721.
(44) Shubin, A. V.; Demidyuk, I. V.; Komissarov, A. A.; Rafieva, L. M.; Kostrov, S. V. Cytoplasmic vacuolization in cell death and survival. *Oncotarget* **2016**, *7*, 55863–55889.
(45) Guo, T.; Guan, R.; Zou, J.; Liu, J.; Ying, L.; Yang, W.; Wu, H.; Cao, Y. Red light-emitting hyperbranched fluorene-alt-carbazole copolymers with an iridium complex as the core. *Polym. Chem.* **2011**, *2*, 2193–2203.
(46) Nilsson, M. Tetrabutylammonium inorganocuprates(I) – $Bu_4N^+CuCl_2^-$, $CuBr_2^-$, CuI_2^- and $Cu(CN)_2^-$. *Acta Chem. Scand.* **1982**, *B36*, 125–126.
(47) Bennett, M. A.; Smith, A. K. Arene ruthenium(II) complexes formed by dehydrogenation of cyclohexadienes with ruthenium(III) trichloride. *J. Chem. Soc., Dalton Trans.* **1974**, 233–241.
(48) Kiel, W. A.; Ball, R. G.; Graham, W. A. G. Carbonyl-η-hexamethylbenzene complexes of osmium. Carbon-hydrogen activation by (η-C_6Me_6)Os(CO)$(H)_2$. *J. Organomet. Chem.* **1990**, *383*, 481–496.
(49) *SAINT-Plus and APEX2*; Bruker-Nonius AXS Inc.: Madison, WI, **2016**.
(50) Sheldrick, G. M. A short history of *SHELX*. *Acta Crystallogr.* **2008**, *A64*, 112–122.
(51) Burnett, M. N.; Johnson, G. K. *ORTEPIII. Report ORNL-6895*; OAK Ridge National Laboratory: Tennessee, **1996**.

Supporting Information
for

Redox-active organoruthenium(II)- and organoosmium(II)-copper(II) complexes, with an amidrazone-morpholine hybrid and $[Cu^{I}Cl_2]^-$ as counteranion, and their antiproliferative activity

Kateryna Ohui,[a,] Maria V. Babak,[b,c] Denisa Darvasiova,[d] Alexander Roller,[a] Daniel Vegh,[e] Peter Rapta,[d] Grace Rui Shi Guan,[f] Yi Hsuan Ou,[f] Giorgia Pastorin,[f] Vladimir B. Arion*,[a]

[a]*University of Vienna, Institute of Inorganic Chemistry, Währinger Strasse 42, A-1090 Vienna, Austria*

[b]*Department of Chemistry, National University of Singapore,3 Science Drive 2, 117543 Singapore*

[c]*Drug Development Unit, National University of Singapore,28 Medical Drive, 117546 Singapore*

[d]*Institute of Physical Chemistry and Chemical Physics, Slovak Technical University of Technology, Radlinského 9, 81237 Bratislava, Slovak Republic*

[e]*Institute of Organic Chemistry, Catalysis and Petrochemistry, Department of Organic Chemistry, Slovak Technical University of Technology, Radlinského 9, 81237 Bratislava, Slovak Republic*

[f]*Department of Pharmacy, National University of Singapore, Singapore*

Keywords: heterometallic complexes, amidrazones, organometallics, ruthenium(II)-copper(II), osmium(II)-copper(II), spectroelectrochemistry, antiproliferative activity, ROS

Content

Figure S11. Concentration-effect curves for HL^H, **1**–**3** and $CuCl_2$ in A2780, A2780cis and HeLa cells lines upon 72 h exposure.

Figure S12. EPR spectra of $^{\bullet}$DMPO-X spin-adducts (X is OR, R and O_2^-) measured in the **2**/DMSO/O_2/DMPO solution.

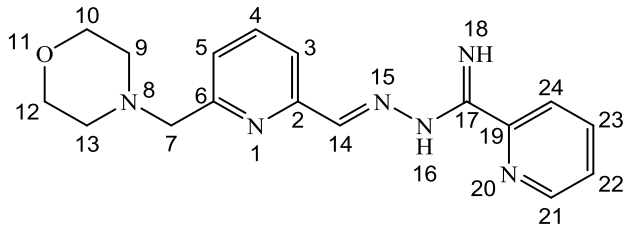

Chart S1. Atom numbering scheme for HL^H for ^1H and ^{13}C NMR data.

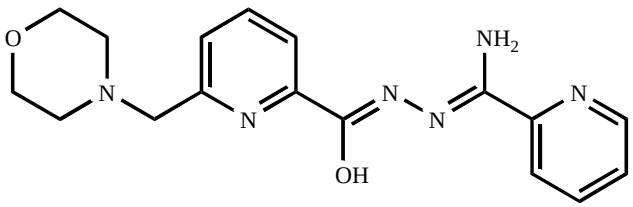

HL^1

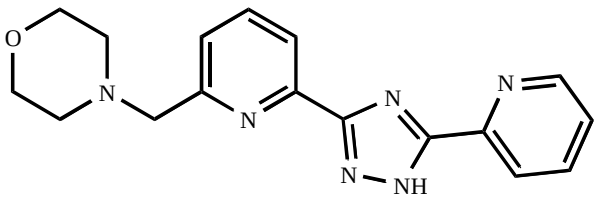

HL^2

Chart S2. Line drawings of the ligands from tetranuclear complex **4**.

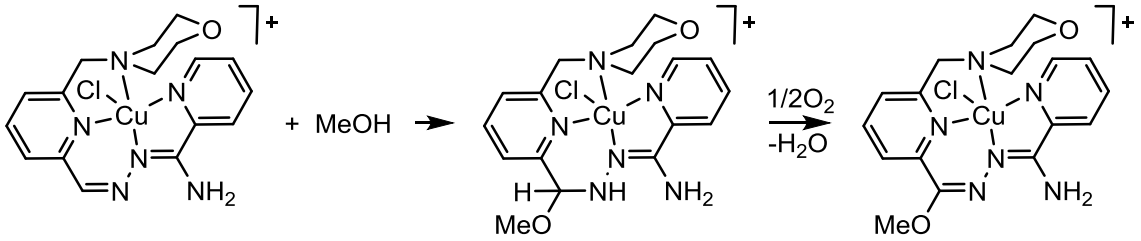

Scheme S1. Transformation of the coordinated ligand HL^{H} into HL^{OMe}.

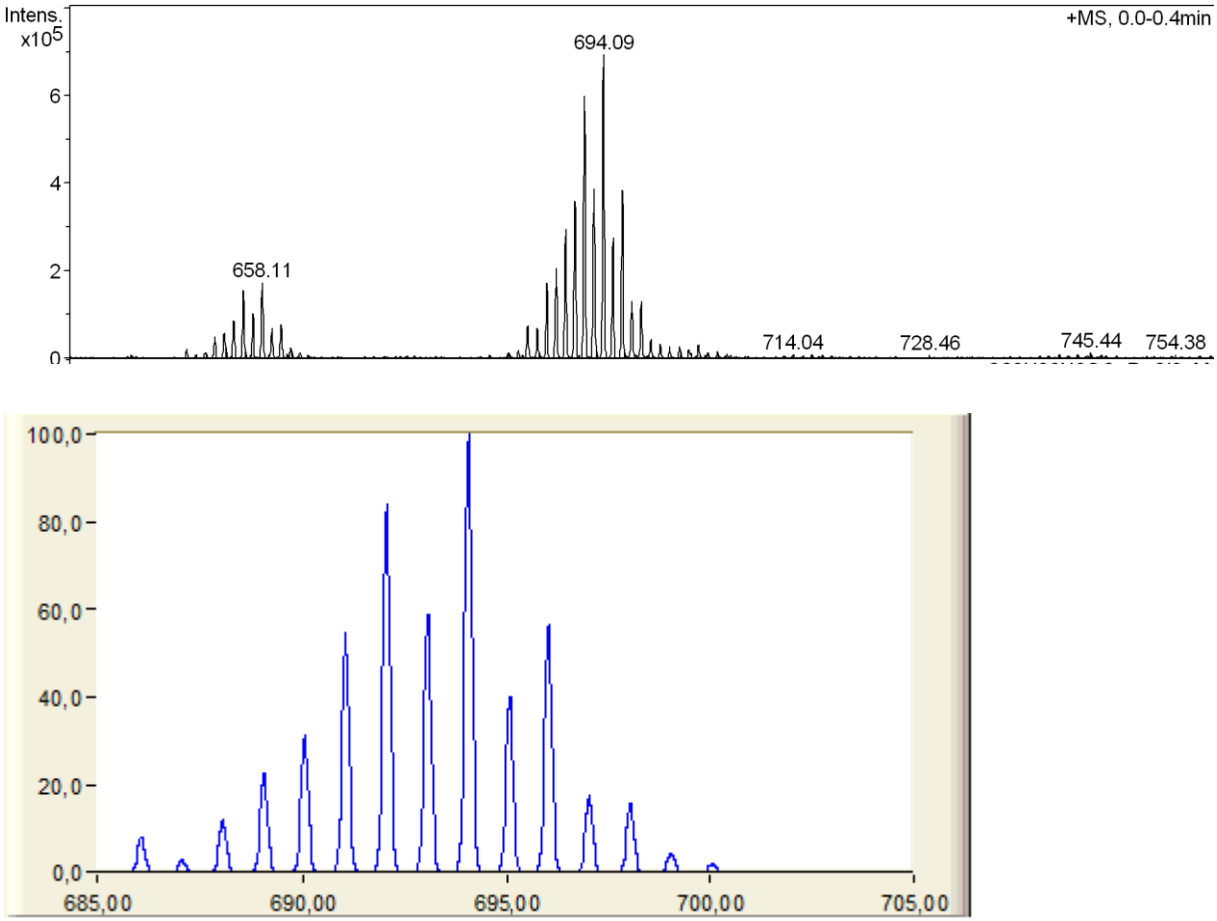

Figure S1. Experimental positive ESI mass spectrum (top) and the calculated isotopic pattern for the peak with *m*/*z* 694.06 (bottom) for $[Cu^{II}Ru^{II}(\eta^{6}\text{-}p\text{-cymene})Cl_2(L^{H})][Cu^{I}Cl_2]$ (**2**).

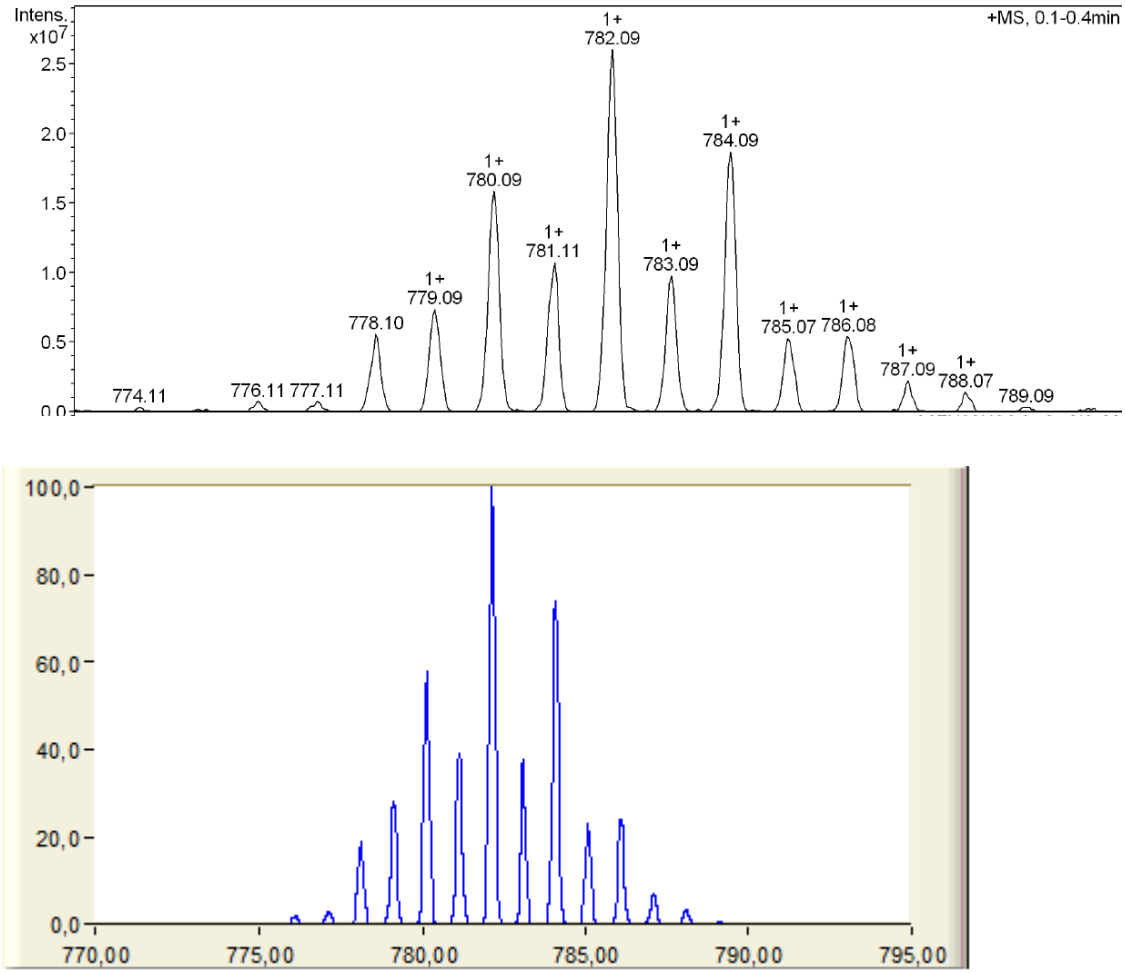

Figure S2. Experimental positive ESI mass spectrum (top) and the calculated isotopic pattern for the peak with *m*/*z* 782.10 (bottom) for $[Cu^{II}Os(\eta^6\text{-}p\text{-cymene})Cl_2(L^H)][Cu^ICl_2]$ (**3**).

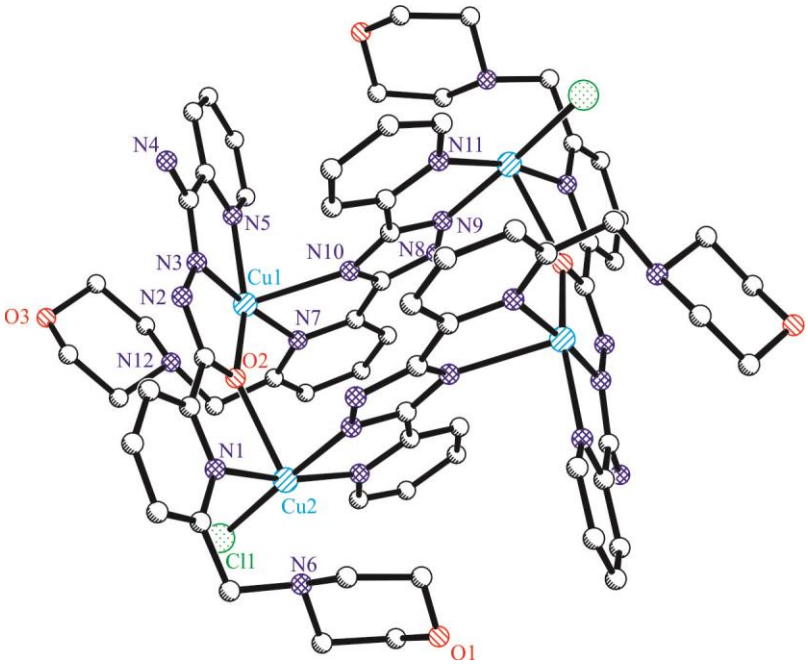

Figure S3. The structure of tetranuclear centrosymmetric complex $[Cu_4(L^1)_2(L^2)_2Cl_2]Cl_2$ (**4**). Selected bond distances (Å), and bond angles (deg) in the complex cation: Cu1–N3 1.912(4), Cu1–N5 2.104(4), Cu1–N7 1.996(4), Cu1–N10 2.378(4), Cu1–O2 2.034(3), Cu2–N1 2.005(4), Cu2–N11 2.061(4), Cu2–N9 1.993(4), Cu2–O2 2.378(3); Cu2–Cl1 2.2736(12), N3–Cu1–N5 78.84(16).

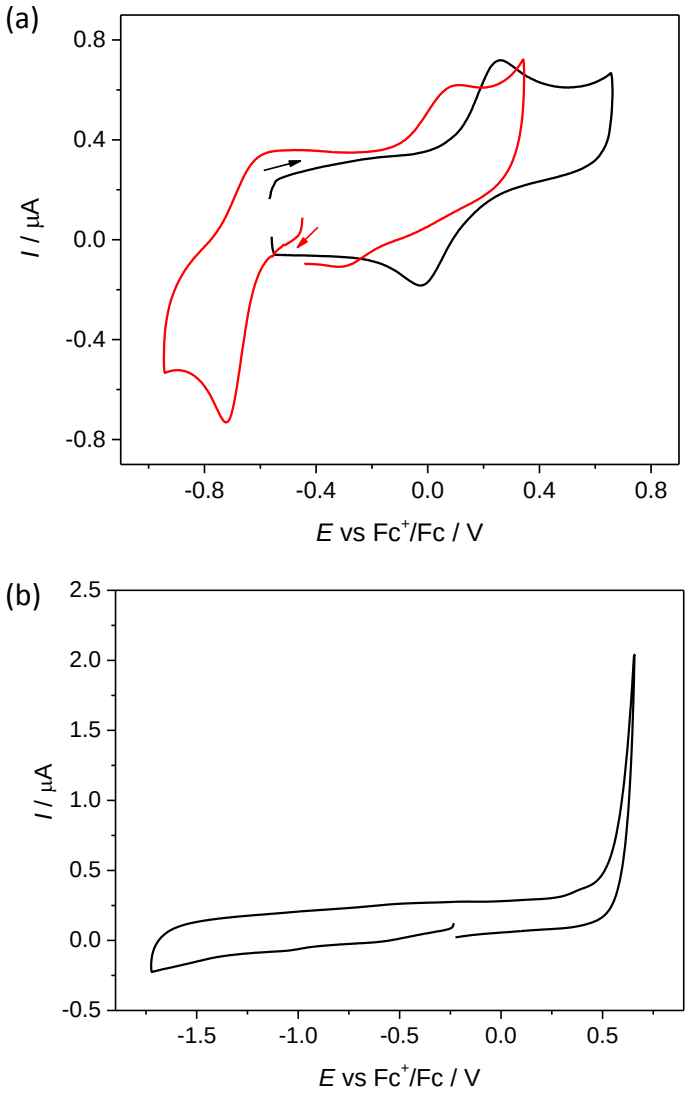

Figure S4. (a) Cyclic voltammograms of heterodinuclear complex **3** (red trace) and *n*-$Bu_4N[CuCl_2]$ salt (black trace) in DMSO/*n*-Bu_4NPF_6 at glassy-carbon working electrode at scan rate of 100 mV s^{-1}. (b) Cyclic voltammogram of proligand HL^H in DMSO/*n*-Bu_4NPF_6 at glassy-carbon working electrode at a scan rate of 100 mV s^{-1}.

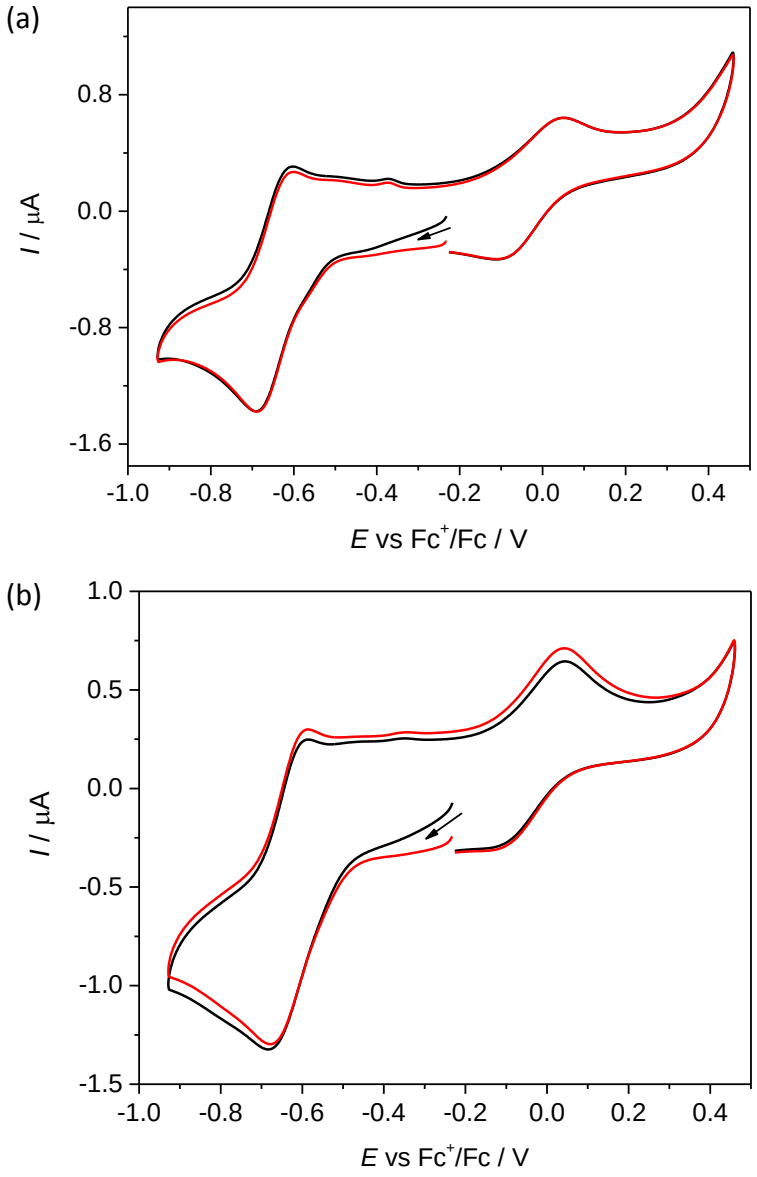

Figure S5. Cyclic voltammograms of heterodinuclear complexes (a) **2** and (b) **3** in methanol/*n*-Bu_4NPF_6 at glassy-carbon working electrode at scan rate of 100 mV s^{-1} (black traces represent the first scan, while red traces the second scan).

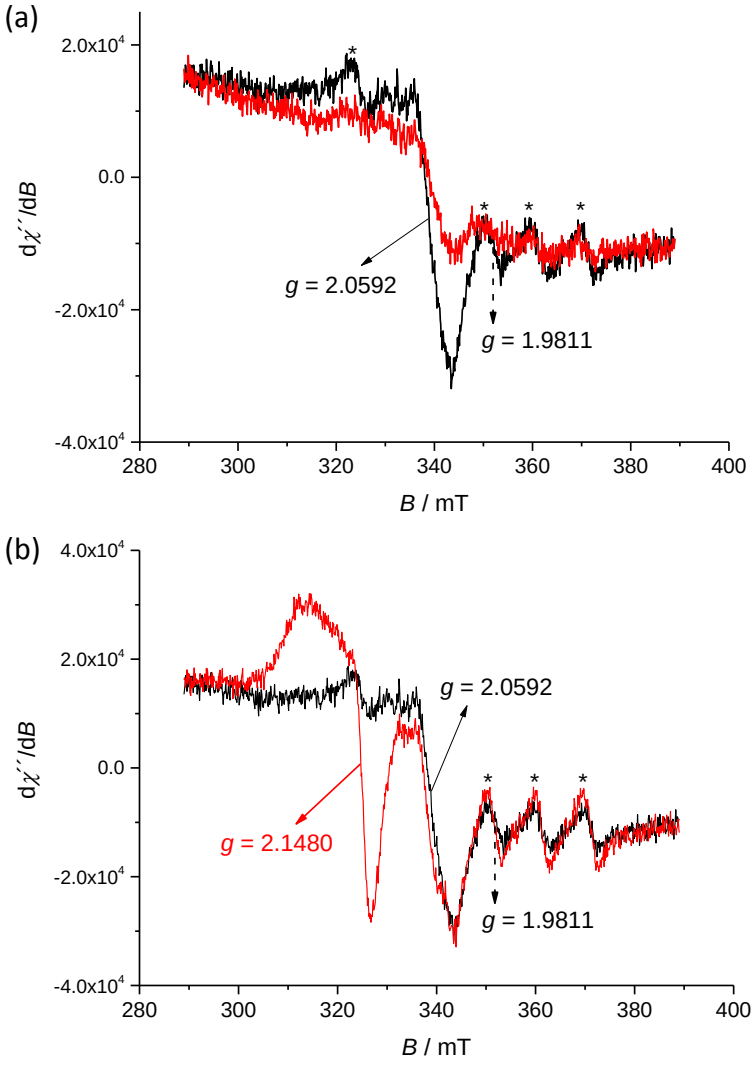

Figure S6. (a) EPR spectra for **2** (black trace) and partially 1-electron reduced $[Cu^{II}Ru^{II}(\eta^6\text{-}p\text{-cymene})Cl_2(L^H)][Cu^ICl_2]$ (red trace) in DMSO/*n*-Bu_4NPF_6 at room temperature; (b) EPR spectra for **2** (black trace) and 1-electron-oxidised $[Cu^{II}Ru^{II}(\eta^6\text{-}p\text{-cymene})Cl_2(L^H)][Cu^ICl_2]$ (red line) in DMSO/*n*-Bu_4NPF_6 at room temperature (*internal Mn(II) standard for g-value determination).

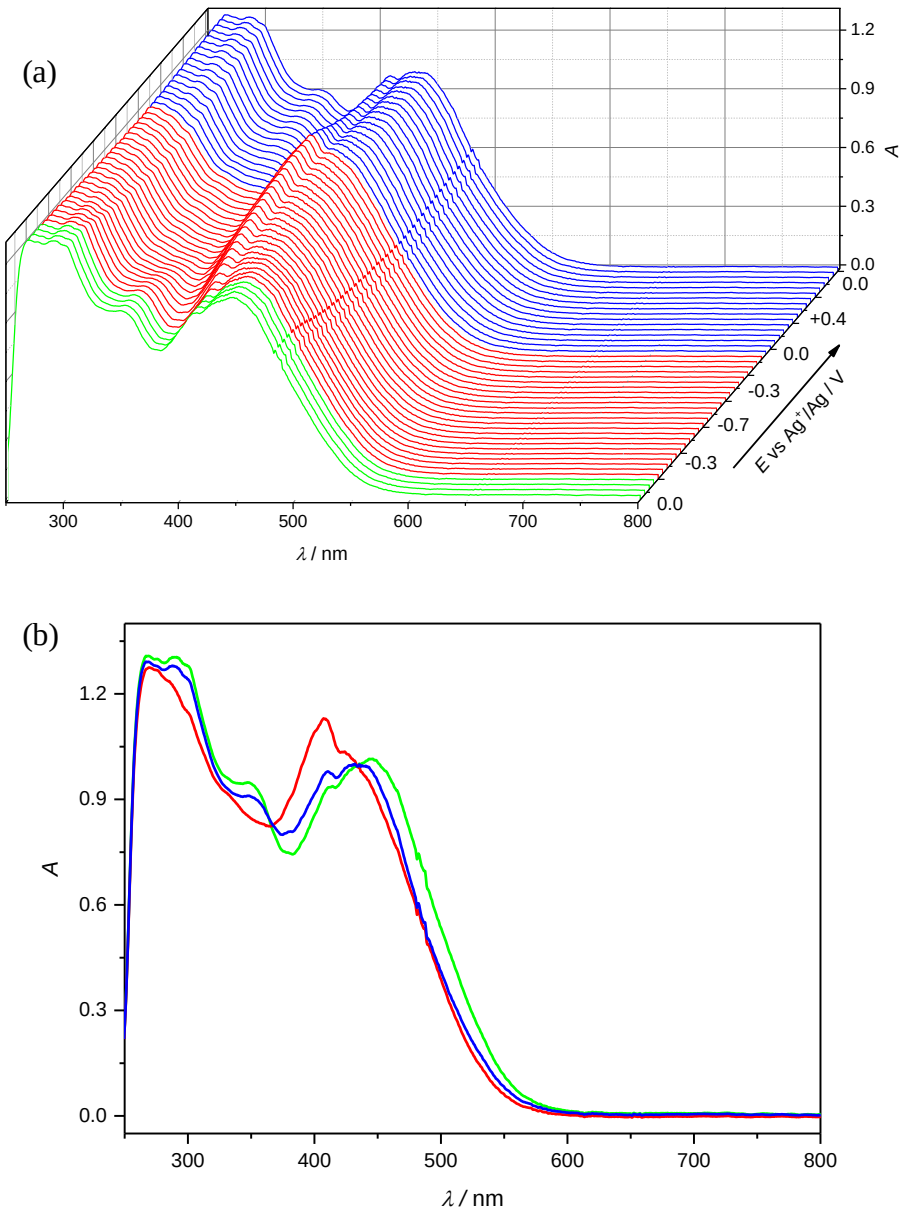

Figure S7. *In situ* UV-vis-NIR spectroelectrochemistry for **2** in DMSO/*n*-Bu_4NPF_6 (scan rate of 10 mV s^{-1}, Pt-microstructured honeycomb working electrode): (a) UV-vis-NIR spectra detected simultaneously upon the cyclic voltammetric scan; (b) UV-vis-NIR spectrum of **2** (green trace), UV-vis-NIR spectra detected after *in situ* reduction of **2** (red trace) and after back reoxidation (blue trace).

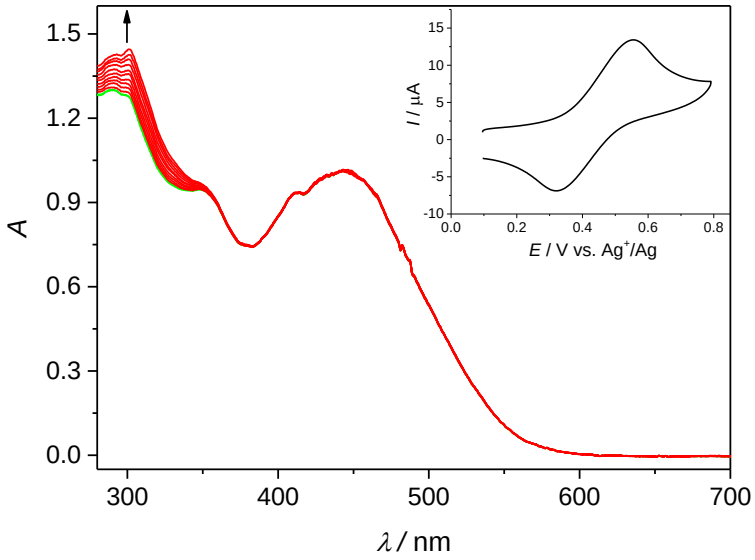

Figure S8. *In situ* optical spectroelectrochemistry **2** in DMSO/*n*-Bu_4NPF_6 (scan rate of 10 mV s^{-1}, Pt-microstructured honeycomb working electrode): UV-vis-NIR spectra recorded simultaneously upon the *in situ* oxidation in the region of the first anodic peak (inset: the corresponding cyclic voltammogram).

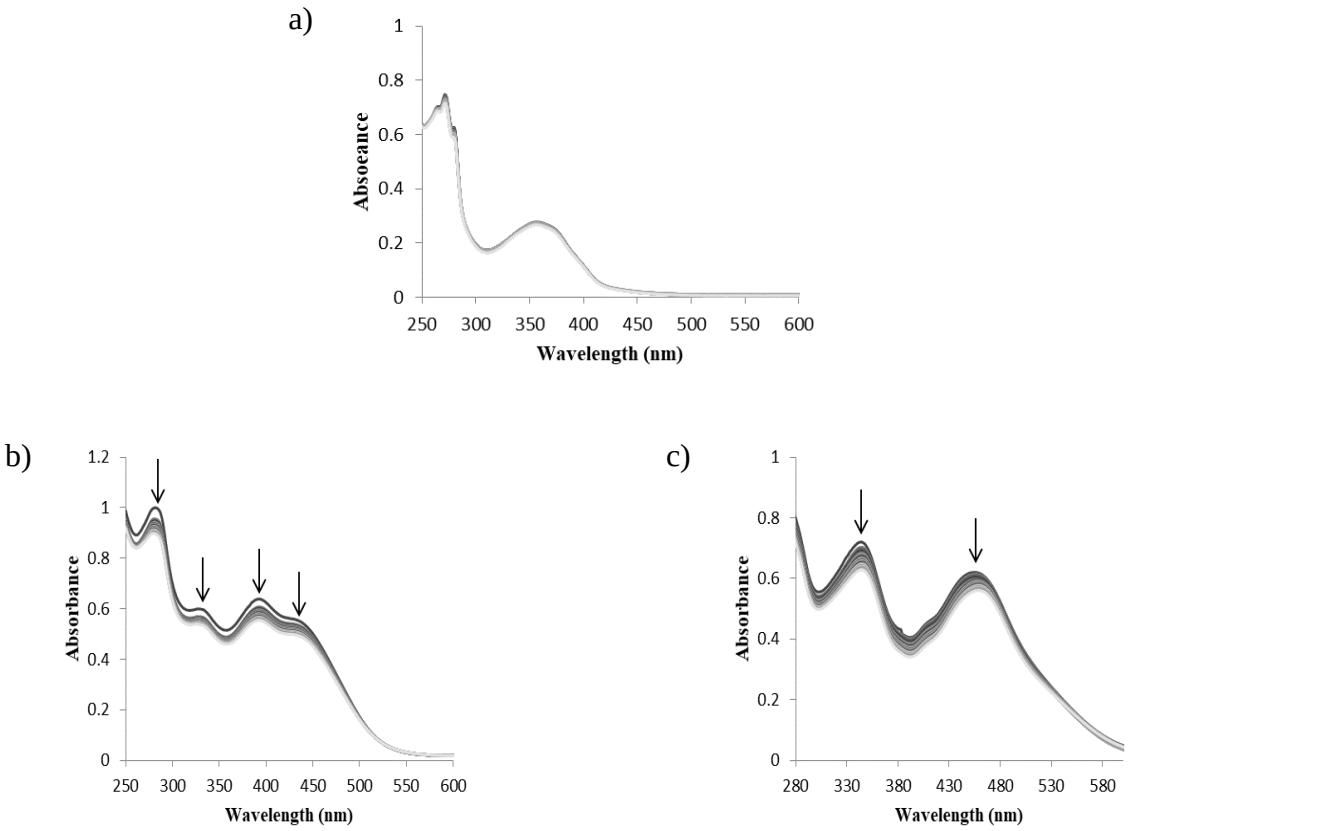

Figure S9. Absorption spectra of **1** (a), **2** (b) and **3** (c) in water measured over 24 h by UV–vis spectrophotometry.

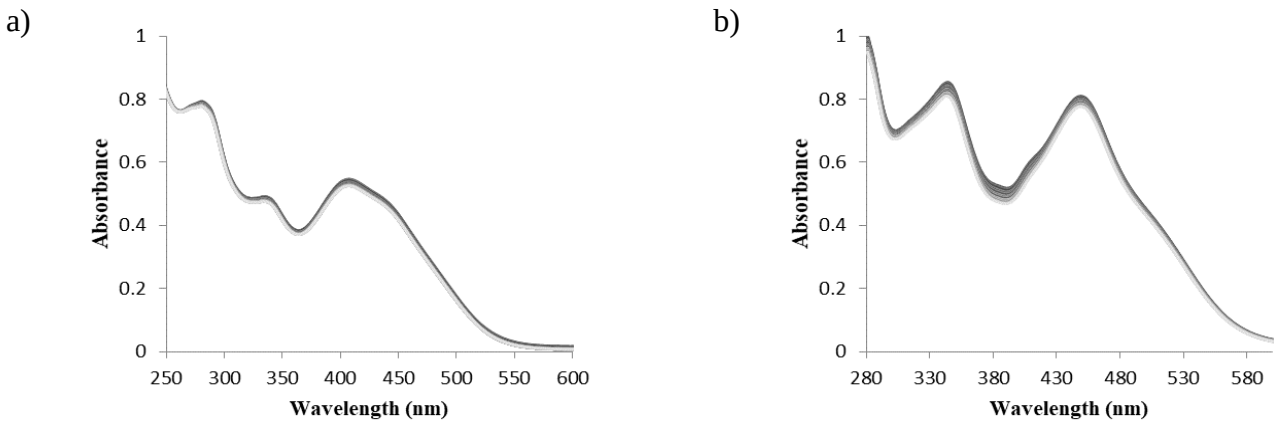

Figure S10. Absorption spectra of **2** (a) and **3** (b) in the presence of 24 μM NaCl in water measured over 24 h by UV–vis spectrophotometry.

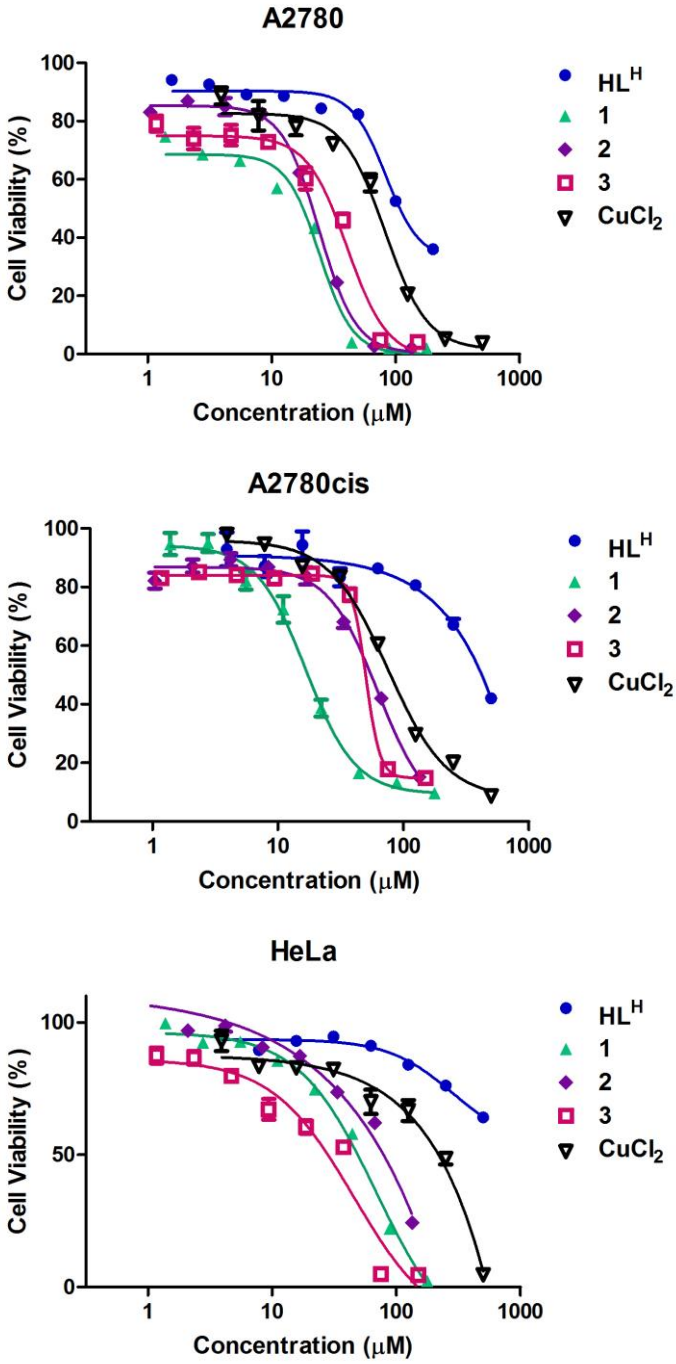

Figure S11. Concentration-effect curves for HL^H, **1**–**3** and $CuCl_2$ in A2780, A2780cis and HeLa cells lines upon 72 h exposure.

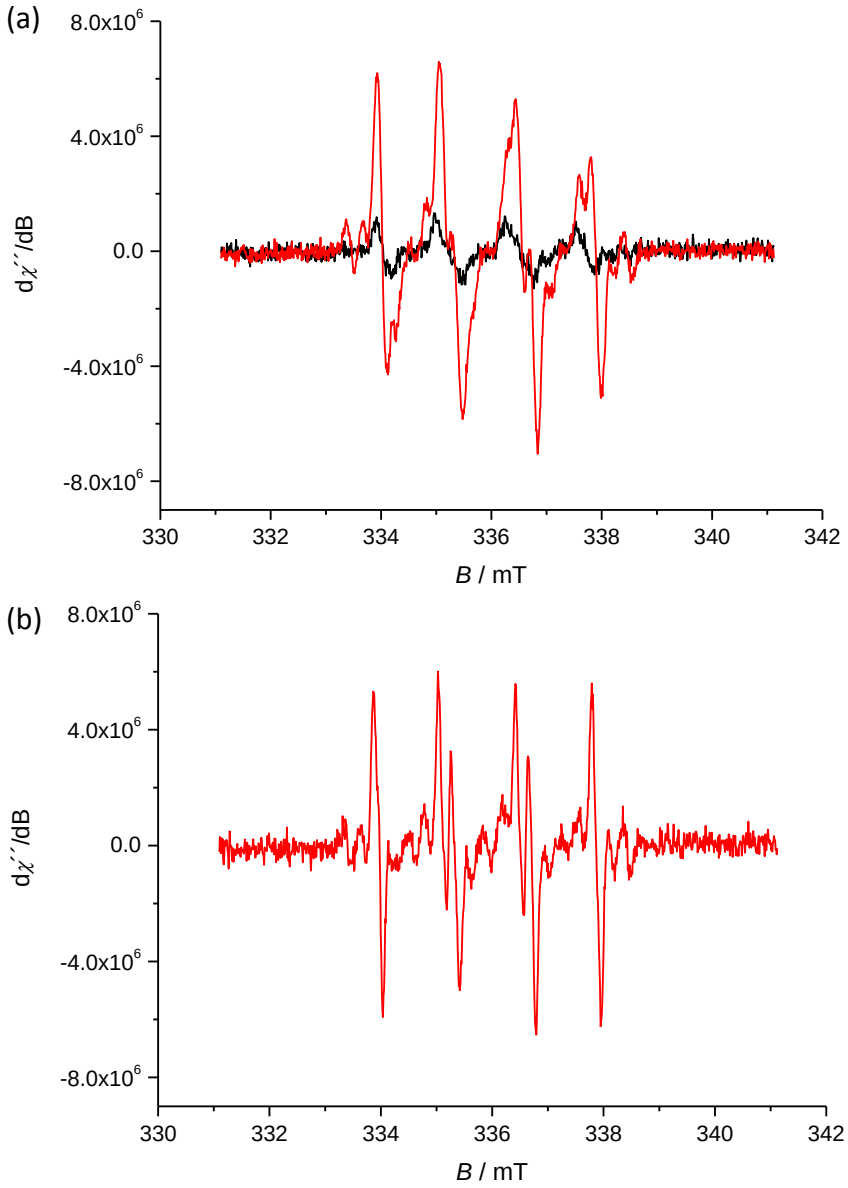

Figure S12. (a) EPR spectra of DMPO spin-adducts measured in the **2**/DMSO/O_2/DMPO solution (red line) and reference DMSO/O_2/DMPO solution (black line) at 298 K. Initial concentrations: c_0(**2**) = 0.3 mM, c_0(DMPO) = 0.04 M; (b) EPR spectra of DMPO spin-adducts measured in the **2**/DMSO/O_2/DMPO system after bubbling the final solution with argon (red line) at 298 K. c_0(**2**) = 0.3 mM, c_0(DMPO) = 0.04 M.

New Triapine Derivatives and their Metal Complexes as Anticancer Agents

Kateryna Ohui,[a,] Maria V. Babak,[b,c] Denisa Darvasiova,[d] Gerald Giester,[e] Daniel Vegh,[f] Peter Rapta,[d] Wee Han Ang,[b,c] Giorgia Pastorin,[g] Vladimir B. Arion*,[a]

[a]*University of Vienna, Institute of Inorganic Chemistry, Währinger Strasse 42, A-1090 Vienna, Austria*

[b]*Department of Chemistry, National University of Singapore,3 Science Drive 2, 117543 Singapore*

[c]*Drug Development Unit, National University of Singapore,28 Medical Drive, 117546 Singapore*

[d]*Institute of Physical Chemistry and Chemical Physics, Slovak Technical University of Technology, Radlinského 9, 81237 Bratislava, Slovak Republic*

[e]*University of Vienna, Department of Mineralogy and Crystallography, Althan Strasse 14, A-1090 Vienna, Austria*

[e]*Institute of Organic Chemistry, Catalysis and Petrochemistry, Department of Organic Chemistry, Slovak Technical University of Technology, Radlinského 9, 81237 Bratislava, Slovak Republic*

[f]*Department of Pharmacy, National University of Singapore, Singapore*

Abstract. Two new proligands **HL^1** and **HL^2** have been prepared by condensation reactions of 2-pyridinamidrazone and S-methylisothiosemicarbazidium iodide with 3-amino-pyridine-2-carboxaldehyde. By reactions of **HL^1·HCl** and **HL^2** with $CuCl_2 \cdot 2H_2O$ in 1:1 mol ratio in methanol the complexes $[Cu^{II}Cl_2(\mathbf{HL^1})]$ (**1**) and $[Cu^{II}Cl_2(\mathbf{HL^2})]$ (**2**) were prepared. The reaction of **HL^2** with $Fe(NO_3)_3 \cdot 9H_2O$ in 2:1 mol ratio in the presence of triethylamine afforded the complex $[Fe^{III}(\mathbf{L^2})_2](NO_3)_3$ (**3**), the reaction of **HL^2** with $ZnCl_2$ the complex $[Zn^{II}Cl_3(\mathbf{H_2L^2})]$ (**4**). The structures of **HL^2** and metal complexes **1**, **2** and **4** were established by X-ray diffraction. Complexes **1** and **2** demonstrated irreversible reduction of Cu(II) ion with the subsequent ligand release, while **3** an almost reversible electrochemical reduction. These observations were also confirmed by UV–Vis and EPR spectroelectrochemical measurements. Complexes **1**–**3** were tested against cisplatin-sensitive and cisplatin-resistant ovarian carcinoma cells and demonstrated significant antiproliferative activity in comparison to proligands.

Keywords: Triapine, amidrazones, isothiosemicarbazones, copper(II), iron(III), zinc(II), spectroelectrochemistry, antiproliferative activity.

Introduction

α-*N*-heterocyclic thiosemicarbazones (TSCs) attract considerable attention since their remarkable antiproliferative properties have been discovered.[1] The most promising representative of this group of compounds is 3-aminopyridine-2-carboxaldehydethiosemicarbazone or Triapine, (3-AP), which has already entered more than 30 phase I and II clinical trials.[2-4] 3-AP was also tested in various combination regiments and was shown to enhance the activity of other anticancer drugs, such as cisplatin,[2,5] gemcitabine,[6] doxorubicin,[7] irinotecan,[4] as well as radiotherapy.[8, 9] It is believed that mode of action of 3-AP is based on the effective inhibition of ribonucleotide reductase (RNR)[10-12] as a result of Fe(III) chelation from diferric-tyrosyl cofactor, followed by the generation of deadly ROS.[13] However, despite promising anticancer effects *in vitro* and *in vivo*, the use of 3-AP in patients is associated with side-effects like neutropenia,[14] methenoglobinemia,[15] nausea, vomiting etc. Additionally, several types of solid tumors demonstrated resistance to 3-AP treatment.[14, 16-18] Since TSCs are known to efficiently chelate first row transition metals, 3-AP and its analogues were coordinated to endogenous metals, such as Cu and Fe.[19-22] TSC coordination to endogenous metals decreased overall toxicity of the drug molecules[23] and increased their activity due to the synergistic action of TSCs and a metal center.[21-23] In general, Cu(II) complexes of thiosemicarbazones were characterized by better anticancer activity than their proligands;[24] whereas complexation to Fe(III) did not always result in the improvement of cytotoxicity.[19,25] Interestingly, both Cu(II) and Fe(III) complexes of 3-AP were less active that 3-AP itself.[12,19]

Carboxamidrazones structurally resemble thiosemicarbazones, but surprisingly their anticancer effects are not very widely studied. These compounds demonstrated antiproliferative activity in a micromolar range and good selectivity to cancer cells over healthy cells.[26-27] Similarly to Cu(II)-TSC complexes, coordination of carboxamidrazones to a Cu(II) center resulted in an improvement of cytotoxicity; however, there are very few examples of reported Cu(II)-carboxamidrazone complexes.[28-30] Therefore, we have prepared novel carboxamidrazones with S-methyl and pyridine substituents, structurally related to 3-AP, as well as their Cu(II) and Fe(III) complexes and investigated their

potential as anticancer drugs. All compounds were fully characterized by analytical and spectroscopic methods and their electrochemical properties were determined by cyclic voltammetry and UV-Vis-NIR spectroelectrochemistry. The anticancer activity of novel compounds was studied in two ovarian cancer cell lines (A2780 and A2780cis), as well as a non-cancerous embryonic kidney cell line (HEK293). Additionally, their intracellular dose-dependent accumulation has been investigated.

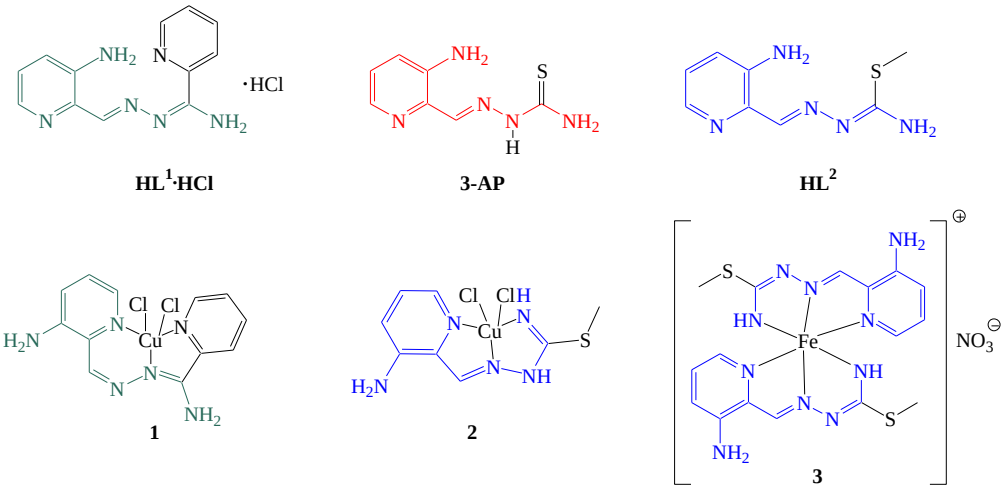

Chart 1. Line drawings of 3-AP, carboxamidrazone proligands (**HL^1, HL^2**) and complexes (**1-3**) reported in this work.

Synthesis and characterization of the HL^1, HL^2, copper(II) complexes 1 and 2 and iron(III) complex 3. HL^1 was obtained by the reaction of 3-N-(*tert*-butyloxycarbonyl)amino-2-pyridinecarboxaldehyde with 2-pyridinamidrazone and hydrochloric acid in 1:1:1 mole ratio in ethanol in 60% yield. The ESI mass spectrum recorded in positive ion mode showed a peak with *m*/*z* 241 attributed to $[L+H]^+$. The ^{1}H NMR spectrum was in agreement with the suggested structure for two tautomeric forms of the **HL^1**. The reaction of the latter with $CuCl_2 \cdot 2H_2O$ in methanol in 1:1 mole ratio afforded a brown solid of **1** that was removed by filtration and purified on preparative HPLC. Slow diffusion of diethyl ether into the solution of the crude product redissolved in methanol afforded brown crystals. The positive ESI mass spectrum showed peaks with *m*/*z* 338 and 303 which could be assigned to $[Cu^{+1}(\mathbf{HL^1})Cl]^+$ and $[Cu(\mathbf{HL^1})]^+$ respectively.

HL^2 was synthesized via a reaction of 3-N-(*tert*-butyloxycarbonyl)amino-2-pyridinecarboxaldehyde with S-methylisothiosemicarbazide hydrochloride and hydrochloric acid in 1:1:0.85 mole ratio in the presence of sodium bicarbonate in water in

67% yield. Slow evaporation of the **HL^2** in ethanol/water (3:1) afforded yellow crystals. The ESI mass spectrum recorded in positive ion mode showed a peak with *m*/*z* 210 attributed to $[L+H]^+$. The ^{1}H NMR spectrum was in agreement with the structure for **HL^2**. The reaction of the proligand with $CuCl_2 \cdot 2H_2O$ in methanol in 1:1 mole ratio afforded dark-green crystals of **2**. The positive ESI mass spectrum showed peaks with *m*/*z* 271 and 307 which could be assigned to $[Cu^{+1}(\mathbf{HL^2})]^+$ and $[Cu(\mathbf{HL^2})Cl]^+$ respectively. Black precipitate of **3** was synthesized by the reaction of **HL^2** with $Fe(NO_3)_3 \cdot 9H_2O$ and triethylamine in 2:1:2 mole ratio in methanol. The positive ESI mass spectrum showed peak with *m/z* 472 which could be assigned to $([Fe(\mathbf{L^2})_2]^+$.

X-ray crystallography. The results of X-ray diffraction studies of **HL^2**, $[Cu(\mathbf{HL^1})Cl_2]$ (**1**), $[Cu(\mathbf{HL^2})Cl_2]$ (**2**) and $Zn(\mathbf{H_2L^2})Cl_3$ (**4**) are shown in Figures 1 and S1, respectively. The proligand **HL^2** and complex 1 crystallized in the monoclinic space group $P2_1/c$, while complexes **2** and **4** in the triclinic centrosymmetric space group *P*-1.

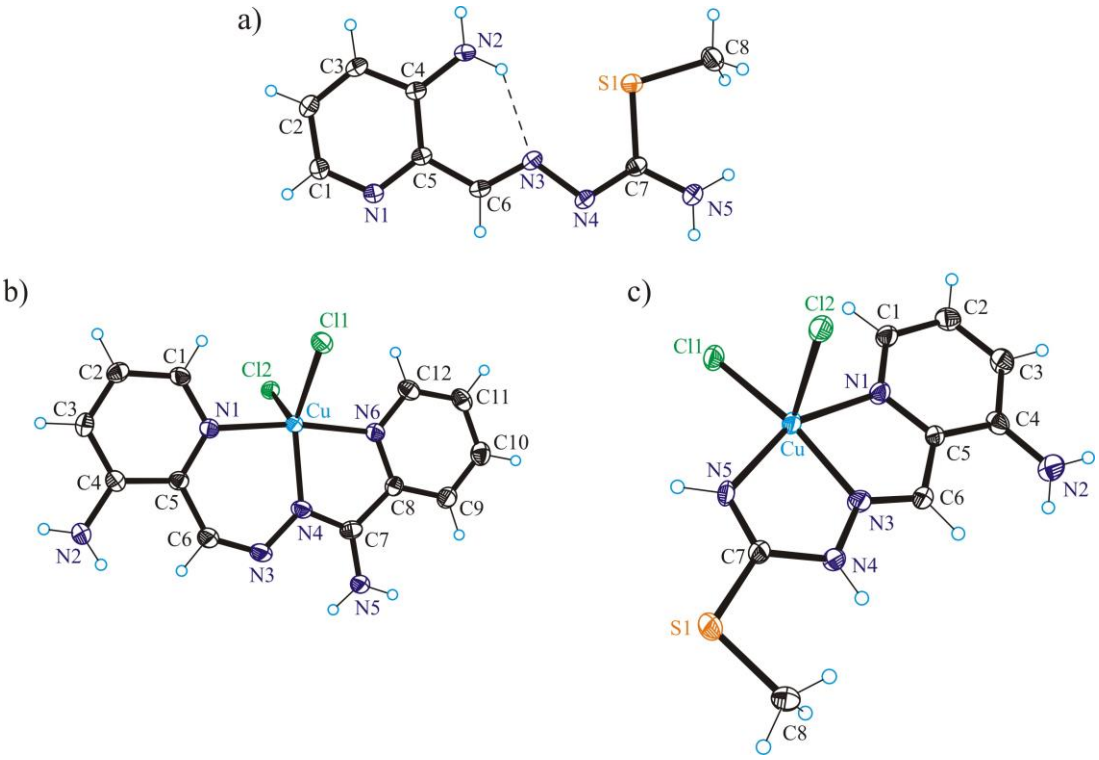

Figure 1. ORTEP views of **HL^2**, (a) $Cu(\mathbf{HL^1})Cl_2$ (**1**) and (b) $Cu(\mathbf{HL^2})Cl_2$ (**2**). Selected bond distances (Å) and bond/torsion angles (deg) in **HL^2**: C4–N2 1.3514(15), C6–N3 1.2828(14), N3–N4 1.3970(12), N4–C7 1.3044(14), C7–N5 1.3471(14), C7–S 1.7643(11), S1–C8 1.8043(12); C1–N1–C5–C6 –179.31(10), N3–N4–C7–N5 –174.898(10); in **1**: Cu–N1 1.997(2), Cu–N4 1.973(2), Cu–N6 2.006(2), Cu–Cl1 2.3255(7), Cu–Cl2 2.5190(6), C6–N3 1.278(4), N3–N4 1.372(3), N4–C7 1.330(3), C7–N5 1.321(3); N1–Cu–N4 91.52(8), N4–Cu–N6 80.12(8), N4–Cu–Cl1 136.54(7), N4–Cu–Cl2 111.58(6); in **2**: Cu–N1 2.063(5), Cu–N3 1.960(5), Cu–

N5 1.990(4), Cu–Cl1 2.2370(17), Cu–Cl2 2.5517(17), C6–N3 1.281(7), N3–N4 1.369(6), N4–C7 1.370(7), C7–N5 1.300(7); C7–S1 1.747(5), S1–C8 1.804(6), N1–Cu–N3 78.50(19), N3–Cu–N5 78.13(19), N3–Cu–Cl1 162.08(17), N3–Cu–Cl2 100.07(16), C1–N1–C5–C6 175.7(5), N3–N4–C7–N5 0.8(8).

Both ligands in **1** and **2** act as neutral tridentate. **HL^1** forms one seven-membered and one five-membered chelate ring upon coordination to copper(II), while **HL^2** two five-membered chelate rings. The coordination polyhedron around Cu(II) in **1** is closer to trigonal-bipyramidal than to square-pyramidal (τ_5 = 0.58). The same distorted coordination geometry was reported previously for a closely related complex [Cu(appc)Cl_2] (appc = 2-acetylpyridine-pyridine-2-carboxamidrazone), in which the coordination geometry of CuN_3Cl_2 is also better described as trigonal bipyramidal (τ_5 = 0.58).[31] The coordination geometry of copper(II) in **2** is very close to square-pyramidal (τ_5 = 0.11)[32] with the ligand bound to Cu(II) via nitrogen atoms N1, N4 and N6 and chloride co-ligand Cl1 in the basal plane and another chloride co-ligand in apical position. The tridentate ligand **HL^2** is bound to Cu(II) via nitrogen atoms N1, N3 and N5. The coordination geometry is further completed by two chloride co-ligands Cl1 and Cl2. The configuration adopted by the ligand in **2** differs considerably from that adopted by proligand **HL^2**. A two-fold rotation around C5–N6 bond and another around N4–C7 in **HL^2** are required to adopt the configuration of the ligand in **2**. As in other copper(II) complexes with tridentate isothiosemicarbazones[33] the thiomethyl group is not involved in coordination to the central metal atom. In complex **4** the protonated ligand is bound to zinc(II) via nitrogen atom N2 in unprecedented monodentate fashion.[33] The tetrahedral coordination geometry is completed by three chloride co-ligands as shown in Figure S1.

Anticancer Activity and Intracellular Accumulation

All novel complexes were tested against two cancer cell lines – ovarian carcinoma A2780 and its cisplatin-resistant analogue A2780cis, as well as noncancerous human embryonic kidney cell line HEK293 (Table 1). Their cytotoxicity was compared to the cytotoxicity of Triapine and cisplatin and is represented by IC_{50} values. The differences in the cytotoxicity between cisplatin-sensitive and cisplatin-resistant cell lines are represented by resistance factors (RF). The selectivity to cancer cells over healthy non-cancerous cells is represented by selectivity factor (SF).

Table 1. Cytotoxicity of proligands **HL^1** and **HL^2**, Cu(II) complexes **1** and **2**, and Fe(III) complex **3**.

Compound	IC_{50} [μM][a]					Cellular accumulation[d], nmol Cu/mg protein
	A2780	**A2780cis**	**RF**[b]	**HEK293**	**SF**[c]	**A2780**
HL[1]	242 ± 84	221 ± 79	0.9	253 ± 39	1.0	-
HL[2]	202 ± 49	211 ± 8	1.0	187 ± 24	0.9	-
1	17 ± 2	15 ± 3	0.9	28 ± 2	1.6	1.1 ± 0.3
2	1.4 ± 0.2	0.92 ± 0.11	0.7	1.5 ± 0.2	1.1	0.76 ± 0.17
3	41 ± 12	36 ± 8	0.9	48 ± 9	1.2	-
Triapine[e]	0.67 ± 0.22	1.1 ± 0.1	1.6	0.39 ± 0.05	0.6	-
Cisplatin[e]	0.44 ± 0.13	4.6 ± 0.3	10.5	n.d.[f]	-	-

[a] 50% inhibitory concentrations (IC_{50}) in human ovarian carcinoma cell lines A2780 and A2780cisR and human embryonic kidney cell line HEK293, determined by means of the MTT assay after 72 h exposure. Values are means ± standard error of mean obtained from at least three independent experiments, [b]Resistance Factor (RF) is determined as $IC_{50\ (A2780cisR)}/IC_{50\ (A2780)}$, [c] Selectivity Factor (SF) is determined as $IC_{50\ (HEK293)}/IC_{50\ (A2780)}$, [d]Cellular accumulation in A2780 cells, determined by Inductively Coupled Plasma Mass Spectrometry (ICP−MS) after 24 h exposure at concentrations, corresponding to their IC_{50} values. Values are means ± SEMs obtained from at least three independent experiments.[e] The IC_{50} values (exposure for 72 h) were taken from the ref 23, [f] n.d. – not determined.

As can be seen from Table 1, carboxamidrazone proligands were only marginally cytotoxic and their coordination to metal centers (Cu(II) or Fe(III)) resulted in the significant improvement of cytotoxicity (14- and 144-fold change for Cu(II) complexes **1** and **2**, respectively, and nearly 5-fold change for Fe(III) complex **3**). Complex **3** was markedly less toxic than complex **2**, possibly due to its lower reactivity in the biological media. Notably, complex **2** was more active than Triapine and cisplatin in cisplatin-resistant A2780cis cell line. In general, all compounds were similarly cytotoxic in both A2780 and A2780cis cells, which is reflected by their low RFs. Unfortunately, these compounds also denstrated comparable toxicity in noncancerous HEK293 cells.

In order to draw the correlations between the cytotoxicity of Cu(II) complexes **1** and **2** and their accumulation in cancer cells, the intracellular Cu content in drug-treated A2780 cells was measured by ICP-MS (Table 1 and Figure 2). Cancer cells were treated with increasing concentrations of complexes **1** and **2** in relation to their IC_{50} values and it was demonstrated that intracellular accumulation of Cu was concentration-dependent. Interestingly, even though the cytotoxicity of complex **1** was about 10 times lower than that of complex **2**, their intracellular Cu content was not significantly different ($p > 0.05$). This result indicates that the differences in the cytotoxicity of Cu(II) complexes are not related to their intracellular content, but rather subsequent reactivity with biomolecular targets.

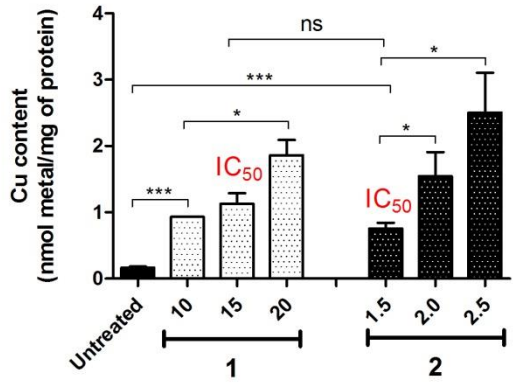

Figure 2. Intracellular Cu accumulation in A2780 cells. A2780 cells were treated with Cu(II) complexes **1** and **2** at 37 °C for 24 h at indicated concentrations and Cu content was measured by ICP-MS. Statistical analysis was performed by two-tailed T-test using GraphPad Prism software (GraphPad Software Inc., CA) with $p < 0.05$ considered as significant (*$p < 0.05$, ***$p < 0.001$).

Electrochemistry

To investigate the redox properties of **1**–**3**, the detailed electrochemical studies were performed using cyclic voltammetry, as well as UV–vis–spectroelectrochemistry. The cyclic voltammogram of **1** in DMSO/*n*-Bu_4NPF_6 at Pt working electrode shows one irreversible reduction peak with cathodic peak potential $E_{pc} = –0.76$ V *vs.* Fc^+/Fc^0 (Figure 3a). The first irreversible reduction step can be attributed to the Cu(II) → Cu(I) process. Consequently, we can propose that the unstable Cu(I)L complex decomposes with ligand release. For complex **2** even more complicated redox behaviour was observed with two irreversible cathodic waves at $E_{pc}^1 = –0.67$ V and $E_{pc}^2 = –1.05$ V *vs.* Fc^+/Fc^0 (Figure 3b). Similarly, as was observed for **1** the complex **2** decomposes upon reduction. On the other hand, ferric complex **3** based on the same proligand as for **2** exhibits different redox behavior with almost reversible electrochemical reduction with the first reduction event at half wave potential of –0.81 V *vs*. Fc^+/Fc. (Figure 3c).

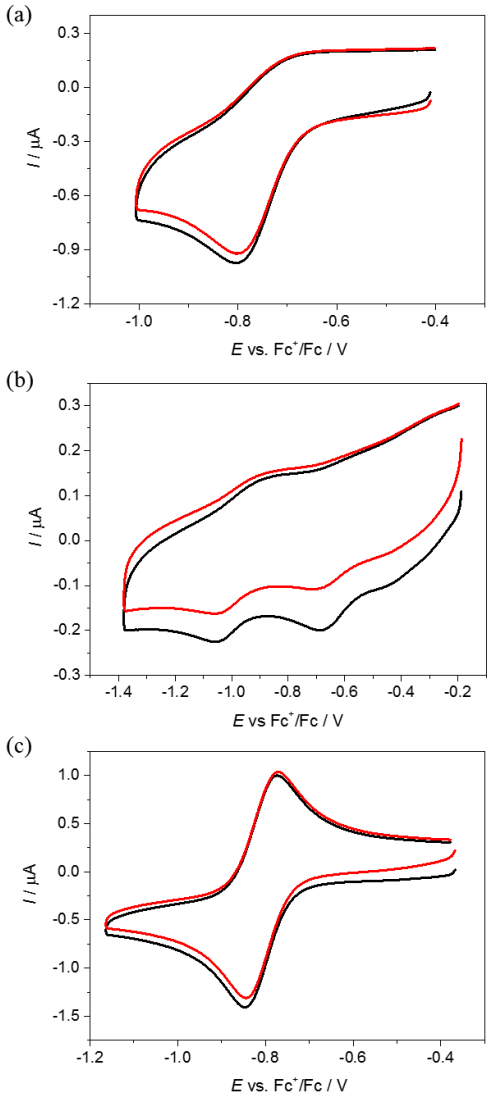

Figure 3. Cyclic voltammograms of 0.5mM (a) **1**, (b) **2** and (c) **3** in DMSO/*n*-Bu_4NPF_6 at scan rate of 100 mV s^{-1} (black traces represent the first scan, while red traces the second scan).

To check the chemical reversibility of the first reduction step for investigated samples, the *in situ* spectroelectrochemical UV-vis-NIR and cyclic voltammetric experiments were carried out under an argon atmosphere in a special thin layer spectroelectrochemical cell with a microstructured honeycomb working electrode. The UV-Vis spectra measured during cathodic reduction of **2** revealed that in the region of the first reduction peak a new optical band at 373 nm emerges. In addition, a decrease of the intensity of the bands at 284 nm and 448 nm is observed (Figure 4a). However, upon scan reversal the product that is formed upon reduction (Cu(II) to Cu(I)) is not reoxidised back to the initial state (Figure 4b). This unambiguously confirms that Cu(I) state is not stable and the complex decomposes with the ligand (or part of the ligand) release. We propose that such released

ligands may act as Fe chelators and inhibit the RNR enzyme, which is highly expressed in cancer cells, and is essential for their DNA synthesis.[34] In addition, the presence of the Cu(II) ion in the cells may lead to the production of ROS *in vivo* because of Cu(II)/Cu(I) redox cycling.

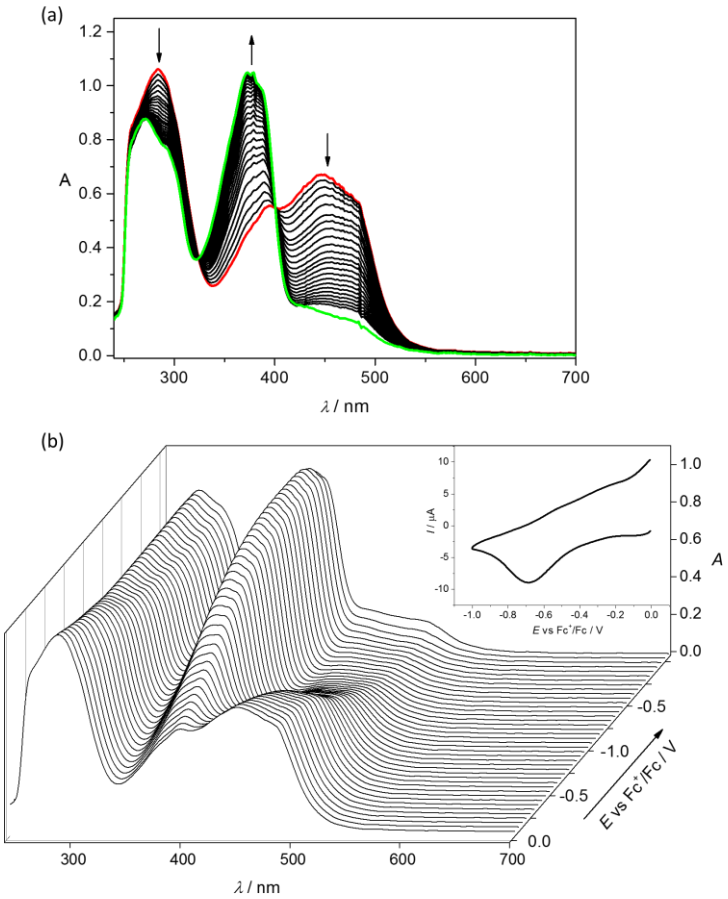

Figure 4. *In situ* UV-vis-NIR spectroelectrochemistry for **2** in DMSO/*n*-Bu_4NPF_6 (scan rate of 10 mV s^{-1}, Pt-microstructured honeycomb working electrode): (a) evolution of UV−vis spectra in 2D projection in forward scan; (b) UV-vis spectra detected simultaneously upon the cyclic voltammetric scan (Inset: respective cyclic voltammogram)

Upon cathodic reduction of **3** in DMSO/*n*-Bu_4NPF_6 at the first electron transfer new absorption bands at 649, 395 and 289 nm arise with a simultaneous decrease of the initial optical band at 500 nm via isosbestic points at 550, 444, 274 and 300 nm (Figure 5a). Additionally, upon voltammetric reverse scan nearly full recovery of the initial optical bands was observed, attesting the chemical reversibility of the cathodic reduction even at low scan rates (Figure 5b). These results are comparable with those reported for other Fe(III)–TSC complexes. Such redox active complexes are able to markedly increase the

amount of ROS in cancer cells. Hydroxyl radicals in such systems can be obtained from Fenton reactions, where the iron cycles between the Fe(II) and Fe(III) oxidation states.[23]

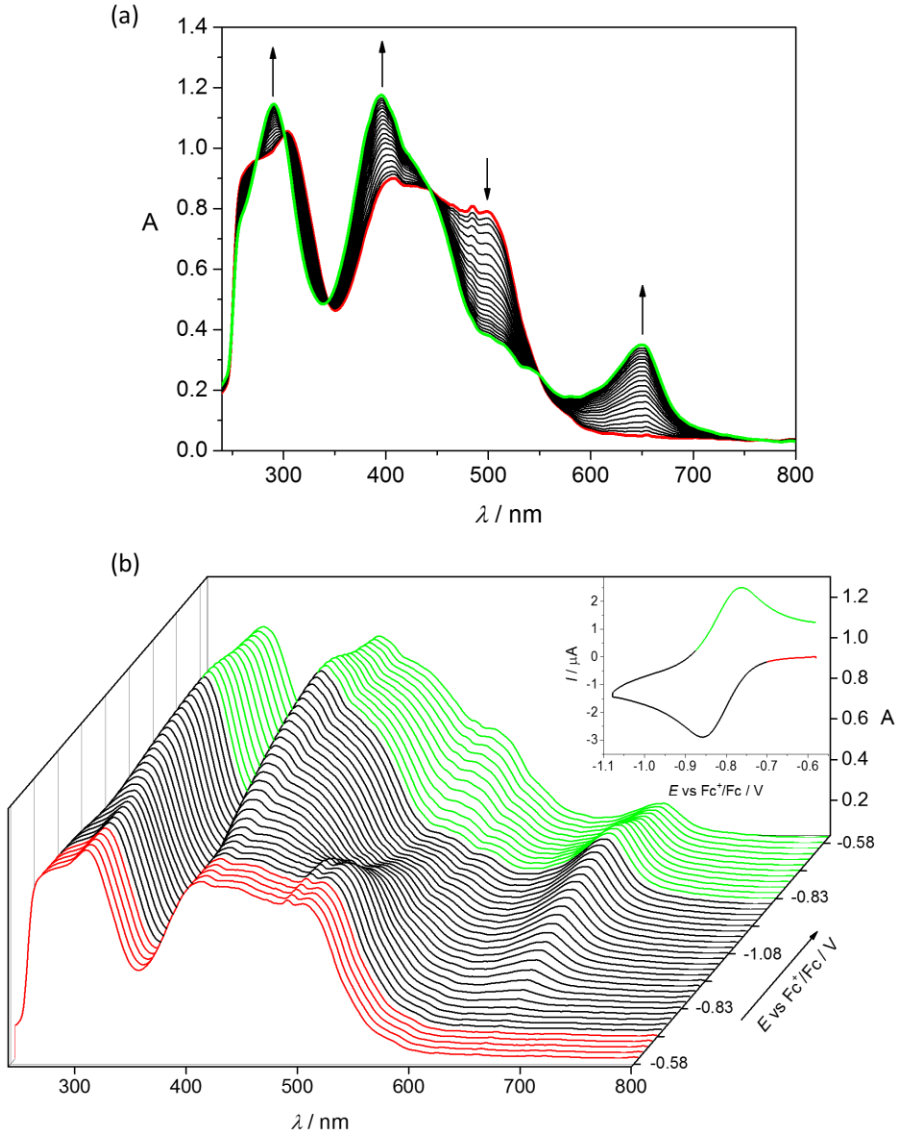

Figure 5. Spectroelectrochemistry of **3** in *n*-Bu_4NPF_6/DMSO in the region of the first cathodic peak. (a) UV-vis spectra detected simultaneously during the in-situ reduction (Pt-microstructured honeycomb working electrode, scan rate v = 10 mV s^{-1}); (b) potential dependence of UV−vis spectra (Inset: respective cyclic voltammogram with color-highlighted potential region, where spectra were taken).

Conclusions

Two new Triapine derivatives, namely (E)-N'-((E)-(3-aminopyridin-2-yl)methylene)picolinohydrazonamide hydrochloride (**HL^1·HCl**) and 3-amino-2-carboxaldehyde S-methylthiosemicarbazone (**HL^2**), were obtained. Further reaction of the proligands with $CuCl_2·2H_2O$ in 1:1 mole ratio afforded five-coordinate copper(II)

complexes [Cu(**HL**^{1})Cl_2] (**1**) and [Cu(**HL**^{2})Cl_2] (**2**). Proligand **HL**^{2} reacted with $Fe(NO_3)_3 \cdot 9H_2O$ in the presence of triethylamine in 2:1:2 mole with formation of bis-ligand octahedral complex [Fe(**L**^{2})$_2$]NO_3 (**3**), while reaction of **HL**^{2} with $ZnCl_2$ in methanol resulted in tetrahedral complex [$Zn^{II}Cl_3$(**H_2L**^{2})] (**4**), in which an unprecedented coordination mode of [**H_2L**^{2}]$^{+}$ is realized. The structures of **HL**^{2} and metal complexes **1**, **2** and **4** were established by X-ray diffraction. Ligands **1** and **2** act in a N,N,N-tridentate manner, while in complex **4** protonated proligand binds to zinc(II) in monodentate fashion via nitrogen atom N2. Complexes **1** and **2** demonstrate one and two irreversible reduction peaks respectively, what could be explained by complex decomposition after reduction with the followed ligand (or part of the ligand) release. These released proligands might act as Fe chelators and inhibit the RNR enzyme. In contrast, ferric complex **3** exhibited different redox behavior with almost reversible electrochemical reduction at –0.81 V *vs*. Fc^{+}/Fc. MTT assays revealed that proligands did not demonstrate significant antiproliferative activity, while complex formation with Cu(II) increased significantly the cytotoxicity in cancer cells. The iron(III) complex **3** was less active than **2**, but much more active than the proligand. Note that in case of 3-AP and its Fe(III) complex the opposite relationship was observed.[19] The reason of that might be in different modes of action of these complexes.

Experimental section

Chemicals. All reagents used were received from commercial sources. 2-cyanopyridine, $CuCl_2 \cdot 2H_2O$ and $Fe(NO_3)_3 \cdot 9H_2O$ were purchased from Sigma-Aldrich. 2-pyridinamidrazone was prepared as a white solid by reaction of 2-cyanopyridine with excess hydrazine hydrate as reported previously.[35] 3-N-(*tert*-butyloxycarbonyl)amino-2-pyridinecarboxaldehyde and S-methylisothiosemicarbazide hydrochloride[36] were obtained via synthetic procedure described in the literature.[37]

(E)-N'-((E)-(3-aminopyridin-2-yl)methylene)picolinohydrazonamide hydrogen chloride (**HL**^{1})

To a suspension of 3-N-(*tert*-butyloxycarbonyl)amino-2-pyridinecarboxaldehyde (0.100 g, 0.45 mmol) with hydrochloric acid (0.014 ml, 0.45 mmol) in ethanol (5 ml) a solution of 2-pyridinamidrazone (0.061 g, 0.45 mmol) in ethanol (10 ml) was added. This was heated to 80 °C and left under the stirring and reflux for 2 h. After this time clear orange solution

was found. Solvent amount was reduced to give fine yellow precipitate. This was filtered off, washed with ethanol, ether and dried on the air. Yield: 0.048 g, 60%. Anal. Calcd for $C_{12}H_{12}N_6 \cdot 2.5HCl \cdot 3H_2O$ (M 384.09 g mol^{-1}): C, 37.39; H, 5.36; N, 21.80. Found: C, 37.46; H, 5.12; N, 21.86; ^{1}H NMR (500.10 MHz, DMSO-d_6): δ 13.17 (s, 1H, H^{10}), 10.18 (s, 1H, H^7), 9.21 (s, 1H, H^{12}), 8.89 (d, J = 4.6 Hz, 1H, H^4), 8.49 (s, 1H, H^8), 8.20 (d, J = 7.8 Hz, 1H, H^2), 7.86-7.81 (m, 1H, H^{17}), 7.78-7.70 (m, 1H, H^3), 7.66 (d, 1H, H^{18}), 7.59 (d, 1H, H^{15}). ^{13}C NMR (125.76 MHz, DMSO-d_6): δ 161.75 (Cq, C^{11}), 157.26 (Cq, C^5), 150.31 (C_{Ar}, C^4), 149.29 (Cq, C^6), 146.98 (Cq, C^{13}), 128.90 (C_{Ar}, C^3), 127.98 (C_{Ar}, C^{17}), 126.52 (C_{Ar}, C^{18}), 124.94 (CH, C^8), 123.64 (C_{Ar}, C^{16}). ESI-MS (positive): *m/z* 241 ($[L + H]^+$). UV-vis (MeOH), λ_{max}, nm (ε, $M^{-1}cm^{-1}$): 399 (23814), 287sh, 264 (25741). IR (ATR, selected bands, $\tilde{\upsilon}_{max}$): 3157, 3050, 2846, 1665, 1605, 1580, 1534, 1476, 1334, 1291, 1164, 990, 791, 741 cm^{-1}.

$Cu(HL^1)Cl_2 \cdot 0.75H_2O$ (**1**$\cdot 0.75H_2O$)

To a solution of **HL^1** (0.100 g, 0.36 mmol) in methanol (10 ml) was added a solution of copper(II) chloride dihydrate (0.062 g, 0.36 mmol) in methanol (10 ml). Mixture was heated to 65 °C and left under the stirring and reflux overnight. The next day brown precipitate was found and filtered off. This was purified on preparative HPLC (water/methanol). The final product was obtained as brown powder after drying *in vacuo*. Yield: 0.031 g, 23.0%. Anal. Calcd for $C_{12}H_{12}N_6CuCl_2 \cdot 0.75H_2O$ (M 388.23 g mol^{-1}): C, 37.12; H, 3.50; N, 21.65; Found: C, 37.62; H, 3.14; N, 21.38; ESI-MS (positive): *m/z* 338 ($[Cu^{+1}(\mathbf{HL^1})Cl^-]^+$), 303 ($[Cu^{+1}(\mathbf{HL^1})]^+$). UV-vis (DMSO), λ_{max}, nm (ε, $M^{-1}cm^{-1}$): 714 (139), 437 (10326). IR (ATR, selected bands, $\tilde{\upsilon}_{max}$): 3209, 3114, 1636, 1578, 1538, 1235, 1151, 1052, 853, 801, 683, 660 cm^{-1}.

3-amino-2-carboxaldehyde S-methylthiosemicarbazone (**HL^2**)

3-N-(*tert*-butyloxycarbonyl)amino-2-pyridinecarboxaldehyde (0.31 g, 1.4 mmol) in ethanol (6 ml) and S-methylisothiosemicarbazide hydrochloride (0.20 g, 1.4 mmol) in water (6 ml) were mixed together and 12 M HCl (0.597 ml, 1.2 mmol) was added. Mixture stirred at 70 °C for 3 h. After cooling to the room temperature the solvent was removed under reduced pressure, residue dissolved in water and neutralized with $NaHCO_3$ (0.16 g, 1.9 mmol). Fine yellow precipitate was washed with ethanol, ether and then dried under the high vacuo. Yield: 0.193 g, 66.6%. Anal. Calcd for $C_8H_{11}N_5S$ (M 209.27 g mol^{-1}): C, 45.91; H, 5.30; N, 33.47; S, 15.32. Found: C, 46.07; H, 5.28; N, 33.29; S, 15.46. ^{1}H NMR

(500.10 MHz, DMSO-d_6): δ 8.31 (s, 1H, H^{10}), 7.83 (dd, J = 6.6, 2.7 Hz, 1H, H^3), 7.08 (d, J = 0.8 Hz, 1H, H^4), 7.06-7.01 (m, 1H, H^2), 6.85 (s, 1H, H^{11}), 6.89 (s, 1H, H^6), 2.41 (s, 3H, H^{14}). ^{13}C NMR (125.76 MHz, DMSO-d_6): δ 166.03 (Cq, C^{10}), 154.19 (CH, C^6), 144.48 (Cq, C^7), 137.30 (CH, C^3), 135.15 (Cq, C^6), 123.91 (CH, C^2), 122.01 (CH, C^4), 12.98 (CH_3, C^{14}). ESI-MS (positive): *m/z* 210 ($[L + H]^+$). UV-vis (MeOH), λ_{max}, nm (ε, $M^{-1}cm^{-1}$): 368 (19932), 269 (18373). IR (ATR, selected bands, $\tilde{\upsilon}_{max}$): 3091, 1652, 1599, 1495, 1443, 1301, 1141, 941, 909, 801, 690 cm^{-1}.

$Cu(HL^2)Cl_2 \cdot 0.2H_2O$ (**2**·$0.2H_2O$)

To a solution of **HL^2** (0.050 g, 0.24 mmol) in methanol (5 ml) was added a solution of copper(II) chloride dihydrate (0.041 g, 0.24 mmol) in methanol (5 ml). Mixture was heated to 50 °C and stirred for 10 min. Then it was left to cool down in the small flask on the air. Dark-green crystals were found the next day. Yield: 0.034 g, 81.9%. Anal. Calcd for $C_8H_{11}N_5SCuCl_2 \cdot 0.1H_2O$ (M 345.52 g mol^{-1}): C, 27.81; H, 3.26; N, 20.27; S, 9.28. Found: C, 28.13; H, 3.30; N, 19.89; S, 8.92. ESI-MS (positive): *m/z* 307 ($[Cu(\mathbf{HL^2})Cl]^+$), 271 ($[Cu^{+1}(\mathbf{HL^2})]^+$). UV-vis (MeOH), λ_{max}, nm (ε, $M^{-1}cm^{-1}$): 696 (122), 441 (11643), 282 (12217). IR (ATR, selected bands, $\tilde{\upsilon}_{max}$): 3250, 1642, 1583, 1525, 1502, 1274, 1217, 913, 877, 794, 643 cm^{-1}.

$[Fe(L^2)_2NO_3] \cdot 1.5H_2O$ (**3**·$1.5H_2O$)

To a solution of **HL^2** (0.059 g, 0.28 mmol) in methanol (5 ml) was added a solution of iron(III) nitrate nonahydrate (0.057 g, 0.14 mmol) in methanol (5 ml) and triethylamine (39 μl, 0.28 mmol). Mixture was heated to 60 °C and stirred for 20 min. After the removal of methanol crude residue was recrystallized from ethanol and fine black precipitate was obtained. This was filtered off, washed with ethanol, ether and dried on the air. Yield: 0.033 g, 24.8%. Anal. Calcd for $C_{16}H_{20}N_{11}S_2O_3Fe \cdot 1.5H_2O$ (M 561.07 g mol^{-1}): C, 34.23; H, 4.13; N, 27.44; S, 11.42. Found: C, 34.61; H, 3.81; N, 27.06; S, 11.22. ESI-MS (positive): *m/z* 472 ($[Fe(\mathbf{L^2})_2]^+$). UV-vis (MeOH), λ_{max}, nm (ε, $M^{-1}cm^{-1}$): 932 (891), 694 (590), 488 (12551), 428 (13956), 401sh, 301(15888), 266 (14206). IR (ATR, selected bands, $\tilde{\upsilon}_{max}$): 3214, 1646, 1579, 1528, 1466, 1319, 1268, 1142, 1057, 970, 849, 736 cm^{-1}.

Crystallographic Structure Determination. X-ray diffraction measurements were performed on a Bruker X8 APEXII CCD, Bruker D8 Venture and STOE diffractometers. Single crystals were positioned at 35, 40, 40 and 30 mm from the detector, and 3319, 5298,

527 and 3096 frames were measured, each for 10, 30, 50 and 5 s over 0.5, 1, 2 and 0.7° scan width for **HL^2**, **1**, **2** and **4**, respectively. The data were processed using SAINT software.[49] Crystal data, data collection parameters, and structure refinement details are given in Table 2. The structures were solved by direct methods and refined by full-matrix least-squares techniques. Non-H atoms were refined with anisotropic displacement parameters. H atoms were inserted in calculated positions and refined with a riding model. The following computer programs and hardware were used: structure solution, *SHELXS-2014* and refinement, *SHELXL-2014*;[38] molecular diagrams, ORTEP;[39] computer, Intel CoreDuo.

Electrochemistry and Spectroelectrochemistry.

Cyclic voltammetric experiments with 0.5 mM solutions of samples **1–3** in 0.1 M *n*-Bu_4NPF_6 (puriss quality from Fluka; dried under reduced pressure at 70 °C for 24 h before use) supporting electrolyte in DMSO (SeccoSolv max. 0.025% H2O, Merck) were performed under argon atmosphere using a three-electrode arrangement with platinum wire as counter electrodes, and silver wire as pseudoreference electrode. Glassy carbon or platinum wire served as working electrodes. Ferrocene purchased from Sigma Aldrich was used as the internal potential standard without further purification. All potentials in voltammetric studies were quoted vs ferricenium/ferrocene (Fc^+/Fc) redox couple. A Heka PG310USB (Lambrecht, Germany) potentiostat with a PotMaster 2.73 software package served for the potential control in voltammetric studies. *In situ* ultraviolet-visible-near-infrared (UV–vis–NIR) spectroelectrochemical measurements were performed on a spectrometer (Avantes, Model AvaSpec-2048x14-USB2 in the spectroelectrochemical cell kit (AKSTCKIT3) with the Pt-microstructured honeycomb working electrode, purchased from Pine Research Instrumentation. The cell was positioned in the CUV-UV Cuvette Holder (Ocean Optics) connected to the diode-array UV-vis-NIR spectrometer by optical fibers. UV-vis-NIR spectra were processed using the AvaSoft 7.7 software package. Halogen and deuterium lamps were used as light sources (Avantes, Model AvaLight-DH-S-BAL).

Cell lines and culture conditions

Human ovarian carcinoma cells A2780 and A2780cis, and human embryonic kidney cells HEK293 were obtained from ATCC. A2780 and A2780cis cells were cultured in RPMI

1640 medium containing 10% fetal bovine serum (FBS). HEK293 were cultured in DMEM medium containing 10% FBS. All cells were grown in tissue culture 25 cm^2 flasks (BD Biosciences, Singapore) 37 °C in a humidified atmosphere of 95% air and 5% CO_2. All drug stock solutions were prepared in DMSO and the final concentration of DMSO in medium did not exceed 1% (v/v) at which cell viability was not inhibited. The amount of actual Cu concentration in the stock solutions was determined by ICP-OES.

Inhibition of cell viability assay

The cytotoxicity of the compounds was determined by colorimetric microculture assay (MTT assay). The cells were harvested from culture flasks by trypsinisation and seeded into Cellstar 96-well microculture plates (Greiner Bio-One) at the seeding density of 6000 cells per well. After the cells were allowed to resume exponential growth for 24 h, they were exposed to drugs at different concentrations in media for 72 h. The drugs were diluted in complete medium at the desired concentration and 100 μl of the drug solution was added to each well and serially diluted to other wells. After exposure for 72 h, drug solutions were replaced with 100 μL of MTT in media (5 mg ml^{-1}) and incubated for additional 45 min. Subsequently, the medium was aspirated and the purple formazan crystals formed in viable cells were dissolved in 100 μl of DMSO per well. Optical densities were measured at 570 nm with a microplate reader. The quantity of viable cells was expressed in terms of treated/control (T/C) values by comparison to untreated control cells, and 50% inhibitory concentrations (IC50) were calculated from concentration-effect curves by interpolation. Evaluation was based on means from at least three independent experiments, each comprising six replicates per concentration level.

Intracellular accumulation

Intracellular accumulation of **1** and **2** was determined in A2780 cells. Cells were seeded into Cellstar 6-well plates (Greiner Bio-one) at a density of 60×10^4 cells/well (2 mL per well). After the cells were allowed to resume exponential growth for 24 h, they were exposed to **1** and **2** at various concentrations for 24 h at 37 °C. The cells were washed twice with 1 mL of PBS and lysed with 100 μL of RIPA lysis buffer (ultrapure water, 5M NaCl, 1M Tris-HCl pH 8.0, 2% sodium deoxycholate, 10% SDS, IGEPAL, protease and phosphatase inhibitor) for 5–10 min at 4 °C. The cell lysates were scraped from the wells and transferred to separate 1.5 mL microtubes. The supernatant was then collected after

centrifugation (13 000 rpm, 4 °C for 15 min) and total protein content of each sample was quantified via Bradford's assay. Cell lysates were transferred to 2 mL glass vials and then digested with ultrapure 60% HNO_3 (50 μL) at 110 °C for 96 h. The resulting solution was diluted to 1 mL (2–4% *v/v* HNO_3) with ultrapure Milli-Q water, sonicated for 45 mins and filtered through 0.45μm filters. Cu content of each sample was quantified by ICP-MS and expressed as per mg of protein. Re was used as an internal standard. Cu and Re were measured at *m*/*z* 64 and *m*/*z* 186, respectively. Metal standards for calibration curve (0, 1, 2, 5, 10, 20, 40 ppb) were prepared. All readings were made in six replicates in He mode.[40]

Table 2. Crystal Data and Details of Data Collection for 3-amino-2-carboxaldehyde S-methylthiosemicarbazone (**HL^2**), Cu(**HL^1**)Cl_2·0.75H_2O **(1),** Cu(**HL^2**)Cl_2·0.2H_2O **(2),** Zn(**H_2L^2**)Cl_3 **(4)**

Compound	**HL^2**	**1**	**2**	**4**
empirical formula	$C_8H_{11}N_5S$	$C_{12}H_{12}Cl_2CuN_6$	$C_8H_{11}Cl_2CuN_5S$	$C_8H_{12}Cl_3N_5SZn$
fw	209.28	374.72	343.72	382.01
space group	$P2_1/c$	$P2_1/c$	P-1	P-1
α, Å	10.9320(4)	8.3933(3)	8.0926(13)	8.5605(3)
b, Å	7.0723(3)	11.5392(2)	8.9713(15)	9.1005(3)
c, Å	12.6838(5)	15.1025(5)	9.1504(15)	9.9953(4)
α, °			78.368(7)	103.5744(12)
β, °	93.627(2)	104.188(2)	78.276(6)	93.6905(13)
γ, °			74.508(6)	109.2890(11)
V [Å^3]	978.29(7)	1418.09(7)	619.15(18)	705.84(4)
Z	4	4	2	2
λ [Å]	0.71073	1.54186	0.71073	1.54178
ρ_{calcd}, g cm^{-3}	1.421	1.755	1.844	1.797
cryst size, mm^3	0.20 × 0.18 × 0.12	0.22 × 0.04 × 0.04	0.20 × 0.18 × 0.07	0.22 × 0.17 × 0.10
T [K]	130(2)	100(2)	200(2)	100(2)
μ, mm^{-1}	0.298	5.662	2.347	8.946
R_1[a]	0.0309	0.0358	0.0555	0.0395
wR_2[b]	0.0873	0.0950	0.2121	0.1104
GOF[c]	1.048	0.958	1.071	1.093

[a] $R_1 = \Sigma||F_o| - |F_c||/\Sigma|F_o|$. [b] $wR_2 = \{\Sigma[w(F_o^2 - F_c^2)^2]/\Sigma[w(F_o^2)^2]\}^{1/2}$. [c] GOF = $\{\Sigma[w(F_o^2 - F_c^2)^2]/(n - p)\}^{1/2}$, where n is the number of reflections and p is the total number of parameters refined.

References

(1) Brockman, R. W.; Thompson, J. R.; Bell, M. J.; Skipper, H. E. Observations on the antileukemic activity of pyridine-2-carboxaldehyde thiosemicarbazone and thiocarbohydrazone. *Carcer. Res.* **1956**, *16*, 167.

(2) Kunos, C. A.; Chu, E.; Beumer, J. H.; Sznol, M.; Ivy, S. P. Phase I trial of daily triapine in combination with cisplatin chemotherapy for advanced‐stage malignancies. *Cancer Chemother. Pharmacol.* **2017**, *79*, 201–207.

(3) Nutting, C. M.; van Herpen, C. M. L.; Miah, A. B.; Bhide, S. A; Machiels, J.-P.; Buter, J.; Kelly, C.; de Raucourt, D.; Harrington, K. J. Phase II study of 3-AP Triapine in patients with recurrent or metastatic head and neck squamous cell carcinoma. *Annals of Oncol.* **2009**, *20*, 1275–1279.

(4) Choi, B. S.; Alberti, D. B.; Schelman, W. R.; Kolesar, J. M.; Thomas, J. P.; Marnocha, R.; Eickhoff, J. C.; Ivy, S. P.; Wilding, G.; Holen, K. D. The maximum tolerated dose and biologic effects of 3-aminopyridine-2-carboxaldehyde thiosemicarbazone (3-AP) in combination with irinotecan for patients with refractory solid tumors. *Cancer Chemother. Pharmacol.* **2010**, *66*, 973–980.

(5) Kunos, C. A.; Chu, E.; Makower, D.; Kaubisch, A.; Sznol, M.; Ivy, S. P. Phase I Trial of Triapine-Cisplatin-Paclitaxel Chemotherapy for Advanced Stage or Metastatic Solid Tumor Cancers. *Front. Oncol.* **2017**, *7*, 1–8.

(6) Mortazavi, A.; Ling, Y.; Martin, L. K.; Wei, L.; Phelps, M. A.; Liu, Z.; Harper, E. J.; Ivy, S. P.; Wu, X.; Zhou, B.-S.; Liu, X.; Deam, D.; Monk, J. P.; Hicks, W. J.; Yen, Y.; Otterson, G. A.; Grever, M. R.; Bekaii-Saab, T. A. A phase I study of prolonged infusion of triapine in combination with fixed dose rate gemcitabine in patients with advanced solid tumors. *Invest. New Drugs* **2013**, *31*, 685–695.

(7) Schelman, W. R.; Morgan-Meadows, S.; Marnocha, R.; Lee, F.; Eickhoff, J.; Huang, W.; Pomplun, M.; Jiang, Z.; Albert, D.; Kolesar, J. M.; Ivy, P.; Wilding, G.; Traynor, A. A phase I study of Triapine in combination with doxorubicin in patients with advanced solid tumors. *Cancer Chemother. Pharmacol.* **2009**, *63*, 1147–1156.

(8) Kunos, C. A.; Ivy, S. P. Triapine Radiochemotherapy in Advanced Stage Cervical Cancer. *Front. Oncol.* **2018**, *8*, 1–7.

(9) Barker, C. A.; Burgan, W. E.; Carter, D. J.; Cerna, D.; Gius, D.; Hollingshead, M. G.; Camphausen, K.; Tofilon, P. J. *In vitro* and *In vivo* Radiosensitization Induced by the

Ribonucleotide Reductase Inhibitor Triapine (3-Aminopyridine-2-Carboxaldehyde-Thiosemicarbazone). *Clin. Cancer Res.* **2006**, *12*, 2912–2918.

(10) Finch, R. A.; Liu, M.-C.; Cory, A. H.; Cory, J. G.; Sartorelli, A. C. Triapine (3-Aminopyridine-2-carboxyldehyde thiosemicarbazone; 3-AP): an Inhibitor of Ribonucleotide Reductase with Antineoplastic Activity. *Advan. Enzyme Regul.* **1999**, *39*, 3–12.

(11) Aye, Y.; Long, M. J. C.; Stubbe, J. Mechanistic Studies of Semicarbazone Triapine Targeting Human Ribonucleotide Reductase *in Vitro* and in Mammalian Cells. *J. Biol. Chem.* **2012**, *287*, 35768–35778.

(12) Popović-Bijelić, A.; Kowol, C. R.; Lind, M. E. S.; Luo, J.; Himo, F.; Enyedy, É. Arion, V. B.; Gräslund, A. Ribonucleotide reductase inhibition by metal complexes of Triapine (3-aminopyridine-2-carboxaldehyde thiosemicarbazone): A combined experimental and theoretical study. *J. Inorg. Biochem.* **2011**, *105*, 1422–1431.

(13) Shao, J.; Zhou, B.; J. Di Bilio, A. J.; Zhu, L.; Wang, T.; Qi, C.; Shih, J.; Yen, Y. A Ferrous-triapine complex mediates formation of reactive oxygen species that inactivate human ribonucleotide reductase. *Mol. Cancer. Ther.* **2006**, *5*, 586–592.

(14) Knox, J. J.; Hotte, S. J.; Kollmannsberger, C.; Winquist, E.; Fisher, B.; Eisenhauer, E. A. Phase II study of Triapine in patients with metastatic renal cell carcinoma: a trial of the National Cancer Institute of Canada Clinical Trials Group. *Invest. New Drugs* **2007**, *25*, 471–477.

(15) Yen, Y.; Margolin K.; Doroshow, J.; Fishman, M.; Johnson, B.; Clairmont, C.; Sullivan, D.; Sznol, M. A phase I trial of 3-aminopyridine-2-carboxaldehyde thiosemicarbazone in combination with gemcitabine for patients with advanced cancer. *Cancer Chemother. Pharmacol.* **2004**, *54*, 331–342.

(16) Traynor, A. M.; Lee, J.-W.; Bayer, G. K.; Tate, J. M.; Thomas, S. P.; Mazurczak, M.; Graham, D. M.; Kolesar, J. M.; Schiller, J. H. A phase II trial of Triapine® (NSC# 663249) and gemcitabine as second line treatment of advanced non-small cell lung cancer: Eastern Cooperative Oncology Group Study 1503. *Invest. New Drugs* **2010**, *28*, 91–97.

(17) Mackenzie, M. J.; Saltman, D.; Hirte, H.; Low, J.; Johnson, C.; Pond, G.; Moore, M. J. A Phase II study of 3-aminopyridine-2-carboxaldehyde thiosemicarbazone (3-AP) and gemcitabine in advanced pancreatic carcinoma. A trial of the Princess Margaret Hospital Phase II consortium. *Invest. New Drugs* **2007**, *25*, 553–558.

(18) Attia, S.; Kolesar, J.; Mahoney, M. R.; Pitot, H. C.; Laheru, D; Heun, J.; Huang, W.; Eickhoff, J.; Erlichman, C.; Holen, K. D. A phase 2 consortium (P2C) trial of 3-aminopyridine-2-carboxaldehyde thiosemicarbazone (3-AP) for advanced adenocarcinoma of the pancreas. *Invest. New Drugs* **2008**, *26*, 369–379.

(19) Kowol, C. R.; Trondl, R.; Heffeter, P.; Arion, V. B.; Jakupec, M. A.; Roller, A.; Galanski, M.; Berger, W.; Keppler, B. K. Impact of Metal Coordination on Cytotoxicity of 3-Aminopyridine-2-carboxaldehyde Thiosemicarbazone (Triapine) and Novel Insights into Terminal Dimethylation. *J. Med. Chem.* **2009**, *52*, 5032−5043.

(20) Jansson, P. J.; Sharpe, P. C.; Bernhardt, P. V.; Richardson, D. R. Novel Thiosemicarbazones of the ApT and DpT Series and Their Copper Complexes: Identification of Pronounced Redox Activity and Characterization of Their Antitumor Activity *J. Med. Chem.* **2010**, *53*, 5759–5769.

(21) Bacher, F.; Dömötör, O.; Chugunova, A.; Nagy, N. V.; Filipović, L.; Radulović, S.; Enyedy, É. A.; Arion, V. B. Strong effect of copper(II) coordination on antiproliferative activity of thiosemicarbazone-piperazine and thiosemicarbazone-morpholine hybrids. *Dalton Trans.* **2015**, *44*, 9071−9090.

(22) Dobrova, A.; Platzer, S.; Bacher, F.; Milunovic, M. N. M.; Dobrov, A.; Spengler, G.; Enyedy, É. A.; Novitchi, G.; Arion, V. B. Structure-antiproliferative activity studies on L-proline- and homoproline-4-N-pyrrolidine-3-thiosemicarbazone hybrids and their nickel(II), palladium(II) and copper(II) complexes. *Dalton Trans.* **2016**, *45*, 13427−13439.

(23) Ohui, K.; Afanasenko, E.; Bacher, F.; Lin Xue Ting, R.; Zafar, A.; Blanco-Cabra, N.; Torrents, E.; Dömötör, O.; May, N. V.; Darvasiova, D.; Enyedy, É. A.; Popović-Bijelić, A.; Reynisson, J.; Rapta, P.; Babak, M. V.; Pastorin, G.; Arion, V. B. New Water-Soluble Copper(II) Complexes with Morpholine-Thiosemicarbazone Hybrids: Insights into the Anticancer and Antibacterial Mode of Action. *J. Med. Chem.* **2019**, *62*, 512–530.

(24) Adsule, S.; Barve, V.; Chen, D.; Ahmed, F.; Dou, Q. P.; Padhye, S.; Sarkar, F. H. Novel Schiff Base Copper Complexes of Quinoline-2-Carboxaldehyde as Proteasome Inhibitors in Human Prostate Cancer Cells. *J. Med. Chem.* **2006**, *49*, 7242−7246.

(25) Milunović, M. N. M.; Dobrova, A.; Novitchi, G.; Gligorijević, N.; Radulović, S.; Kožiček, J.; Rapta, P.; Enyedy, E. A.; Arion, V. B. Effects of Terminal Substitution and Iron Coordination on Antiproliferative Activity of L-Proline-salicylaldehyde-Thiosemicarbazone Hybrids. *Eur. J. Inorg. Chem.* **2017**, 4773–4783.

(26) Pogorzelska, A.; Sławiński, J.; Kawiak, A.; Żołnowska, B.; Chojnacki, J.; Stasiłojć, G.; Ulenberg, S.; Szafrański, K.; Bączek, T. Synthesis, molecular structure, and metabolic stability of new series of N'-(2-alkylthio-4-chloro-5-methylbenzenesulfonyl)-1-(5-phenyl-1*H*-pyrazol-1-yl)amidine as potential anti-cancer agents. *Eur. J. Med. Chem.* **2018**, *155*, 670–680.

(27) Al-Qtaitat, M. A.; El-Abadelah, M. M.; Sabbah, D. A.; Bardaweel, S.; Sweidan, K.; Sabri, S. S.; Mubarak, M. S. Synthesis, characterization, and bioactivity of new bisamidrazone derivatives as possible anticancer agents. *Med. Chem. Res.* **2018**, *27*, 1419–1431.

(28) Gokhale, N.; Padhye, S.; Rathbone, D.; Billington, D.; Lowe, P.; Schwalbe, C.; Newton, C. The crystal structure of first copper(II) complex of a pyridine-2-carboxamidrazone – a potential antitumor agent. *Inorg. Chem. Commun.* **2001**, *4*, 26–29.

(29) Mazur, L.; Modzelewska-Banachiewicz, B.; Paprocka, R.; Zimecki, M.; Wawrzyniak, U. E.; Kutkowska, J.; Ziółkowska, G. Synthesis, crystal structure and biological activities of a novel amidrazone derivative and its copper(II) complex – A potential antitumor drug. *J. Inorg. Biochem.* **2012**, *114*, 55–64.

(30) Ohui, K.; Babak, M. V.; Darvasiova, D.; Roller, A.; Vegh, D. Rapta, P.; Guan, G. R. S.; Ou, Y. H.; Pastorin, G.; Arion, V. B. Redox-Active Organoruthenium(II)− and Organoosmium(II)−Copper(II) Complexes, with an Amidrazone−Morpholine Hybrid and $[Cu^{I}Cl_2]^-$ as Counteranion and Their Antiproliferative Activity. *Organometallics* 10.1021/acs.organomet.9b00229

(31) Gokhale, N. H.; Padhye, S. S.; Padhye, S. B.; Anson, C. E.; Powell, A. K. Copper complexes of carboxamidrazone derivatives as anticancer agents. 3. Synthesis, characterization and crystal structure of [Cu(appc)Cl2], (appc = N1-(2-acetylpyridine)pyridine-2-carboxamidrazone). *Inorg. Chim. Acta* **2001**, *319*, 90–94.

(32) Addison, A. W.; Rao, T. N.; Reedijk, J.; van Rijn, J.; Verschoor, G. C. Synthesis, structure, and spectroscopic properties of copper(II) compounds containing nitrogen–sulphur donor ligands; the crystal and molecular structure of aqua[1,7-bis(*N*-methylbenzimidazol-2′-yl)-2,6-dithiaheptane]copper(II) perchlorate. *J. Chem. Soc. Dalton Trans.* **1984**, 1349–1356.

(33) Arion, V. B. Coordination chemistry of S-substituted isothiosemicarbazides and isothiosemicarbazones. *Coord. Chem. Rev.* **2019**, *387*, 348–397.

(34) Milunović, M. N. M.; Dobrova, A.; Novitchi, G.; Gligorijević, N.; Radulović, S.; Kožiček, J.; Rapta, P.; Enyedy, E. A.; Arion, V. B. Effects of Terminal Substitution and Iron Coordination on Antiproliferative Activity of L-Proline-salicylaldehyde-Thiosemicarbazone Hybrids. *Eur. J. Inorg. Chem.* **2017**, 4773−4783.

(35) Guo, T.; Guan, R.; Zou, J.; Liu, J.; Ying, L.; Yang, W.; Wu, H.; Cao, Y. Red light-emitting hyperbranched fluorene-alt-carbazole copolymers with an iridium complex as the core. *Polym. Chem.* **2011**, *2*, 2193–2203.

(36) Freund, M.; Paradies, T. Zur Kenntnis des Tetrazols. *Ber. Dtsch. Chem. Ges*. **1901**, *34*, 3110–3122.

(37) Venuti, M. C.; Stephenson, R. A.; Alvarez, R.; Bruno, J. J.; Strosberg, A. M. Inhibitors of cyclic AMP phosphodiesterase. 3. Synthesis and biological evaluation of pyrido and imidazolyl analogs of 1,2,3,5-tetrahydro-2-oxoimidazo[2,1-b]quinazoline. *J. Med. Chem.* **1988**, *31*, 2136–2145.

(38) Sheldrick, G. M. A short history of SHELX, *Acta Crystallogr.* **2008**, *A64*, 112–122.

(39) Burnett, M. N.; Johnson, G. K. ORTEPIII. Report ORNL-6895. OAK Ridge National Laboratory; Tennessee, **1996**.

Supporting Information

for

New Triapine Derivatives and their Metal Complexes as Anticancer Agents

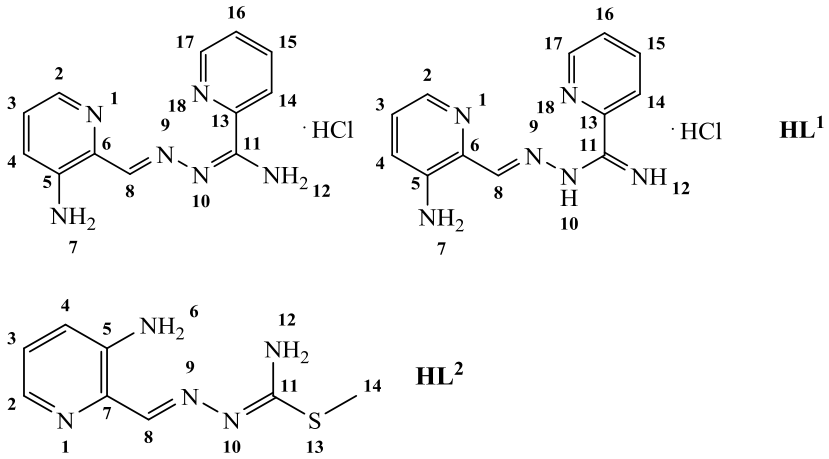

Scheme S1. Atom numbering used for proton and carbon resonances assignment in ^{1}H and ^{13}C NMR spectra of **HL**^{1} and **HL**^{2}.

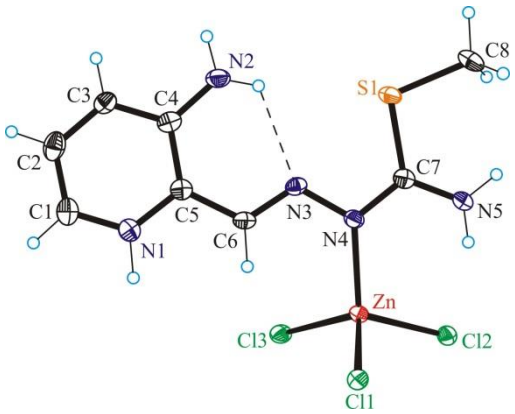

Figure S1. ORTEP view of Zn(**H$_2$L**^{2})Cl$_3$.

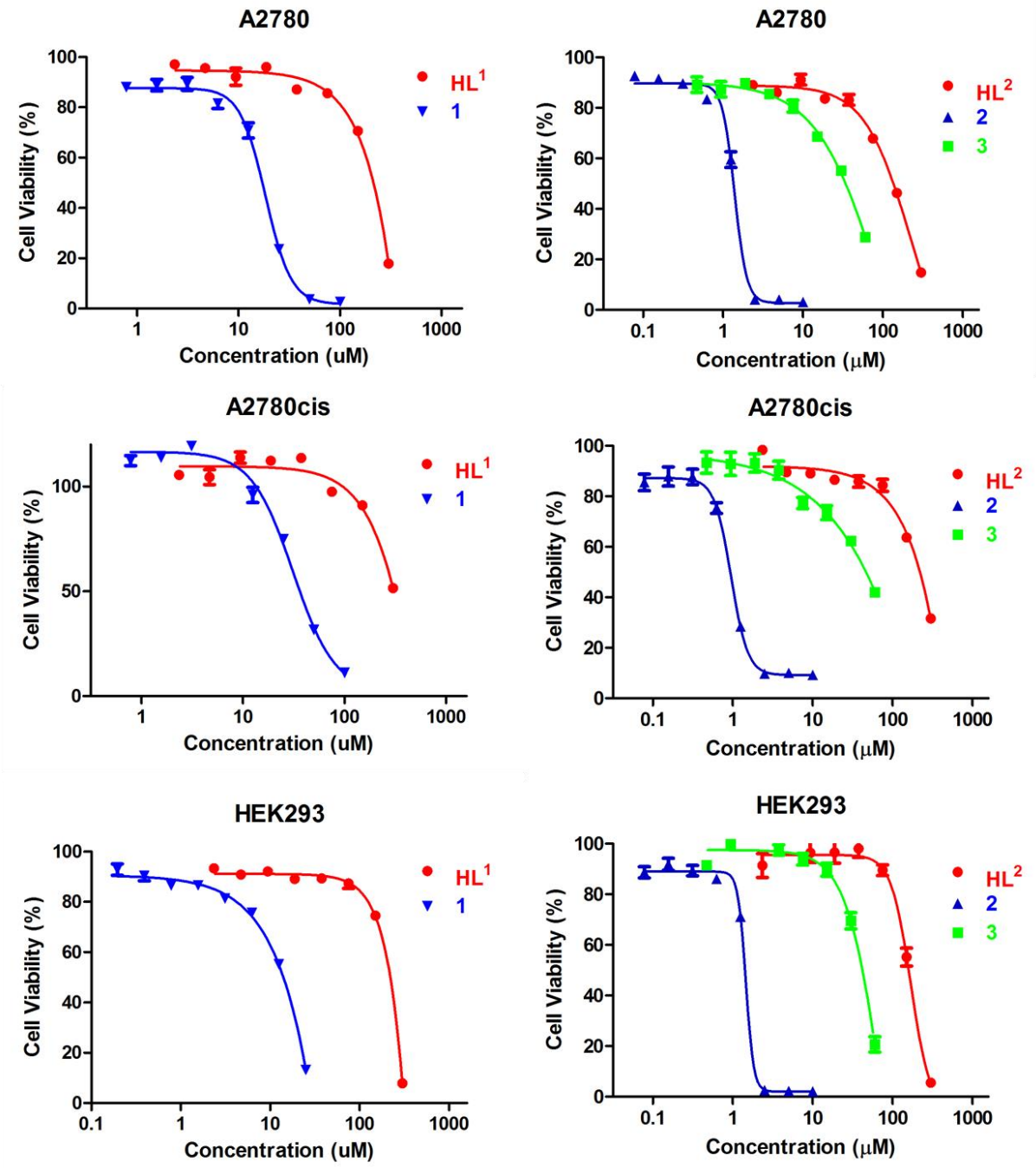

Figure S2. Concentration-effect curves for **HL**^{1}, **HL**^{2} and **1**–**3** in A2780, A2780cis and HEK293 cell lines upon 72 h exposure.

Other Synthesis

Synthesis of N,N'-(((2-(2-((Z)-(6-(morpholinomethyl)pyridin-2-yl)methylene)hydrazine-1-carbothioamido)ethyl)azanediyl)bis(ethane-2,1-diyl))bis(2-((6-(morpholinomethyl)pyridin-2-yl)methylene)hydrazine-1-carbothioamide)

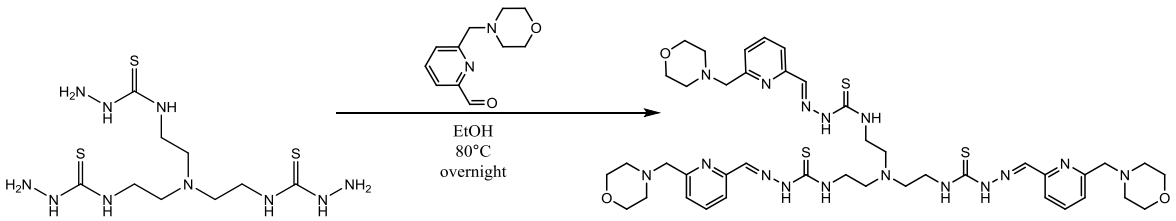

Reagents:

6-(moprpholinomethyl)pyridine-2-carboxaldehyde	0.168 g, 0.82 mmol
Tris(2-aminoethyl)amine	0.100 g, 0.27 mmol
Ethanol	15 ml

To 6-(morpholinomethyl)pyridine-2-carboxaldehyde dissolved in ethanol was added *tris*(2-aminoethyl)amine. Mixture was heated to 80 ºC and left under the stirring and reflux for 48 h. After this time clear yellow solution was obtained. The amount of ethanol was reduced under the high vacuo and mixture was left to stand at –20 ºC for 72 h to give yellow precipitate.

Yield: 0.1 g (39.5%).

Anal. Calcd for $C_{42}H_{60}N_{16}O_3S_3 \cdot 1.65H_2O$ (Mr = 962.96): C, 52.39; H, 6.63; N, 23.27; S, 9.99. Found: C, 52.78; H, 6.63; N, 22.88; S, 9.68.

ESI-MS (positive): *m/z* 933 ($[L + H]^+$).

Synthesis of N,N'-(((2-(2-((Z)-(6-(morpholinomethyl)pyridin-2-yl)methylene)hydrazine-1-carbothioamido)ethyl)azanediyl)bis(ethane-2,1-diyl))bis(2-((6-(morpholinomethyl)pyridin-2-yl)methylene)hydrazine-1-carbothioamide) copper(II) chloride

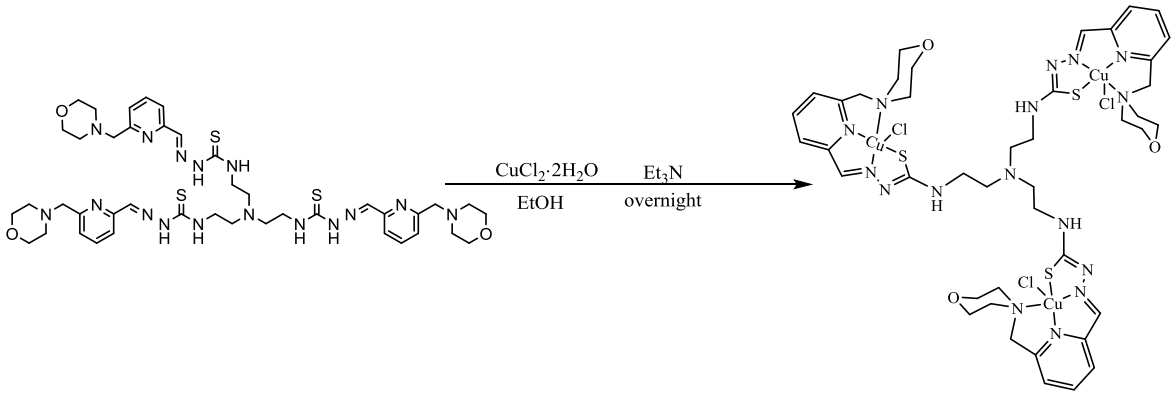

Reagents:

Proligand	0.050 g, 0.05 mmol
copper(II) chloride dihydrate	0.027 g, 0.16 mmol
triethylamine	0.022 ml, 0.16 mmol

To a solution of N,N'-(((2-(2-((Z)-(6-(morpholinomethyl)pyridin-2-yl)methylene)hydrazine-1-carbothioamido)ethyl)azanediyl)bis(ethane-2,1-diyl))bis(2-((6-(morpholinomethyl)pyridin-2-yl)methylene)hydrazine-1-carbothioamide) in methanol was added a solution of copper(II) chloride dihydrate in methanol and then triethylamine. Dark-green solution was stirred for 20 min at 60 ºC and the precipitate was filtered off. The filtrate was concentrated and allowed to stand at –20 ºC overnight to give a dark-green powder.

Yield: 0.058 g, 16.9%.

ESI-MS (positive): *m/z* 577.6 ($[M_3(L)Cl]^{2+}$).

Synthesis of Polypropyleniminetetrathiosemicarbazonedendrimer with Morpholine moiety

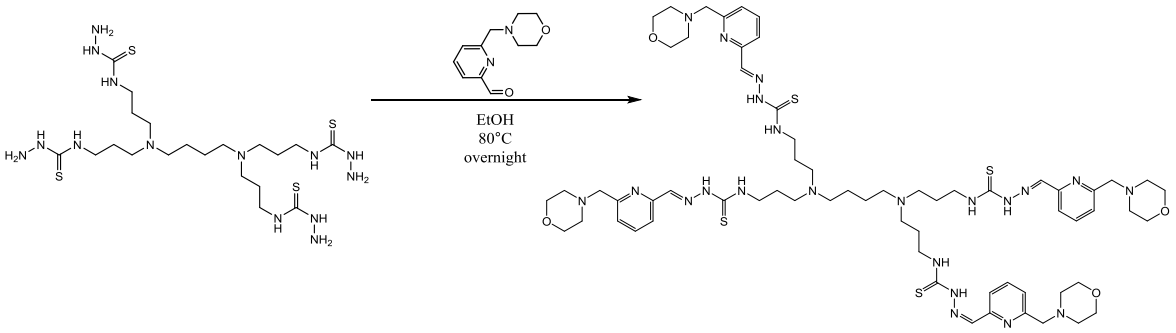

Reagents:

Tetrameric carbazide	0.100 g, 0.16 mmol
6-(morpholinomethyl)pyridine-2-carboxaldehyde	0.134 g, 0.65 mmol
Ethanol	15 ml

To 6-(morpholinomethyl)pyridine-2-carboxaldehyde dissolved in ethanol was added N,N',N'',N'''-((butane-1,4-diylbis(azanetriyl))tetrakis(propane-3,1-diyl))tetrakis (hydrazinecarbothioamide). Mixture was heated to 80 ºC and left under the stirring and reflux overnight. The next day the amount of ethanol was reduced under the high vacuo and mixture was left to stand at +4 ºC for 48 h to give yellow precipitate.

Yield: 0.059 g (26.3%)

ESI-MS (positive): *m/z* 1365 ($[L + H]^+$).

Final Remarks

The aim of this work was synthesis of novel mono-, di- and polynucleating thiosemicarbazones, amidrazones and/or aminoguanizones as well as their metal complexes, which could possess anticancer activity and additionally antibacterial/antiviral activity and act dual pharmaceutical agents. α-*N*-heterocyclic thiosemicarbazones possess a broad spectrum of biological activity and are perfect metal chelators especially for the first row transition metals, namely zinc(II), copper(II), iron(III), etc. Recently, two new thiosemicarbazones, DpC and COTI-2, have entered clinical trials rekindling the interest to this class of the compounds. The attachment of morpholine-scaffold to thiosemicarbazone backbone in position 5 to 2-formylpyridine moiety resulted in six novel water-soluble morpholine-(iso)thiosemicarbazone hybrids and their copper(II) complexes. Compounds displayed remarkable activity in nanomolar and submicromolar concentration range against cisplatin-sensitive and cisplatin-resistant ovarian carcinoma cells. As R2 RNR is believed to be one of the main biological targets of thiosemicarbazones, the inhibition potency of novel compounds toward this enzyme was tested. Studies with R2 RNR showed that copper(II) complexes with new hybrid ligands only moderately quench the tyrosil radical. Therefore, the antiproliferative activity of this family of compounds might be caused not only by R2 RNR inhibition but also by other mechanisms, such as MAPK activation, ER stress, etc. Additionally it was discovered that complex formation with new hybrid ligands results in enhancement of antibacterial activity against Gram-positive *S. aureus*.

Amidrazones possess a broad spectrum of biological activity and are good metal chelators. Attachment of morpholine-scaffold to the amidrazone backbone was expected to not only provide an additional coordination site but also increase aqueous solubility and improve biological properties of the compounds, since incorporation of morpholine into the chemical structure of drugs is known to result in good pharmacological profiles. Good examples are the worldwide used drugs Aprepitant and Gefinitib. In the presented work new redox-active mono- Cu(II) and heterodinuclear Cu(II)-Ru(II) and Cu(II)-Os(II) complexes with amidrazone scaffold and $[CuCl_2]^-$ as counteranion were synthesized. In case of copper(II)-amidrazone complex aldimine bond was highly polarized triggering the substitution of H by MeO group by two step suggested mechanism. All three complexes have demonstrated moderate activity against ovarian carcinoma and cervical carcinoma

cells in micromolar concentration range. In addition, all three complexes were selective to cancer cells over healthy cells. Spin-trapping experiment in cell-free media and confocal microscopic imaging in ovarian carcinoma cells showed that compounds are able to generate reactive oxygen species (ROS), which could explain their antiproliferative activity. Interestingly, even though intracellular accumulation of Cu(II)-Ru(II) and Cu(II)-Os(II) complexes was higher, they demonstrated lower cytotoxicity. This might be explained by their less efficient ROS production.

Triapine (3-aminopyridine-2-carboxaldehyde thiosemicarbazone , 3-AP) is one of the most potent antitumor drug and inhibitor of R2 RNR. The drug has already entered more than 30 phase I and II clinical trials. Two new derivatives with S-methyl and pyridine substituents and their Cu(II) and Fe(III) complexes were synthesized and tested against ovarian cancer cells and non-cancerous embryonic kidney cells. Complexes showed significant cytotoxicity in comparison to their proligands, but, unfortunately, were not selective to cancer cells. The Fe(III) complex with S-methyl derivative was less active that Cu(II) complex, but nearly 5 times more active than the proligand. It has to be noted that in case of Fe(III) complex of Triapine the opposite relationship was observed.

Finally, attempts to obtain polynucleating thiosemicarbazone-derivatives were undertaken as dendrimers are known to build an interesting class of compounds which could be potent drug-delivery agents. Efforts to obtain new derivatives resulted in the synthesis of a novel *tris*-thiosemicarbazone with morpholine moiety and its tricopper(II) complex. The investigation of this class of compounds is going on and will be reported in due course.